

Some pages of this thesis may have been removed for copyright restrictions.

If you have discovered material in AURA which is unlawful e.g. breaches copyright, (either yours or that of a third party) or any other law, including but not limited to those relating to patent, trademark, confidentiality, data protection, obscenity, defamation, libel, then please read our [Takedown Policy](#) and [contact the service](#) immediately

**All Optical Networking Beyond 10 Gbit/s;
OTDM Networks Based on Electro-Optic
Modulators and Fibre Ring Lasers.**

Andrew D Ellis

Doctor of Philosophy

The University of Aston in Birmingham

April 1997.

This copy of the thesis has been supplied on condition that anyone who consults it is understood to recognise that its copyright rests with its author and that no quotation from the thesis and no information derived from it may be published or otherwise disclosed without proper acknowledgement. Material within is reproduced with permission from publications of the IEE and John Wiley and Sons Limited.

The University of Aston in Birmingham

All Optical Networking Beyond 10 Gbit/s; OTDM Networks Based on Electro-Optic Modulators and Fibre Ring Lasers.

Andrew D Ellis

Doctor of Philosophy

1997.

This thesis examines options for high capacity all optical networks. Specifically optical time division multiplexed (OTDM) networks based on electro-optic modulators are investigated experimentally, whilst comparisons with alternative approaches are carried out. It is intended that the thesis will form the basis of comparison between optical time division multiplexed networks and the more mature approach of wavelength division multiplexed networks.

Following an introduction to optical networking concepts, the required component technologies are discussed. In particular various optical pulse sources are described with the demanding restrictions of optical multiplexing in mind. This is followed by a discussion of the construction of multiplexers and demultiplexers, including favoured techniques for high speed clock recovery. Theoretical treatments of the performance of Mach Zehnder and electroabsorption modulators support the design criteria that are established for the construction of simple optical time division multiplexed systems.

Having established appropriate end terminals for an optical network, the thesis examines transmission issues associated with high speed RZ data signals. Propagation of RZ signals over both installed (standard fibre) and newly commissioned fibre routes are considered in turn. In the case of standard fibre systems, the use of dispersion compensation is summarised, and the application of mid span spectral inversion experimentally investigated. For green field sites, soliton like propagation of high speed data signals is demonstrated. In this case the particular restrictions of high speed soliton systems are discussed and experimentally investigated, namely the increasing impact of timing jitter and the downward pressure on repeater spacings due to the constraint of the average soliton model. These issues are each addressed through investigations of active soliton control for OTDM systems and through investigations of novel fibre types respectively.

Finally the particularly remarkable networking potential of optical time division multiplexed systems is established, and infinite node cascability using soliton control is demonstrated. A final comparison of the various technologies for optical multiplexing is presented in the conclusions, where the relative merits of the technologies for optical networking emerges as the key differentiator between technologies.

To Dad.

Acknowledgements

First, and foremost, I would like to thank Mum and Dad for the gift of life, and Jackie and Daniel for giving life its meaning. Thanks also for putting up with the whirr's and clicks during the preparation of this thesis.

To Nick Doran and David Cotter and Keith Blow, thanks for the encouragement and the opportunity, and of course Terry Widdowson for the ever present "useful comments". For reviewing the thesis, particular thanks are due to Nick, Terry, Dave Richardson, Dominique Marcenac, Mike Brierley, Paul Gunning, Julian Lucek, and not forgetting Dave Spirit who heroically checked the references.

Much of this work would not have been possible without the assistance of a great many friends and colleagues, not least Derek Malyon, who set me upon the right track way back when and Dave Spirit for continuous support. More specifically thanks to; Gary Wickens and Peter Barnsley for their early pioneering work, Paul Gunning for assistance with understanding gain switched DFB's, Xuekang Shan for constructing stabilised mode locked fibre ring lasers, Lutz Blank for a wealth of ideas, Dave Davies for work on semiconductor loop mirrors, Dave Moodie and colleagues for the development of electroabsorption modulators, Ian Lealman for the supply of high speed DFB lasers, Doug Williams, Joe Antos and Mark Newhouse for the supply of optical fibres, Dave Richardson for anything to do with dispersion profiled fibre, Terry Widdowson for assistance with recirculating loops and clock recovery circuits, Liam Pender for assistance in demonstrating non-linear fibre circuits and optical regenerators, Martin Tatham for assistance with mid span spectral inversion, Ahmet Altuncu for the characterisation of distributed amplifiers, Ewart Lowe for permission to include cost modelling data, Phil Watkinson, Laraunt Noel, Finlay Knox, Jel Hueting and Damian Flannery for all round support and Mahlen Fox for development of data acquisition tools. The contributions, friendship and support of everybody else who knows me at BT labs, Aston, ICL, UCL, KCL, Essex and Southampton is also implicitly acknowledged, as is the stimulating research carried out at research establishments world-wide.

Finally, the author gratefully acknowledges the IEE for permission to use material originally published in Electronics Letters and Colloquium digests and John Wiley and Sons of Chichester for permission to reproduce previously published material from D.M.Spirit, M.J.O'Mahony, "High Capacity Optical Transmission Explained", © John Wiley and Sons Limited.

Statement of Originality

Except where indicated above, or by reference, all of the ideas and results presented in this thesis are solely attributable to the author. Similarly, the author participated in the design and implementation of all experiments presented except where explicitly indicated. Precise details of collaborators may be ascertained from lists of co-authors in Chapter 8.

Contents

1. Introduction	1
1.1 Optical Communications	1
1.2 General Optical Multiplexing Concepts	1
1.3 World Status	5
1.3.1 Point to point systems	5
1.3.2 Optical Networking	7
1.4 Overview of Thesis	8
2. Theory of Optical Communications	12
2.1 Properties of Transmission Links	12
2.1.1 Optical Receivers	12
2.1.2 Optical Fibre	12
2.1.2.1 Approach	13
2.1.2.2 Attenuation	13
2.1.2.3 Dispersion	14
2.1.2.4 Birefringence	16
2.1.2.5 Non-linearity	17
2.1.3 Optical Amplifiers	19
2.2 Optical Pulse Transmission	20
2.2.1 Propagation Equation	20
2.2.2 Optical Solitons	21
2.2.3 Ideal soliton communication systems	22
2.2.4 Practical soliton transmission	23
2.3 Systems Impairments of OTDM systems	27
2.3.1 Demultiplexer performance	28
2.3.2 Multiplexer performance	29
2.3.3 System Specification	30
2.4 Chapter summary	32
3. OTDM Transmitters	34
3.1 Picosecond Pulse Sources	35
3.1.1 Linear Compression	35
3.1.2 Gain Switched DFB	37
3.1.2.1 Jitter Suppression of Gain Switched DFB's	37
3.1.2.2 Pulse width optimisation of gain switched DFB's	39
3.1.2.3 Benefits of high FM efficiency	41
3.1.3 Mode Locked External Cavity Lasers	43
3.1.4 Mode Locked Fibre Ring Lasers	44
3.1.4.1 Electro-optic modulator based ring lasers	44
3.1.4.2 Ring laser cavity length stabilisation	45
3.1.4.3 Optically mode locked ring lasers	45
3.1.5 Electro-Optic Mach Zehnder Modulator	48
3.1.6 Electroabsorption Modulators	48
3.1.6.1 Soliton Pulse Generation Using Electroabsorption Modulators	49
3.1.6.2 Modulated soliton pulse train generation using EA modulators	52
3.1.7 Other Sources	57
3.1.8 Assessment of pulse source options	57
3.2 Pulse Compression Techniques	58
3.2.1 Soliton Pulse Compression	58
3.3 OTDM Multiplexer	63
3.3.1 Mach Zehnder Modulators	64
3.3.2 Full OTDM Multiplex	65
3.3.3 Passive OTDM Multiplexers	67
3.4 Alternative OTDM data generation	68
3.4.1 Generation of 40 GHz pulse train by beat frequency conversion	69
3.4.2 Systems evaluation of beat frequency conversion source	72
3.4.2.1 All optical modulation with a non-linear optical loop mirror	74

3.4.2.2 All optical modulation with a Kerr rotation gate.....	77
3.5 Chapter Summary	79
4. OTDM Receivers	80
4.1 Clock Recovery	80
4.1.1 Electronic Clock Recovery	81
4.1.2 All Optical Clock Recovery	82
4.1.3 Alternative OTDM clock recovery techniques.....	87
4.2 Demultiplexers	88
4.2.1 Mach Zehnder Modulators.....	89
4.2.2 Electroabsorption modulators.....	92
4.2.2.1 Theoretical Performance at 40 Gbit/s.....	92
4.2.2.2 80 Gbit/s systems based on electroabsorption modulators.....	93
4.2.2.3 Simultaneous photodetection and demultiplexing.....	96
4.3 Chapter Summary	97
5. OTDM Transmission.....	98
5.1 Standard Fibre Systems	98
5.1.1 Mid Span Spectral Inversion	99
5.2 Soliton Systems	104
5.2.1 40 Gbit/s soliton transmission.....	104
5.2.2 Theory of Soliton Transmission Control.....	109
5.2.3 20 Gbit/s soliton control	114
5.2.4 Soliton control using electro-optic frequency doubling.....	117
5.2.5 Soliton shepherding	120
5.2.6 Novel Transmission Fibres for Soliton Transmission	122
5.2.6.1 Distributed Amplification	122
5.2.6.2 Loss Compensating Dispersion Decreasing Fibre.....	125
5.3 All Optical Regeneration	131
5.3.1 Two stage all-optical regenerator.....	133
5.3.2 Self Synchronising All Optical Regeneration	137
5.4 Chapter Summary	139
6. OTDM Networks	141
6.1 Network Concepts	141
6.2 D&I Nodes based on Mach Zehnder Modulators.....	143
6.3 A 40 Gbit/s, 3 Node OTDM Network	146
6.4 OTDM Network Scalability	149
6.5 OTDM Network Connectivity	153
6.6 Chapter Summary	156
7. Conclusions	158
8. Publications and Conference Presentations.....	162
9. References.....	166

Figures

Figure 1-1 Schematic diagram of basic WDM (top) and OTDM (bottom) systems.....	2
Figure 1-2 Simple WDM bus network with channels dropped at intermediate nodes.....	3
Figure 1-3 Multi-layer Model of an advanced telecommunications network, illustrating transport connectivity in both optical and SDH layers.	3
Figure 1-4 Illustration of network optimisation using an optical layer comprising four channel WDM systems based on BT's current network, showing allowed node locations and duct routes (left), and optimised WDM system and switch locations (right), from [3].....	4
Figure 1-5 Evolution of maximum fibre capacity (open triangles) and bit rate distance product (closed circles) for WDM (red), OTDM (blue), electronic (green) multiplexing formats. Active soliton control also shown (crosses).	5
Figure 1-6 Evolution of standard fibre transmission capacity (open triangles) and bit rate distance product (closed circles) for WDM (red), OTDM (blue), electronic (green) multiplexing formats. ...	6
Figure 1-7 Schematic diagram of a typical WDM network node (after MWTN).....	7
Figure 1-8 Theoretical limitation of WDM node cascading [from 12].....	8
Figure 2-1 ; Attenuation of single mode fibre.....	13
Figure 2-2 Illustration of the relationship between group delay, its dispersion and the dispersion in the propagation constant.	15
Figure 2-3 Theoretical phase change due to cross phase modulation as a function of inverse group velocity. Calculation assumes 50 mW mean power for a 10 GHz stream of 10 ps pulses propagating along a 10 km fibre. Effects of dispersive pulse broadening and loss have been neglected for simplicity.....	18
Figure 2-4 Illustration of the limitations on soliton system design. This example; 5 Gbit/s transmission over 10,000 km fibre with 0.5 ps/nm/km dispersion, 5.2 dB noise figure amplifiers with input and output coupling efficiencies of 0.2 and 1.7 dB and a fibre loss coefficient of 0.23 dB/km.	25
Figure 2-5 Soliton design diagram showing capacity limits for 2,000 km transmission with a mean dispersion of 0.15 ps/nm/km and a repeater spacing of 33 km. All other parameters as Figure 2-4.	26
Figure 2-6 Illustration of the relative impact of various jitter sources in a 4000 km 40 Gbit/s transmission system. Parameters as described for the system below, but with a PMD of 0.1 ps/√km.....	27
Figure 2-7 Theoretical performance of an N channel OTDM system as a function of the extinction ratio of the transmitted pulses. Solid lines drawn as a guide to the eye.	31
Figure 2-8 Theoretical variation in receiver sensitivity penalty as a function of demultiplexer extinction ratio for a four channel OTDM system. Solid line drawn as a guide to the eye.....	31
Figure 3-1 Conceptual diagram of OTDM Transmitter, illustrating the functions of pulse generation, parallel data encoding and interleaving. Taken from figure 1.1.	34
Figure 3-2 Illustration of the effect of compression fibre on a chirped gaussian pulse as a function of the of chirp.....	37
Figure 3-3 Schematic diagram of jitter suppressed gain switched DFB laser.....	38
Figure 3-4 Temporal and spectral output of simple gain switched DFB in low and high bias regimes. Histograms for measurement of temporal jitter also shown.....	39
Figure 3-5 Spectra of Gain Switched DFB Pulses with (right) and without (left) reflective self seeding, illustrating pulse to pulse wavelength jitter by the smearing of the modes without jitter suppression.	40
Figure 3-6 Dependence of output spectral and temporal widths of Gain Switched DFB Laser as a function of RF drive power at a fixed dc bias current of 45 mA.....	40
Figure 3-7 Compression of gain switched DFB output using normally dispersive fibre to compensate for linear chirp.	41
Figure 3-8; D.C. output power (circles) and optical frequency (triangles) characteristics of high speed (filled symbols) and high FM efficiency DFB's (open symbols).....	42
Figure 3-9; Compression of pulses from a high FM efficiency DFB gain switched at 2.5 GHz by linear chirp compensation.....	42
Figure 3-10 Schematic diagram of an external cavity semiconductor mode locked laser (EC-MLL).....	43

Figure 3-11; Typical output of mode locked semiconductor external cavity laser, showing autocorrelation (left) and optical spectrum (right).	43
Figure 3-12 ; Schematic diagram of typical erbium fibre mode locked ring laser.	44
Figure 3-13 ; Schematic diagram of optically mode locked erbium fibre ring laser.	46
Figure 3-14 ; Typical output of FM mode locked ring laser when driven at 40 Gbit/s, illustrating a resolution limited rms timing jitter of < 1 ps.	46
Figure 3-15 ; Performance of a 12.6 km FM/AM mode locked fibre ring laser, illustrating variation of jitter (circles) and pulse width (squares) as a function of control signal power. Previous results without a polariser, and subsequent results using a polariser and 1 km cavity length are shown for comparison.	47
Figure 3-16 ; Output spectra (right) and autocorrelation (left) of 1 km FM/AM ring laser mode locked at 10 GHz.	47
Figure 3-17; Typical absorption characteristic of an electro-absorption modulator (after reference 123) showing exponential loss characteristic for reverse bias' between 2 and 4 volts.	49
Figure 3-18; Pulse profiles for an ideal sech ² pulse (dashed line) and as generated by an ideal electro-absorption modulator (solid line) with 10 dB/V absorption characteristic and 10V _{p-p} , 10 GHz drive signal.	50
Figure 3-19; Experimental arrangement for generation and measurement of short pulses from electro absorption modulators.	50
Figure 3-20; Observed pulse widths from sinusoidally driven electro absorption modulators, with (circles) and without (squares) linear chirp compensation for device #1 (10 GHz drive, filled symbols) and device #2 (20 GHz drive, open symbols).	51
Figure 3-21 Optical spectrum and autocorrelation of linearly chirp compensated 10 GHz pulses for a reverse bias of 8.5 V	52
Figure 3-22 Principle of modulated pulse generation using an electroabsorption modulator.	53
Figure 3-23 Schematic diagram of modulated soliton pulse stream formation experiment, omitting electrical amplifiers.	53
Figure 3-24 Output of electro absorption modulator driven by sine wave and data signals simultaneously and independently.	54
Figure 3-25 ; Absorption characteristics of "polarisation insensitive" EA modulator.	55
Figure 3-26 ; Modulated pulse streams from a single electro absorption modulator driven at 10 GHz, showing outputs for single wavelength (left) and two simultaneous wavelengths (right), following -7.6 ps/nm dispersion.	56
Figure 3-27 Schematic diagram of distributed erbium fibre amplifier based pulse compression experiment.	59
Figure 3-28 Adiabatic soliton pulse compression in a 60 km distributed erbium doped fibre amplifier, showing variation in gain, pulse width and time bandwidth product as a function of launched power.	60
Figure 3-29 Output spectra following non-linear pulse compression in a 60 km distributed amplifier for input signal input powers of -9 dBm (left), +3 dBm (centre) and +6.5 dBm (right) with autocorrelations shown as insets.	60
Figure 3-30 Experimental arrangement for the compression of soliton pulses in a dispersion decreasing fibre.	61
Figure 3-31 Output pulse width as a function of mean launch power for DDF compression of soliton pulses at 10 and 20 GHz. The theoretical compression (from Equation 3-51) corresponding to the required launch power for a fundamental soliton also shown for comparison (open circles).	61
Figure 3-32 Autocorrelation (top) and spectra (bottom) following maximum observed soliton compression in a 2 km dispersion decreasing fibre for 10 GHz (left) and 20 GHz (right) pulses.	62
Figure 3-33 General schematic of an OTDM transmitter, showing pulse source, optional pulse compression, source / data synchronisation and modulator array.	63
Figure 3-34 Interface between OTDM terminal and SDH network. Clock synchronisation paths shown in green. Note that any element (ADM, RF Clock, Pulse Source, SSU clock) may be used as a master clock source, with all other elements synchronised to it.	64
Figure 3-35 Amplitude and instantaneous chirp of 8 ps pulses modulated at 10 Gbit/s using an 8 GHz Mach Zehnder modulator.	65
Figure 3-36 Schematic diagram of full OTDM multiplexer (MUX-1).	66

Figure 3-37 Theoretical RF spectrum for a 40 GHz OTDM data signal, showing residual 10 GHz components from slightly imperfect multiplexing (left), along with experimental 40 Gbit/s autocorrelation showing high uniformity of correctly interleaved data(right).	67
Figure 3-38 Schematic diagram of four path passive OTDM multiplexer (MUX-2)	67
Figure 3-39 Schematic diagram of multistage partial OTDM multiplexer (MUX-3)	68
Figure 3-40 ; Schematic diagram of beat frequency conversion source.	69
Figure 3-41; Typical beat frequency seed spectrum using Lithium Niobate Mach Zehnder modulator driven at 17.5 GHz and biased at the transmission null	70
Figure 3-42 ; Typical spectral output of 40 GHz beat frequency to soliton conversion source. Autocorrelation shown as inset	71
Figure 3-43 ; Output of 40 GHz beat frequency source (upper trace) and RF drive signal (lower trace) applied to modulator, displayed on a digital sampling scope	71
Figure 3-44 ; Jitter measurement of beat frequency source, showing the microwave source (centre) and soliton pulse trains with (left) and without (right) SBS suppression.	72
Figure 3-45 ; Schematic diagram of beat frequency source and source evaluation experiments (modulation and transmission)	73
Figure 3-46 ; Schematic diagram of NOLM based all optical modulator.	74
Figure 3-47 ; Performance of 40 Gbit/s NOLM based all optical modulator with zero walk through, showing input (solid line) transmitted (long dashes) and reflected (short dashes) pulse shapes and the effect of fibre length (normalised to π peak phase shift)	75
Figure 3-48 ; Variation of through signal attenuation (red), reflected power (light blue) and adjacent channel crosstalk (dark blue) of NOLM based 40 Gbit/s optical modulator as a function of control pulse width	76
Figure 3-49 ; Anticipated Performance of 40 Gbit/s NOLM modulator as a function of walk off rate between 5 ps signal and 6.4 ps control pulses, with a fixed fibre length and a signal power adjusted for a peak phase shift of π	76
Figure 3-50; Output eye diagram (right) and spectra (left) of beat frequency source modulated at 40 Gbit/s using a NOLM modulator	77
Figure 3-51; Schematic diagram of Kerr gate	77
Figure 3-52 ; Modulated output of beat frequency source using Kerr gate. Showing eye diagram (left) and autocorrelation (right). The upper trace on autocorrelation represents modulation by all ones and the lower trace by a PRBS data sequence	78
Figure 3-53; BER characteristics for 40 Gbit/s modulation of a beat frequency source, showing 1545 nm back to back at 10 Gbit/s (filled circles) and 40 Gbit/s (filled squares) along with all four channels of the modulated beat frequency source at 1557 nm. Signal powers are measured at the input to the photodiode	78
Figure 4-1 Options for the location of an OTDM clock recovery circuits	80
Figure 4-2 Schematic diagram of electronic clock recovery circuits	81
Figure 4-3 : Erbium fibre ring laser clock recovery	83
Figure 4-4 Output of 1 km clock recovery circuit, driven by 10 Gbit/s (left) and 40 Gbit/s (right) data signals, showing spectra (top) and autocorrelations (bottom)	84
Figure 4-5 Variation of jitter (triangles) and spectral mode contrast (circles) for 40 Gbit/s clock recovery in a 12 km mode locked ring laser with data (filled) and clock (open) inputs. Solid lines represent parabolic data fits to guide the eye	84
Figure 4-6; Jitter measurement of 12.6 km fibre ring laser 40 GHz clock recovery	85
Figure 4-7 RF spectra of 40 GHz clock recovery, showing lock condition (left) and the downconverted 40 GHz harmonic (right)	86
Figure 4-8 Switching windows of Mach Zehnder modulators driven by a 10 GHz signals;	89
Figure 4-9 Output of cascaded Mach Zehnder modulator demultiplexer for an 8 ps input pulse train at 40 GHz	90
Figure 4-10 Signal to crosstalk ratio of cascaded Mach Zehnder modulator demultiplexer as a function of input 40 Gbit/s pulse width.	90
Figure 4-11 Illustration of the operation and performance of Mach Zehnder modulator based demultiplexer driven by a pulsed electrical drive (final diagram assumes 8 ps pulses at 40 Gbit/s)	91
Figure 4-12 Schematic diagram of proposed 160 Gbit/s demultiplexer	92
Figure 4-13 Signal to crosstalk ratio of electro-absorption modulator demultiplexer with 6.3 ps 40 Gbit/s input signal, 24 dB extinction ratio, 11.8 dB/V absorption slope and a 10 V peak to peak 10 GHz drive signal.	93

Figure 4-14 Schematic diagram of electroabsorption modulator, 80 Gbit/s data source.....	94
Figure 4-15 Schematic diagram of polarisation insensitive electroabsorption modulator based 80 Gbit/s demultiplexer.....	94
Figure 4-16 80 Gbit/s OTDM system employing four electroabsorption modulators. Showing autocorrelation (top left) and eye diagram (top right) of 80 Gbit/s data signal, and BER measurements (bottom left) of demultiplexed signal (bottom right).....	96
Figure 4-17 Schematic diagram showing simultaneous switching and detection of OTDM data channels using an electroabsorption modulator.....	96
Figure 4-18 Electrical extraction of a weak data signal from a mixture of clock and data.....	96
Figure 5-1 Operating principle of mid span spectral inversion, showing pulse broadening in the first fibre link, and restoration in the second, symmetric fibre link.....	99
Figure 5-2 Schematic diagram of 202 km transmission system employing MSSSI.....	100
Figure 5-3 Optical spectrum of 40 Gbit/s MSSSI experiment. LEFT - Output of SLA showing input signal, pump, and phase conjugate signal. RIGHT - Output of final filter with and without input data signal, illustrating the achieved signal to noise ratio.....	100
Figure 5-4 Peak signal power of phase conjugate signal as a function of signal/pump detuning.....	101
Figure 5-5 BER performance of MSSSI without fibre as a function of signal-pump detuning.....	102
Figure 5-6 Overall performance of 202 km transmission of a 40 Gbit/s OTDM signal over standard fibre using MSSSI.....	103
Figure 5-7 Schematic diagram of OTDM recirculating loop.....	105
Figure 5-8 Spectral evolution of pulses during 40 Gbit/s soliton transmission experiment with a centre wavelength of 1549.2 nm.....	107
Figure 5-9 Eye Diagram after 2,200 km and evolution of 40 GHz RF component with distance (right) for 40 Gbit/s soliton transmission at 1549.2 nm.....	107
Figure 5-10 Theoretical and experimental performance of 40 Gbit/s transmission system.....	108
Figure 5-11 Illustration of the effect of guiding filter (exaggerated) showing the spectral profile of a jittered pulse (dotted), a gaussian filter (solid) and the resultant output pulse (dashed).....	109
Figure 5-12 Typical variation in error rate for a 40 Gbit/s, 3000 km transmission system as a function of guiding filter width using parameters from experimental demonstration above.....	110
Figure 5-13 Schematic diagram of a generic active soliton control module.....	112
Figure 5-14 Theoretical error ratio performance as a function of transmission distance for the 20 Gbit/s transmission experiment described below.....	115
Figure 5-15 Transmission of 20 Gbit/s soliton signal over 125,000 km showing path averaged optical spectrum for pulse widths of 5.65 and 8 ps (right), the received 20 Gbit/s eye diagram (top left) and the demultiplexed and bandlimited eye diagram (bottom right).....	115
Figure 5-16 Spectral evolution of 20 Gbit/s data under active retiming soliton control.....	116
Figure 5-17 Error ratio performance of 40 Gbit/s transmission in the absence of soliton control (circles), with control elements in place (squares) and with soliton control applied (triangles).....	117
Figure 5-18 Evolution of 40 GHz RF spectral component for 40 Gbit/s soliton control (horizontal scale 5 ms/div, vertical scale 5 dB/div).....	118
Figure 5-19 Spectral evolution of 40 Gbit/s soliton data under transmission control.....	119
Figure 5-20 20 GHz RF component (bottom) and eye diagrams (top) for 10 Gbit/s soliton transmission over 7,500 km, with (right) and without (left) soliton shepherding.....	120
Figure 5-21 Eye diagram of 20 Gbit/s soliton data transmission over 5,000 km with soliton shepherding (top), along with the corresponding demultiplexed and bandlimited 10 Gbit/s base rate signal (bottom).....	121
Figure 5-22 Schematic diagram of distributed erbium fibre link with low signal power excursion used for 40 Gbit/s transmission experiments.....	122
Figure 5-23 Gain variation along a 68 km distributed erbium doped fibre amplifier directly observed using an OTDR, standard fibre also shown for reference.....	123
Figure 5-24 Autocorrelation trace before and after 68 km transmission at 40 Gbit/s.....	124
Figure 5-25 BER performance of a 68 km distributed amplifier at 10 and 40 Gbit/s (left) and received 40 Gbit/s eye diagram (right).....	125
Figure 5-26 Transmission line section of recirculating loop used for dispersion decreasing fibre based transmission experiments.....	126
Figure 5-27 Spectral evolution of 6.5 ps pulses along a transmission line comprising concatenated 38 km DDF's.....	127

Figure 5-28 Spectral evolution of pulses along a transmission line comprising concatenated 18 km DDF's.	127
Figure 5-29 Theoretical and experimental performance of 18 km DDF system for 11ps pulses. Theoretical performance calculated jitter from appropriate mean dispersion values.....	128
Figure 5-30 Spectral evolution of pulses along a transmission line comprising concatenated 18 km DDF's for a signal injected ≈ 5 nm above the design wavelength.....	129
Figure 5-31 Spectral evolution of 4.7 ps pulses through a 20 km DDF (1.5 dB / contour).....	129
Figure 5-32 Theoretical and experimental error ratio performance of 20 km low dispersion DDF using 4.7 ps pulses.	130
Figure 5-33 Schematic diagram of all optical regenerator.....	131
Figure 5-34 Schematic diagram of NPR based all optical regenerator.	133
Figure 5-35 Theoretical switching performance of Kerr gate used in 10 Gbit/s all optical regenerator with input signal having 5% amplitude noise and 5 ps peak to peak timing jitter .Showing the input signal with noise and jitter (left), the resultant switching window (centre) and anticipated output pulse train following modulation of an ideal clock (right). Other parameters detailed in column 1 of Table 16.....	133
Figure 5-36 Error rate performance following 10 Gbit/s all optical regeneration (circles) and back to back (crosses).....	134
Figure 5-37 Schematic diagram of the experimental demonstration of 40 Gbit/s all optical regeneration.	135
Figure 5-38 Output of the clock recovery section of a 40 Gbit/s all optical regenerator.....	135
Figure 5-39 Eye diagram and autocorrelation of 40 Gbit/s signal following all-optical regeneration. .	136
Figure 5-40 Error rate performance of a demultiplexed 10 Gbit/s channel following 40 Gbit/s all optical regeneration.....	136
Figure 5-41 Schematic diagram of 40 Gbit/s self synchronising all optical regenerator.....	137
Figure 5-42 Autocorrelations of recovered clock (top left) and regenerated signal (top right) from self synchronising 40 Gbit/s all optical regenerator, along with eye diagram of regenerated data (bottom).	138
Figure 5-43 Illustration of the anticipated modulator switching window (red) and recovered clock pulse (green) along with resultant theoretical output pulse train for 1 ps peak to peak jitter (right) in a 40 Gbit/s self synchronising all optical regenerator.	139
Figure 6-1 Illustration of a simple OTDM drop and insert network.....	141
Figure 6-2 Schematic diagram of an OTDM time slot interchange constructed from a pair of add drop multiplexers	142
Figure 6-3: Schematic Diagram of D&I Node with Sine Wave Driven 2 x 2 Modulators	143
Figure 6-4 : Signal to crosstalk ratio (circles) and incoherent interference (squares) of a the inserted channel in a 4 x 10 Gbit/s, 2x2 Mach Zehnder switch based, D&I node, following demultiplexing in an identical node.	144
Figure 6-5 Schematic diagram of D&I node based on broadband modulators.	145
Figure 6-6 Signal to crosstalk ratio (circles) and incoherent interference (squares) of a 4 x 10 Gbit/s, Broadband Mach Zehnder switch based D&I node.	146
Figure 6-7 Experimental demonstration of 40 Gbit/s optical drop and insert using electro-optic modulators.	147
Figure 6-8 RF signal processing to derive pulsed signal from 10 GHz recovered clock	147
Figure 6-9 Eye diagrams of dropped (left) and through (right) signals at the intermediate node, along with the electrical switching signals (upper traces).	148
Figure 6-10 Eye diagrams of received signals at third node, showing the input comprising three channels from node 1 and one channel from node 2 (top) and a demultiplexed eye diagram of a channel from node 1 (middle) and the inserted channel from node 2 (bottom).	148
Figure 6-11 Error ratio performance of signals demultiplexed at node three, originating from node 1 (circles) and node 2 (squares).	149
Figure 6-12 Schematic diagram of 20 Gbit/s D&I node.....	150
Figure 6-13 Eye diagram of input (upper) and output (lower) of the 244th D&I node with the same channel dropped at each node, measured using 15 and 32 GHz detectors respectively.....	151
Figure 6-14 Evolution of the pulse peak power as a function of transmission distance for compressed (crosses) and uncompressed (circles) pulses.	152
Figure 6-15 Illustration of the soliton control functionality of a broadband modulator based D&I node showing representative soliton train (yellow) and the modulator switching window (blue).....	153
Figure 6-16 Schematic diagram of a branched OTDM network.....	153

Figure 6-17 Schematic diagram of branched network synchronisation experiment of Widdowson.....	154
Figure 6-18 Schematic diagram of a bi-directional OTDM D&I node, with local traffic terminating on SDH terminals.....	155
Figure 6-19 Schematic diagram of a bi-directional OTDM D&I node, with local traffic routed via a single SDH ADM.....	156
Figure 7-1 Multi Layer model of an optical network employing WDM for rich interconnectivity on a regional level, and OTDM for a global scale backbone network.....	160

Lists of Symbols and Abbreviations

Symbol	Meaning	Units
α_{dB}	Device Absorption Coefficient	dB
α_m	Modulator Chirp Parameter	
α	Fibre Loss	m^{-1}
β	Propagation Constant	m^{-1}
β_0	Propagation Constant at ω_0	m^{-1}
β_x, β_y	Geometric Terms of Propagation Constant	m^{-1}
$\delta\nu_n$	nth Resonance Frequency	Hz
$\delta\tau$	Error in Arrival Time	s
$\delta\omega$	Carrier Frequency Chirp	rads
Δ	Excess Signal Strength	
$\Delta\beta$	Propagation Constant Difference	m^{-1}
$\Delta\tau$	Differential Group Delay	s
$\Delta\tau_{FW}$	Change in Pulse Width	s
$\Delta\omega$	Pulse Spectral Width	$rad\ s^{-1}$
$\Delta\omega_{TL}$	Spectral Width of Transform Limited Pulse	$rad\ s^{-1}$
ΔG	Guiding Filter Excess Gain	
$\Delta G'$	Amplitude Modulator Excess Gain	
ΔL_{mux}	Multiplexer Path Length Difference	m
Δm	Effective Modulation Depth	
ΔP	Change in Power	W
$\Delta P_{(dB)}$	Power Penalty	dB
Δt	Arrival Time Difference (jitter)	s
Δf_{opt}	Optical Filter Bandwidth	Hz
Δf_{elect}	Electrical Filter Bandwidth	Hz
$\chi^{(n)}$	Susceptibility	
ϵ	Dielectric Constant	
ϕ	Instantaneous Phase	rad
ϕ_{SPM}	Phase Shift Induced by Self Phase Modulation	rad
ϕ_{XPM}	Phase Shift Induced by Cross Phase Modulation	rad
γ	Coefficient of Non-linearity	$W^{-1}\ m^{-1}$
λ	Wavelength	m
λ_0	Centre Wavelength	m
λ_{3dB}	Equivalent Gaussian Guiding Filter Width	m
ν	Frequency	Hz
τ	Pulse Width Coefficient	s
τ_{FW}	FWHM Pulse Width	s
τ_{in}	Input Pulse Width	s
τ_{out}	Output Pulse Width	s
τ_g	Group Delay	s
ω	Angular Frequency	$rad\ s^{-1}$
ω_0	Angular Frequency of Carrier	$rad\ s^{-1}$
A	Pulse Amplitude	
A_{eff}	Fibre Effective Area	m^2
c	Speed of Light in a Vacuum	$m\ s^{-2}$
C	Chirp Parameter of Gaussian Pulse	
c_{in}	Input Coupling Loss	
c_{out}	Output Coupling Loss	
D	Dispersion Coefficient	$s\ m^{-2}$
D_{in}	Input Dispersion Coefficient	$s\ m^{-2}$
D_{out}	Output Dispersion Coefficient	$s\ m^{-2}$
D_p	Polarisation Mode Dispersion	$s\ m^{-1/2}$
E	Electric Field Vector	V
f	Frequency	Hz
f_c	RF carrier frequency	Hz

f_{GH}	Reduction in Mean Squared Timing Jitter	
f_m	Effective Modulation Frequency	Hz
g	Gain Coefficient	m^{-1}
G	Gain	
G_{int}	Intrinsic Gain	
G_i	Gain of Amplifier Associated With i th Link	
h	Planks Constant	
I	Optical Intensity	$W m^{-2}$
k	Absorption Characteristic Gradient	dB/V
L	Fibre Length	m
L_b	Beat Length	m
L_{coll}	Soliton Collision Length	m
L_D	Dispersion Length	m
L_i	Lumped Loss of i th Transmission Link	
L_{rep}	Repeater (Amplifier) Spacing	m
L_{mux}	Multiplexer Path Length	m
L_{sol}	Soliton Period	m
L_{sys}	System Length	m
n	Refractive Index	
N	Number of Amplifiers / Channels / Ports	
n_0	Linear Part of Refractive Index	
n_2	Non-linear Refractive Index (Kerr coefficient)	$m^2 W^{-1}$
NF	Noise Figure	dB
n_{sp}	Spontaneous Emission Coefficient	
\underline{P}	Polarisation Vector	
P	Mean Power	W
P_{sig}	Mean Power of Signal	W
P_{peak}	Peak Power	W
P_{spc}	Mean Power of Spontaneous Emission	W
P_{sol}	Soliton Peak Power	W
P_k	Mean Power of k 'th Channel	W
$P_k(t)$	Time Dependant Power of k 'th Channel	$W s^{-1}$
P_{out}	Output Power	W
P_{in}	Input Power	W
P_N	RF Noise Power	W
P_C	RF Power of Spectral Harmonic	W
SNR	Signal to Noise Ratio	
SNR_{elect}	Electrical Signal to Noise Ratio	
SNR_k	Signal to Noise Ratio of k 'th Channel	
SXR	Signal to Crosstalk Ratio	
t	Time	s
T	Bit Period or Pulse Spacing	s
u	Optical Pulse Envelope Function	
V	Applied Voltage	V
V_0	Maximum Reverse Bias for Minimum Absorption	V
V_1	Reverse Bias for Maximum Absorption	V
V_{pp}	Peak to Peak Drive Amplitude	
v_g	Group Velocity	$m s^{-1}$
v_p	Phase Velocity	$m s^{-1}$
V_π	Required Switching Voltage of Modulator	V
x	Effective Guiding Filter Strength	
X	Extinction Ratio	
XR	Maximum Extinction Ratio	dB
xr	Extinction Ratio	
z	Co-ordinate of Axial Distance	m
z_{opt}	Optimum Length for Linear Compression	m

Abbreviations.

ACTS	A European Community Funded Research Programme
ADM	Add Drop Multiplexer
AM	Amplitude Modulation
ARPA	A US Government Funded Research Programme
ATM	Asynchronous Transfer Mode
BER	Bit Error Ratio
bit/s	bits per second
cw	Continuos Wave
DCF	Dispersion Compensating Fibre
DDF	Dispersion Decreasing Fibre
DEDFA	Distributed Erbium Doped Fibre Amplifier
DFB	Distributed Feedback Laser
DS	Dispersion Shifted
DSF	Dispersion Shifted Fibre
D&I	Drop and Insert
EAM	Electroabsorption Modulator
EDFA	Erbium Doped Fibre Amplifier
EC-MLL	External Cavity Mode Locked Laser
eTDM	Electrical time division multiplexing
FM	Frequency Modulation
FWHM	Full Width at Half Maximum
FWM	Four Wave Mixing
ISI	Inter Symbol Interference
LCDDF	Loss Compensating Dispersion Decreasing Fibre
LTE	Line Terminating Equipment
MI	Modulation Instability
MWTN	Multi Wavelength Transport Network
MQW	Multiple Quantum Well
MSR	Mark to Space Ratio
MSSI	Mid Span Spectral Inversion
MZ	Mach Zehnder
NF	Noise Figure
NOLM	Non-linear Optical Loop Mirror
NPR	Non-linear Polarisation Rotation

NRZ	Non Return to Zero
OPC	Optical Phase Conjugation
OTDM	Optical time division multiplexing
OTDR	Optical Time Domain Reflectometer
PALM	Parametric Loop Mirror
PLL	Phase Locked Loop
PM	Polarisation Maintaining
PMD	Polarisation Mode Dispersion
PRBS	Pseudo Random Bit Sequence
RACE	A European Community Funded Research Programme
RF	Radio Frequency
rms	Root Mean Squared
RZ	Return to Zero
SDH	Synchronous Digital Hierarchy
SLA	Semiconductor Laser Amplifier
SMCR	Spectral Mode Contrast Ratio
SNR	Signal to Noise Ratio
SONET	Synchronous Optical Networks
SPM	Self Phase Modulation
SXR	Signal to Crosstalk Ratio
TDM	Time division multiplexing (see eTDM)
TE	Transverse Electrical Mode
TM	Transverse Magnetic Mode
TOAD	Terahertz Optical Asymmetric Demultiplexer
VCO	Voltage Controlled Oscillator
WDM	Wavelength division multiplexing
XPM	Cross Phase Modulation

1. Introduction

1.1 Optical Communications^{1,3,5,6,9,21,28}

It is well known that the telecommunications industry has experienced a remarkably constant increase in the demand for capacity, with little evidence of saturation. This increase has been driven by two factors, enhancements to the available telecommunications services, from telegraphy, through voice to data transfer (including internet and video conferencing) and by an increased user base for each service. Fortunately continuous technological innovations have enabled the capacity of communications networks to keep pace with this demand. These innovations include coaxial cable, digital transmission, optical fibre, single mode optical fibre and optical amplification, each new technology enhancing a particular aspect of state of the art systems. Along the way, several promising technological advances were implemented, and later abandoned. These solutions include graded index optical fibre and coherent transmission systems. Today's state of the art transmission networks operate with electronic switching systems, interconnected by optical transmission lines, where fibre loss is often overcome by optical amplification, up to a maximum capacity of 10 Gbit/s. Attention is now focused world-wide on the application and deployment of optical multiplexing systems to further increase the available transmission capacity, towards the maximum transmission capacity of optical fibre. Indeed towards the end of this study, widespread deployment of commercial wavelength division multiplexed (WDM) systems within North America has commenced, with up to sixteen 2.5 Gbit/s electronic switch pairs interconnected via a single fibre pair using a product supplied by Ciena Inc. However, despite continual technological revolution in transmission technologies, the basic approach to signal switching has remained more or less constant since the onset of digital switches. That is, whilst the actual signal structure has been continuously defined, redefined and optimised, the core of the switch remains a large array of digital electronic switches. These switches are designed to route a large number of low capacity circuits (typically in the range of 2 - 155 Mbit/s).

1.2 General Optical Multiplexing Concepts

Two main approaches have been taken to enhance the capacity (or data throughput) of an optical transmission system¹. For a wavelength division multiplexing (WDM) system many signals of a conventional format are simultaneously launched into a single optical fibre, and distinguished by virtue of a unique, predetermined, wavelength. Optical time division multiplexing (OTDM) *recodes* each of the data signals into a format comprising short optical pulses, which may be interleaved in time. The appropriate time slot is then used to identify each data signal. These concepts are illustrated in Figure 1-1 below. In the case of WDM, each incoming data sequence is used to modulate the output of a wavelength selected DFB. The signals are combined passively and routed along a single fibre. At the far terminal, wavelength selective

much lower capacity is required to be "dropped" and the majority of the traffic simply bypasses the intermediate nodes. This network may be further enhanced by re-using the dropped wavelengths to transmit signals from the intermediate nodes, forming a simple "drop and insert" network^{4,5,6}.

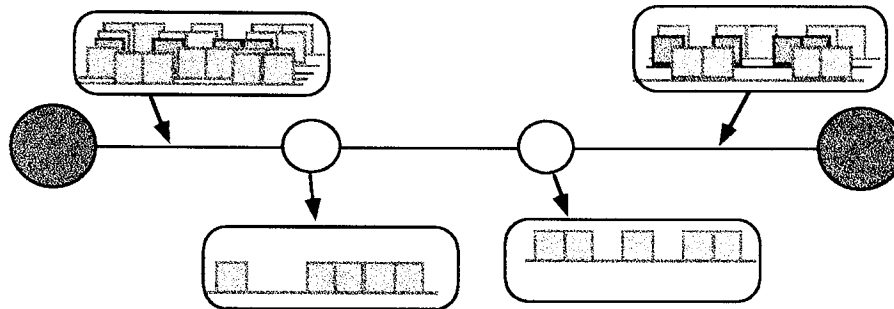


Figure 1-2 Simple WDM bus network with channels dropped at intermediate nodes.

To understand the traffic flow through such a network, it is necessary to consider a multi-layer model for the network, as shown, for example, in Figure 1-3. In this figure different network technologies are considered as independent, but interconnected networks. Each technology is represented by a unique layer and offers functionality (including transmission and switching) to other layers. Traffic is thus routed from customer premises through a concentrator (for example, an ATM router) from whence it is passed into the SDH transport layer. Complex connectivity exists within this layer, with SDH switches at various nodes interconnected via established regenerative links. However, where a large degree of connectivity is required along a particular route, the physical transport should occur in an "optical layer" using either WDM or OTDM technology. In this case, traffic may be further concentrated within the SDH layer itself, using the existing transport infrastructure, before long haul transmission within the optical layer. The scale of this optical layer is of course minimised by the use of drop and insert, such that separate optically multiplexed systems are not required to interconnect several nodes along a single fibre route. Similarly, traffic flowing through the optical layer may, if appropriate, be reconfigured by utilising the switching functionality of the SDH or ATM layers.

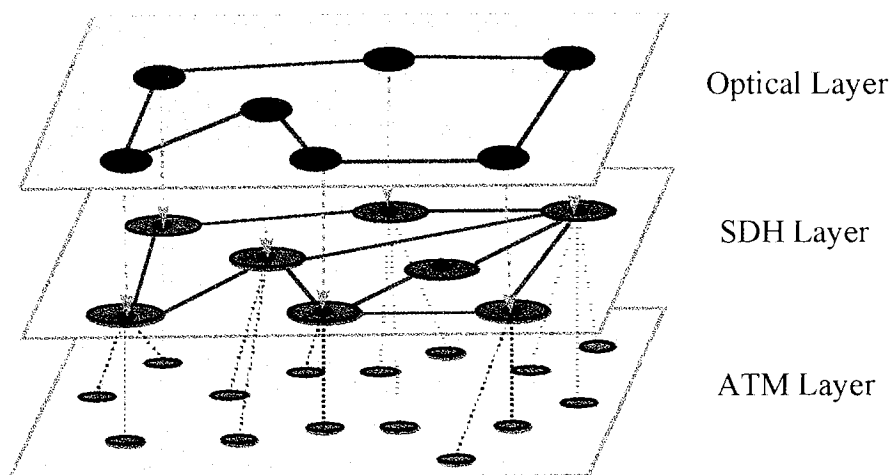


Figure 1-3 Multi-layer Model of an advanced telecommunications network, illustrating transport connectivity in both optical and SDH layers.

Using Figure 1-2 and Figure 1-3, the traffic flow may be envisioned for all required traffic patterns, with signals flowing between and across both physical transport layers. Note that in this system, individual channels are routed through the optical layer and dynamic switching (reconfiguration) is only carried out in the SDH layer. It is anticipated that this basic approach will allow several significant benefits to be readily exploited, not least the immediate cost savings pertaining to reduced line plant. However, with simple modifications to the optical layer, allowing a small degree of dynamic reconfiguration, additional benefits of network flexibility and enhanced reliability may be obtained.

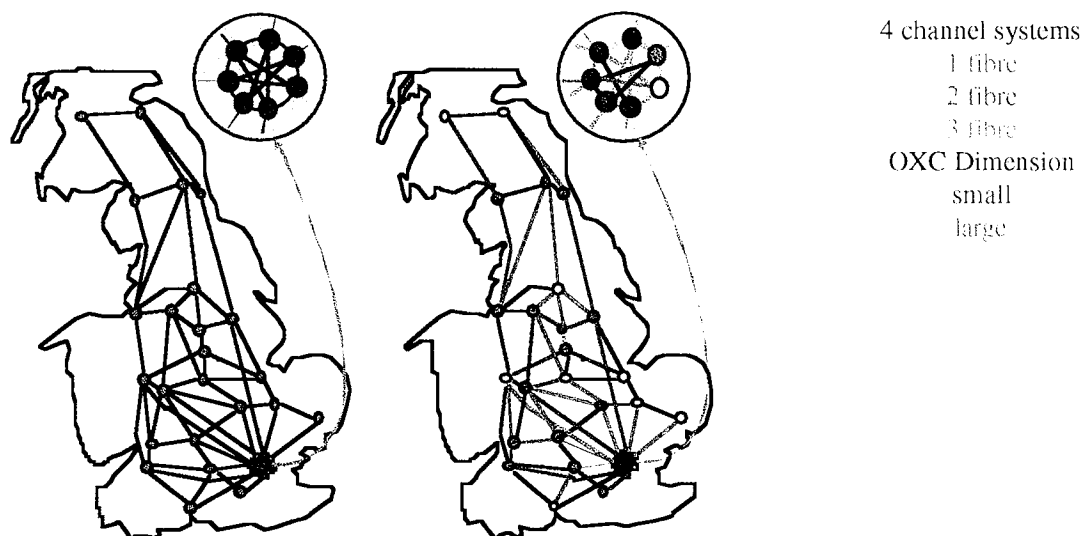


Figure 1-4 Illustration of network optimisation using an optical layer comprising four channel WDM systems based on BT's current network, showing allowed node locations and duct routes (left), and optimised WDM system and switch locations (right), from [3].

Recent detailed studies by Ewart Lowe and Paul Botham³ have demonstrated the real cost savings anticipated for a WDM network using realistic network constraints and traffic patterns. This study modelled optical layer comprising optical amplifiers, 16 x 16 optical switches for reconfigurability, 4 channel WDM systems and an SDH layer comprising 2.5 Gbit/s SDH line systems and cross connects. This model is based on uniform growth of statistical traffic flows from current Mega Stream Private Circuits, in contrast to previous studies based on uniform traffic densities. It was shown that for a meagre 5 fold increase in traffic levels, a 30 % cost saving results from the implementation of the optical layer, despite the additional overhead of optical switch provision. A 50 % cost saving is anticipated for a 20 fold increase in traffic levels. Increased savings are anticipated for higher levels of optical multiplexing (eg 16 wavelength WDM systems).

Clearly care must be taken in the interpretation and generalisation of these results. They firmly establish however, the advantages of the coarse routing concept, which allows SDH switches to be bypassed for sufficiently high traffic densities. This general principle is clearly technology independent, and would be obtained for WDM, OTDM or even electrical TDM implementations. The specific cost savings would be determined

by the actual level of course multiplexing, the degree of reconfigurability implemented, and the specific terminal costs.

1.3 World Status

Optical multiplexing experiments began shortly after the development of optical fibres¹⁸. WDM in particular was seen as a useful technique to increase the transmission capacity of a highly dispersive multi-mode fibre⁷. Efforts in this direction resulted in transmission capacities in excess of 10 Gbit/s as early as 1985⁸. However, during the same period the developments of graded index and single mode fibres allowed a steady growth in the fibre capacity for a single optical channel⁹. In addition to allowing transoceanic systems to be constructed without the need for submerged high speed electronics, EDFA's were used to overcome losses within system terminals. This allowed the high losses associated with optical multiplexing and demultiplexing technologies to be overcome²⁸. This has allowed practical realisation of both OTDM and WDM technologies as realistic alternatives to ever increasing electronic terminal capacities.

1.3.1 Point to point systems

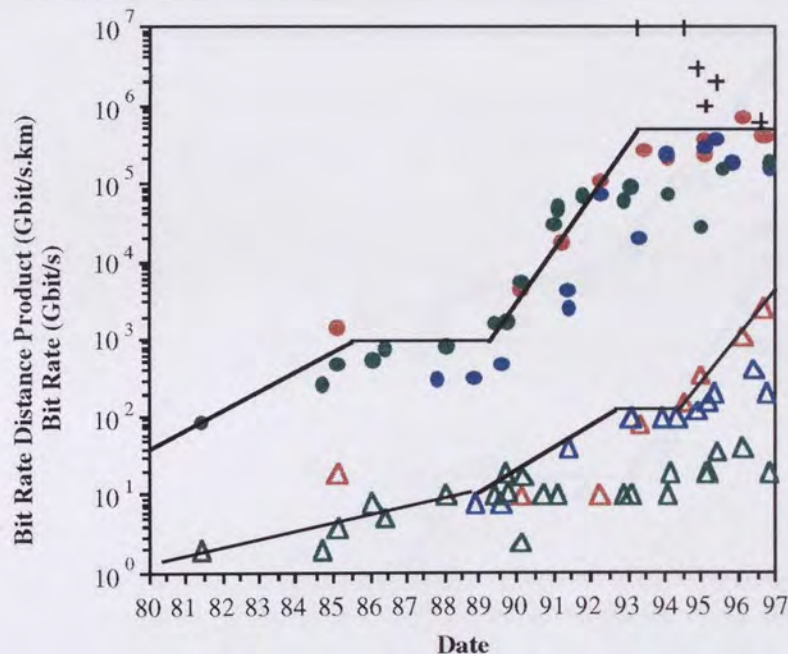


Figure 1-5 Evolution of maximum fibre capacity (open triangles) and bit rate distance product (closed circles) for WDM (red), OTDM (blue), electronic (green) multiplexing formats. Active soliton control also shown (crosses).

The overall historical development of point to point transmission systems is summarised in Figure 1-5, where a selection of reported laboratory transmission experiments is used to illustrate the maximum achieved system capacity. The data is presented both in terms of transmitted bit rate (capacity), and in terms of the maximum bit rate distance product for all three multiplexing technologies. For brevity, specific references are not cited. Two distinct plateaux are evident. The first corresponds to achievement of loss limited transmission in the absence of optical amplifiers in the

1980's. The second plateau, attained in the mid 90's, is restricted by a balance between optical signal to noise ratio and fibre non-linearities. This gives a maximum bit rate distance product of the order 1 Tbit/s.Mm. We may readily conclude that this data fails to indicate any *significant* performance differentiation between the two optical multiplexing technologies. However, it has become apparent during the course of this thesis that single channel systems based on electronic multiplexing are no longer competitive.

The second conclusion that may be drawn from this figure is that marked improvement in bit rate distance product will rely on a further revolution in optical communications technology (following single mode fibre and optical amplifiers). Results of active soliton control (shown in Figure 1-5 for comparison) suggests that the most likely evolution path would be the development of fundamentally digital transmission techniques. Bit rate distance products in excess of 10 Tbit/s.Mm are readily achieved in soliton control experiments²⁸¹, and compare favourably to demonstrations of electronically regenerated systems (≈ 4 Tbit/s.Mm)²⁸¹. Indeed the particle like nature of these soliton systems suggests that the required move towards a fundamentally digital optical transmission format that will yield the required rewards of multi Terabit transmission over transoceanic distances has already begun.

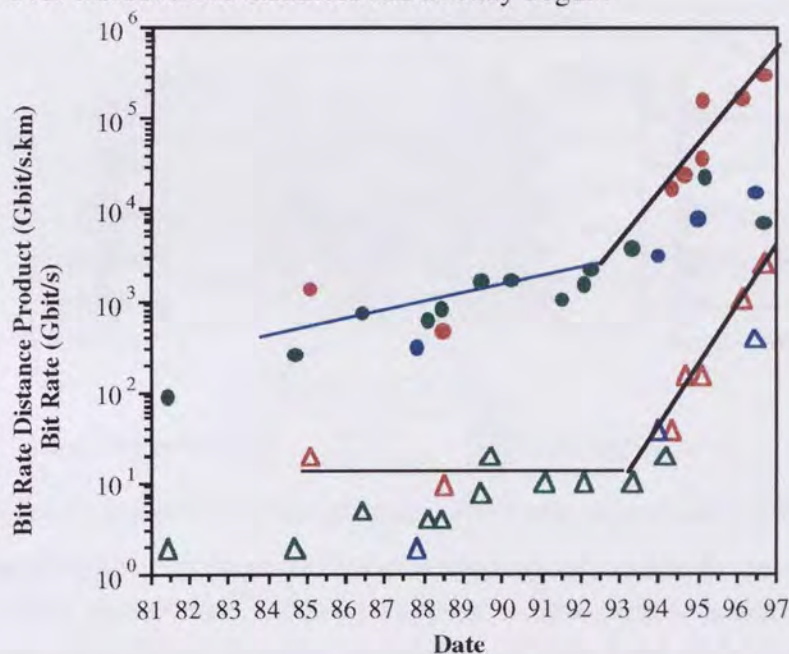


Figure 1-6 Evolution of standard fibre transmission capacity (open triangles) and bit rate distance product (closed circles) for WDM (red), OTDM (blue), electronic (green) multiplexing formats.

A more important facet of recent research in optical communications is the exploitation of existing fibre plant. A substantial investment in standard single mode fibre has already been made by the majority of telecommunications operators world-wide. Any advanced optical technology would consequently be unlikely to be rapidly exploited outside the submarine environment if new cable build became a prerequisite. Figure 1-6 illustrates the same evolution discussed above, but restricted to standard fibre systems. From this figure we observe a 2-3 year delay in the exploitation of optical amplifiers, and a steady exponential growth has been observed throughout the course of this thesis.

The transmission of high capacity OTDM systems on standard fibre is discussed in chapter 4.

1.3.2 Optical Networking

With optical multiplexing now firmly established as the natural choice for increased transmission capacity, much attention has been focused on optical networking, as described in section 1.2. A wealth of architectural detail has been produced, purporting the benefits of various configurations of optical nodes. Large co-ordinated programs within the ACTS and ARPA frameworks are now exploring the networking technologies required to allow flexibility, survivability and reconfigurability of future optical networks⁶. In the case of a WDM network node, the majority of proposals are based on large NxN space switches. A particular example from the RACE project MWTN is shown in Figure 1-7, where each fibre is terminated with an optical amplifier, before the entire multiplex is separated into individual spatial channels¹⁰. This is followed by a loss equalised space switch, allowing full reconfiguration prior to a re-multiplexing of the channels and onward transmission via a second bank of optical amplifiers.

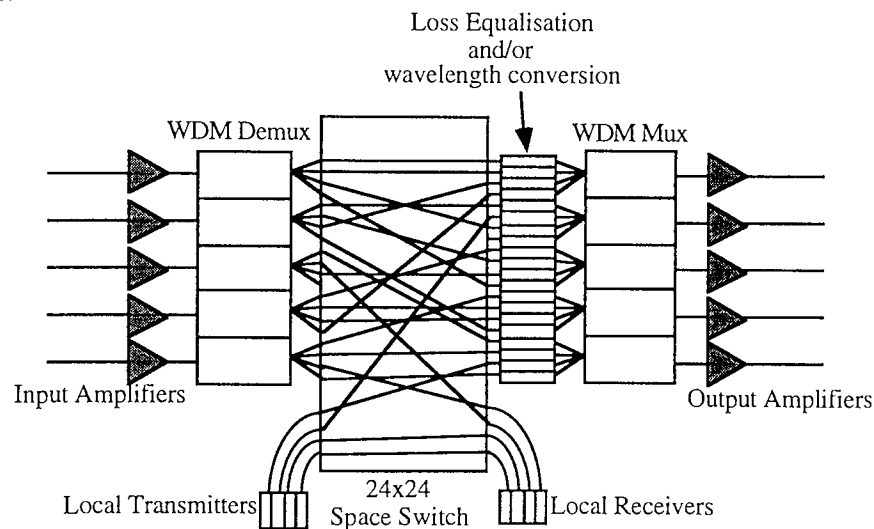


Figure 1-7 Schematic diagram of a typical WDM network node (after MWTN).

This "full demultiplex - space switch" technique may of course be applied to OTDM systems, or even hybrid WDM/OTDM systems¹¹. The switch architecture is prone however to crosstalk due to imperfect switching and large intra node losses reduce the overall network scalability considerably. The network scalability restrictions due to signal to noise ratio degradations for a 3 fibre, 4 wavelength full cross connect system have been theoretically demonstrated by Zhou and O'Mahony, and are summarised in Figure 1-8¹².

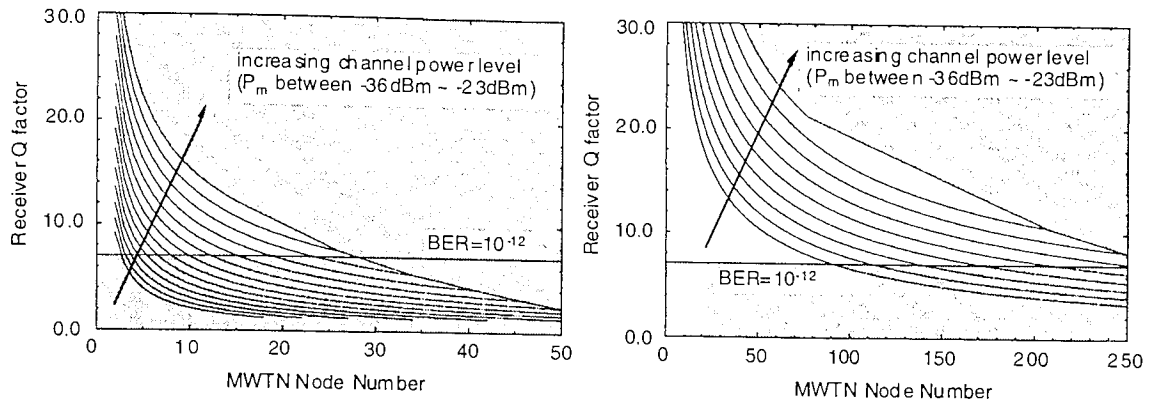


Figure 1-8 Theoretical limitation of WDM node cascadability [from 12].

The theoretical predictions of Figure 1-8 have been recently verified (towards the end of this study) in 8 and 10 node WDM network demonstrations^{13,14}, and overall switch throughputs of 320 Gbit/s have been demonstrated¹⁵. Simultaneously, large scale WDM network demonstrations have been carried out utilising opto-electronic regeneration at each node¹⁶. Unfortunately, this approach does appear to remove the fundamental benefit of optical networking, being the avoidance of costly opto-electronic interfaces. Indeed such systems may easily replace the optical space switch with the more mature electronic equivalent, reverting the role of optical multiplexing to point to point linkages. A considerable simplification is of course achieved for non reconfigurable drop and insert type architectures, based on, for example fibre grating technology¹⁷. Such fixed D&I networks are now approaching commercial availability.

1.4 Overview of Thesis

As we have seen, optical multiplexing techniques, both in the time domain (OTDM) and the wavelength domain (WDM) offer many advantages to future telecommunications networks designers. In addition to the obvious increase in point to point capacity^{18,19}, optical multiplexing provides many additional interesting features. Capacity upgrades may be installed simply by adding extra channels (time slots or wavelengths) without the development of additional electronics. Similarly drop and insert (D&I) functionality may be implemented all optically, allowing a full circuit switched network to be deployed without returning to the electrical domain with its consequent restrictions^{11,20}. The overall aim of this thesis is to perform a detailed evaluation of one of these multiplexing options (OTDM) both in terms of signal generation, transmission and potential for optical networking. Particular investigations into standard fibre transmission, fundamentally digital transmission technologies and optical networking are completed. The approach adopted is largely one of experimental demonstration of concepts, with a brief theoretical analysis where appropriate used to verify system performance, and produce typical design optimisation rules. The results presented in this thesis are restricted to OTDM applications of electro-optic modulators and fibre ring lasers. Consequently, given the maturity of electro-optic modulators, many of the concepts described in this thesis could be rapidly brought to market.

We shall consider initially the components required to construct a simple OTDM system, namely pulse sources, modulator arrays, clock recovery circuits and

demultiplexers. Whilst a single common specification may be defined for each function, many different implementations exist, each with its own unique features and advantages. In particular, the development of appropriate pulse sources is crucial for all OTDM systems, and whilst high quality transform limited pulses may be required for soliton transmission, considerably poorer quality pulses may often be used to drive all optical switches. Timing synchronisation is also an important issue, and accuracy is required on a picosecond time scale. Electronic and optical clock recovery means will be discussed in detail, as well as the practical issues involved in the deployment of clock recovery circuits in OTDM systems. Subsequently, the transmission of OTDM signals will be considered using a variety of standard and advanced fibre types, prior to a demonstration of the networking potential of OTDM.

A degree of familiarity with standard optical communications systems is assumed throughout the thesis. However, **Chapter 2** reviews general background material required to understand the remainder of the thesis, and is deliberately restricted to particular essential aspects. The general properties of optical fibres, and conventional single channel communications systems are discussed, including optical amplification and Kerr type non-linearities. References are provided to suitable text book material for further background information. The necessary adaptations to extend standard theories are discussed during an illustration of the effect of crosstalk in an OTDM system.

In **Chapter 3** the construction of an OTDM transmitter is discussed, beginning with detailed investigations into various pulse source options, and brief descriptions of existing pulse sources used throughout these investigations. In particular the following investigations are described in some detail;

- Jitter suppressed gain switched DFB lasers
- Mode locked fibre ring lasers
- Electro-absorption modulators
- Non-linear pulse compression

The chapter is completed by details of the actual OTDM multiplexers employed in this thesis, and an alternative transmitter construction based on beat frequency conversion sources.

Chapter 4 applies the same approach to an OTDM receiver, discussing initially the problems of synchronisation and clock extraction. A favoured option of electronic phase locked loops is presented, along with a summary of alternative schemes. Work carried out on optical clock recovery is also discussed at this point. Following this, the construction of OTDM demultiplexer from electro-optic modulators is discussed.

Having discussed the development of OTDM transmitters and receivers, we shall consider the transmission of OTDM signals in **Chapter 5**. Transmission over standard fibre is essential for the near term deployment of OTDM where exploitation of the existing fibre plant will be an essential pre requisite for any new network architectures. In this chapter we shall review the available techniques before discussing the application of mid span spectral inversion to 40 Gbit/s OTDM systems. Allowing for longer term developments, and the migration of OTDM technologies to new networks allows the use of non standard transmission fibre, and the transmission of OTDM data signals

using dispersion shifted fibre with and without active soliton control will be discussed. Next, the use of novel transmission fibre designs is considered, where the aim is to alleviate some of the problems encountered for high bit rates (> 20 Gbit/s) and allow the eventual deployment of soliton control in ultra high capacity systems. Finally, the alternative of truly digital optical transmission using all optical regenerators is described with a demonstration of the worlds highest capacity regenerator.

In **Chapter 6**, and perhaps most importantly, the remarkable networking potential of OTDM is illustrated via two experiments employing electro-optic modulators. In particular, the chapter illustrates that by combining the effects of soliton control and optical switching, an infinitely cascable global OTDM network is feasible. Furthermore, particularly simple reconfigurable architectures are proposed without the use of optical space switches.

Finally, in **Chapter 7**, the material presented in this thesis is summarised, and used as the basis for a brief comparison with the alternative technologies. The thesis is closed with two visions of future communications networks, the first representing the logical evolution of traditional networks. The second represents a revolutionary future communication network which, as this thesis is completed, is beginning to receive widespread attention.

The main contributions of this thesis to the field of optical time division multiplexing are summarised below;

Pulse Sources

- Lowest reported duty cycle obtained from an electroabsorption modulator without non-linear compression (6.3 %) ^{125,129}.
- Worlds first generation of a modulated train of solitons using a single electroabsorption modulator without high speed electrical signal processing.
- Worlds first demonstration of low jitter beat frequency conversion source ¹⁷⁶.
- Worlds first modulation and error ratio characterisation of a beat frequency conversion source ³⁴⁹.

Clock Recovery

- Continued demonstration of electronic phase locked loop clock recovery for OTDM systems, including addition of harmonic mixer to simplify circuit and allow flexible upgradability beyond 100 Gbit/s ¹⁸³.

Signal Processing

- Demonstration of 80 Gbit/s OTDM system with electroabsorption modulators ¹²⁹.
- Proposal for simultaneous channel drop and photo-detection using an electroabsorption modulator.

OTDM Transmission

- Worlds first demonstration mid span spectral inversion at 40 Gbit/s ¹²⁸.
- Worlds first pseudo linear transmission of 40 Gbit/s data in a single polarisation over distances in excess of 1,000 km ³¹⁵.
- Worlds first demonstration of 40 Gbit/s soliton transmission over distances in excess of 2,000 km without soliton control or dispersion management ³¹⁵.

- Worlds first demonstration of global scale transmission at 20 Gbit/s using active soliton control^{258,286}.
- Highest repetition rate error ratio measurement over a long distributed erbium amplifier, with exceptionally low signal power excursion³²².
- Worlds first demonstration of periodically amplified transmission over loss compensating dispersion decreasing fibres³³⁰.
- Worlds first error ratio measurements of truly all optical regeneration³⁵⁰.
- Demonstration, using all optical regenerator, of the highest reported repetition rate regenerator using any technology²¹⁰.
- Proposal for self synchronising all optical regenerator.

OTDM Networks

- Worlds first demonstration of 40 Gbit/s three node OTDM network¹¹⁸.
- Demonstration of the feasibility of a truly global scale OTDM network, with almost infinitely cascable network nodes²⁰.

Furthermore, this thesis represents the most comprehensive review of 40 Gbit/s OTDM technology presented to date, and forms an excellent base for comparison with electronic and wavelength multiplexing systems.

2. Theory of Optical Communications

In this chapter, we will review the basic properties of standard optical communications systems, the fundamental principles of optical multiplexing and the required component subsystems. We shall begin by considering a simple single channel point to point communications link. This will entail describing in outline the fundamental properties of the transmission medium which limit the ultimate performance. This discussion will be extended to the fundamental properties of optical solitons, a particularly stable solution the equations governing the propagation of light along a transmission link. Finally we shall describe the additional system impairments of OTDM systems

2.1 Properties of Transmission Links

2.1.1 Optical Receivers

In a traditional communication system, signal processing is carried out electronically, and consequently any transmission link should comprised opto-electronic interfaces. The performance of these interfaces is well understood, and will not be described in detail²¹. It is important however to note that any practical optical receiver will introduce thermal noise into a communications link. This results in a minimum receiver power below which error free detection of the incoming optical data signal is not possible. This minimum power is typically characterised by the receiver sensitivity, which defines the received light level for which an error ratio of 10^{-9} is achieved²¹. In high speed systems however (> 5 Gbit/s) it is usual associate an optical amplifier with each opto-electronic receiver, boosting the signal power and allowing error free operation for considerably reduced signal powers (at the input to the optical amplifier). The improvement in the effective sensitivity of a correctly designed combination is limited by the noise added by the optical amplifier²⁸ as discussed in Section 2.1.3. In this thesis, the terms receiver sensitivity and pre-amplified receiver sensitivity refer to the received light levels at the input to a photodiode and the input to the first optical amplifier within an OTDM node respectively.

2.1.2 Optical Fibre

Perhaps the most significant recent development in communications networks was the optical fibre waveguide, proposed in 1966 by Kao and Hockham²² and first produced by Corning Glass Works in 1970. This development allowed the construction of the first optical communications systems in 1977, and today the media has almost completely replaced copper based coaxial transmission lines for trunk and international networks world-wide. The properties of the transmission medium dictate the performance of any given link within a communications network, defining parameters such as carrier frequency (traditionally referred to in terms of wavelength in the case of optical fibre based systems), repeater spacing and maximum line rate before limits imposed by practical terminal equipment are even considered. In this section, we shall

review some of the more important properties of single mode fibre, namely; attenuation, dispersion, birefringence and non-linearity. By the nature of the maturity of this technology, a certain amount of rigorous detail, found in many texts^{21,24,28}, will be omitted.

2.1.2.1 Approach

The propagation of an optical signal is governed by the wave equation^{2,3}

$$\left[\nabla^2 + \frac{\epsilon}{c^2} \frac{\partial^2}{\partial t^2} \right] \underline{E} = 0 \quad \text{Equation 2-1}$$

where E represents the electric field vector, c the velocity of light and ϵ the dielectric constant of the medium. For a cylindrically symmetric waveguide, the boundary conditions reduce the equation to a single spatial dimension (z) and a set of allowed guided modes with associated propagation constants. For pulse propagation, solutions to the wave equation for guided modes are usually represented as optical waves in the slowly varying envelope condition²⁴. That is, that the light intensity varies slowly with respect to the optical carrier. In this approximation (which is valid for pulses longer than ≈ 200 fs) we look for solutions of the form

$$u(t, z)e^{i(\omega_0 t - \beta z)} \quad \text{Equation 2-2}$$

where u represents the pulse envelope (related to the optical intensity by $I = |u|^2 / A_{\text{eff}}$ where A_{eff} is the effective area of the fibre), ω_0 the carrier frequency and β the propagation constant at that frequency.

2.1.2.2 Attenuation

In a high quality optical fibre optical signals are attenuated (reduced in power) by; electronic absorption, phonon absorption, impurities, Rayleigh scatter and bending losses.

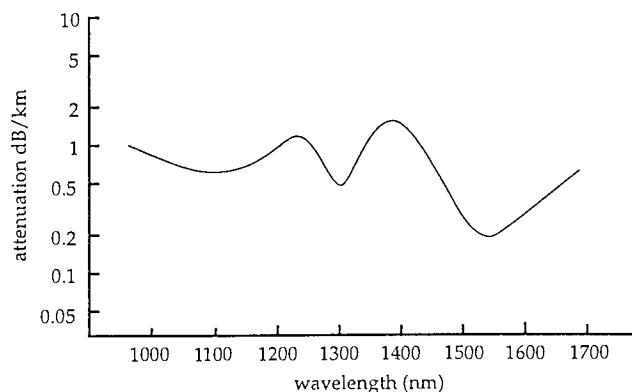


Figure 2-1 ; Attenuation of single mode fibre.

These features lead to the fibre loss exhibiting a strong wavelength dependence as shown in Figure 2-1. Note the occurrence of low loss windows around 1300 and 1500 nm. Denoting the signal power as P and the total fibre loss per unit length as α , then the evolution of signal power with distance (z) is governed by the equation.

$$\frac{dP}{dz} = -\alpha z \quad \text{Equation 2-3}$$

or in terms of the slowly varying envelope approximation,

$$\frac{\partial u}{\partial z} = -\frac{\alpha}{2} z \quad \text{Equation 2-4}$$

For the two lowest loss windows of interest (Figure 2-1) typically $\alpha = 0.046 \text{ km}^{-1}$ at 1550 nm and 0.073 km^{-1} at 1300 nm. Simple calculations based on these figures may be used to determine the impact of fibre loss for a simple point to point link. For example for a system with a minimum detectable power of -42 dBm and a launch power of 10 mW, a system could accommodate 52 dB of loss, giving maximum transmission spans of 260 km @ 1550 nm and 157 km @ 1300 nm. Clearly from the point of view of signal loss, operation in the 1550 nm window is preferred.

2.1.2.3 Dispersion

The two major causes of error in a simple, communication system are power loss and signal distortion. Different wavelengths travel at different speeds within an optical fibre, due to the wavelength dependence of the material refractive index and the effects of the waveguide itself. Since an optical pulse has a finite spectral bandwidth, different parts of the pulse will travel at different velocities, leading to dispersive pulse broadening. This is interpreted as the frequency dependence of the mode propagation constant of Equation 2-2²⁴. Several important relationships may be derived from this constant. These include the phase velocity, $v_p = \omega/\beta$ (the velocity at which a constant phase front would move through the material), the group velocity $v_g = (d\beta/d\omega)^{-1}$ (the velocity at which a pulse envelope moves through the material) and the related quantity, the group delay ($\tau_g = 1/v_g$) used to directly calculate the time of flight of a pulse. To simplify the theoretical treatment²⁴, it is normal to consider the Taylor series expansion of the propagation constant about the carrier frequency.

$$\beta(\omega) = \frac{\omega \cdot n(\omega)}{c} = \beta_0 + \beta' \cdot (\omega - \omega_0) + \frac{\beta'' \cdot (\omega - \omega_0)^2}{2} + \dots \quad \text{Equation 2-5}$$

Where ω represents the instantaneous angular frequency and prime represents differentiation with respect to angular frequency. To mathematicians pulse spreading is governed by the second and higher derivatives of the propagation constant with respect to frequency ($d^2\beta/d\omega^2 = \beta''$). Communications engineers on the other hand consider the derivatives of the group delay (τ_g) with respect to wavelength. These quantities are interrelated to each other and fundamental parameters by

$$D = \left(\frac{1}{z}\right) \frac{d\tau_g}{d\lambda} = -\left(\frac{\lambda}{c}\right) \frac{d^2n}{d\lambda^2} = -\frac{2\pi c}{\lambda^2} \beta'' \quad \text{Equation 2-6}$$

where D is the dispersion coefficient and z is the fibre length. The wavelength at which the derivative of the propagation constant (or the dispersion coefficient) is zero is referred to as the zero dispersion wavelength, λ_0 . At this wavelength, higher order

dispersive terms such as third order dispersion, $d^3\beta/d\omega^3 = \beta'''$ dominate the pulse propagation. This is related to the dispersion coefficient, and its slope $dD/d\lambda$, by ;

$$\beta''' = \left(\frac{\lambda}{2\pi c} \right) \left(\frac{2D}{\lambda} + \frac{dD}{d\lambda} \right) \quad \text{Equation 2-7}$$

Using this notation, pulse propagation is governed by;

$$\frac{\partial u}{\partial z} = -\beta' \dot{u} - \frac{i}{2} \beta'' \ddot{u} + \frac{1}{6} \beta''' \ddot{\ddot{u}} + \dots \quad \text{Equation 2-8}$$

where the first term represents group delay, the second the dispersion and the, third higher order dispersion. The relationship between these various terms is shown in Figure 2-2, where the group delay and dispersion coefficients (D and β'') are shown for a dispersion shifted fibre with 1550 nm dispersion zero and a constant dispersion slope of 0.075 ps/nm²/km. Note that two signals whose centre wavelengths are equally spaced (in wavelength) around the zero dispersion point experience the same group delay. Such signals with equal propagation velocities are said to be velocity matched.

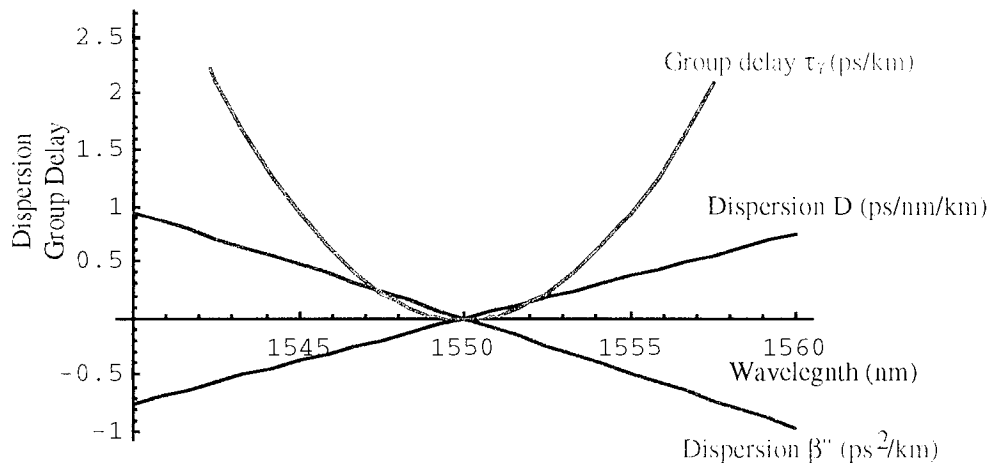


Figure 2-2 Illustration of the relationship between group delay, its dispersion and the dispersion in the propagation constant.

For a gaussian input pulse, neglecting higher order dispersion terms, it can be shown that the output pulse is also gaussian, but with an increased pulse width, given by;

$$\left(\frac{\tau_{out}}{\tau_{in}} \right)^2 = 1 + \left(\frac{\beta'' z}{[\tau_{in}/1.665]^2} \right)^2 \quad \text{Equation 2-9}$$

where τ_{out} represents the output pulse widths (measured at full width at half maximum, or FWHM) and τ_{in} the input FWHM pulse width. If such broadening is allowed to become excessive, then the tails of the pulse begin to impinge on the adjacent time slot and eventually the detected signal will be degraded by intersymbol interference (ISI). This initially causes a reduction in the receiver sensitivity without introducing errors (a sensitivity penalty), but eventually producing irretrievable errors, and an error rate floor.

2.1.2.4 Birefringence

Single mode optical fibre, now used exclusively throughout core networks world-wide, in actual fact supports two distinct modes, differentiated by the polarisation of the signal. In an ideal fibre, these two modes are degenerate and indistinguishable. However, the exact fibre geometry has a profound influence on the group delay characteristics. Consequently, applied stress, or intrinsic ovality (as a result of a practical manufacturing process) leads to an orientation specific geometry and consequently a polarisation dependence of the group delay, known as birefringence. Conventionally, the propagation along one axis is faster than the other, and the two orthogonal states are known as the fast and slow axis. For short lengths of fibre, the differential group delay between the two orthogonal modes, $\Delta\tau$ may be expressed in terms of the difference between the geometric terms of the propagation constant, β_x, β_y as;

$$\Delta\tau = \Delta\beta \cdot L \cdot \frac{\lambda}{2\pi c} \quad \text{Equation 2-10}$$

Where $\Delta\beta = \beta_x - \beta_y$. However, for a signal launched at an angle to these specific polarisation's, by delaying the two modes relative to each other, the birefringence will cause the linear polarisation state to evolve into an elliptical state (circular if launched at 45°), eventually returning to its original linear state. The length scale over which this occurs is known as the beat length, representing the period over which any arbitrary polarisation will return to its original state. The beat length L_b is given by ;

$$L_b = \frac{2\pi}{\Delta\beta} \quad \text{Equation 2-11}$$

Unfortunately, for long lengths of fibre, the orientation of the geometric disturbance varies randomly, and the net differential group delay between the fastest and slowest polarisation states will not increase linearly with distance. The picture is further complicated by polarisation scattering, causing power to be transferred between the local fast and slow axis (known as mode coupling). It has been observed however²⁵ that such a fibre behaves very similarly to a short length of birefringent fibre, with the fast and slow axes are replaced by two principle states (not necessarily of orthogonal launch polarisation's) of maximum and minimum group delay. Under these conditions it is perhaps more appropriate to consider the accumulation of differential delay as a random walk process, whereby the mean group delay is statistically likely to increase with the square root of distance. Under these conditions, a typical value of mean differential group delay (D_p) would be around 0.03 ps/ $\sqrt{\text{km}}$ for fibres on shipping drums, whilst the same fibre when cabled may under certain circumstances give an increased value of up to 0.3 ps/ $\sqrt{\text{km}}$. In a similar way to chromatic dispersion, polarisation mode dispersion (PMD) gives rise to pulse broadening, eventually leading to ISI.

2.1.2.5 Non-linearity

The fourth cause of signal distortion in an optical fibre arises from the non-linear response of the medium. Two types of non-linearity exist, involving the interaction of the incident radiation with bound electrons (Kerr effect) and phonons (Scattering) respectively. Whilst traditionally of negligible importance, non-linear effects are of increasing significance as the overall fibre lengths are increased through the use of optical amplification and launch powers are increased to maintain an adequate signal to noise ratio at higher capacities.

For a general optical signal, the electronic non-linearity is normally accounted for in the solution of Equation 2-1 by allowing a polynomial relationship between the polarisation vector \underline{P} and the applied field \underline{E} , given in tensor notation as²⁶;

$$P_i = \epsilon_0 [\chi_{ij}^{(1)} E_j + \chi_{ijk}^{(2)} E_i E_k + \chi_{ijkl}^{(3)} E_j E_k E_l] \quad \text{Equation 2-12}$$

The various terms of the electric susceptibility, and the fibre properties they govern, are detailed in Table 2-1.

component	tensor rank (#elements)	typical value for fibre (1.5 μ m)	real part determines	imaginary part determines
general			Effects due to phase	Amplitude effects
$\chi^{(1)}$	matrix (9)	0.89	refractive index (n)	attenuation (α)
$\chi^{(2)}$	third (27)	0		
$\chi^{(3)}$	fourth (81)	$6 \cdot 10^{-14} \text{ J m}^{-1}$	non-linear refractive index (n_2)	non-linear loss (α_{NL})

Table 2-1 : Properties of the electric susceptibility tensors.

Note that in a perfect centro symmetric media, such as a fibre, all 27 elements of $\chi^{(2)}$ are zero (for an appropriate co-ordinate system), and thus the dominant non-linearity in silica based optical fibres is due to $\chi^{(3)}$. Geometric constraints also simplify this fourth rank tensor, and when appropriate axes are chosen to we find that a simple relationship exists between the non zero components²⁷;

$$\begin{aligned} \chi_{xxxx}^{(3)} &= \chi^{(3)} \\ \chi_{xxyy}^{(3)} &= \chi_{xyxy}^{(3)} = \chi_{yyxx}^{(3)} = \chi^{(3)} / 3 \\ x, y &\in \{1, 2, 3\}, x \neq y \end{aligned} \quad \text{Equation 2-13}$$

It is more common however to utilise a related parameter, the Kerr coefficient or non-linear refractive index n_2 , defined such that ;

$$\begin{aligned} n &= n_0 + n_2 I \\ n_2 &= \frac{3\chi^{(3)}}{4\epsilon_0 n_0^2 c} \end{aligned} \quad \text{Equation 2-14}$$

A typical value of the Kerr coefficient is $3.2 \cdot 10^{-20} \text{ m}^2 \text{W}^{-1}$. Following the approach of Equation 2-2, a further related coefficient is the coefficient of non-linearity γ (with a

typical value of $2.6 \text{ W}^{-1}\text{km}^{-1}$), giving rise to the equation of motion for a single optical carrier²⁴;

$$\frac{\partial u}{\partial z} = i\gamma|u|^2 u$$

$$\gamma = \frac{\omega_0 n_2}{cA_{\text{eff}}} = \frac{3\omega_0 \chi^{(3)}}{4\epsilon_0 c^2 A_{\text{eff}} n_0^2}$$

Equation 2-15

It should be noted that the refractive index change is purely real, and so only phase changes may be induced by the electronic non-linearity described here and the total optical power is conserved. The total phase change, ϕ_{SPM} , induced by a signal on itself is directly proportional to the integral of the signal power with length;

$$\phi_{\text{SPM}} = \gamma \int_0^L P dz$$

Equation 2-16

This particular manifestation of the electronic non-linearity is often referred to as self phase modulation (SPM). When two co-polarised signals interact, the non-linear phase change, ϕ_{XPM} , on one due to the other (cross phase modulation, XPM) is given by;

$$\phi_{\text{XPM}}^{(1)} = 2\gamma \int_0^L P^{(2)}(z/\Delta v_g) dz$$

Equation 2-17

where $P^{(2)}(t)$ represents the power of the second signal in a frame of reference moving with the first. This is illustrated in Figure 2-3, where the effects of imperfect velocity matching are examined by varying the relative group delays ($\Delta\tau_g$). Cross phase modulation may be exploited in the construction of optical switches, where the temporal profile of the phase change profile determines the temporal properties of the switch.

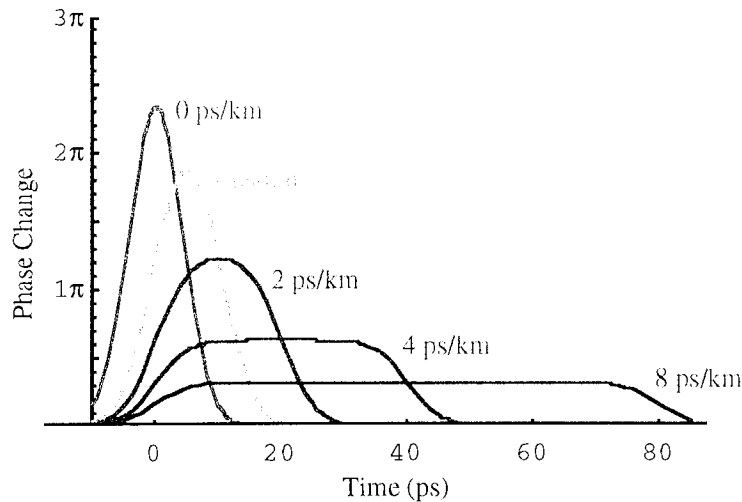


Figure 2-3 Theoretical phase change due to cross phase modulation as a function of inverse group velocity. Calculation assumes 50 mW mean power for a 10 GHz stream of 10 ps pulses propagating along a 10 km fibre. Effects of dispersive pulse broadening and loss have been neglected for simplicity.

Other particular manifestations of the electronic non-linearity include four wave mixing (FWM) and modulation instability (MI), which will not be discussed in this thesis.

2.1.3 Optical Amplifiers

The maximum transmission distance of an optical communications system was historically limited by simple fibre attenuation coupled with a finite receiver sensitivity (or minimum received power), and a transmission system would comprise many independent optical fibre spans. With the advent of optical amplifiers²⁸, this simple constraint is lifted, and many fibre spans may be traversed before signal regeneration is required. However, whilst advantageously removing power budget limitations, optical amplifiers have allowed the impairments of each fibre span (eg dispersion) to accumulate along an essentially analogue transmission link. Furthermore, optical noise is added to the system by the amplifiers. In this section the accumulation of optical noise for a generic optical amplifier is described.

The noise added to the transmission line by an individual optical amplifier is a function of the amplifier gain, the component losses (WDM couplers and optical isolators) and the amplifier noise figure, and arises from the spontaneous emission process within the amplifier. The total noise power (or spontaneous emission power) in a single polarisation state P_{ase} for a gain G and an optical bandwidth Δf_{opt} for a single amplifier is given by³⁰;

$$P_{ase} = n_{sp} (G - 1) h \nu \Delta f_{opt} \quad \text{Equation 2-18}$$

where h is Plank constant, ν the optical frequency and n_{sp} the population inversion parameter. In close analogy with electrical amplifiers, it is useful to describe the system performance in terms of the amplifier noise figure NF (usually quoted in dB). For an optical amplifier this is directly related to the population inversion n_{sp} by ;

$$NF = 10 \log_{10} 2n_{sp} \quad \text{Equation 2-19}$$

In a system with optical amplifiers, the electrically detected signal will comprise noise sources from the receiver thermal noise and the signal shot noise (which in the absence of optical noise determines the receiver sensitivity) plus shot noise from the spontaneous emission, beat noise between the signal and spontaneous emission and beat noise between the various spectral components of the spontaneous emission spectrum. Clearly, for the beat noise terms, only the spectral components of the beat noise within the electrical bandwidth of the receiver ($\Delta \nu_{elect}$) are of concern. For most practical systems, a narrow-band optical filter (of bandwidth $\Delta \nu_{opt}$) is usually placed prior to the receiver, making the contributions of spontaneous shot noise and spontaneous beat noise negligible, whilst a sufficiently high gain amplifier will cause the remaining optical amplifier induced noise terms to dominate over the receiver thermal noise²⁹. Consequently the system performance can usually be specified by considering only signal shot noise and signal spontaneous beat noise terms. In this case the electrical signal to noise ratio is given by³⁰;

$$SNR_{elect} = \frac{P_{sig}}{2h\nu\Delta f_{elect} + 4P_{spont} \frac{\Delta f_{elect}}{\Delta f_{opt}}} \quad \text{Equation 2-20}$$

Thus, in order to calculate the performance of a simple transmission line, it is sufficient to calculate the signal and amplified spontaneous emission powers P_{sig} and P_{spon} respectively. This is complicated slightly by the practical realisation of an optical amplifier, where component losses on the amplifier input (c_{in}) and the amplifier output (c_{out}) demand a higher intrinsic gain (G_{int}) than the actual required amplifier gain (G). In this case, the amplifier spontaneous emission from a single amplifier is given by ;

$$P_{spon} = c_{out} n_{sp} (G_{int} - 1) h\nu \Delta f_{opt}$$

or

Equation 2-21

$$P_{spon} = \left[\frac{1}{c_{in}} n_{sp} \right] (G - c_{in} c_{out}) h\nu \Delta f_{opt}$$

By comparison with Equation 2-18, if the amplifier we considered to be a “black box”, its apparent noise figure would be, for large gains, governed by the term in square brackets. We may thus deduce that the major effect of the component losses is to increase the apparent noise figure of the amplifier by the input coupling loss. This therefore favours the location of extraneous components, such as isolators and filters, on the amplifier output.

It remains to calculate the evolution of the signal and spontaneous emission along an arbitrary transmission link comprising fibre lengths of loss L_i , amplifiers with gains G_i .

$$P_{sig}(out) = P_{sig}(in) \prod_i^N G_i L_i$$

$$P_{spon} = \left[\frac{1}{c_{in}} n_{sp} \right] h\nu \Delta f_{opt} \sum_i^N \left\{ (G_i - c_{in} c_{out}) \prod_{j=i}^N G_j L_j \right\}$$

Equation 2-22

For the case of a chain of N similar amplifiers exactly overcoming the fibre loss between them, this becomes quite simply;

$$P_{sig}(out) = P_{sig}(in)$$

$$P_{spon} = \left[\frac{N}{c_{in}} n_{sp} \right] h\nu \Delta f_{opt} (G - c_{in} c_{out})$$

Equation 2-23

From these equations we can calculate the minimum signal power in order to obtain a given error rate, given the known relationship between error rate and signal to noise ratio.

2.2 Optical Pulse Transmission

2.2.1 Propagation Equation

In the above discussion, it was noted that each fibre property could be described in terms of an equation of motion, with a solution in the form of Equation 2-2. It is useful however, to consider the fibre as a whole, rather than the individual properties

independently. It is possible to show, that the equation of motion of an optical fibre, taking into account loss, dispersion and Kerr type non-linearities is given by^{24,23};

$$\frac{\partial u}{\partial z} = -\frac{\alpha}{2}u + i\gamma|u|^2u - \beta'u - \frac{i}{2}\beta''\ddot{u} + \frac{1}{6}\beta'''\ddot{\ddot{u}} \quad \text{Equation 2-24}$$

Solutions to this equation are generally complicated, and the application to a specific communications system normally requires the use of numerical techniques. However, certain simplifying assumptions are often made. In particular, if a frame of reference moving with the pulse is chosen (by making the transformation $t \Rightarrow t - z/v_g$), second and higher order dispersion is neglected and the action of optical amplifiers is assumed to make the fibre loss-less (without the addition of noise, generally added later as a small perturbation) then we have the non-linear Schrödinger equation.

$$\frac{\partial u}{\partial z} = i\gamma|u|^2u - \frac{i}{2}\beta''\ddot{u} \quad \text{Equation 2-25}$$

Again, this equation may be solved numerically to predict the performance of any given system, allowing approximate limits on transmission performance to be derived³¹. However, in certain special cases, Equation 2-25 may be solved exactly. A solution of particular interest are the optical soliton, a pulse of specific spectral and temporal profile that propagates with no change in shape. Physically, in soliton transmission the phase changes induced by dispersion and non-linearity are balanced exactly, preventing any distortion in the pulse shape. The propagation of an optical soliton without distortion makes this solution particularly attractive, and will be discussed in more detail in 2.2.2. This solution is a stable solution, by which it is meant that if a small perturbation is made to the pulse, it will tend to reform into a soliton.

2.2.2 Optical Solitons

Due to its importance to optical communications, we shall end this discussion on the properties of the transmission link by examining the propagation of optical solitons. The precise solutions to the Schrödinger equation may be obtained directly by inverse scattering transforms³², however, with hindsight, substitution of known solutions is generally sufficient to derive the properties of any given soliton. The optical soliton was first theoretically demonstrated in 1973³³, and observed experimentally in 1980³⁴. Solitons are proposed as a technique for allowing ultra high speed long haul optical communications via an exact balance of dispersion and non-linearity, however, solitons also exist as solutions to many physical phenomena; for example in fluid mechanics, river bores and tsunamis are soliton solutions to the relevant equations. We shall of course restrict ourselves to the optical soliton, and its use in optical communications. The field amplitude of a fundamental soliton is, in general, described by a hyperbolic secant of the form

$$|u(t,z)| = A \cdot \text{Sech}\left(\frac{t}{\tau}\right) \quad \text{Equation 2-26}$$

where τ represents the sech width of the pulse and A its amplitude. In order for Equation 2-26 to represent a solution to the Schrödinger equation, we must insist on certain relationships between the parameters in this equation. In particular, the amplitude (A) or peak power (P_{sol}), sech width (τ) or pulse FWHM ($\tau_{FW} = 1.76275\tau$) and propagation constant (β) or fibre dispersion (D) should be related by

$$P_{sol} = \frac{0.766\lambda^3 DA_{eff}}{\pi^2 cn_2 \tau_{FW}^2} \quad \text{Equation 2-27}$$

Higher order solitons have complex pulse shapes, which evolve with propagation along a fibre. However, the pulse shape repeats periodically, and the length scale on which this repetition occurs is known as the “soliton period”. This pulse shape evolution is of course accompanied by a periodic phase variation, which is also present in the fundamental soliton (which propagates without changes in shape), and the concept of soliton period remains valid. For a fundamental soliton, the soliton period (L_{sol}) is given by

$$L_{sol} = \frac{0.322\pi^2 c \tau_{FW}^2}{\lambda^2 D} \quad \text{Equation 2-28}$$

and is clearly inversely related to the soliton power, as shown below.

$$L_{sol} P_{sol} = 0.246 \frac{A_{eff} \lambda}{n_2} \quad \text{Equation 2-29}$$

The properties of these optical solitons were first investigated at a wavelength of $1.55\mu\text{m}^{34}$ and later at $1.3\mu\text{m}^{35}$. Today interest is mainly focused on the utilisation of dispersion shifted fibres at $1.55\mu\text{m}$ for low pulse energy, high capacity, long haul systems. Recently however, investigations of solitons on standard fibre have promised valuable upgradability routes for the installed fibre base^{36,37}.

2.2.3 Ideal soliton communication systems

More detailed treatments of the fundamental properties of optical solitons are readily available in the literature, and will not be reproduced here^{32,38}. Instead, we turn to the practical implications of optical communications systems. A typical launched pulse train, comprising fundamental solitons, would be ;

$$P(t) = P_{sol} \sum_n \left| A_n \text{Sech}\left(\frac{t-nT}{\tau}\right) e^{i\phi_n} \right|^2 \quad \text{Equation 2-30}$$

where A_n represents the data sequence, taking value 1 for a logical “1” and zero for a logical “0”, ϕ_n the relative phase of the n 'th pulse and T the pulse spacing. One significant difference between the propagation of an ideal soliton pulse train and the modulated pulse stream is that the modulated train is not a simple solution of Equation 2-26. In fact, it may be shown³⁹ that neighbouring pulses may be more readily described in terms of interaction forces that decrease exponentially with separation, and vary sinusoidally with phase. This interaction force will cause a pair of solitons to change their relative positions, and gives rise to a pattern dependent arrival time jitter.

Neglecting the relative phase, we may physically understand this interaction in terms of the non-linearity by considering that the presence of the exponentially decaying pulse tail from one pulse changes the refractive index experienced by the second, and hence results in a change in velocity. Incorporating the pulse phase merely reflects the dependence of the non-linearity on the total intensity, governed by the addition of the two optical fields either constructively or destructively. Taking this effect into account allows for both attractive (constructive interference) and repulsive (destructive interference) forces between solitons. This effect has also been studied by perturbation theory⁴⁰, numerically^{41,42} and experimentally⁴³. A significant result of these investigations is that pulses initially in phase will periodically collapse and separate with a period given by;

$$L_{collision} = \frac{2\pi L_{sol}}{4 \operatorname{Sech}\left(\frac{1.76.T}{2.\tau_{FW}}\right)} \quad \text{Equation 2-31}$$

Since an optical communication system will contain random data (the sequence A_n will be uncorrelated) interaction forces must simply be avoided by spacing the pulses sufficiently to ensure that the resultant jitter is minimised. Rather than perform exact jitter calculations however, it is usually sufficient to impose the condition that the pulse spacing (T) is large enough to ensure that the collapse period is at least four times the system length.

2.2.4 Practical soliton transmission.

Fibre attenuation implies that an ideal soliton only exists at most at a single point in the fibre, where the amplitude generates the appropriate non-linear chirp to balance the dispersive chirp. However, it was shown that a fundamental soliton will be recovered at the fibre output provided the launch power is within 50% of the ideal launch power (P_{sol}) for the launched pulse width in a loss-less fibre^{44,45}. For a launched power of $P_{sol}(1+\Delta)^2$, the resultant soliton is of the form

$$P(t) = P_{sol}(1+2\Delta)^2 \operatorname{Sech}^2\left(\frac{1.76t}{\tau_{FW}(1+2\Delta)}\right) \quad \text{Equation 2-32}$$

that is, the peak power is increased, and the pulse width reduced due to the compression of the pulse. It was proposed⁴⁶ that if a pulse is launched with an initial amplitude up to 50% greater than the soliton power (for a loss-less fibre), then soliton transmission will be possible in a cascade of real fibres and optical amplifiers, provided the power never falls below 50% of the required soliton power. The technique is known as preemphasis, or dynamic soliton control, since. Preemphasis sets a limit on the amplifier spacing for soliton transmission by virtue of the large, but finite soliton dynamic range.

A more physically appealing property of periodically amplified solitons arises from the viewpoint of the Average Soliton Model⁴⁷ or the Guiding Centre Soliton⁴⁸. It was been shown by analysis that a soliton arises from a balance between non-linear phase shift

and dispersion over the length scale of the soliton period (Equation 2-28). Thus, provided ANY perturbation to parameters governing the soliton propagation occurs periodically, with a length scale substantially less than the soliton period, then the soliton will behave according to the average value of the parameter. This was initially demonstrated by the author for large periodic changes in both dispersion and signal power^{49,50}. Here the non-linear phase shift was accumulated in a 67 km length of normally dispersive (non soliton supporting) fibre, and the average dispersion was determined by a 4.5 km length of standard fibre. Remarkable agreement between analytical theory, numerical modelling and experimental results were achieved for this experiment. Subsequently, many soliton transmission experiments⁵¹ have employed exactly this technique to fine tune the balance between dispersion and non-linearity. More recently, this technique of dispersion management within the soliton period has been proposed for use with installed dispersion shifted fibres, where a large spread in fibre dispersion zeroes exists^{52,53}.

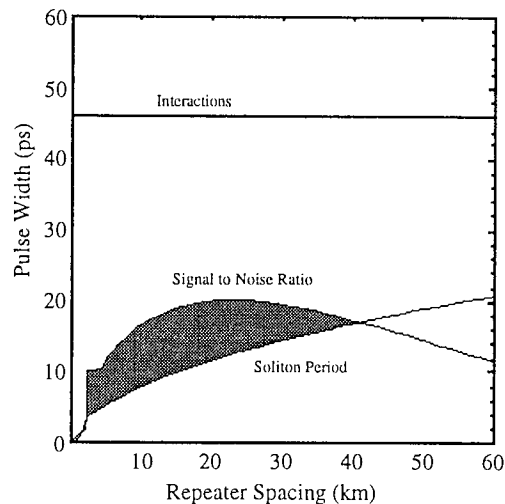


Figure 2-4 Illustration of the limitations on soliton system design. This example; 5 Gbit/s transmission over 10,000 km fibre with 0.5 ps/nm/km dispersion, 5.2 dB noise figure amplifiers with input and output coupling efficiencies of 0.2 and 1.7 dB and a fibre loss coefficient of 0.23 dB/km.

So for stable soliton transmission, we must ensure that any periodic disturbances to the transmission path occur with a length scale shorter than the soliton period by, say, a factor of 6, and set the soliton power according to the average value of these parameters. If this condition is not maintained, then energy is lost from the solitons in the form of dispersive wave radiation and eventually results in unacceptable error ratio's. For mild violations of this rule phase matching between the dispersive wave components generated from each span result in resonance's within the spectrum of the soliton. It has been shown that the frequencies of these resonance's is given (empirically) by⁵⁴

$$\delta v_n = \pm \frac{1}{2\pi\tau_{FW}} \sqrt{1 + 8n \frac{L_{sol}}{L_{rep}}} \quad \text{Equation 2-33}$$

With three major constraints on the system (low pulse width to avoid interactions, high launch powers for good signal to noise and short repeater spacings to allow average solitons) we may begin to construct a Soliton Design Diagram^{55,56}, as shown in Figure

2-4. The shaded region of this diagram indicates the allowed values of the pulse width and repeater spacings to simultaneously satisfy all three criteria for a given bit rate and system configuration (see figure for details).

Gordon and Haus considered the interaction of solitons with spontaneous emission theoretically in some detail, with the basic premise that certain noise modes are added to the soliton which then reforms into a slightly different soliton on subsequent propagation⁵⁷. Amplifier noise may be added to both the amplitude or phase (frequency) of the soliton. In the case of amplitude noise, the soliton peak power is modified, and provided the soliton remains within its dynamic range, a new soliton reforms with slightly different energy. Upon detection however, this process is indistinguishable from the simple linear addition of noise (section 2.1.3), provided other non-linear effects (such as the soliton self frequency shift⁶⁴) may be neglected.

The case of phase noise, often neglected for linear transmission systems, does however have a significant effect for a soliton system. Noise added by optical amplification shifts the mean central frequency of the pulse, and a new soliton forms around this new central frequency upon subsequent propagation. The frequency change, coupled with chromatic dispersion along the remainder of the (potentially dispersion managed) transmission link, results in a change in the pulse arrival time. The random nature of this effect thus imposes a random arrival time (or timing jitter) for the pulses, known as Gordon Haus jitter. The magnitude of this jitter for a system of uniform dispersion is given by ;

$$\langle \Delta t^2 \rangle = \frac{n_2 n_{sp} h c_{out} (G_{int} - 1) (1 - e^{-\alpha L_{rep}}) D L_{sys}^3}{9 A_{eff} \alpha L_{rep}^2 \frac{\tau_{FW}}{1.76}} \quad \text{Equation 2-34}$$

where L_{sys} is the overall system length, and L_{rep} the repeater spacing. Pulses arriving outside the appropriate time slot (determined by the effective bandwidth of the receiver) will be erroneously detected and this gives rise to the well known maximum bit rate distance product limit for soliton systems. For an error rate better than 10^{-9} an rms. jitter levels less than 1 sixth of the detection window (conventionally taken as half of the bit period for an ideal receiver) are required. The growth of the rms. jitter has been studied directly⁵⁸ by monitoring the inferred pulse width from the RF spectrum of soliton pulses, which appears to narrow as the jitter accumulates. Direct measurements of this RF spectrum as a function of system length thus provide an excellent diagnostic tool for a soliton system. Similarly many soliton transmission experiments have verified this limit.

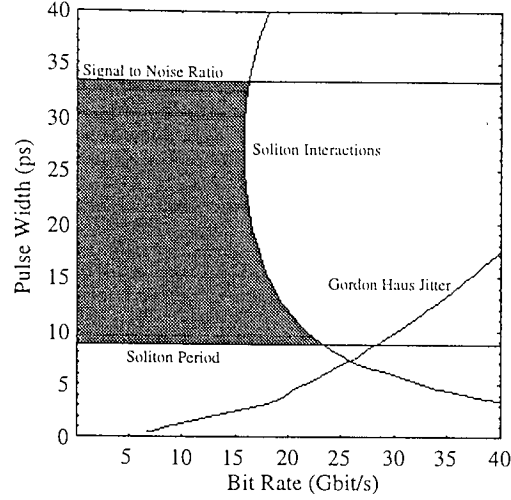


Figure 2-5 Soliton design diagram showing capacity limits for 2,000 km transmission with a mean dispersion of 0.15 ps/nm/km and a repeater spacing of 33 km. All other parameters as Figure 2-4.

Further sources of timing jitter in a soliton system include pulse to pulse wavelength jitter of the source⁵⁹, the soliton self frequency shift⁶⁰ (coupled with amplitude noise), interaction with fibre birefringence⁶¹ and the acousto-optic effect⁶². The latter is particularly significant for high speed OTDM systems and arises from an interaction between the optical signal and vibrational modes within the transmission medium. The passage of a signal pulse through the fibre can lead to an electrostrictional excitation of acoustic (sound) waves, which propagate radially out of the fibre. Upon reflection from physical boundaries in the fibre, this acoustic wave modifies the refractive index of the fibre core, resulting in a temporal jitter given by

$$\langle \Delta t^2 \rangle = 1.9 \cdot 10^{-31} \frac{D^4 L_{sys}^4}{T^3} \left(1 - 1.18 \cdot 10^9 T \right) \quad \text{Equation 2-35}$$

Fibre birefringence is of course problematic for both linear and soliton systems and can affect the stability of a soliton itself⁶³. It has been shown that, provided the non-linear effects are sufficiently strong, a soliton is stable in a birefringent fibre. This condition translates to a simple inequality between the fibre dispersion and the birefringence of the fibre (Equation 2-36). Provided this inequality is maintained, the only effect of the birefringence is to introduce timing jitter^{61,63};

$$D_{p(ps/\sqrt{km})} \leq 0.3 \sqrt{D_{(ps/nm/km)}} \quad \text{Equation 2-36}$$

$$\langle \Delta t^2 \rangle = \frac{(G_{int} - 1) \left(1 - e^{-\alpha L_{rep}} \right) c_{out} n_{sp} hc^2 D_p^2 L_{sys}^2 \tau_{FW}}{2.85 \alpha L_{rep}^2 \lambda^3 D}$$

Intra pulse stimulated Raman scattering gives rise to the soliton self frequency shift, where the rate of change of the pulse central frequency along the fibre length is given by⁶⁴;

$$\frac{df}{dz} = 2.2 \cdot 10^{-15} g(\tau) \frac{\lambda^2}{2\pi c} \frac{D}{\tau^4} \quad \text{Equation 2-37}$$

For a perfect train of solitons, this effect is benign, simply changing the central frequency, however, it is strongly pulse width dependant, and consequently any pulse to pulse width variations (from the source laser, or induced by the incorporation amplifier noise into the soliton) will give rise to differing frequency shifts, and consequently, through chromatic dispersion, timing jitter. It is easy to show that a change in pulse power (ΔP) or width ($\Delta\tau_{FW}$) will give rise to a mean timing shift of;

$$\Delta t = 27 \cdot 10^{-15} \frac{\lambda^4}{4\pi^2 c^2} \frac{D^2 L_{sys}^2}{\tau_{FW}^4} \left(\frac{\Delta\tau_{FW}}{\tau_{FW}} + \frac{\Delta P}{P_0} \right) \quad \text{Equation 2-38}$$

A simple variant of the soliton design diagram (Figure 2-5), for a fixed, optimum, repeater spacing, illustrates the major obstacles to system capacity, whilst theoretical error rate curves (Figure 2-6) illustrate the relative effects of these jitter sources. Control of soliton interactions and jitter are clearly key aspects to the production of high capacity soliton systems. Careful choice of fibre dispersion, to control the soliton period will also be required, where low mean values are preferred. Indeed, recent work has illustrated that precise dispersion management in a soliton system offers significant benefit⁶⁵.

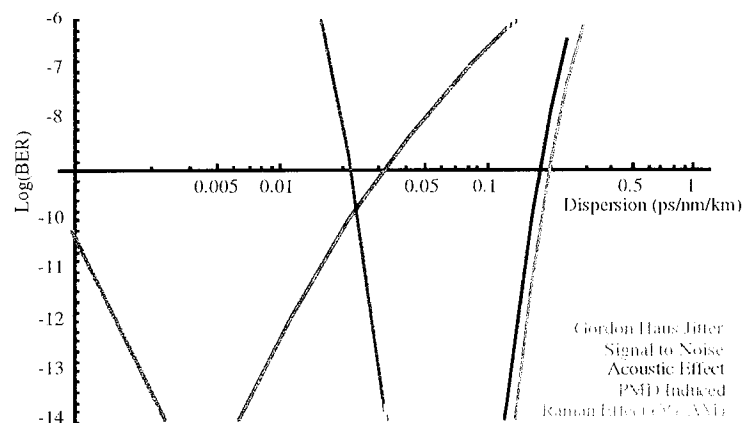


Figure 2-6 Illustration of the relative impact of various jitter sources in a 4000 km 40 Gbit/s transmission system. Parameters as described for the system below, but with a PMD of 0.1 ps/√km.

2.3 Systems Impairments of OTDM systems

The above discussion allows a rudimentary evaluation of the performance of a single channel optical communication system. However, with optical multiplexing techniques, further factors must be taken into account. In a WDM system for example, crosstalk is generated in the transmission fibre from four wave mixing and Raman scattering, and in the terminals from incomplete demultiplexing. To calculate the error ratio performance of any given OTDM system, it is of course necessary to determine the incidence of errors due to amplitude noise, jitter and intersymbol interference as described above, or by other means. However, slight modifications are immediately imposed by the presence of the demultiplexer. For example, in the case of signal to noise ratio, the demultiplexer rejects some of the noise as well as unwanted signals resulting in an improvement in receiver sensitivity⁶⁶.

In terms of timing jitter a pulse can in principle be jittered to the extremes of the demultiplexer switching window and still be passed through to the electrical detector. The band-limiting effect of the receiver (operating at the base rate) will integrate the jittered pulse such that it can be detected without an error occurring, due to the larger jitter tolerance of the low bit rate receiver. Of course, once a soliton has jittered out of the OTDM demultiplexer acceptance window an error will result from the loss of the pulse. In practice the actual shape of the demultiplexer switching window results in an effective conversion from phase noise (jitter) to amplitude noise⁶⁷. Consequently OTDM systems should be designed with the demultiplexer switching window setting the allowed rms. timing jitter of the system. This being so the demultiplexer defines the pulse arrival time within a restricted range, and no further errors from jitter would be anticipated.

In addition to these traditional system impairments (jitter, intersymbol interference and signal to noise ratio), the multiplexing and demultiplexing of the optical signals is liable to lead to finite levels of cross talk between the various OTDM channels^{68,69,70}. These effects are discussed below.

2.3.1 Demultiplexer performance

For a demultiplexer, where incomplete rejection of the unwanted channels leads to crosstalk, two types of degradation are present. Firstly, the unwanted signals contributes to the total power of the signal incident upon the receiver (reducing the proportion that is actually wanted data) and simultaneously reduces the eye opening⁷¹, and hence a simple power penalty is recorded at this point (i.e. at the input to the opto-electronic receiver). The demultiplexed receiver sensitivity is degraded by

$$\Delta P_{(dB)} = 10 \text{Log}_{10} \left(\frac{P_i + \sum_{k \neq i} P_k}{P_i - \sum_{k \neq i} P_k} \right) \quad \text{Equation 2-39}$$

Where $\Delta P_{(dB)}$ represents the penalty (in dB) P_i the signal power after demultiplexing and P_k the power of the unwanted channels after demultiplexing. It is useful to write this equation in terms of a “signal to crosstalk” ratio (SXR). In this case the penalty becomes ;

$$\Delta P_{(dB)} = 10 \text{Log}_{10} \left(\frac{SXR + 1}{SXR - 1} \right), SXR = \frac{P_i}{\sum_{k \neq i} P_k} \quad \text{Equation 2-40}$$

In order to ensure a penalty of less than 0.5 dB, the signal to crosstalk ratio should exceed 12.4 dB. Secondly, in addition to simply reducing the eye opening the unwanted data channels may interact with any optical noise originating from optical amplifiers, irredeemably reducing the error ratio of the system (i.e. worsening any error floor). This is especially true for an ideally band-limited receiver where each pulse (and its associated noise) is spread over the entire bit interval. In particular, since the eye opening is reduced in line with the signal to cross talk ratio, the optical signal to noise ratio will be similarly degraded. Furthermore, additional noise terms are introduced as a

consequence of beat noise between the unwanted channels and the spontaneous emission, again in line with the signal to crosstalk ratio, and from shot noise from the unwanted channels. Consequently the signal to noise ratio (neglecting receiver thermal noise, spontaneous-spontaneous beat noise and spontaneous shot noise and the effect of the demultiplexer on spontaneous emission powers) becomes

$$\begin{aligned}
 SNR_{elect} &= \frac{P_{sig}(1 - SXR^{-1})}{2h\nu\Delta f_{electt}(1 + SXR^{-1}) + 4P_{spont}(1 + SXR^{-1}) \frac{\Delta f_{electt}}{\Delta f_{opt}}} \\
 &= \frac{P_{sig}}{2h\nu\Delta f_{electt} + 4P_{spont} \frac{\Delta f_{electt}}{\Delta f_{opt}}} \cdot \frac{SXR - 1}{SXR + 1}
 \end{aligned}
 \tag{Equation 2-41}$$

From which we, unsurprisingly, deduce that the signal to noise ratio (and consequently the level of any error floor) is degraded exactly in line with the demultiplexer penalty. A finite demultiplexer extinction ratio will thus result in both a direct X dB receiver sensitivity penalty and a further X dB degradation in the apparent signal to noise ratio, with an associated additional penalty.

2.3.2 Multiplexer performance

For a multiplexer, incoherent interference between channel “i” and the other channels may become critical, and the signal to noise ratio after demultiplexing must be calculated allowing for the temporal overlap of the pulses. Four different classes of multiplexer must be considered, characterised by the overall path length L_{mux} , and absolute path length differences ΔL_{mux} . Note that whilst it is necessary that each path length difference ensures that each channel is inserted into the correct time slot, there are no restrictions as to the absolute lengths. Indeed the path length differences may be several ns long.

- a) $\Delta L_{mux} >$ Source coherence length. Under these conditions, penalties arise from incoherent interference between different channels where ever temporal overlap occurs.
- b) $\Delta L_{mux} <$ Source coherence length $< L_{mux}$. In this case, interference still occurs, but is coherently, producing extinction ratio penalties, but not error floors. Furthermore, unless the system is absolutely stable, this extinction ratio penalty will vary slowly with changes in path length differences causing drifts between constructive and destructive interference.
- c) $L_{mux} \ll$ Coherence length. With particularly short optical path lengths, it should be possible to produce a stable multiplexer with well defined, stable interference characteristics, producing static extinction ratio penalties.
- d) Each channel is of a slightly different centre wavelength (as would be the case for a drop and insert node). In this case, a static extinction ratio penalty would be produced. However, it would be almost impossible to guarantee that the wavelengths were not the same, in which case, the conditions of case (a) would be replicated.

Of these cases, (a) is most representative of interleavers fabricated from pigtailed components, whilst (c) would be an ideal target for an integrated device. Note that attempts to simulated case (c) without the inclusion of independent electro optic modulators (passive interleaver) would produce OTDM data patterns with very little de-correlation of the respective PRBS test patterns. In extreme cases, the OTDM data pattern may actually represent an N pulse per bit base rate transmission system, totally obscuring all aspects of the OTDM system other than the pulse transmission characteristics. Within this thesis, all OTDM sources are constructed as case (a or d) The resultant signal to noise ratio (after opto electronic conversion) of channel i (SNR_i) in the case of incoherent interference (cases a and d) is given simply by ;

$$SNR_i = \frac{\int P_i(t).dt}{\sum_n \sum_{m \neq n} \int \sqrt{P_n(t)P_m(t)}.dt} \quad \text{Equation 2-42}$$

where $P_j(t)$ represents the time dependence of the power of channel “j” after demultiplexing. Equation 2-42 dictates the pulse width required for a given crosstalk level when multiplexing ideal signals together, and the level of background radiation from a practical source which may be tolerated. However, the integrals depend directly upon the demultiplexer switching window and it could be envisioned that the pulse requirements would vary acing to the demultiplexer technology employed. In general two values of signal to noise ratio are of interest: 15.8 dB (giving an error ratio of 10^{-9} for comparison with experimental results), and 18 dB (giving an error ratio of 10^{-15} for system design, and to ensure negligible penalty). Note however, that when calculating the performance of a system, both multiplexer and demultiplexer degradations must be taken into account simultaneously, along with the influence of pulse dispersion, jitter and spontaneous emission. For example, error ratio floors from incoherent interference and degradations in optical signal to noise ratio should be added together, whilst any calculation of demultiplexed signal powers should take account of the full characteristics of the source, demultiplexer and jitter added by the transmission line.

2.3.3 System Specification

Using the formalism described above, it is possible to derive a basic system specification for an arbitrary OTDM system, and to verify the performance of specific systems. Consider for example an N_{ch} channel OTDM system with sech squared signal pulses whose FWHM is 12% of the bit period T and a peak to background extinction ratio of X_{Tx} and a raised cosine demultiplexer whose FWHM is 40% of the bit period, and a maximum extinction ratio of X_{demux} . The extinction ratio requirements are quite strict and this example is particularly illustrative. Assuming a demultiplexer extinction ratio of 40 dB, Figure 2-7 illustrates the error ratio performance of 4, 8 and 16 channel OTDM systems as a function of the extinction ratio of the base rate pulses. We would anticipate the system to be limited by incoherent interference between the OTDM channels.

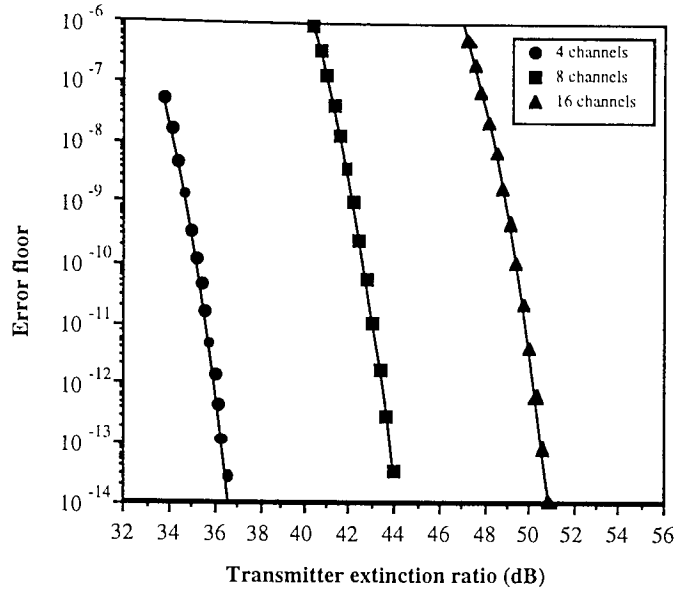


Figure 2-7 Theoretical performance of an N channel OTDM system as a function of the extinction ratio of the transmitted pulses. Solid lines drawn as a guide to the eye.

These results illustrate the rapid deterioration in performance usually associated with incoherent interference effects, with significant error floors appearing with only a few dB change in extinction. As we would expect, the required extinction ratio for a given error floor varies according to $20 \log_{10}(N_{ch}-1)$, and for a four channel system, a minimum extinction ratio of 38 dB is required.

Figure 2-8 illustrates the variation in penalty arising from the finite extinction ratio of the demultiplexer in a 4 channel system, assuming an extinction ratio of 40 dB for the transmitted pulses. In this figure, the double logarithmic scale, used to illustrate the curve fit, disguises the rapid deterioration in receiver sensitivity below an extinction ratio of 15 dB. A value of some 20 dB or more is required to ensure a negligible demultiplexer penalty in a 4 channel OTDM system.

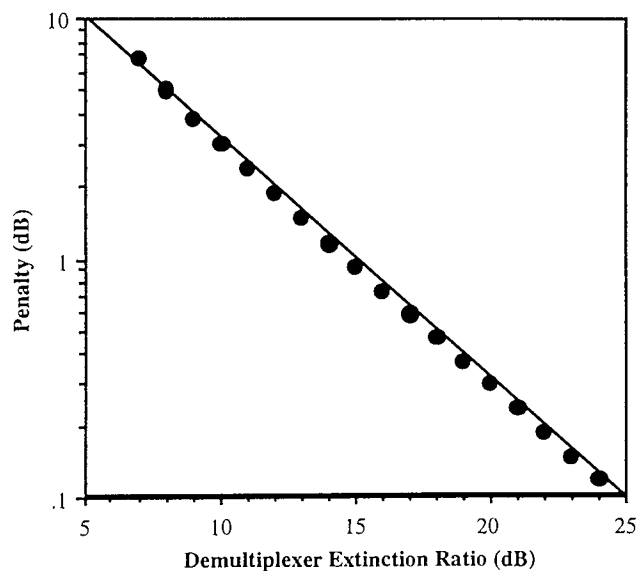


Figure 2-8 Theoretical variation in receiver sensitivity penalty as a function of demultiplexer extinction ratio for a four channel OTDM system. Solid line drawn as a guide to the eye.

For pulse widths, and demultiplexer switching window, the limitations are not as clear cut, with the performance for a particular pulse width dependant upon the specific temporal profile of the demultiplexer. Some examples are discussed in the following chapter and suggest that for a 40 Gbit/s system, the pulse width should be less than 8 ps, whilst the demultiplexer switching window should be somewhat less than 15 ps. Table 1 summarises the outline specification of an OTDM system with these considerations in mind.

System Parameter	Specification
Transmitter Extinction Ratio	$28.5 \text{ dB} + 20 \text{ Log}_{10}(N_{ch} - 1)$
Transmitter Pulse Width	< 33% of bit period
Demultiplexer Extinction Ratio	$15.0 \text{ dB} + 10 \text{ Log}_{10}(N_{ch} - 1)$
Demultiplexer Switching Window	< bit period - 2 minimum rise time

Table 2 System specification for OTDM terminal equipment comprising N_{ch} OTDM channels.

2.4 Chapter summary

In this chapter we have reviewed the fundamental properties of pulse transmission using optical fibres and ideal optical amplifiers. This allows the performance of simple communications links to be predicted analytically, provided that one impairment dominates the system. However, where several impairments are of equal importance, a more numerical approach is required, in extreme cases requiring a full numerical solution of the non-linear Schrodinger equation. The particular case of optical solitons were also considered, where analytical solutions may be found for a much broader range of system configurations due to the fundamental balance of dispersion and non-linearity, and the particle like nature of the optical solitons. This analytical approach enables the construction of detailed "design diagrams" and accurate calculation of the error rate performance of the system. Typically the feasibility of a system, and the optimum implementation strategy would be examined using variants of the design diagram, whilst the performance of a given system would be verified through error ratio calculations.

In the final section this standard theoretical treatment has been applied to the specific case of OTDM systems, and a generic OTDM system specification has been defined. In particular it was asserted that, large penalties may be anticipated from incoherent interference for pulses with poor extinction ratio's or excessive temporal width. These penalties are of course minimised using stable planar integrated multiplexers, whereby rather than producing interferometric noise, the overlap of pulses simply produces static degradations in the eye closure (or extinction ratio penalties). However, care must be taken in the interpretation of results taken using a single data modulator followed by a physically short passive optical interleaver, since identical performance may only be obtained using a similar interleaver comprising the appropriate number of independent data modulators. Furthermore, design rules for the development of demultiplexers have been presented, placing a minimum bound on the extinction ratio of such devices in

order to avoid excessive penalties. Whilst unlikely to directly produce error floors, a poor extinction ratio will exaggerate any low level error floor through an increase in noise terms. Again, the detrimental effects of a poorly designed demultiplexer may be inadvertently avoided by the construction of a passive OTDM interleaver with relative delays of less than a few bit periods which do not sufficiently decorrelate the data patterns. In an extreme case an N channel OTDM system constructed with an interleaver whose maximum differential delay is less than a bit period results in a N pulse per bit signal at the base rate.

3. OTDM Transmitters

In this chapter we describe the options for the OTDM transmitter in some detail. Two distinct transmitter configurations have been investigated. The first, traditional^{18,69}, implementation of OTDM (Figure 3-1) relies on a single high quality pulse source operating at the base rate (eg 10 Gbit/s) with a very low duty cycle. This base rate source may then be encoded with data in the usual manner (once for each time slot), before interleaving to form an OTDM data stream. However, as we have seen in chapter 2, the source specification is quite demanding. In addition to low duty cycles, an extremely high extinction ratio is required for stable multiplexing, whilst good spectral and temporal characteristics are essential for optimised transmission performance. These requirements have in general lead to the use of advanced erbium doped fibre ring lasers for soliton transmission experiments, although less complex sources may be used for processing applications.

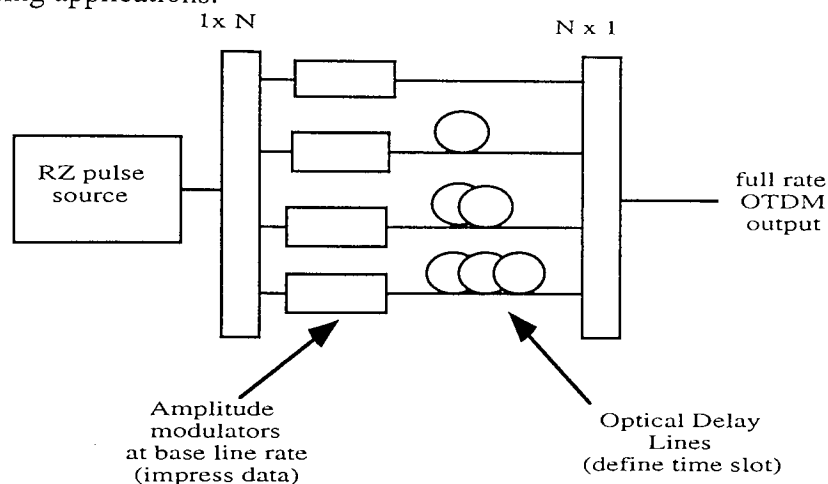


Figure 3-1 Conceptual diagram of OTDM Transmitter, illustrating the functions of pulse generation, parallel data encoding and interleaving. Taken from figure 1.1.

An alternative approach has been investigated where high quality soliton pulse trains are generated at the overall line rate (eg 40 GHz) using a Mach Zehnder modulator and a dispersion profiled fibre circuit. This source fundamentally generates pulses of the correct spectral and temporal quality, and optical interleaving is not required. The natural affinity of this technique to higher line rates (> 100 Gbit/s) suggests that this form of pulse generation holds great promise for the highest capacity point to point links. However, this approach is unlikely to be employed at line rates accessible to electronics, and thus necessitates the development of all optical data encoding techniques *a-priori*.

In this chapter the fundamental building blocks of a traditional OTDM transmitter will be discussed in turn, namely picosecond pulse generation, data modulation and interleaver construction. Finally, the alternative approaches to OTDM data generation will be discussed.

3.1 Picosecond Pulse Sources

The most critical component within an OTDM system is the source of picosecond optical pulses, which must have an appropriate duty cycle and extinction ratio to allow multiplexing and demultiplexing operations. Prior to the commencement of this thesis, two pulse sources were routinely used, namely mode locked semiconductor⁷² and erbium fibre ring lasers⁷³. Whilst the former produces, upon linear compression, adequate pulses for driving 40 Gbit/s all optical gates, the pulse quality is in general insufficient to allow the successful operation of theoretically optimised transmission systems⁷⁴. In this case, the fibre ring laser was deployed as a source of transform limited pulses. The suitability of a pulse source is assessed in terms of its temporal pulse width, its spectral width (and associated time bandwidth product), timing jitter, extinction ratio and wavelength stability. These parameters may be accurately determined using standard measurements techniques and a high speed sampling oscilloscope, an autocorrelator, an optical spectrum analyser, an RF spectrum analyser, a self homodyne interferometer and a high speed photodiode.

Source Type.	Traditional limitations.	Contribution of thesis.
Gain Switched DFB.	Jitter. Pulse Quality. Pulse Width.	Jitter reduction technique. Direct generation of <3 ps pulses.
Mode Locked ECL.	Chirp.	None
Fibre Ring Laser.	Complexity.	Development of optically mode locked ring laser.
Electroabsorption modulator.	Extinction Ratio. Pulse Width.	Cascaded for 40 & 80 Gbit/s interleaving. Lowest reported duty cycle. Simultaneous pulse generation and data encoding. Multiple wavelength operation.

Table 3 Picosecond pulse sources investigated in the thesis, and contributions made.

In addition to the continued development of these sources, which will be described briefly below, several other options were considered for either simplicity and ease of use or potentially enhanced performance. The options considered in this thesis, and the developments achieved are summarised in Table 3. Following a description of these sources, soliton pulse compression is examined as an appropriate method of increasing flexibility of the pulse sources. Various other proposed sources are then discussed taking into account the stringent limitations of OTDM systems, and the section will be concluded with a critical assessment of source options. Initially however, due to its almost ubiquitous presence in the pulse sources described below, pulse compression through linear chirp compensation is discussed.

3.1.1 Linear Compression

We saw in chapter 2 that a gaussian pulse propagating in a dispersive fibre will be temporally broadened on a length scale known as the dispersion length. As the pulse temporally broadens without change in spectral width, it acquires chirp, that is, the instantaneous frequency differs from the central frequency across the pulse. It can easily be shown that the instantaneous frequency for a gaussian pulse is given by²⁴;

$$\delta\omega(t) = \frac{2 \left(\frac{\beta''z}{[\tau_{FW}/1.665]^2} \right) t}{1 + \left(\frac{\beta''z}{[\tau_{FW}/1.665]^2} \right)^2} \quad \text{Equation 3-43}$$

from which we observe that the frequency varies linearly across the centre of the pulse. This condition is known as linear chirp. This chirped pulse may of course be compressed back to its original pulse width by propagation through a fibre of equal magnitude but opposite sign, dispersion. This, in essence, is the principle of linear chirp compression⁷⁵ used for semiconductor based pulse sources. In this case, the pulse is initially chirped, not through propagation in fibre, but from dynamic changes in the semiconductor refractive index. However, provided the chirp is linear, the pulse will behave as if it was chirped through fibre propagation. Describing the chirped gaussian pulse by;

$$P(t) = P_{peak} \exp \left\{ -1.665^2 (1 + iC) \frac{t^2}{\tau_{FW}^2} \right\} \quad \text{Equation 3-44}$$

where C represents the degree of chirp, and is given, in terms of measurable pulse parameters (spectral width $\Delta\omega$ and spectral width if the pulse were transform limited $\Delta\omega_{TL}$) by;

$$C^2 = \left(\frac{\Delta\omega}{\Delta\omega_{TL}} \right)^2 - 1 \quad \text{Equation 3-45}$$

we find that the evolution of the pulse width is given by;

$$\frac{\tau_{out}}{\tau_{in}} = \sqrt{\left(1 + C \frac{\beta''z}{(\tau/1.665)^2} \right)^2 + \left(\frac{\beta''z}{(\tau/1.665)^2} \right)^2} \quad \text{Equation 3-46}$$

which, in the case of zero chirp ($C=0$), reverts to Equation 2.9. Note that the chirp parameter C may take either sign, depending upon whether the leading edge of the pulse is blue shifted ($C > 0$) or red shifted ($C < 0$). Typically, for a semiconductor laser device with a finite population inversion, generated optical pulses are red shifted on leading edge. This leads to an optimum length of fibre to produce a transform limited pulse (whose temporal width is therefore determined by the input spectral width) of

$$z_{opt} = L_D \frac{|C|}{1 + C^2} \quad \text{Equation 3-47}$$

$$L_D = \frac{(\tau_{FW}/1.665)^2}{\beta''}$$

This behaviour is illustrated in Figure 3-2, where the normalised pulse width is plotted against transmission distance (in dispersion lengths) for a variety of chirp parameters C. Further verification may be found in Figure 3-9 below, where Equation 3-46 was used to plot the theoretical curve, and by the many experimental pulse sources, where the appropriate length of compression fibre was estimated using Equation 3-47. It is

interesting to note that the maximum possible compression fibre length is half of the dispersion length of the pulse, corresponding to a compression factor of $1/\sqrt{2}$. In order to achieve greater compression factors, proportionally less compression fibre is required (to a first approximation).

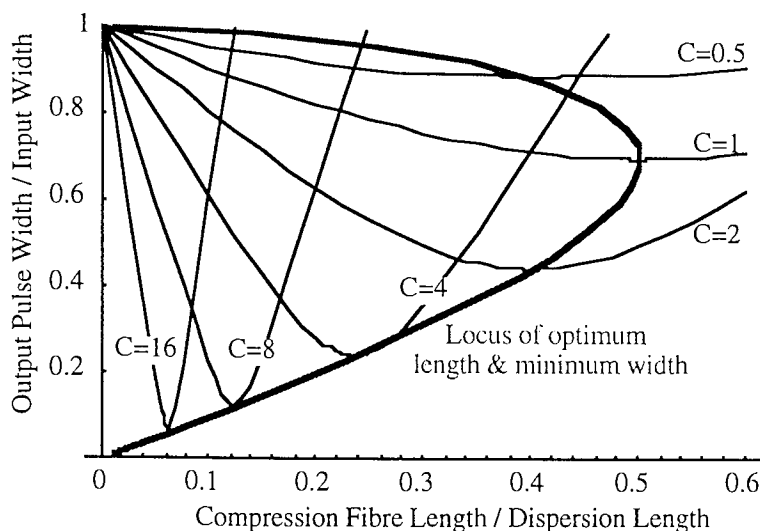


Figure 3-2 Illustration of the effect of compression fibre on a chirped gaussian pulse as a function of the degree of chirp.

3.1.2 Gain Switched DFB

It is well known that short optical pulses may be obtained by applying a high power RF signal to a DFB laser biased close to threshold, and that this represents perhaps the simplest form of optical pulse source^{76,77,78}. However, it is also well known that the spontaneous emission process that seeds each gain switched pulse produces both timing and wavelength jitter^{78,79}. The rms timing jitter is typically around 7 ps and uncorrelated, making such sources useless for high speed OTDM applications. In this section, a simple feedback technique is described which reduces the jitter to acceptable levels, allowing the use of gain switched DFB lasers in OTDM systems to be contemplated. The generation of low jitter 6 ps pulses following linear compression^{80,24} is then described, and techniques for the generation of shorter pulses are indicated.

3.1.2.1 Jitter Suppression of Gain Switched DFB's

The high power sine wave drive applied to a DFB laser produces a corresponding variation in the population inversion within the device. Once the population inversion is sufficient, photons generated previously by spontaneous emission are amplified, rapidly depleting the carrier density by the stimulated emission process. Consequently, short optical pulses are generated, globally timed by the driving frequency, and constrained in wavelength by the laser grating. However, on a pulse to pulse basis, the exact wavelength an emission time of each pulse is determined by the spontaneous emission process. The exact magnitude of the jitter is dependant upon the carrier lifetimes/recovery rates and upon the relative drive signal amplitude and frequency, however, in order to eliminate it, the spontaneous emission must be controlled.

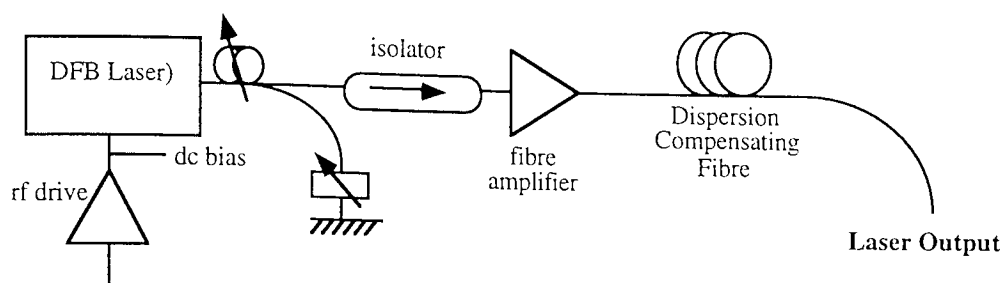


Figure 3-3 Schematic diagram of jitter suppressed gain switched DFB laser

A schematic diagram of a jitter suppressed gain switched DFB is shown in Figure 3-3. By feeding back part of a previously generated pulse into the DFB laser, at the appropriate time, instead of being seeded from spontaneous emission, each gain switched pulse is seeded by an earlier pulse, vastly reducing fluctuations in wavelength and timing jitter. The excellent performance of this technique to suppress spectral (Figure 3-5) and temporal jitter enables the use of gain switched DFB lasers in practical OTDM systems⁸¹. This approach, known as reflective self seeding⁸² and originally developed for Fabry Perot lasers, is closely analogous with mode locking. Two types of high speed DFB laser we tested for gain switching in this configuration, with centre wavelengths in the region of 1545 nm and 1563 nm. All the devices had threshold currents between 21 and 35 mA and 3 dB bandwidths between 7 and 12 GHz (increasing with increasing bias current) dominated by the device relaxation oscillation frequency.

When operated at low frequencies (2.5 and 5 Gbit/s) with no feedback, as expected gain switched operation was obtained at 1563 nm when the DFB was biased near threshold. However, when driven at 10 GHz it was necessary to increase the bias current by 20% to approximately 50 mA. Even so, although the device gain switched producing a spectral width in excess of 1 nm, the output signal comprised a train of 5 GHz pulses (see Figure 3-4, note that the “eye diagram” effect, top left hand corner, arises simply because the scope is triggered at 10 GHz). This may be anticipated from the device characteristics⁷⁷ whereby the carrier density has insufficient time to recover to the appropriate level between cycles of the drive frequency. Note the corresponding presence of strong 5 GHz components within the RF spectrum. Whilst clearly of little use as a pulse source, a device operated in this regime may find applications in high speed clock division. Upon a further increase of the dc bias level to above 63 mA, good quality gain switching was obtained producing 11 ps pulses with a spectral width of 1.06 nm and an rms timing jitter less than 1.8 ps (measurement limited by sampling scope). In this high bias current regime, the timing jitter has reduced significantly, albeit accompanied by a high proportion of background radiation. Whilst such a pulse source may be used in a short multiplexer⁸³ (type c), use with any practical multiplexer, excepting a fully integrated modulator array⁸⁴, is precluded by incoherent interference.

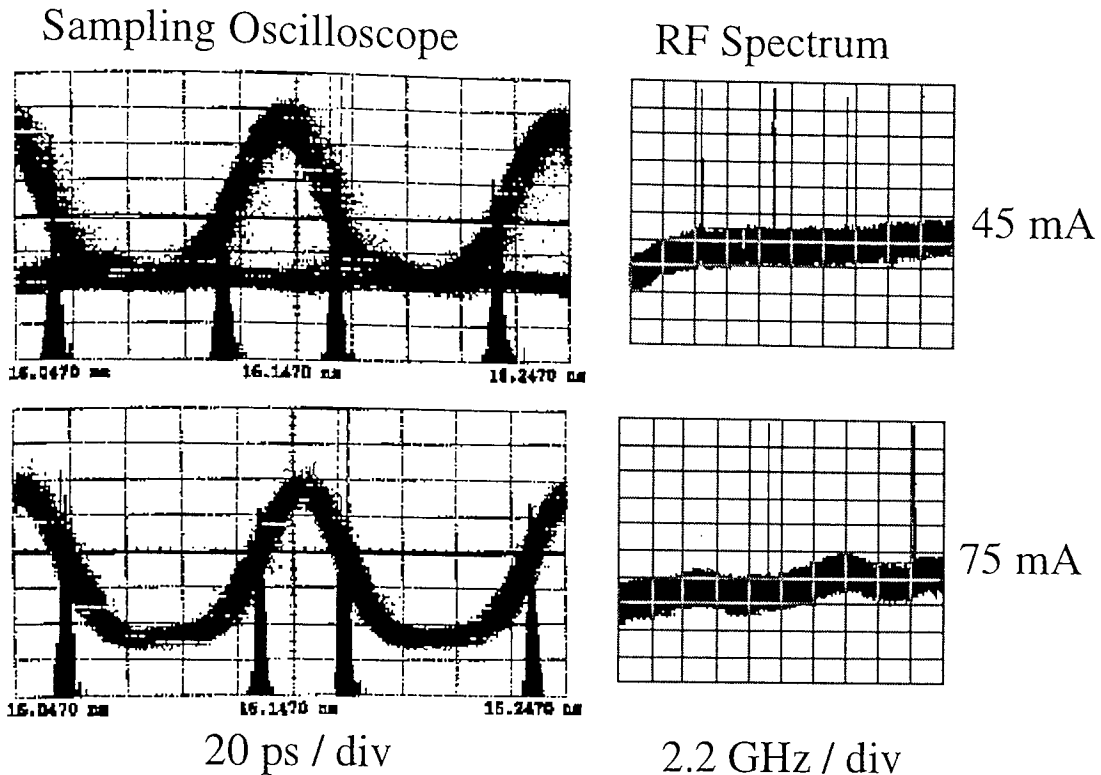


Figure 3-4 Temporal and spectral output of simple gain switched DFB in low and high bias regimes. Histograms for measurement of temporal jitter also shown.

The application of an optimised level of feedback (typically ≈ -8 to -14 dB) allowed 10 GHz operation of the device with a dc bias much closer to the threshold current, producing 16 ps pulses with a 0.43 nm spectral width, a resolution limited jitter of 2.2 ps, and a low level of background radiation. However, in this case as the bias current was increased, competition between gain switching and mode locking lead to the formation of multiple pulses and a rapid degradation on the device performance.

3.1.2.2 Pulse width optimisation of gain switched DFB's

Similar results were obtained using the 1545 nm device and this device was used to assess the effect of applied RF power, linear compensation of pulse chirp and the suitability of the source for 40 Gbit/s OTDM systems. Typical spectral outputs obtained with this device are shown in Figure 3-5, with and without reflective self seeding. Jitter in the carrier frequency is clearly evident from the un seeded spectra (left) due to the smearing of the modes, whilst strong modes spaced at the driving frequency for self seeded pulses indicate a high degree of coherence between individual pulses (right). Under these conditions, it was possible to obtain temporal jitters wholly attributable to the RF source (<500 fs) with a feedback level of -14 dB and a dc bias current of 45 mA.

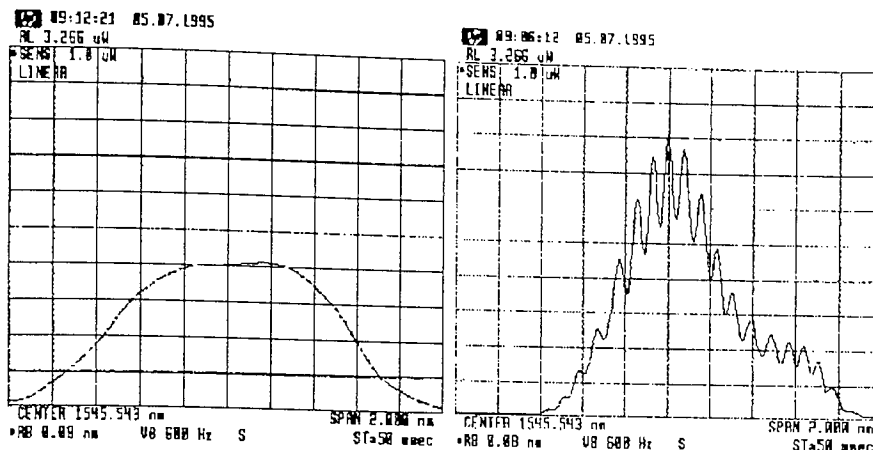


Figure 3-5 Spectra of Gain Switched DFB Pulses with (right) and without (left) reflective self seeding, illustrating pulse to pulse wavelength jitter by the smearing of the modes without jitter suppression.

Figure 3-6 illustrates the variation in pulse spectral and temporal widths as a function of the applied RF power (measured into a 50Ω load) with a constant bias current of 45 mA. The time bandwidth product remained approximately constant, with a value in the region of 0.95 (assuming gaussian pulses) and indicating considerable chirp, and gain switching was clearly observed for RF power levels in excess of 25 dBm ($\approx 12.6 V_{p-p}$). Significantly, neither spectral width or temporal width shows any evidence of reaching a limiting value, thus offering the promise of enhanced performance with correctly impedance matched, higher power drive circuitry.

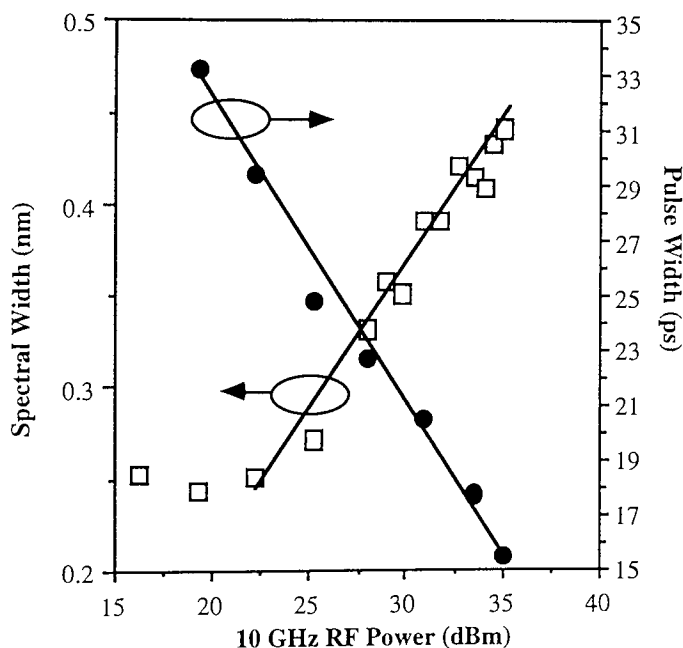


Figure 3-6 Dependence of output spectral and temporal widths of Gain Switched DFB Laser as a function of RF drive power at a fixed dc bias current of 45 mA.

To produce sufficiently short pulses, linear compensation of the pulse chirp was investigated⁸⁰. This was achieved using fibre with a (non soliton supporting) dispersion coefficient of $D = -38 \text{ ps/nm/km}$. The results are illustrated in Figure 3-7 where the output pulse width is plotted against the net measured group delay of the fibres used. A third order polynomial fit to the data is also shown as a guide to the eye. At the optimum fibre length (Group delay -18 ps/nm), a pulse width of 6.3 ps was achieved,

and the spectral width remained un-altered at around 0.5 nm, giving almost transform limited gaussian pulses (time bandwidth product of 0.4).

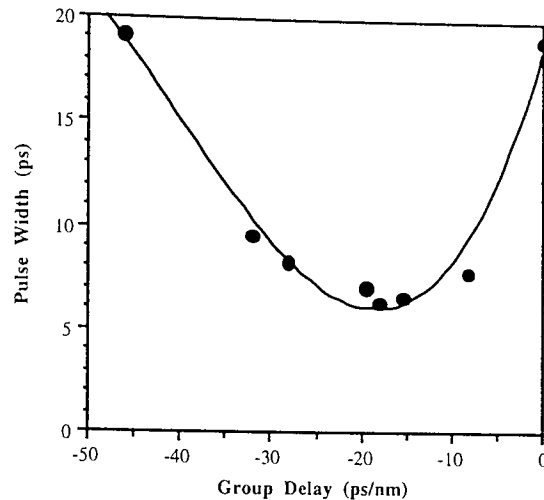


Figure 3-7 Compression of gain switched DFB output using normally dispersive fibre to compensate for linear chirp.

Pulses so produced (<8 ps width, low jitter and background free) are certainly excellently suited to driving intensity dependant all optical switches, where the non ideal pulse spectrum is unlikely to deteriorate the system performance^{81,85,86}. However, for use in transmission systems, further processing is required to reduce the non-linear chirp and reduce the inevitable generation of dispersive wave radiation from any subsequent soliton transmission line^{87,59}. Further optimisation of the source would enable the practical and wide spread use of such devices within optical processing nodes. Indeed, recent developments suggest that injection locking may be a suitable technique for jitter reduction^{77,88,89} whilst higher RF drive powers and tuned fibre grating chirp compensation techniques^{90,91} would enable the quality of the optical pulses to be improved.

3.1.2.3 Benefits of high FM efficiency

It is interesting to note that whilst the minimum uncompressed pulse width obtainable from a gain switched DFB is dependant upon the RF drive conditions (amplitude and pulse width) and the laser slope efficiency (mW/mA) and relaxation oscillation frequency, the actual useable pulse width after compression is clearly dominated by the degree and linearity of the available chirp, which is more directly related to the FM efficiency of the laser. In order to verify this assumption a, low speed, high FM efficiency Hitachi DFB laser was investigated for pulse production at 2.5 GHz. The dc characteristics of this device are contrasted with the high speed DFB lasers used above in Figure 3-8.

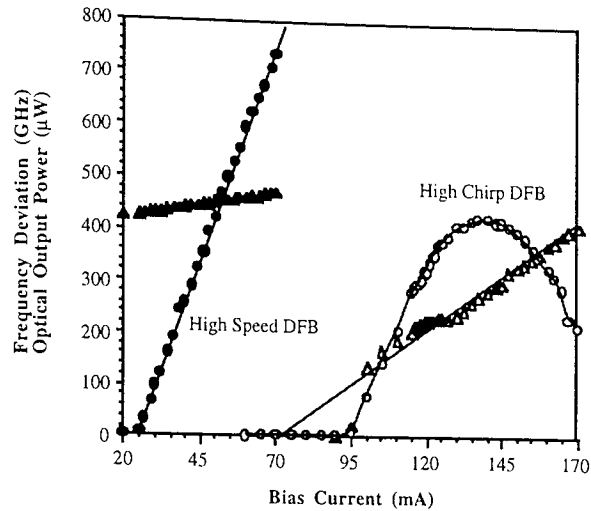


Figure 3-8; D.C. output power (circles) and optical frequency (triangles) characteristics of high speed (filled symbols) and high FM efficiency DFB's (open symbols).

Clearly, although complicated in terms of slope efficiency, the FM efficiency is increased significantly from 0.87 GHz/mA to approximately 4.2 GHz/mA. This in principle should result in highly chirped pulses, suited to linear compression in normally dispersive fibre. When biased at threshold and modulated with a 2.5 GHz, +27 dBm RF signal, 25 ps pulses were produced with a spectral width of 0.8 nm (time bandwidth product of 2.5).

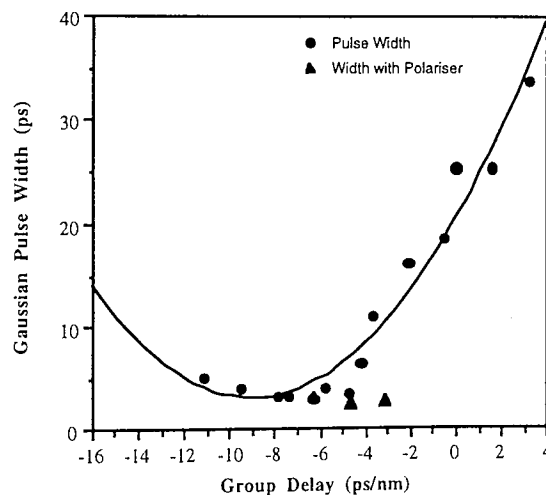


Figure 3-9; Compression of pulses from a high FM efficiency DFB gain switched at 2.5 GHz by linear chirp compensation.

This compares to a typical time bandwidth product of ≈ 0.95 for the high speed devices. From the view point of FM efficiency alone, and all other things being equal, we would expect the time bandwidth product to increase by a factor of 4.8, comparing favourably with the observed value of 3.1. As shown in Figure 3-9 a minimum pulse width of 2.9 ps was obtained upon subsequent compression in normally dispersive fibre, for a group delay of -6.3 ps/nm. The resultant time bandwidth product of 0.29 suggests that the complicated spectral structure has led to the formation of highly chirped non gaussian pulses. This figure also shows that slightly shorter pulses (2.6 ps) may be obtained, if a polariser is placed after the chirp compensation fibre, whereby some of the non-linear

chirp in the spectral wing of the pulses is spectrally filtered⁹² through a combination of PMD and the action of the polariser.

In summary, we have seen how a simple pulse source, producing unsuitable highly chirped and jittered pulses may be transformed into a low jitter, background free source of pulses wholly suited to use in 40 Gbit/s OTDM processing systems. This is achieved by the controlled reflection of pulses back into the laser to control jitter, and the application of normally dispersive fibre to compress the pulses by compensating for the linear chirp. We have also seen how large FM efficiencies will allow a greater control of the pulse widths, giving the potential of operation at significantly higher bit rates (eg 100 Gbit/s).

3.1.3 Mode Locked External Cavity Lasers

It is similarly well known that short optical pulses may be obtained from a mode locked semiconductor external cavity⁷² (Figure 3-10). Indeed many commercially available external cavity lasers may now be mode locked. The laser cavity is formed between the front facet of a semiconductor device and a bulk optic diffraction grating positioned behind the rear facet. The grating provides wavelength tuning and optical feedback of an appropriate spectral bandwidth for the desired pulse width (determined by the grating pitch and the spot size). A typical output from one of the mode locked lasers used throughout this thesis is shown in Figure 3-11. When correctly aligned, pulse widths from 15 ps (no pulse compression) to as short as 4.2 ps (maximum RF drive power and linear chirp compensation^{93,94}) have been obtained over the entire erbium amplifier window, with jitter levels determined by the electrical drive signal only.

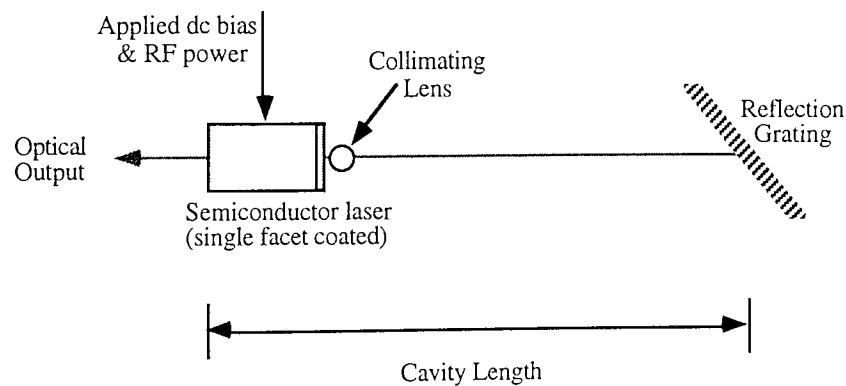


Figure 3-10 Schematic diagram of an external cavity semiconductor mode locked laser (EC-MLL).

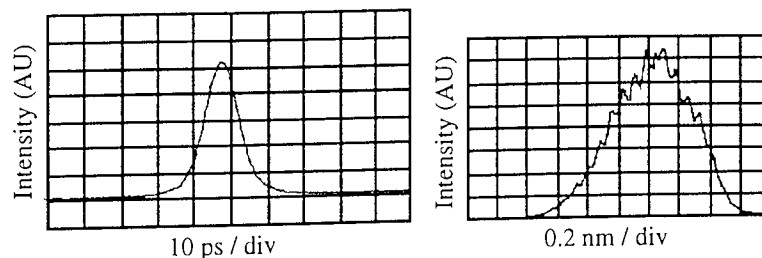


Figure 3-11; Typical output of mode locked semiconductor external cavity laser, showing autocorrelation (left) and optical spectrum (right).

A significant advantage of a mode locked laser, is that the extinction ratio (pulse amplitude to background level) is guaranteed to be high. The source is easily tuneable in terms of pulse width, repetition frequency and wavelength. Recent advances in mode locked laser technology include the incorporation of a saturable absorber⁹⁵ or electro absorption modulator⁹⁶ within the laser cavity, enabling the generation of significantly shorter pulses.

3.1.4 Mode Locked Fibre Ring Lasers

3.1.4.1 Electro-optic modulator based ring lasers

Perhaps the highest quality pulses obtained to date have been generated using mode locked fibre ring lasers^{97,98}. Such sources produce transform limited pulse trains of particularly high quality and have been used as the main pulse source for countless soliton and OTDM experiments. A typical laser cavity is shown in Figure 3-12. Note that the cavity length is rather long (typically in excess of 100 m) resulting in the necessity to develop cavity length stabilisation schemes⁹⁹ and techniques to prevent mode competition^{100,101,102,103,104,105,106} when harmonic modulation is employed to obtain 10 GHz pulse trains.

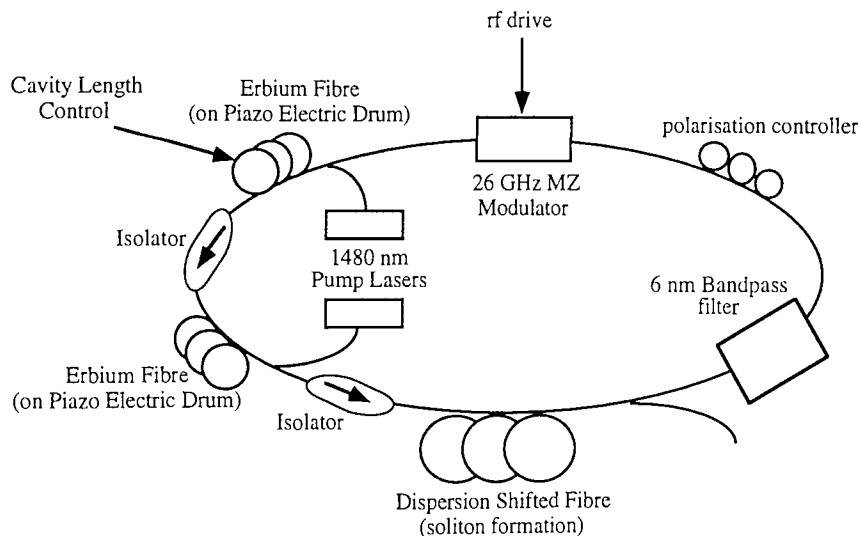


Figure 3-12 ; Schematic diagram of typical erbium fibre mode locked ring laser

During the course of this thesis, existing fibre ring lasers have been modified to produce shorter pulses and higher frequency pulse trains. In order to reduce the pulse width from 6 ps to as short as 3 ps at 10 GHz and 4.5 ps at 20 GHz, the amplifier output power has been increased and the length of dispersion shifted fibre re-optimised for stable soliton propagation within the cavity for these pulse widths. Initially, a cavity filter with a spectral width of 5 nm was employed to allow the formation of shorter pulses within this modified cavity, in accordance with standard mode locking theory¹⁰⁷. However, due to the presence of polarisation mode dispersion within the non polarisation maintaining cavity, the laser would support two distinct polarisation states with slightly different central wavelengths. Whilst it was possible to carefully align the cavity to allow for only one polarisation mode to oscillate, the long term stability of the

laser was adversely affected by any minor change of the cavity polarisation. Consequently, the cavity filter bandwidth was reduced to 2.7 nm, surprisingly with little increase in pulse width (> 4 ps at 10 GHz), enabling excellent long term stability of the ring laser.

3.1.4.2 Ring laser cavity length stabilisation.

For this ring laser, the issue of cavity length stability was addressed in three ways; For ease of operation, and consistent pulse quality without user intervention, a phase locked approach was employed^{103,108,109}, whereby the drive frequency was matched to the drifting ring laser cavity length and stable operation over several weeks was possible. Where an exact operating frequency was required, cavity length stabilisation was employed, using a combination of piezo electric transducers and heat pumps to compensate for rapid and long term drifts respectively. Initially, the cavity length error signal was derived from the relative phase of the laser output and the RF drive signal⁹⁹ requiring the use of high speed RF electronics. Subsequently a technique proposed by NTT for polarisation maintaining cavities¹⁰⁴ was extended for use in non polarisation maintaining cavities¹⁰⁶. In both cases, the action of the control signal is to vary either fibre stress or temperature. Unfortunately this can have an adverse effect on the laser stability because of subtle changes in the intra cavity polarisation. In one implementation of the system, both erbium doped fibre, and dispersion shifted fibres were carefully wound on piezo electric drums, enabling cavity length control over several days, with less than 10 % variation in the output pulse width over the entire control range.

3.1.4.3 Optically mode locked ring lasers

In this thesis, in addition to developments of fibre ring lasers using Mach Zehnder modulators as the mode locking element, ring lasers based on all optical mode locking were also investigated^{110,111}. The schematic diagram of this configuration is shown in Figure 3-13. Initially 12.6 km of dispersion shifted fibre was used, in a configuration analogous to previous work¹¹². The main difference being the inclusion of a fibre polariser to provide additional AM in addition to the usual FM processes governing the dynamics of fibre ring lasers¹¹³. With no control pulses present, the ring laser will lase continuous wave as a fibre ring laser at the wavelength to which the bandpass filter is tuned. When driven by a regular stream of pulses (in this case derived from a 10 GHz harmonically mode locked external cavity laser, passively interleaved to 40 GHz where appropriate), at a frequency equal to a harmonic of the cavity resonance frequency (3.965 kHz in this case), a periodic frequency modulation (FM) is imposed on the recirculating light as it co-propagates with the injected pulses via cross phase modulation. The efficiency of this interaction is optimised by arranging for the fibre dispersion zero to lie halfway between the wavelength of the injected pulses and the recirculating light, such that the group velocities are nearly equal. Due to the natural birefringence of the fibre, the cross phase modulation is accompanied by non-linear polarisation rotation (Kerr effect), which is converted into amplitude modulation (AM)

by the fibre polariser. When correctly aligned, both FM and AM processes serve to mode lock the ring laser to the driving frequency, and a regular stream of transform limited optical pulses is obtained.

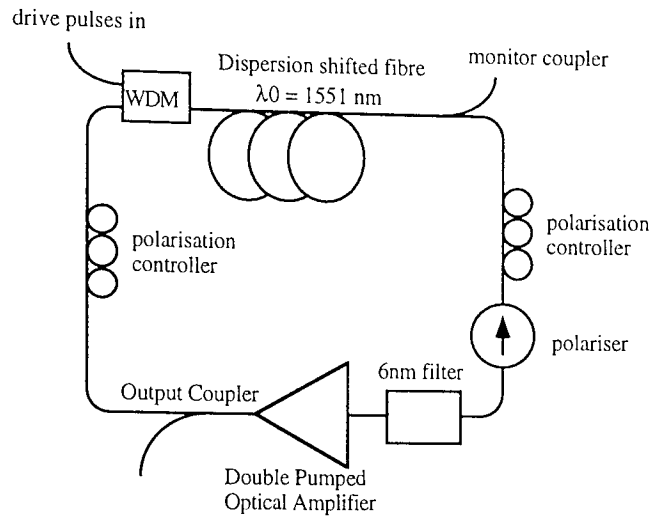


Figure 3-13 ; Schematic diagram of optically mode locked erbium fibre ring laser

The mode locking characteristics of this laser were investigated at frequencies up to 40 GHz. Pulse widths as short as 2.9 ps were achieved for a mean drive signal power of +13.8 dBm compared to the 5.5 ps achieved previously without the fibre polariser, resulting from changes in the mode locking conditions in accordance with the standard Kuizenga-Siegman mode locking theory¹⁰⁷, which predicts that the output pulse τ_{FW} width is proportional to

$$\tau_{FW} \propto \frac{1}{\sqrt{f_m \Delta f_{opt} \Delta m}} \quad \text{Equation 3-48}$$

where f_m is the effective modulation frequency (which we may take as inversely proportional to the driving pulse width), Δf_{opt} the intra cavity optical filter bandwidth and Δm the effective modulation depth.

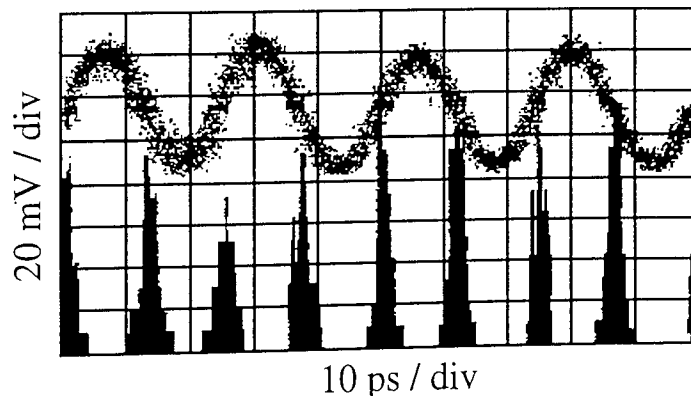


Figure 3-14 ; Typical output of FM mode locked ring laser when driven at 40 Gbit/s, illustrating a resolution limited rms timing jitter of < 1 ps.

In our case, this simple picture is clearly complicated by soliton effects within the laser, but the trends should be the same. In particular, increasing the filter width from 2.7 nm¹¹² to 6 nm, and reducing the driving pulse width from 12 ps to 6.4 ps predicts a

reduction in ring laser output pulse width from 5.5 ps to 2.7 ps, in excellent agreement with experimental observations. A typical 40 GHz output pulse train, measured using a high speed photo detector and sampling oscilloscope, is shown in Figure 3-14. The sampling oscilloscopes statistic features were used to demonstrate resolution limited temporal jitter of the recovered clock.

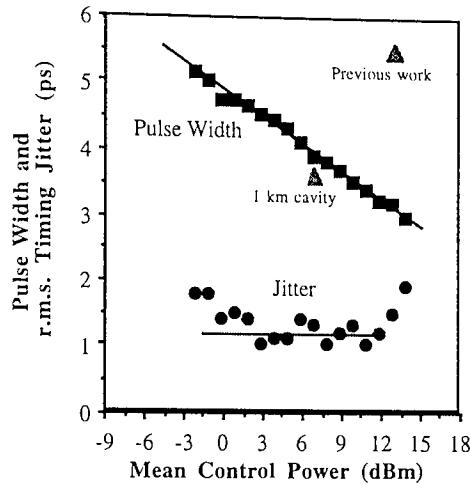


Figure 3-15 ; Performance of a 12.6 km FM/AM mode locked fibre ring laser, illustrating variation of jitter (circles) and pulse width (squares) as a function of control signal power. Previous results without a polariser, and subsequent results using a polariser and 1 km cavity length are shown for comparison.

The ring laser performance is summarised in Figure 3-15, showing the variation in pulse width and jitter (measured using sampling oscilloscope) against control signal power. Low jitter operation is observed over more than 10 dB of dynamic range, with a minimum required power in the region of +0.5 dBm. This corresponds to a very small peak phase shift of approximately 0.1 radians (assuming exact phase matching) for sub 5 ps pulses, compared with approximately 0.96 radians for 5.5 ps pulses without the inclusion of the fibre polariser.

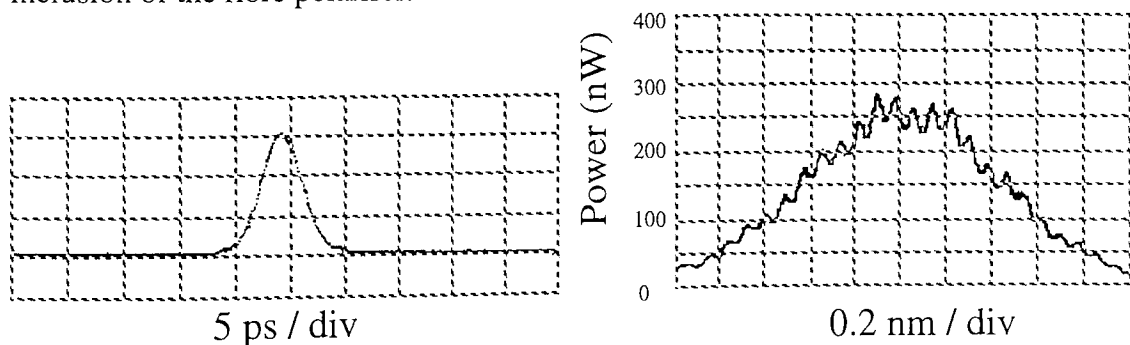


Figure 3-16 ; Output spectra (right) and autocorrelation (left) of 1 km FM/AM ring laser mode locked at 10 GHz.

The large dynamic range available with this configuration enable a significant reduction in the length of dispersion shifted fibre used for cross phase modulation, improving the environmental stability. In a second laser cavity, the 12.6 km of fibre was replaced with a 1 km length of fibre with a dispersion zero at 1.55 μm , and the monitor coupler was replaced with an 80:20 split ratio fused fibre coupler. Under these conditions, stable mode locking was again achieved with a peak phase shift as low as 0.02 radians,

typically giving 2.6 ps pulses at 10 GHz and 3.6 ps at 40 GHz, both with approximately +6.9 dBm mean control signal power. The 40 GHz result is also shown in Figure 3-15 for comparison where we clearly observe that the change in the length of dispersion shifted fibre has had little effect on the 40 GHz performance of the ring laser. Phase locked operation of this laser was possible over a period of several hours. A typical output of the laser, driven by 10 GHz control pulses, is shown in Figure 3-16, illustrating a time bandwidth product of ≈ 0.35 . Both of the FM ring lasers studied are soliton supporting at the ring laser wavelength (anomalous dispersion), giving pulse compression via soliton effects within the cavity. It has been demonstrated however, that a non soliton supporting ring cavity would produce broader, linearly chirped pulses¹¹⁴. Subsequent linear compression in a short length of fibre results in transform limited pulses as short as 1.2 ps in a 10 GHz FM mode locked ring laser¹¹³.

Both types of ring laser studied here (electro-optic and all optically mode locked) produce near transform limited pulse width and wavelength tuneable pulses with an immeasurable extinction ratio. Fibre ring lasers, albeit complex, represent a highly promising source of optical pulses for OTDM applications, as evidenced by the multitude of system demonstrations in which they are employed.

3.1.5 Electro-Optic Mach Zehnder Modulator

The use of traditional Mach Zehnder modulators for pulse generation has been considered by several authors^{115,116,117}. The techniques proposed generally rely on exploiting the sinusoidal transfer function of the modulator. One further technique is to employ pulsed electrical drives to the modulator, which therefore simply acts as a pulse shaping element. Whilst perfectly capable of producing optical pulses¹¹⁸ these approaches suffer several drawbacks. Firstly, they in general require complex electronic drive circuits to ensure that the RF drive signal is of the correct temporal form. Secondly, any minor imperfections in the drive signal, will by nature of the sinusoidal transfer function of the modulator, lead to high levels of background radiation, and consequent cross talk penalties. Finally, and perhaps most significantly, the techniques produce relatively broad optical pulses with a finite extinction ratio (typically less than 30 dB), which are perfectly suited to applications in single channel soliton systems but allow only modest levels of optical multiplexing above the data rate available from the modulator directly. Consequently, given the advances in other technology areas, it is unlikely that this form of electro optic modulator would find application as a pulse generator for OTDM networks in the absence of subsequent pulse compression¹¹⁹.

3.1.6 Electroabsorption Modulators

There has been considerable recent interest in the use of electro-absorption modulators for pulse generation^{66,120,121}. The non-linear absorption characteristic of an EAM has been shown to generate pulses whose temporal intensity profile closely approximates the sech^2 shape required for soliton transmission. The simple source configuration (Figure 3-19) compares favourably with the alignment issues of complex mode locked laser cavities, and to match simplicity of gain switched DFB laser, monolithic

integration may be pursued^{122,123}. With these advantages in mind, it is clear why it is widely believed that electro absorption modulators will have a significant impact on soliton transmission systems. Whilst devices have been investigated at many laboratories world-wide, until this work, the minimum mark to space ratios achieved were close to 14% at 10 GHz¹²⁴, clearly precluding the application of electro absorption modulators to 40 Gbit/s OTDM systems. In this thesis, the generation of duty ratios of 6.3 % is discussed, along with a particularly simple method of generating a modulated stream of pulses from a single modulator.

3.1.6.1 Soliton Pulse Generation Using Electroabsorption Modulators

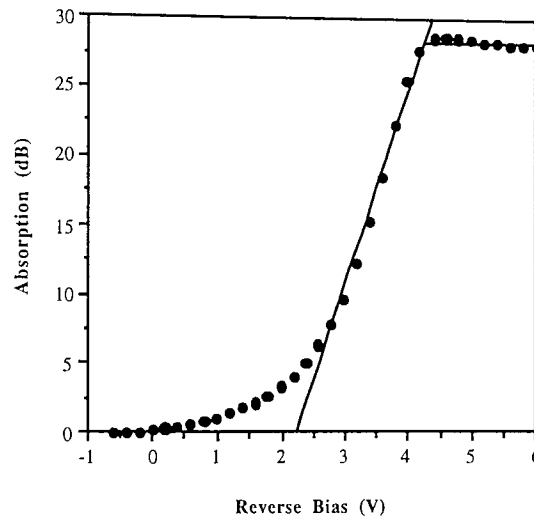


Figure 3-17; Typical absorption characteristic of an electro-absorption modulator (after reference 125) showing exponential loss characteristic for reverse bias' between 2 and 4 volts.

A typical absorption characteristic of a 325 μm multiple quantum well device is shown in Figure 3-17, the packaged device performance included, typically, an additional 8.4 dB insertion loss¹²⁵. To first order, the modulation characteristic may be expressed by considering an idealised relationship between the absorption (in dB) and the applied reverse bias (V) ;

$$\alpha_{dB} = \begin{cases} 0 & V \leq V_0 \\ k(V - V_0) & \dots V_0 < V < V_1 \\ XR = k(V_1 - V_0) & V_1 \leq V \end{cases} \quad \text{Equation 3-49}$$

where k represents the gradient of the absorption characteristic in dB/V, V_0 the maximum reverse bias for zero absorption and V_1 the reverse bias at which maximum absorption is achieved. XR represents the associated parameter of extinction ratio (dB), critical for the deployment of electroabsorption modulators in OTDM systems. For a sinusoidal drive signal, it is easy to show¹²⁶, that provided the applied bias voltage remains below V_0 at all points during its cycle, the resultant pulse width is given by ;

$$\tau_{FWHM} = \frac{1}{\pi f} \left(\frac{12}{kV_{pp}} \right)^{\frac{1}{2}} \quad \text{Equation 3-50}$$

where V_{pp} represents the peak to peak amplitude of the drive signal of frequency f . From this equation, we may deduce that the shortest pulses are produced for the highest drive frequencies, and for the steepest absorption characteristics. A comparison of an idealised pulse generated according to Equation 3-49 and a sech squared pulse, whose width is determined by Equation 3-50 is shown in Figure 3-18.

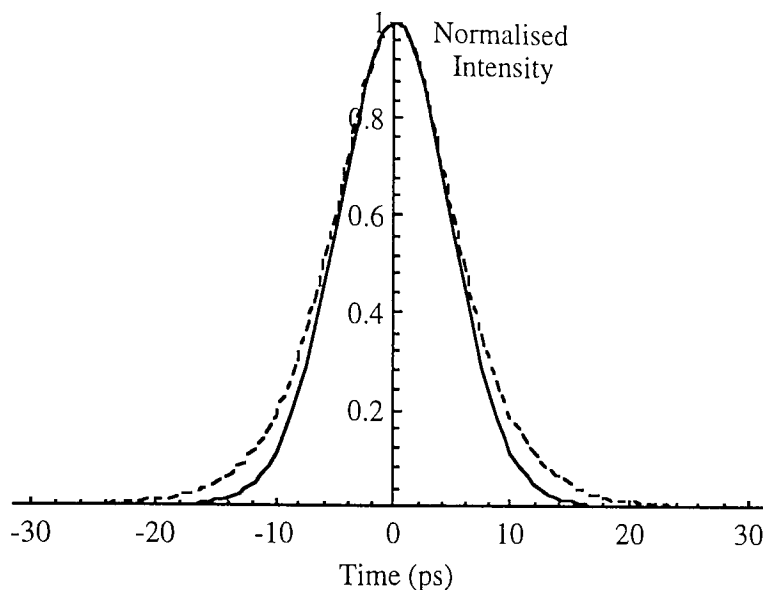


Figure 3-18; Pulse profiles for an ideal sech² pulse (dashed line) and as generated by an ideal electro-absorption modulator (solid line) with 10 dB/V absorption characteristic and $10V_{pp}$, 10 GHz drive signal.

Note that the wings of the electro-absorption modulator pulse are somewhat reduced in extent, a fundamental characteristic for pulses generated with this technique. The precise nature of the deviation from an ideal sech squared pulse will of course be determined, in practice, by the precise absorption characteristic. This enhanced confinement of the optical pulse is of clear benefit for optical multiplexing, by reducing the level of crosstalk.

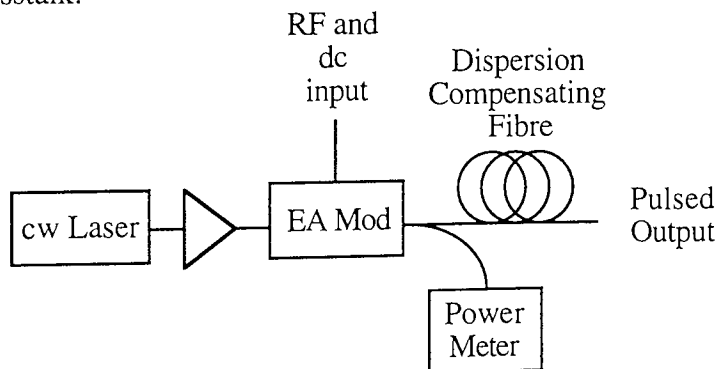


Figure 3-19; Experimental arrangement for generation and measurement of short pulses from electro-absorption modulators.

Figure 3-19 illustrates the experimental configuration used to assess the generation of pulses from electro-absorption modulators. An external cavity laser was used as cw light source at the wavelength of maximum extinction ratio. A polarisation controller selected the TE polarisation state. Two devices were employed (devices #1 and #2),

whose characteristics are summarised in Table 4, along with typical operating conditions. The output signals were passed to appropriate measurement equipment via an erbium amplifier, and where appropriate, a length of dispersion compensating fibre for pulse compression via linear chirp compensation.

	Modulator #1	Modulator #2	Modulator #3	Modulator #4	Modulator #5
Bandwidth (GHz)	10.7	> 20		15	16
Absorption Slope (dB/V)	11.8	8	2.5	> 10	11
Max Extinction (dB)	28	40	20	> 20	23
Input Power (dBm)	+3.7	0	-2	< +3	< +2
Drive frequency (GHz)	10	20	10	10	10
Drive Amplitude (V_{r-n})	10.7	10.1	2.5 + data	data+clock	11

Table 4 Summary of electro-absorption modulator characteristics and operating conditions.

The experimental FWHM pulse duration for both devices (Figure 3-20) was estimated assuming a sech squared profile, although strictly, for low reverse bias voltages, a lower conversion factor should be used to represent the increasing rectangular nature of the pulses.

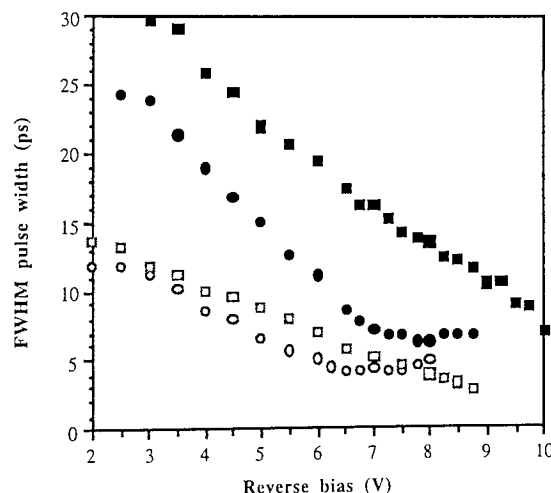


Figure 3-20; Observed pulse widths from sinusoidally driven electro absorption modulators, with (circles) and without (squares) linear chirp compensation for device #1 (10 GHz drive, filled symbols) and device #2 (20 GHz drive, open symbols).

For the 10 GHz device, although pulses as short as 7 ps were generated for a reverse bias of 10 V, satisfying the $\leq 8\%$ duty ratio criterion for four fold OTDM (Table 2), this corresponded to a region where the pulse extinction ratio was somewhat reduced because of the high absorption at the peak of the drive cycle. A 400m of dispersion compensating fibre (of dispersion coefficient -38 ps/nm/km) was used to linearly counteract the chirp inevitably accompanying the amplitude modulation imposed by the EAM (A fibre Bragg grating may also be used to linearly compress the pulses¹²⁷). For a dc bias of 8.5V the pulse width after the DCF was 6.8 ps as shown in Figure 3-21. For reverse biases between 7 and 8.5V the measured time bandwidth products were

very close to 0.315 indicating that the pulses were approximately of the required sech^2 profile and pulses as short as 6.3 ps were observed over a range of bias conditions.

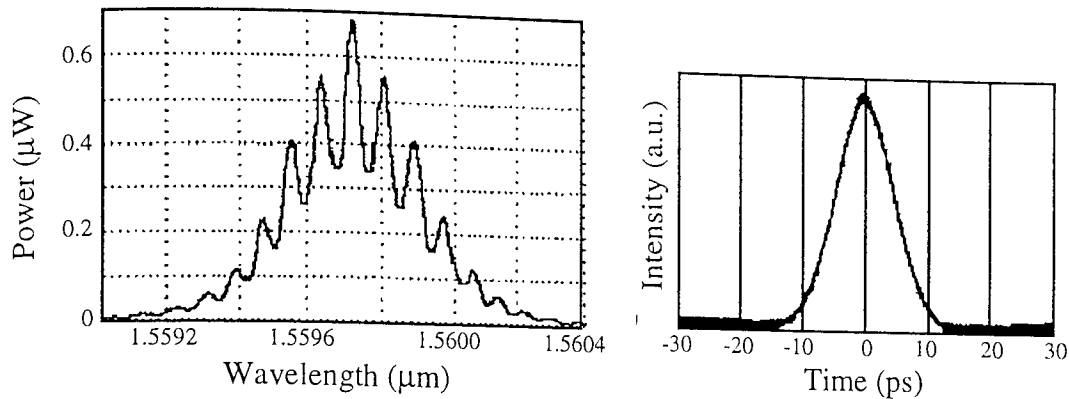


Figure 3-21 Optical spectrum and autocorrelation of linearly chirp compensated 10 GHz pulses for a reverse bias of 8.5 V

Similar results were obtained at 20 GHz using device #2. Uncompressed pulse widths as short as 2.8 ps were obtained in the region where the device extinction ratio was compromised, and transform limited pulses of 4.1 ps duration were obtained after 100 m of identical DCF for reverse bias voltages between 6 and 7.25 V. Furthermore, this performance was achieved with a peak extinction ratio (measured at dc) in excess of 40 dB, suggesting that the device is well suited to OTDM applications. In both cases, the minimum compressed pulse widths were approximately two thirds (62% and 67% respectively) of the theoretically predicted values (Equation 3-50). The theoretically anticipated pulse widths were obtained (≈ 10 and 6 ps respectively) without compression at the highest dc bias that did not compromise the pulse extinction ratio.

The 6.3% duty ratio achieved at a 10 GHz repetition rate and 8.2% duty ratio achieved at 20 GHz meets the requirements for 4 channel OTDM systems and are both believed to be significantly less than the lowest previously reported value for an EAM at such a high repetition rates without using non-linear compression. Furthermore, the 40 dB extinction ratio of device #2 is sufficient for 4 fold optical multiplexing. These results confirm for the first time that the EAM is a compact, stable, low jitter source of short pulses suitable for use in high bit-rate OTDM systems, this was recently confirmed in a 40 Gbit/s transmission experiment¹²⁸ and in the construction of an 80 Gbit/s all electroabsorption modulator system¹²⁹.

3.1.6.2 Modulated soliton pulse train generation using EA modulators.

Traditionally, data modulation for a single channel soliton system usually requires the addition of a second modulator (either electro-absorption¹²⁹ or Mach Zehnder⁷³), increasing the loss and complexity of a modulated pulse source. It has been shown however, that an appropriately processed electrical signal may be used to generate 75 ps pulses at 2.5 Gbit/s using an integrated laser modulator¹³⁰, and modulated trains of 70 ps pulses at 2.5 Gbit/s utilising a laser array¹²³. This approach is in fact suitable for use with all forms of modulator (see section 3.1.5), and indeed similar techniques have been used to demultiplex a 40 Gbit/s data stream directly to 10 Gbit/s using a single

Mach Zehnder modulator¹¹⁸. With suitable modifications to the drive electronics, this Mach Zehnder modulator could produce a modulated stream of 19 ps optical pulses. The optical simplicity of the schemes is particularly attractive, and may even be used in OTDM systems, allowing the pulse source to be replaced with a simple cw laser, provided the pulse quality and extinction ratio from the modulator is sufficiently good.

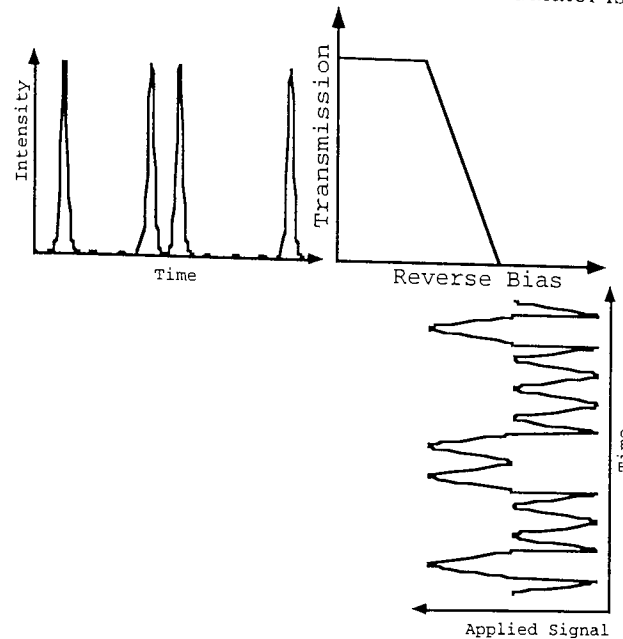


Figure 3-22 Principle of modulated pulse generation using an electroabsorption modulator.

This thesis demonstrates that the technique may in fact be simplified in the electrical domain by utilising the unique transfer function of electro absorption modulators. This is achieved simply by applying an appropriate sine wave and a data signal simultaneously to the same device such that the signal amplitudes are added. Biased appropriately, the modulator will only give an output when both the sine wave and data signals are high, since the modulator maintains high loss for increasing reverse bias (figure 3-22). The signals may be combined either through a power splitter (increasing the power demand placed upon the drive electronics), or, using packaged devices developed at BT labs¹²⁵, contra-directionally, without loss of power. In both cases, it is essential that the outputs of the two signal sources (sine wave and data) are well impedance matched to 50Ω at the point of combination to minimise spurious reflections and the potential of unwanted electrical standing waves.

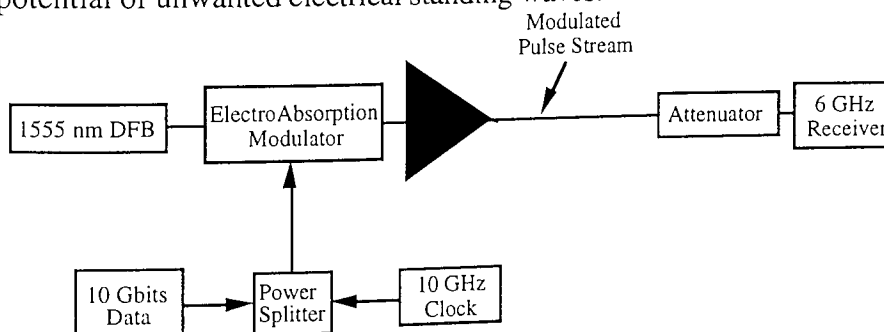


Figure 3-23 Schematic diagram of modulated soliton pulse stream formation experiment, omitting electrical amplifiers.

Figure 3-23 illustrates the experimental arrangement used to initially demonstrate this single modulator pulse source. A synchronous 10 GHz sine wave drive is added to a 10 Gbit/s data sequence via a simple power splitter, initially both with 2.5 V peak to peak amplitudes. The signal now comprises a sine wave with an offset voltage determined by the data signal. It is a sufficient condition to ensure that the entire 10 GHz cycle remains in the high absorption region for a data 'zero' and precise adjustment is not necessary. Ideally however, the amplitude of the sine wave is chosen to give the desired pulse width, whilst the data amplitude is set to give the necessary extinction ratio. The signal is then applied to electroabsorption modulator #3, and the dc bias adjusted to ensure that the entire clock cycle for a data zero gives high extinction, whilst the peaks of the cycle for a data one give a low loss. Consequently, soliton like pulses are formed for data ones in the usual way, whilst a high extinction is maintained for data zeros. Figure 3-24 illustrates the output of the transmitter when either data (lower trace) or sine wave (middle trace) are applied to the modulator independently, and the output when both signals are applied simultaneously (upper trace). Autocorrelations of the pulse stream reveal that no degradation in pulse quality occurs when the EA modulator is used with both drives applied compared to when a single sine wave drive is used. Note however, that a short length of dispersion compensating fibre is used to compress the chirped pulses generated from the modulator, decreasing the output pulse width from 26 ps to 18 ps (assuming Sech profiles) and resulting in a time bandwidth product below 0.35. The bit error ratio performance of the system demonstrated a receiver sensitivity of -12.5 dBm with no observable error floor using an overall receiver bandwidth of around 6 GHz, which equalises the optical return to zero eye.

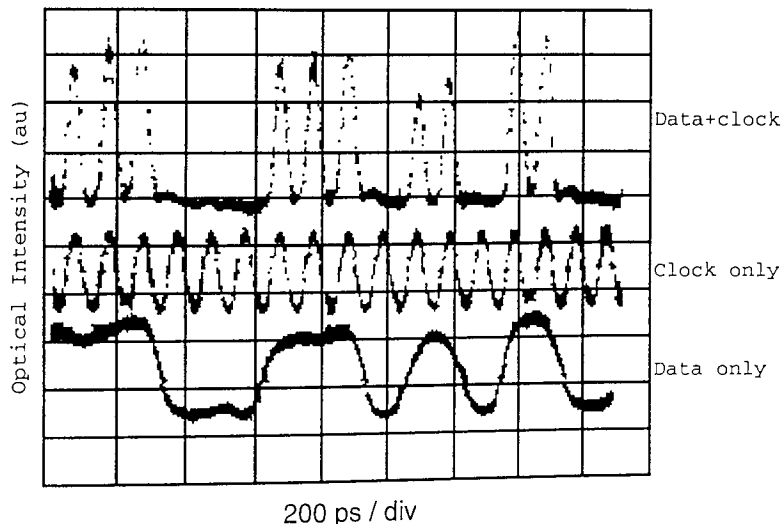


Figure 3-24 Output of electro absorption modulator driven by sine wave and data signals simultaneously and independently.

The experiment was repeated using a 15 GHz electro absorption modulator (device #4) demonstrating remarkable wavelength and polarisation insensitive extinction ratio¹³¹. This is illustrated in Figure 3-25, where the absorption characteristic is plotted for a variety of wavelengths and polarisation states. Note that although the insertion loss and maximum extinction ratio are insensitive to polarisation, in orthogonal polarisation's, modulator absorption begins at different voltages (difference of approximately 0.8 V at

1550 nm). However, again the unique trapezoidal transfer function of the electroabsorption modulator may be used to advantage, since it is only necessary to switch the modulator between the maximum absorption state and a state close to minimum insertion loss. Thus provided the applied signal amplitude exceeds a critical value, many wavelengths can be simultaneously modulated with high extinction ratio, independent of polarisation.

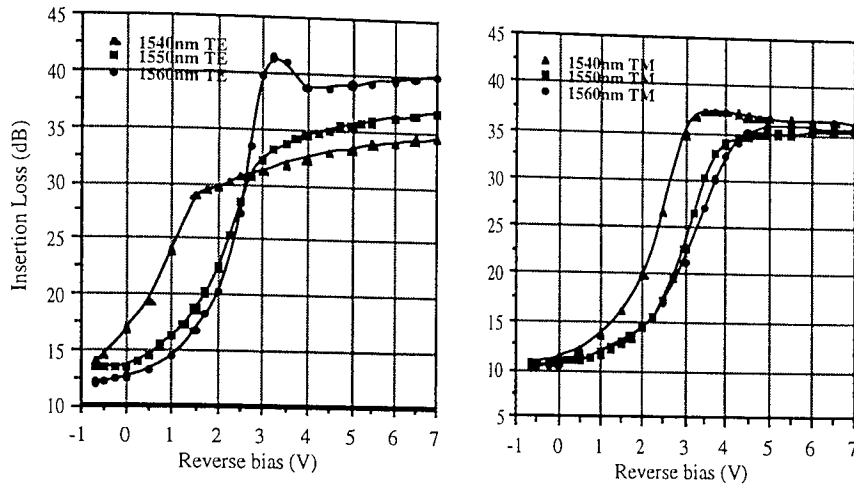


Figure 3-25 ; Absorption characteristics of "polarisation insensitive" EA modulator

Using this modulator it was possible to simultaneously generate 10 GHz soliton pulse trains at 12 different wavelengths, without the use of multiple modulators or polarisation controllers, the pulse widths obtained after linear compression (dispersion of -7.6 ns/nm) are summarised in Table 5 below. The minimum pulse width of 7.5 ps corresponds to a wavelength exactly aligned with the low loss axis of the modulator, whilst the 2.4 ps peak to peak variation represents the combined effects of differing wavelength and polarisation on the effective bias point (any changes of course degrading the output pulse width). Whilst clearly significant, the range of pulse widths produced are entirely consistent with operation of each wavelength in a 20 Gbit/s soliton system, with negligible compression required for 40 Gbit/s operation.

Frequency (THz)	Approximate Wavelength (nm)	Pulse Width (ps)
191.9	1563.1	8.4
192.0	1562.5	9.2
192.1	1561.69	8.0
192.2	1560.87	8.7
192.3	1560.06	8.2
192.4	1559.25	9.0
192.5	1558.44	7.7
192.6	1557.63	7.5
192.7	1556.82	8.7
192.8	1556.02	8.7
192.9	1555.21	10.0
193.0	1554.4	9.7

Table 5 Simultaneously obtained pulse widths from 12 single electroabsorption modulator driven at 10 GHz. Each signal has a random polarisation state.

Typical outputs with the data signal simultaneously applied to the modulator (in this case the signals are combined before amplification) are shown in Figure 3-26, where the ratio of 10 GHz clock amplitude to 10 Gbit/s data amplitude driving the modulator was fixed at 5.9 : 1 before amplification via a 15 GHz electrical amplifier.

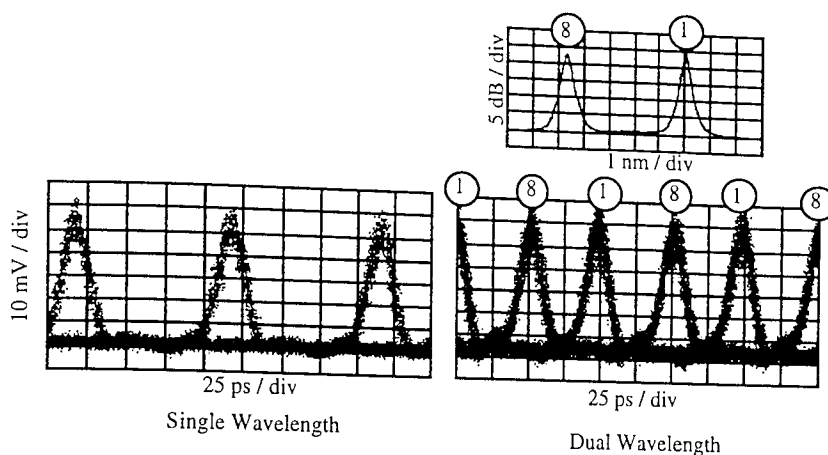


Figure 3-26 ; Modulated pulse streams from a single electro absorption modulator driven at 10 GHz, showing outputs for single wavelength (left) and two simultaneous wavelengths (right), following -7.6 ps/nm dispersion.

Interestingly, with the multiple wavelength source, the linear pulse compression fibre not only reduces the optical pulse width, but introduces time delays between the pulses. The right hand trace of Figure 3-26 illustrates the output for channels 1 and 8, with a wavelength spacing of 700 GHz. With appropriate variation in either the exact wavelength spacing, or the fibre dispersion/length (or both) it is possible to arrange for any reasonable time delay, enabling the generation of OTDM test patterns and probe signals for non-linear gates. In combination with suitable optical logic gates and dispersive delay lines, these multi wavelength pulse trains enable, for example, time slot interchange, regenerative drop and insert, multiple output demultiplexing and OTDM to WDM format conversion, whilst the ability to modulate these trains allows access to lower line rates without the need for resonant comb generators or multiple RF signals^{124,132,133}. These applications are of course in addition to the generation of multiwavelength pulses for WDM applications.

3.1.7 Other Sources

In this section, we have reviewed pulse sources, either used or directly studied during the period of this thesis, and have attempted to quantify the particular advantages and drawbacks of each technique. However, this is by no means an exhaustive survey of all possible pulse sources, and the table below illustrates some of the sources recently proposed in the literature. In addition to this list, note that many demultiplexers may be configured to act as pulse sources (see chapter 4)

Type of Laser	Maximum Reported Rate (GHz)	MSR	Minimum Width (ps)	Comments	Ref
Supercontinuum	10	0.6%		Ideally suited to OTDM	134, 135
Phase modulator + external filter + loop mirror	10 2	10% 33%	10 ps	Simple source suited to single channel soliton systems	136 137
Passive ring laser	MHz 2 GHz		350 fs 480 fs	No Synchronisation to system clock	138 139
MZ modulator	2.5	20%	80 ps	One of many such schemes Also used for dark solitons.	117 140
Phase modulator + guiding filters	10	n/a	n/a	Pulses form on propagation	
beat frequency conversion in NOLM	32	14%	4.3 ps	Alternative to DDF beat frequency conversion.	141
Mode locked fibre grating laser	2.5	4.8 %	20 ps	Alternative to EC-MLL	142
Monolithic colliding pulse laser	15.8 40-350	10% 2-5%	6.4 ps	Fixed repetition rate alternative to EC-MLL	143
Mode Locked	16.3	0.9%	550 fs	Alternative to EC-MLL	96
Kerr Gate	10	6.6%	6.6 ps	Cleans up poor pulses	144
NOLM	5			Cleans up poor pulses	50, 145
XPM in an SLA	10	7%	7 ps	Cleans up poor pulses WDM operation possible	146, 147

Table 6 A selection of optical pulse sources.

3.1.8 Assessment of pulse source options

Recalling the requirements of an OTDM pulse source, pulse width and extinction ratio are the first criteria to be met before issues of stability and jitter are even considered. As a general rule, any mode locked laser is likely to produce pulses with a high extinction ratio suitable for OTDM applications. For sources based on gain switching or modulation, the obtained extinction ratio performance will necessarily restrict the level of multiplexing available. A great level of simplicity and flexibility is achieved through

the use of electro-absorption modulators, even if two cascaded devices are required in order to meet these exacting extinction ratio requirements. This type of source is particularly important when supplementary requirements such as low wavelength and timing jitter, chirp and tunability are considered. For the most demanding application of high speed OTDM soliton transmission, the erbium doped fibre ring laser remains the most promising candidate (with the possible exception of the supercontinuum source, which is itself based on a ring laser), whilst electroabsorption modulators come a close second. For applications where transmission is not required, the simplicity of gain switched sources and the flexibility of EC-MLL become attractive.

3.2 Pulse Compression Techniques

In the previous section, various pulse sources were described for use in 4 and 8 times 10 Gbit/s OTDM systems, with mark to space ratios as low as 4% readily achieved. However, for higher capacity systems, either higher, non-standard base rates must be employed, or the mark to space ratio of the pulse stream must be increased. Whilst it is possible to increase the RF drive power to the various laser sources and attempt to continue the monotonic decrease in pulse width or decrease the pulse width of the drive signal this becomes increasingly difficult, with reducing benefit. This is illustrated in figure 3-6 and equation 3-50 the pulse width certainly decreases more slowly than the RF power increases. To achieve mark to space ratios below $\approx 5\%$, pulse compression is perhaps the most efficient approach, and is employed by many laboratories world-wide. In general pulse compression comprises a manipulation of the pulse spectrum, either within the pulse source or via non-linearity (SPM or XPM) accompanied by a temporal manipulation through dispersive effects. These effects may either be carried out separately^{148,149,150,151}, or dynamically (eg soliton effect compressors).

3.2.1 Soliton Pulse Compression

The principles of soliton pulse compression are well established^{152,153,154,155}. It was initially demonstrated that a soliton pulse propagating in a long optical fibre will remain a soliton, continuously adjusting (broadening) its pulse width in sympathy with the fibre loss, provided that the overall loss is small compared to the soliton period¹⁵⁶, whilst Tajima suggested that if the product of dispersion coefficient and effective area varies proportionally to the accumulated fibre attenuation, then a soliton would propagate without variation in width¹⁵⁷. Additionally, it has been shown that pulse compression will be obtained if the soliton is amplified adiabatically or if the dispersion slowly decreases along the fibre length but more rapidly than suggested by Tajima^{152,158}. In order to allow reasonable adiabatic compression, the gain coefficient (or alternatively the rate of change of dispersion) should be less than ≈ 1 dB per soliton period¹⁵⁹ (Note that the soliton period is not necessarily constant). We then anticipate that the ratio of the output pulse width to the input pulse width would be given by;

$$\frac{\tau_{out}}{\tau_{in}} \approx \frac{D_{out}}{D_{in}} e^{-gL} \frac{1}{1+2\Delta} \quad \text{Equation 3-51}$$

$$P_{peak} = P_{sol} (1+\Delta)^2$$

Where the first term represents compression due to slowly varying dispersion¹⁵³, the second adiabatic amplification¹⁶⁰ and the third term, the tendency of pulses launched above the soliton power to form into a soliton of slightly narrower width (pre-emphasis)¹⁶¹. Particularly impressive results have been achieved by using a linearly decreasing dispersion in a lightly doped erbium fibre (to ensure that the soliton energy remains constant) resulting in a compression factor of 17.6 with no observable pedestal¹⁶². Similar results are obtained in an undoped fibre whose dispersion coefficient decreased hyperbolically over a 1.6 km length¹⁶³.

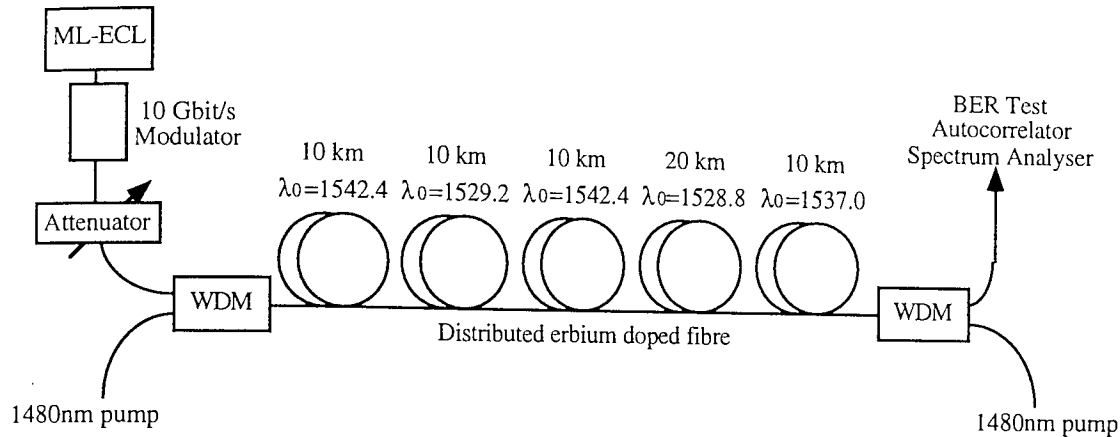


Figure 3-27 Schematic diagram of distributed erbium fibre amplifier based pulse compression experiment.

In order to investigate the potential of adiabatic soliton pulse compression, two experiments were carried out. In the first, a 60 km long optical amplifier, comprising lightly doped dispersion shifted fibre, was used to provide adiabatic amplification of a 10 Gbit/s soliton pulse train as shown in Figure 3-27. The mean dispersion zero of the 5 concatenated fibres was 1534.76 nm, with the local dispersion zero alternating between ≈ 1542 and ≈ 1529 nm along the fibre length to minimise the accumulated dispersion. For a signal wavelength of 1537.5 nm and a pulse width of 6.4 ps, this gives a soliton period of ≈ 87 km and a soliton peak power of 5.7 mW (-4.9 dBm mean power) assuming an effective area of $50\mu\text{m}^2$. Measurements of the output error ratio characteristics, pulse width and amplifier gain were carried out and are summarised in Figure 3-28 below. The system operated error free with negligible penalties for mean input powers as low as -10.5 dBm.

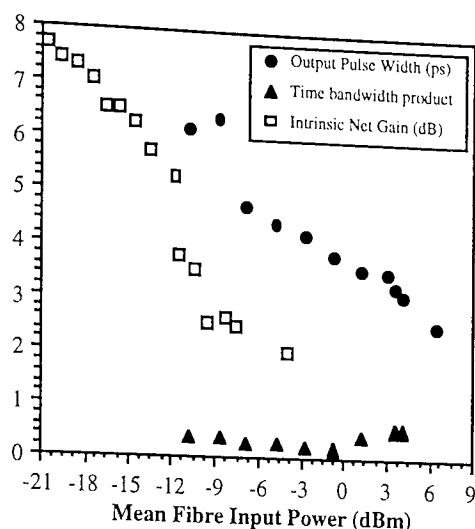


Figure 3-28 Adiabatic soliton pulse compression in a 60 km distributed erbium doped fibre amplifier, showing variation in gain, pulse width and time bandwidth product as a function of launched power.

For a mean fibre input power of -4.8 dBm, close to the fundamental soliton power, the intrinsic fibre gain of 1.8 dB suggests an ideal adiabatic compression factor of 1.5 in excellent agreement with the observed compression factor of factor of 1.52 . This input power also closely corresponds to the minimum output time bandwidth product confirming near adiabatic soliton compression despite the use of gaussian pulses from an EC-MLL. For higher signal powers, the output pulse width monotonically decreases to a minimum value of 2.5 ps at the maximum mean signal input power of $+6.5$ dBm, corresponding to a compression factor of 2.6 . Given a net loss through the fibre of around 3 dB, this compression may not be attributed to the adiabatic compression anticipated for soliton propagation. Figure 3-29 shows the output pulse spectrum for signal launch powers of $+6.5$, $+3$ dBm and -9 dBm, illustrating the occurrence of a complex compression process. However, the reduced net fibre loss (0.05 dB/km), and the restrictive gain bandwidth of the amplification process resulted in the generated of pedestal free compressed pulses (see insets)¹⁵⁸, and the technique clearly merits further investigation.

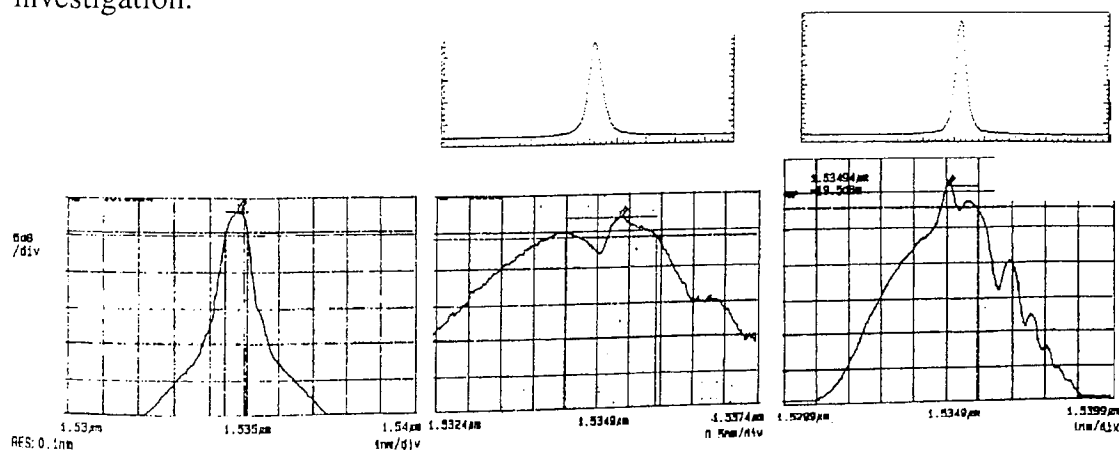


Figure 3-29 Output spectra following non-linear pulse compression in a 60 km distributed amplifier for input signal input powers of -9 dBm (left), $+3$ dBm (centre) and $+6.5$ dBm (right) with autocorrelations shown as insets.

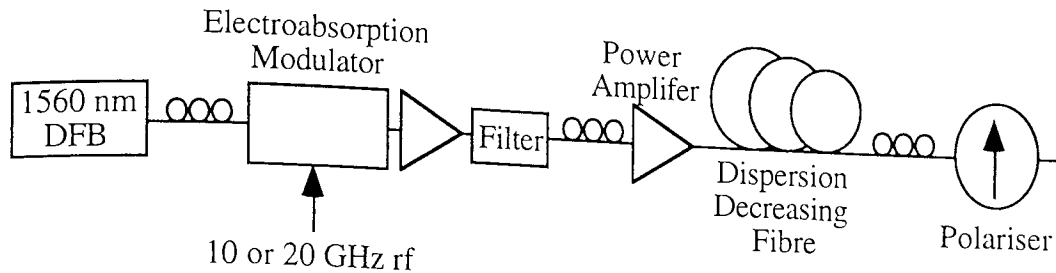


Figure 3-30 Experimental arrangement for the compression of soliton pulses in a dispersion decreasing fibre.

In a second experiment, the alternative, passive, approach of dispersion decreasing fibre was employed, in conjunction with a sinusoidally driven electro absorption modulator to generate the initial soliton pulses. The experimental arrangement is illustrated in Figure 3-30. Two different electro absorption modulators were employed (devices #1 and #2 from Section 3.1.6) to generate pulses at 10 and 20 GHz repetition rates. The pulses so generated were linearly compressed in a short length of normally dispersive fibre (≈ -3.8 ps/nm dispersion) to produce transform limited pulses. These pulses were amplified and subsequently compressed in a 2 km length of dispersion decreasing fibre with input and output dispersions of +8 and +3 ps/nm/km respectively. A small pedestal component generated during the pulse compression was effectively suppressed using a fibre polariser and the residual birefringence of the DDF. The relatively large birefringence of the fibre was characterised by a peak differential group delay of ≈ 3 ps.

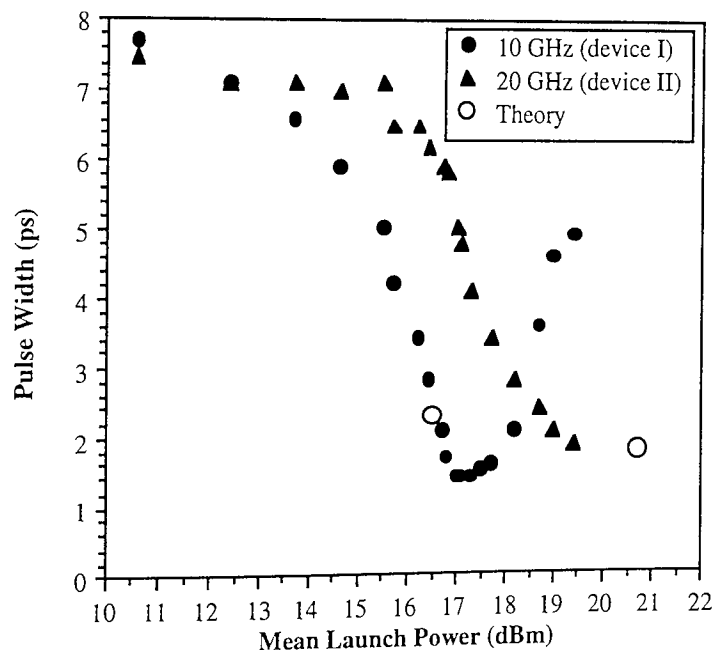


Figure 3-31 Output pulse width as a function of mean launch power for DDF compression of soliton pulses at 10 and 20 GHz. The theoretical compression (from Equation 3-51) corresponding to the required launch power for a fundamental soliton also shown for comparison (open circles).

At 10 GHz, 6.3 ps transform limited soliton pulses were generated at 1560 nm following linear compression, theoretically requiring a mean power of 16.5 dBm to generate a fundamental soliton with a soliton period of 1.9 km at the input to the DDF. As the launch power was increased to towards this value, there was a corresponding

decrease in the pulse width due to soliton compression in the DDF. Optimum compression to a pulse width of 2.1 ps was achieved for a mean launch power of around +17 dBm. Similarly, at 20 GHz, a launch power of 20.2 dBm was required to generate a fundamental soliton of 5.1 ps pulse width at the input to the DDF. For the maximum launch power of +19.4 dBm, compression to a pulse width of 1.9 ps was achieved.

These results are summarised in Figure 3-31, along with the predicted performance for ideal soliton compression. The excellent agreement between theory and experiment is apparent. At 10 GHz, as the power increases beyond the soliton power, compression continues due to pre-emphasis to the minimum pulse width of 1.3 ps, in accordance with Equation 3-51. Beyond this point rapid broadening of the pulse width was observed. At 20 GHz, the maximum mean launch power was insufficient to generate ideal soliton pulses for the minimum available pulse width. The autocorrelation and spectrum of the shortest pulses generated at each frequency are shown in Figure 3-32. Although the compression is in excellent agreement with theoretical predictions, a slight residual pedestal component is accompanied by spectra with suppressed central components. The origin of these deformations is probably due to the excess SPM resulting from a breach of the adiabatic condition (rate of change in dispersion of ≈ 2.5 dB per soliton period). Indeed, during analysis by others of a femtosecond compression experiment, similar spectral dips were observed when the compression process was no longer adiabatic¹⁶¹.

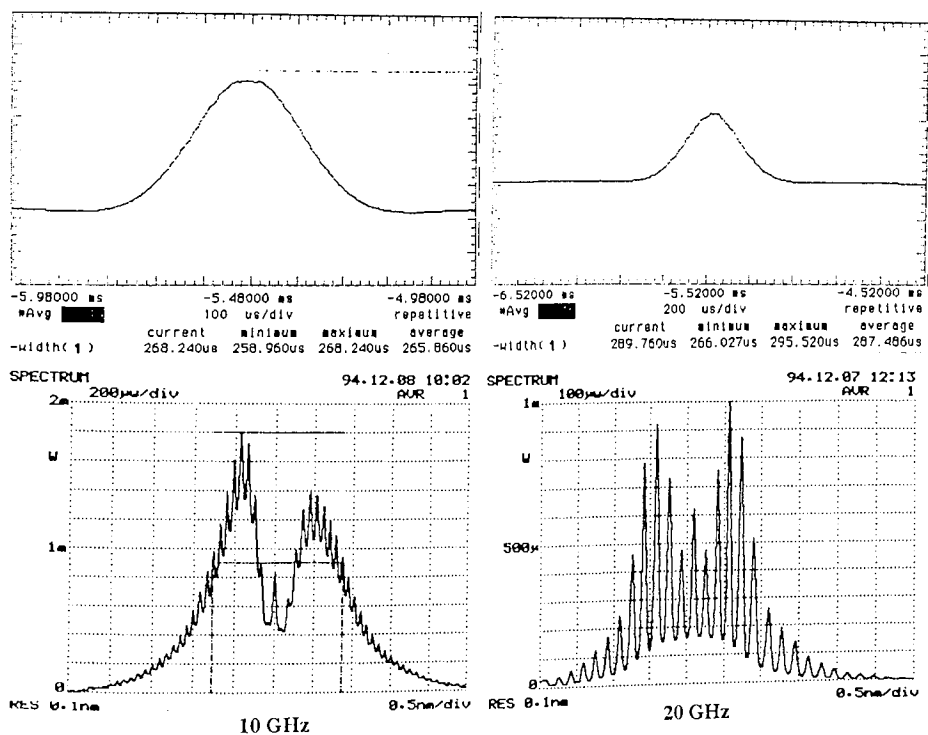


Figure 3-32 Autocorrelation (top) and spectra (bottom) following maximum observed soliton compression in a 2 km dispersion decreasing fibre for 10 GHz (left) and 20 GHz (right) pulses.

In summary, we have confirmed that adiabatic soliton compression techniques may be used to produce pulses with pulse widths ≈ 2 ps from typical sources described above, either via adiabatic amplification, or via effective amplification in a DDF. The results at

20 GHz, whilst not producing the shortest reported pulses by this technique¹⁶², were the shortest reported pulses at that repetition rate for any reported compression technique, and indicate an easy route to upgrade a 4 * 10 Gbit/s OTDM system to either an 8 * 10 Gbit/s or a 4 * 20 Gbit/s OTDM system.

3.3 OTDM Multiplexer

Having generated sufficiently short pulses, it remains to encode N copies of the pulse train with N channels of data, and interleave the resultant data streams into a single OTDM data stream^{69,73}. Note that in this case the electro optic modulators are simply used to gate pulses on and off, and are not required to shape the pulses. This is in marked contrast the requirements of a modulator for a standard NRZ formatted signal, where the rise time and chirp of the pulses formed by the modulator have a significant impact on the system performance. However it is crucially important to ensure that incoming data streams are synchronised to the pulse train to within a small fraction of the base rate bit period. This would typically be achieved using a buffer store, as shown in Figure 3-33.

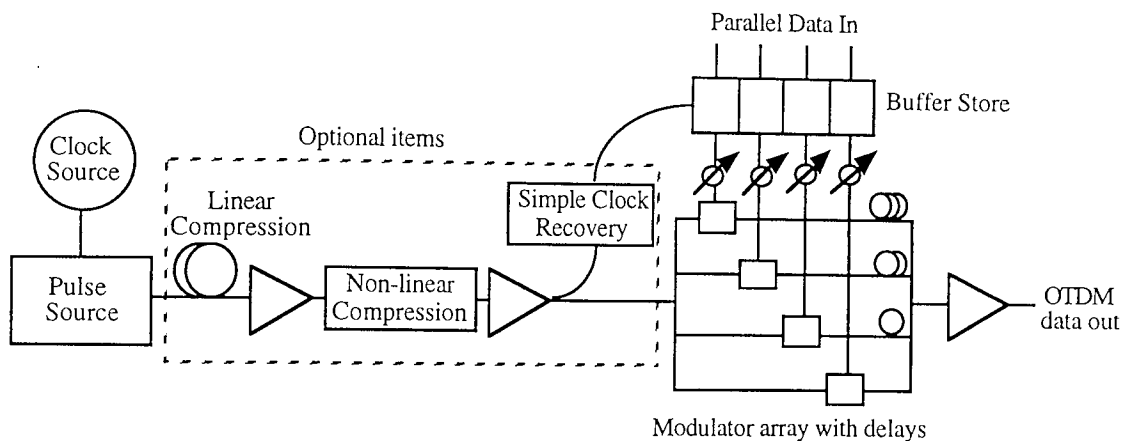


Figure 3-33 General schematic of an OTDM transmitter, showing pulse source, optional pulse compression, source / data synchronisation and modulator array.

In this figure, the optical pulse source is driven by a local clock. This clock may be a local master clock, locked to an incoming data signal, derived from the locally generated data signals, or in special cases may form part of the actual pulse source (eg Phase locked ring lasers) provided the drift rate and offset from the intended base rate are within prescribed limits. If necessary, the pulse source is followed by various stages of pulse compression, which will necessarily introduce some low frequency timing variations with respect to the clock source, unless non-dispersive compression techniques or chirped fibre gratings are employed. Any *non-linear* pulse compression should almost always come BEFORE the interleaving, not only to reduce the mean power required to generate sufficient non-linearity, but also to eliminate the possibility of cross talk between the various overlapping channels. If necessary, a simple clock recovery circuit, comprising an opto electronic receiver and a low Q microwave filter is used to gate the incoming electrical data onto the modulator array. Throughout this thesis, this function is simulated by gating the 10 Gbit/s pulse pattern generator with this recovered clock signal. Alternatively, the phase variations may be compensated for

using optical or electrical delay lines or a distributed phase locked loop. Of course, when interfacing to SDH terminals, a high degree of buffer storage already exists and synchronisation of clock pulses and data streams is ensured through the adoption of an appropriate clock distribution strategy (Figure 3-34). Similarly, for low data rate input channels, synchronisation may be neglected completely by oversampling²². In the following part of this section we shall discuss the generation of a 40 Gbit/s OTDM data stream from synchronised optical and electrical inputs according to Figure 3-33.

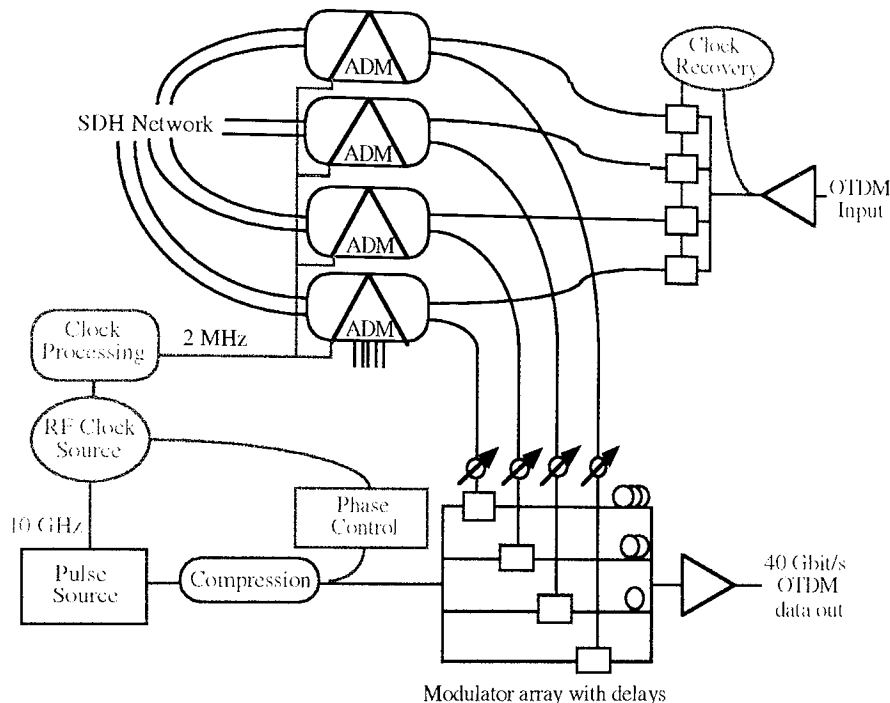


Figure 3-34 Interface between OTDM terminal and SDH network. Clock synchronisation paths shown in green. Note that any element (ADM, RF Clock, Pulse Source, SSU clock) may be used as a master clock source, with all other elements synchronised to it.

3.3.1 Mach Zehnder Modulators

Whilst several options exist to encode the optical pulse trains with data, including electro-absorption modulators and all optical techniques, Lithium Niobate Mach Zehnder modulators have been used for this function throughout this thesis by virtue of their ready availability. It is well known that the output of a Mach Zehnder modulator (P_{out}) is governed by the following equations for amplitude and phase (ϕ)¹⁶⁴;

$$P_{out} = P_{in} \left\{ xr + \frac{(1 + xr)(1 + \cos(\pi V/V_{\pi}))}{2} \right\} \quad \text{Equation 3-52}$$

$$\frac{\partial \phi}{\partial t} = \left(\frac{\alpha_m}{2P_{out}} \right) \frac{\partial P_{out}}{\partial t}$$

where V is the applied voltage, V_{π} the switching voltage (minimum transmission to maximum), P_{in} the input power and α_m the modulator chirp parameter. The chirp

parameter α_m is dependant upon the device geometry and driving conditions and is given by;

$$\alpha_m = \frac{\Delta V_a + \Delta V_b}{\Delta V_a - \Delta V_b}, \text{ independent twin electrodes (e.g. AT\&T M2420C)}$$

$$0 \quad \text{, balanced push-pull (e.g. BT\&D IOC2010)}$$

$$\pm 1 \quad \text{, single ended drive (e.g. Sumitomo T.MZ1.5-5).}$$

These equations allow the calculation of system performance for NRZ system applications and various components within an OTDM system. Consider for example, the use of an 8 GHz single ended drive modulator to encode 10 Gbit/s data onto a train of 8 ps pulses, for use in a 40 Gbit/s OTDM system.

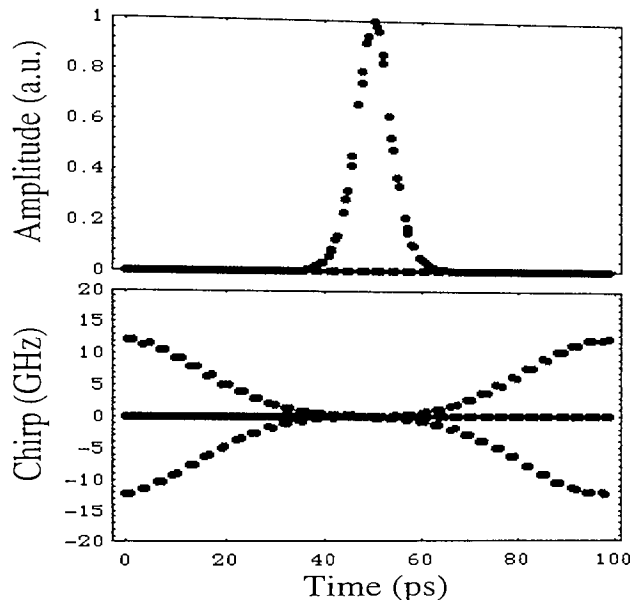


Figure 3-35 Amplitude and instantaneous chirp of 8 ps pulses modulated at 10 Gbit/s using an 8 GHz Mach Zehnder modulator.

Figure 3-35 illustrates the intensity eye diagram for an 8 bit pattern, along with the calculated chirp. Clearly, for the RZ system, the small amount chirp that exists is passed onto only the wings of the pulse, and will have negligible influence on the transmission performance.

3.3.2 Full OTDM Multiplex

The OTDM sources used during the early part of this thesis were unique in their ability to code each data stream completely independently, by using an independent modulator for each channel of the OTDM system. As well as ensuring complete decorrelation of the PRBS patterns applied to each modulator (essential to reveal penalties associated with subsequent components), many engineering issues are revealed in the attempt to construct a full transmitter. In addition to the obvious problems of loss, and the large number of polarisation controllers required for a non polarisation maintaining fibre laboratory system, these include differing degrees of chirp and depolarisation of pulses. In work predating this thesis, it was observed that a back to back system with a small, but obvious variation in the receiver sensitivity (due experimentally to mis-alignment of polarisations and modulator bias conditions) of around 0.5 dB, rapidly leads to quite severe and unpredictable variations of up to 2.5 dB in the receiver sensitivity following

soliton transmission. This reveals the care required to ensure a high degree of uniformity between the channels of an OTDM system for propagation through anything but the most ideal linear transmission line, and the importance of measuring all of the N channels where theoretically it may be anticipated that identical performance would always occur.

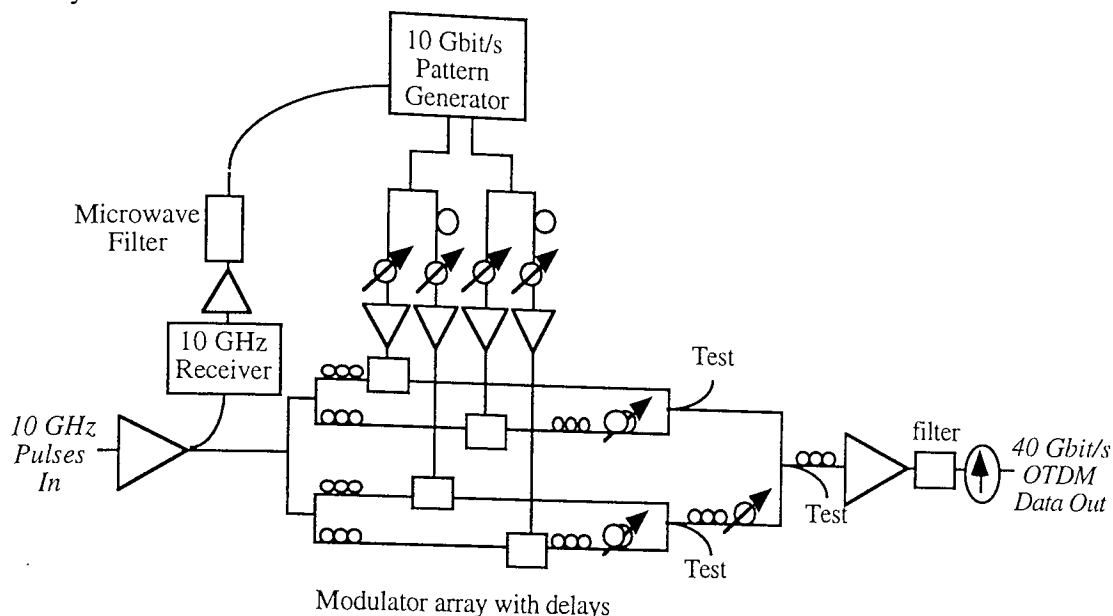


Figure 3-36 Schematic diagram of full OTDM multiplexer (MUX-1).

Figure 3-36 illustrated the experimental configuration used for these experiments, and from which all later configurations are derived. The clock recovery circuit simply comprises a 10 GHz receiver circuit (with a resonance at around 9.5 GHz) followed by a microwave amplifier and a 10 GHz filter ($Q \approx 35$). The resultant clock signal was used to trigger the 10 Gbit/s pattern generator, whose data and data bar outputs were each used to drive two 8 GHz balanced lithium niobate Mach Zehnder modulators. Unfortunately, the frequency response of the prototype drive amplifiers used had several deleterious features, particularly around 5 GHz and below 10 MHz, effectively limiting the operation of the transmitter to pattern lengths of 2^7-1 . The independent data channels were passed through fibre stretcher based optical delay lines to align the channel with the appropriate time slot, whilst following the final stage of amplification, a filter and fibre polariser were used to reject unwanted spontaneous emission and ensure single polarisation operation respectively.

Note that the modulators are arranged in pairs to produce two 20 Gbit/s data streams, which are then multiplexed to form the final 40 Gbit/s OTDM data stream. The test points indicated after each multiplexer allow for the quality of interleaving to be assessed. In particular, in the RF domain of a correctly interleaved 20 Gbit/s OTDM signal the 10 GHz spectral component should be indistinguishable from spectral lines arising from the PRBS data signal. Thus by minimising the 10 GHz RF component at all test points, and the 20 GHz RF component after the final interleaver stage, correct interleaving is assured. The cross correlation of the final 40 Gbit/s OTDM signal may also be used to verify the interleaving quality through a comparison of the widths of the central autocorrelation and the successive cross correlations (see Figure 3-37).

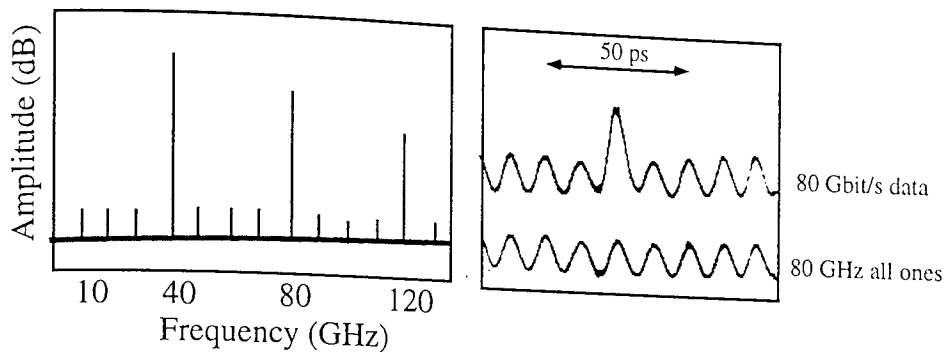


Figure 3-37 Theoretical RF spectrum for a 40 GHz OTDM data signal, showing residual 10 GHz components from slightly imperfect multiplexing (left), along with experimental 40 Gbit/s autocorrelation showing high uniformity of correctly interleaved data (right).

3.3.3 Passive OTDM Multiplexers

Given the complexities of set up involved with a full OTDM multiplex, for experimental investigations of some of the more complex nodes within an OTDM network, it is more convenient to employ a single modulator and a passive interleaver network. Indeed this is the approach adopted by most laboratories world-wide. However, experience of full multiplexers suggests some important design rules for partial multiplexers. These relate in particular to the relative delays of the optical paths through the network, to ensure adequate decorrelation of the PRBS patterns between the OTDM data channels. Without such decorrelation, error rate floors from inadequate demultiplexer performance will not be totally apparent (Equation 2-41), and in the extreme case of total correlation (path length difference less than the base rate bit period), even power penalties are absent (Equation 2-40).

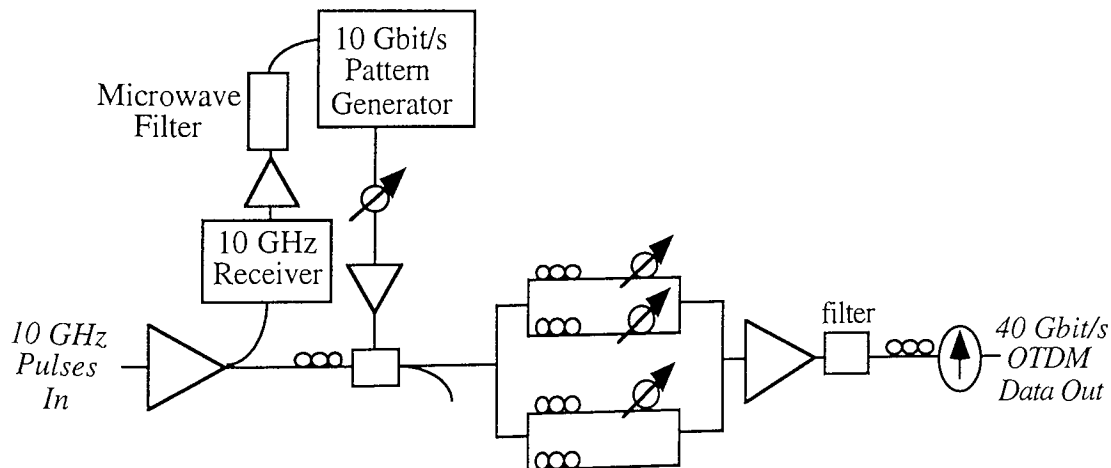


Figure 3-38 Schematic diagram of four path passive OTDM multiplexer (MUX-2).

Figure 3-38 illustrates the reconstruction of the testbed to allow the use of a single modulator format. A test port is included after the modulator to optimise its performance for single channel operation. The differential delays between each channel through the passive multiplexer were 1.16 ns, 6.03 ns, 7.17 ns and 18.51 ns, the last three of which were adjustable by up to 90 ps using fibre stretcher based optical delay lines. Whilst this arrangement preserves the correct number and arrangement of optical paths,

the only simplification in set up arises from the reduction in the number of modulators. Still further simplification of the passive OTDM multiplexer may be achieved by the use of cascaded delay line pairs as shown in Figure 3-39.

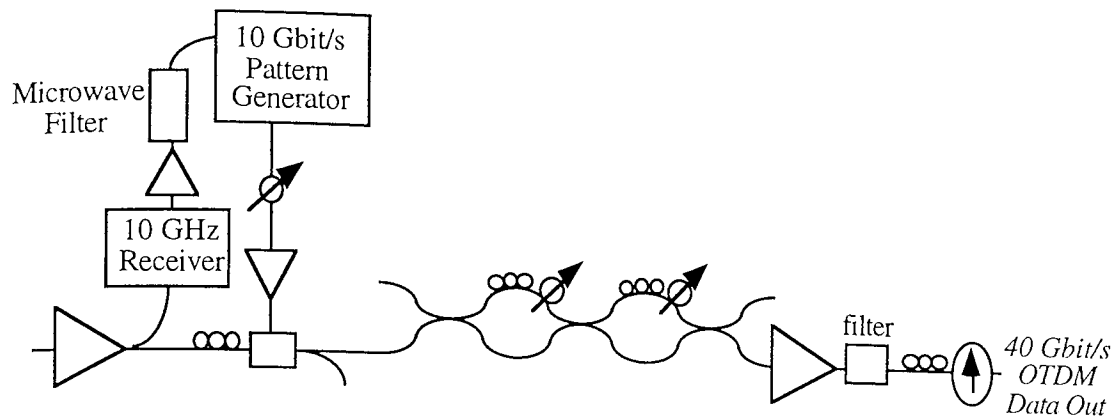


Figure 3-39 Schematic diagram of multistage partial OTDM multiplexer (MUX-3).

Note that in this arrangement, multiplexing is only possible in factors of two. However, considerable benefit is derived in terms of insertion loss, reducing from a minimum value of $10 \text{ Log}[N]$ (i.e. 6 dB for a 40 Gbit/s system) to 3 dB irrespective of the multiplexing factor (neglecting the excess loss of the couplers used). The differential delay in each interleaving stage was approximately 200 ns, ensuring significant decorrelation of the PRBS bit patterns.

3.4 Alternative OTDM data generation.

As we have seen, the most demanding constraints for OTDM pulse generation are mark to space ratio ($< 8\%$ for four fold multiplexing) and pulse to background extinction ratio ($> 38 \text{ dB}$ for four fold multiplexing) to ensure stable interleaving. As the system line rate (level of multiplexing) increases, these constraints become increasingly severe. One alternative solution is to generate a soliton train at the *line rate* and eliminating the need for multi-path optical multiplexing. There has been considerable recent interest in the generation of high frequency soliton trains based on non-linear optical beat signal to soliton train conversion in dispersion profiled fibre circuits^{165,166,167}. The technique offers the advantages of ultra-high repetition rates, high pulse quality, and broad, continuous wavelength and repetition rate tunability. In its simplest form, the output of two cw lasers of differing central frequencies generate a sinusoidal beat frequency corresponding to the target repetition rate, which is adiabatically compressed into a soliton pulse train in a non-linear fibre circuit.

Although many impressive results have been obtained, particularly for the generation of ultra high speed pulse trains¹⁶⁸ a number of practical issues must be resolved for the implementation of such a technique within a communications environment. Firstly, since the beat frequency signal nominally originates from a diode pair, the finite laser line width, and thermal drift in the laser centre wavelengths gives rise to high and low frequency timing jitter respectively. Several techniques may be used to stabilise the beat frequency drift, including the use of dual mode lasers^{169,170} and phase locked loops¹⁷¹. In both cases, the beat frequency is locked to an external clock signal, ensuring

operation at the required repetition rate. Alternatively, a single wavelength cw laser may be used, along with an electro optic modulator¹⁶⁸. The particular approach adopted in this thesis however relies upon the frequency doubling characteristics of Mach Zehnder modulators biased at maximum extinction. Appropriately driven such a scheme generates the beat frequency with high efficiency from a sine wave drive at half of the required frequency.

The second major difficulty arises from unwanted non-linear effects within the soliton compression fibres. In particular, stimulated Brillouin scattering¹⁷² limits the launched power, resulting in poor pulse formation^{173,166}. In order to increase the launch power (and allow for improvements in pulse quality) SBS suppression techniques must be employed taking care not to induce source timing jitter. Ideally, a single laser source should be used (this work and simultaneously by Swanson and Chin¹⁷⁴), or the diode pair linewidths should be broadened by synchronous modulation, either via bias current modulation or using an external modulator¹⁷³.

Finally, in order to initially verify the suitability of the technique to communications networks, "relatively low" repetition rate pulse trains (eg 40 GHz) must be generated to enable testing and comparison with traditional OTDM implementations. It is well known that for a simple soliton compressor comprising dispersion decreasing fibre, the net fibre length increases with decreasing repetition rate. It has been shown however, that if the input seed spectrum is spectrally enhanced (through SPM in a length of uniform dispersion shifted fibre), fibre lengths are reduced to a manufacturable level of a few kilometers^{167,175}. In this thesis, such a fibre circuit is evaluated for pulse generation at repetition frequencies between 35 and 40 GHz, using a Mach Zehnder modulator for the generation of a stable pulse train¹⁷⁶. Whilst offering little advantage over conventional techniques at this low bit rate, this investigation serves to verify the suitability of the technique to communications applications. This work was carried out as part of a EU funded collaborative project with the University of Southampton (ARTEMIS).

3.4.1 Generation of 40 GHz pulse train by beat frequency conversion

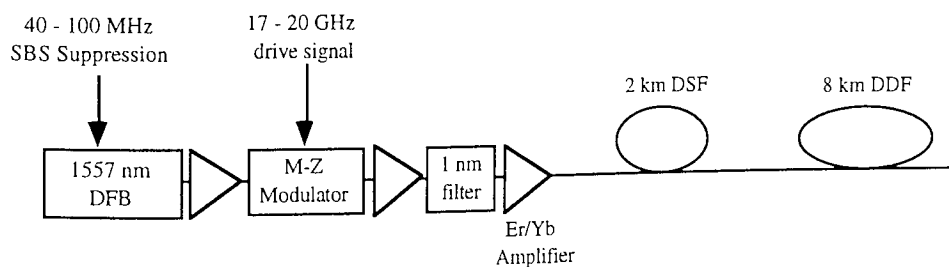


Figure 3-40 ; Schematic diagram of beat frequency conversion source.

The source configuration used is shown in Figure 3-40. In order to obtain a low timing jitter beat signal a 20 GHz amplitude modulator was tuned to a transmission null and driven at between 17.5 and 20 GHz to obtain 35-40 GHz sinusoidal modulation of the output from a DFB laser diode. The output from the beat signal source as measured on a scanning Fabry Perot interferometer (1 GHz resolution) and is shown in Figure 3-41

illustrating an almost complete rejection of the carrier. The DFB laser was itself modulated at 100 MHz to eliminate Brillouin scattering within the DDF. The $\text{Er}^{3+}/\text{Yb}^{3+}$ power amplifier provided up to +21 dBm of beat signal. The dispersion decreasing fibre section consisted of 2 km of DSF to spectrally enrich the input beat signal, and an 8 km DDF. The DDF was designed to have a hyperbolic dispersion profile (at 1550 nm) tapering from 13 ps/(nm.km) at the input to 2.75 ps/(nm.km) at the output. The relatively high value of output dispersion was selected to reduce the absolute physical length of fibre required to obtain high quality, adiabatic 40 GHz pulse generation at an MSR of 5:1, whilst maintaining a practical optical power requirement on the input beat signal (theoretically 80 mW).

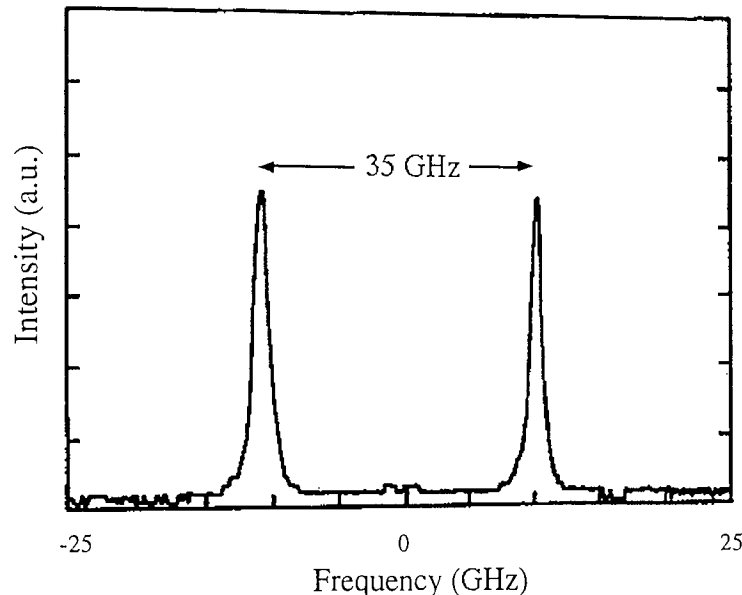


Figure 3-41; Typical beat frequency seed spectrum using Lithium Niobate Mach Zehnder modulator driven at 17.5 GHz and biased at the transmission null.

High quality soliton generation could be obtained in the repetition rate range 32-40 GHz with pulse duration's in the range 4.5-6.5 ps obtainable for input beat signal powers <20 dBm over the entire tuning range of the available diodes 1547-1563 nm. A typical autocorrelation and spectrum of a 40 GHz pulse train at the source output are shown in Figure 3-42. It should be noted that the amplitudes of the autocorrelation (central peak) and nearest neighbour cross correlation's are identical, indicating excellent pulse amplitude stability and low jitter. Furthermore, the output shows no degradation in spectrum when compared to traditional dual diode beat frequency sources. In particular, no observable spectral components at the RF frequency (20 GHz) are observed.

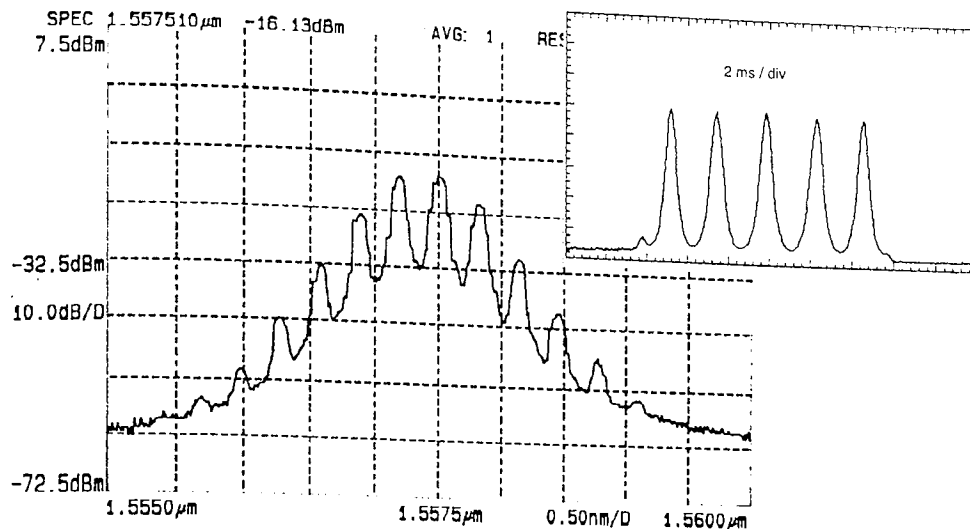


Figure 3-42 ; Typical spectral output of 40 GHz beat frequency to soliton conversion source. Autocorrelation shown as inset.

Whilst the performance was tolerant to small changes in the RF power level, variations in the dc bias point rapidly degraded both the spectral and temporal outputs. This technique however, allowed the output of the beat frequency conversion source to be displayed on a sampling oscilloscope for the first time¹⁷⁶, and a typical example, along with the RF drive signal, is shown in Figure 3-43 .

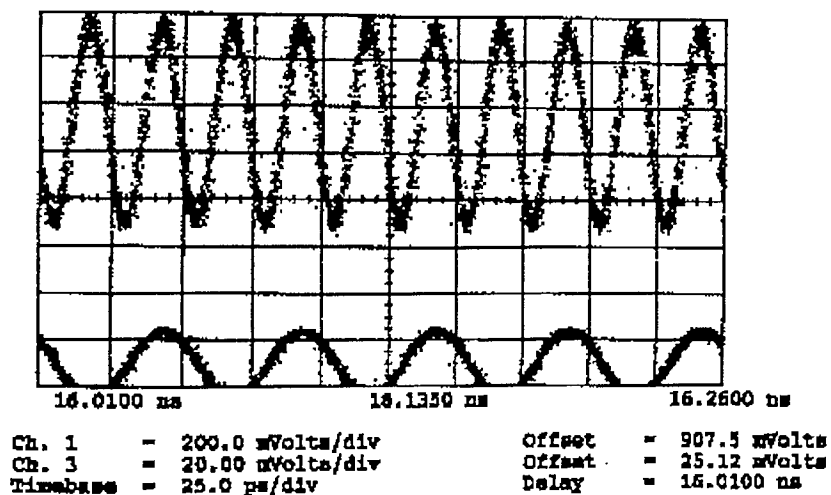


Figure 3-43 ; Output of 40 GHz beat frequency source (upper trace) and RF drive signal (lower trace) applied to modulator, displayed on a digital sampling scope.

Furthermore, accurate jitter analysis was possible by measuring the RF noise spectral density using microwave mixers and an RF spectrum analyser. The beat signal was detected using a 32 GHz bandwidth photodetector, and mixed with the frequency doubled output of a separate frequency synthesiser tuned to 19.8 GHz. The resultant 400 MHz beat frequency was displayed and analysed by comparing the total power within the signal harmonic and the noise sidebands in the usual manner⁷⁸. Having integrated the noise power spectral density, the rms. timing jitter is given by;

$$\sqrt{\langle \delta t^2 \rangle} = \frac{1}{2\pi n f_c} \sqrt{\frac{P_N(n)}{P_C(n)}}$$

Equation 3-53

Where n represents the harmonic number (1st harmonic or fundamental, second harmonic etc), f_c the fundamental repetition frequency $P_C(n)$ the total power of the n 'th harmonic and $P_N(n)$ the total RF power of the associated phase noise side bands. It is usual to analyse a series of harmonics of the pulse repetition frequency to allow the separation of phase noise contributions to the noise side bands (which grow with the square of the harmonic number) and contributions due to amplitude noise (which grow in proportion to the harmonic number).

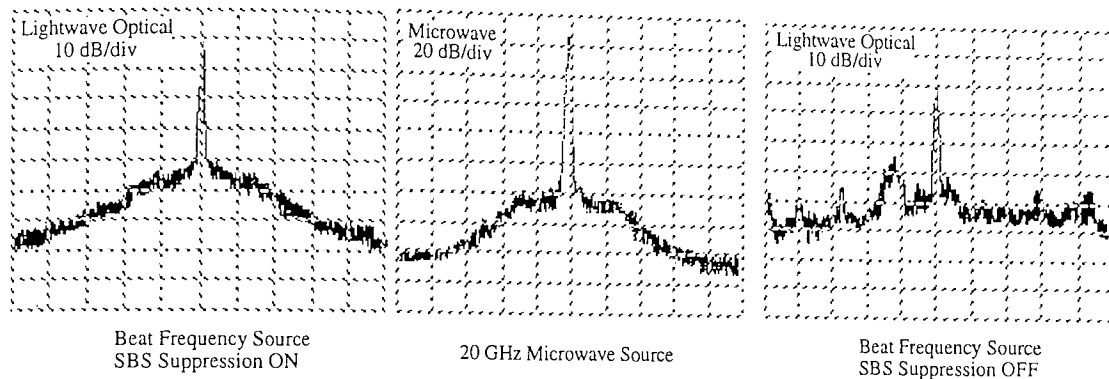


Figure 3-44 ; Jitter measurement of beat frequency source, showing the microwave source (centre) and soliton pulse trains with (left) and without (right) SBS suppression.

Typical measured beat frequencies from the soliton conversion source are shown in Figure 3-44. Attributing all of the noise to phase noise (rather than amplitude noise), yields a maximum rms. pulse to pulse jitter of less than 300 fs, equivalent to the known jitter of the electrical drive signal.

In summary, by constructing a low jitter beat frequency seed signal using an electro optic modulator, the world's first stable, low jitter soliton pulse streams based on beat frequency conversion have been generated at 40 GHz with a mark to space ratio of between 4 and 6.

3.4.2 Systems evaluation of beat frequency conversion source.

The motivation for studying this source configuration was to determine its suitability for communications applications, with 40 Gbit/s operation a means rather than an end in itself. Initially simple pulse propagation experiments using the source (tuned to give a 35 GHz pulse train) were performed over a previously investigated transmission line^{177,73} incorporating four 50 km spans of dispersion shifted fibre and 3 EDFAs (Figure 3-45). However, the results of these experiments, which represent the first long distance, multi-amplifier stage pulse transmission experiments using a beat-signal source, will not be described in this thesis. More importantly, because the source generates a train of fundamental solitons, at the maximum *line rate* of the system base rate modulation is precluded. Consequently, all optical modulation, or serial electro-optical modulation schemes must be pursued¹⁷⁸.

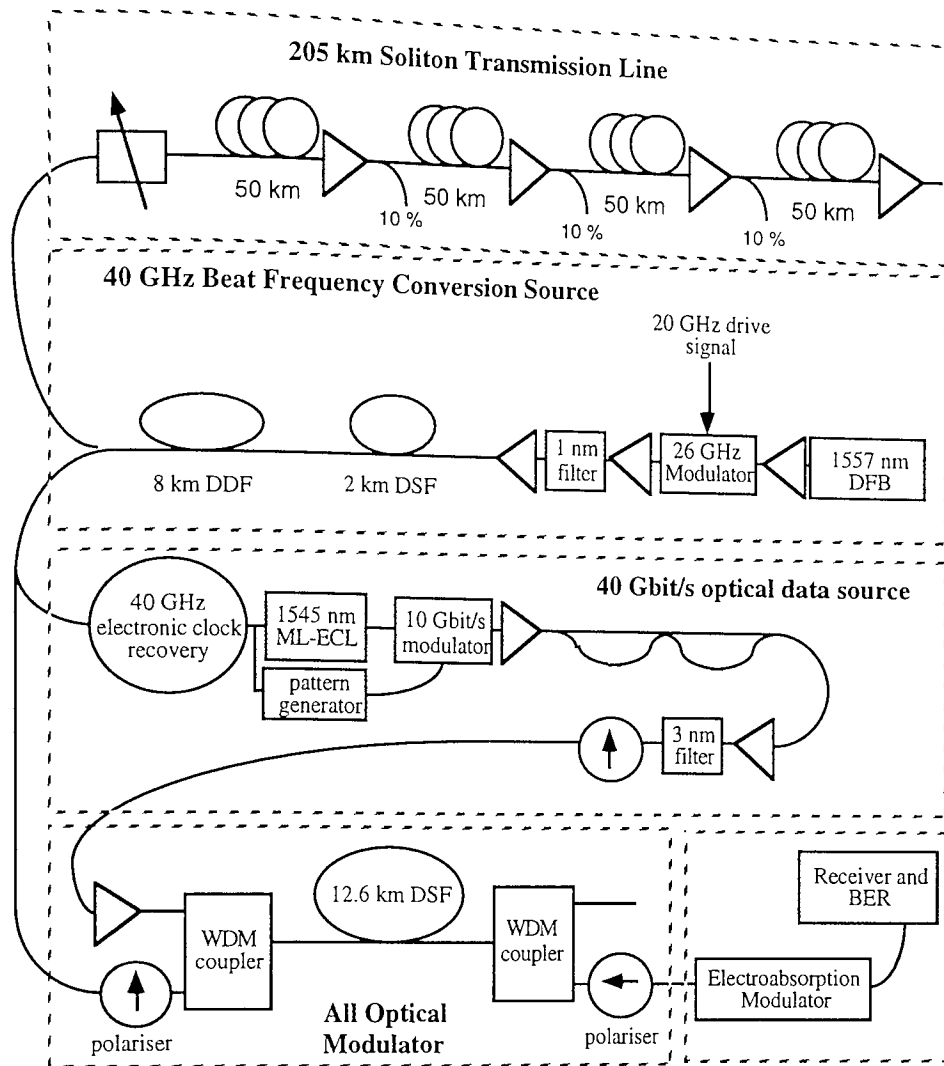


Figure 3-45 ; Schematic diagram of beat frequency source and source evaluation experiments (modulation and transmission)

The modulation scheme used should of course be carried out using an approach which may potentially produce data streams at bit rates exceeding 100 Gbit/s. Several promising candidates exist, including compact semiconductor switches⁸¹, four wave mixing devices¹⁷⁹ and devices based on cross phase modulation in optical fibres¹⁴⁴. However, in order to maintain the spectral and temporal purity of the source, it is imperative that the modulator does not excessively chirp the pulses. Thus for example, if a four wave mixing gate were employed, any chirp present in the data signal would be transferred to the outgoing data signal. Similarly, if semiconductor amplifier based switches are employed, the chirp associated with the simple amplification of the pulse train through the amplifier may significantly degrade the pulse quality. The demonstrations of all optical modulation of a 40 GHz soliton train reported in this thesis employed cross phase modulation interactions in dispersion shifted optical fibre. As such they are largely independent of the spectral purity of the driving signal. Two approaches were taken, utilising a non-linear optical loop mirror (NOLM)^{180,181}, and a fibre based Kerr gate¹⁸², and these two devices will now be described in turn.

3.4.2.1 All optical modulation with a non-linear optical loop mirror.

Figure 3-46 illustrates the layout of a typical NOLM gate. The 40 GHz beat frequency signal is applied to the signal input, and interaction with 40 Gbit/s control pulses would occur within the dispersion shifted optical fibre. Ideally, the dispersion zero of the fibre would be placed midway between the signal and control wavelengths to ensure the appropriate velocity matching. The 40 Gbit/s data source used to switch the soliton laser can, for example, be comprised of 6 to 10 ps pulses derived from almost any of the pulse sources described above, giving rise to peak powers up to ≈ 500 mW for a mean power of 50 mW. With zero walk through a π phase shift from cross phase modulation is then predicted for a 2.5 km length of dispersion shifted fibre. With a dispersion zero of 1550 nm, tuning the control and soliton signal wavelengths within the erbium amplifier window allows a walk through of between zero and ± 2.7 ps/km to be selected. Thus, with a fibre length of just under 10 km a total walk through equivalent to the system bit period of 25 ps is easily achieved. However, it is unlikely that such a large walk off would be required for this application due to the low duty cycles (of the 40 GHz soliton train) and negligible source timing jitter.

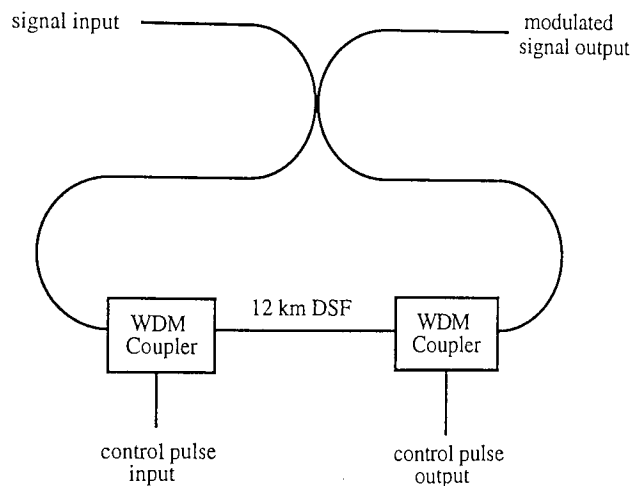


Figure 3-46 ; Schematic diagram of NOLM based all optical modulator.

Parameter	Without Walk Off	With Walk Off
Probe pulse width (ps)	5	
Control pulse width (ps)	6.4	
α (km^{-1})	0.046	
n_2 ($\text{m}^2 \text{W}^{-1}$)	$3.2 \cdot 10^{-20}$	
A_{eff} (m^2)	$50 \cdot 10^{-12}$	
Fibre Length (km)	12.6	3
Mean Control Power (mW)	8	25

Table 7 : Default parameters used to model the performance of a NOLM based all optical modulator.

Modelling results of this configuration has been carried out with zero walk off, for a range of pulse widths. The results for a NOLM biased to be normally reflecting are

shown in Figure 3-47. The results in this figure have been calculated with a simple analytical model (based on the cosine of the phase shift predicted by equation 2-17), Athens¹⁸³. In this simple theory, pulse shaping effects due to self phase modulation and dispersion have been neglected. Non-inverting modulation is achieved since a signal pulse is transmitted from the loop mirror for each control pulse. Since the instantaneous intensity of the 6.4 ps control pulse and the 5 ps soliton pulse are varying simultaneously, complete switching is not possible over the entire pulse width and in this case a significant portion of the energy ($\approx 10\%$) will be reflected from the loop mirror. For the calculated optimum length for a π phase shift, we would expect 100% transmission at the pulse peak, and the pulse wings would be strongly attenuated. This may be of benefit for improving the pulse quality if any pulse wings are present from the 40 GHz source, but only serves to degrade the pulse quality of ideal pulses from the beat frequency source. A greater total energy throughput may be achieved if the fibre length is optimised so that the peak phase shift is greater than π .

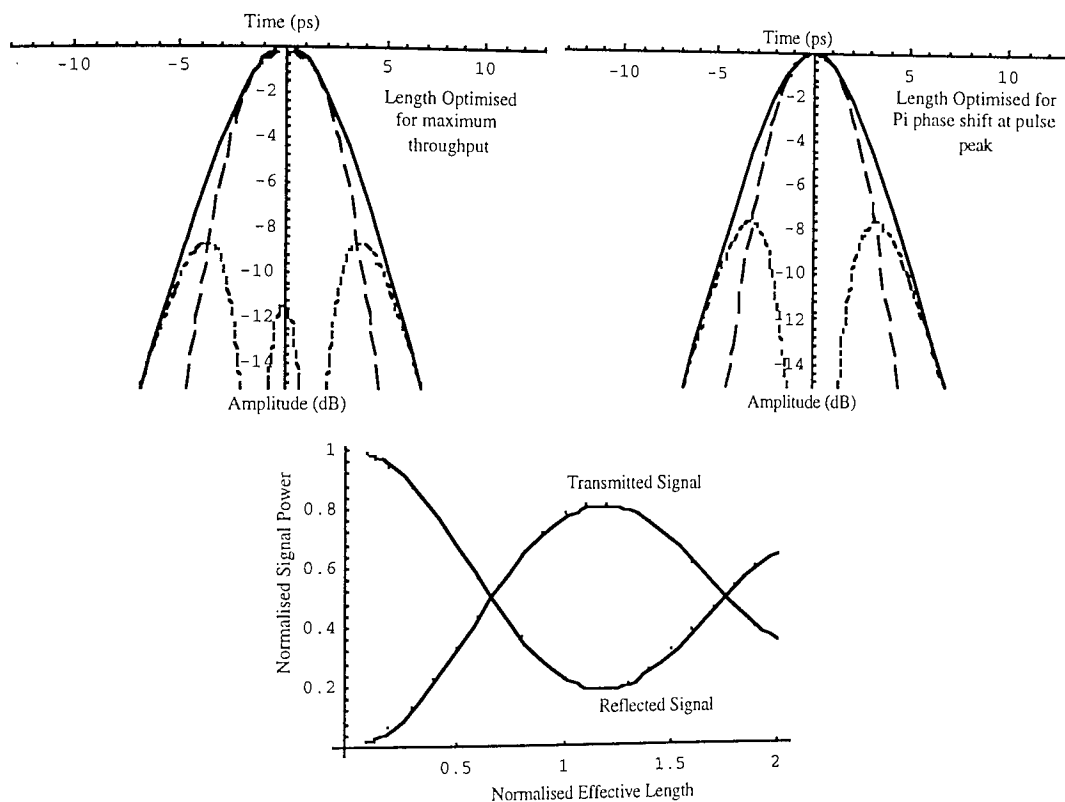


Figure 3-47 ; Performance of 40 Gbit/s NOLM based all optical modulator with zero walk through, showing input (solid line) transmitted (long dashes) and reflected (short dashes) pulse shapes and the effect of fibre length (normalised to π peak phase shift)

As may be expected, as the ratio of control pulse width to signal pulse width is increased, the transmission efficiency is increased, as shown in Figure 3-48. This follows simply from the fact that a greater portion of the signal pulse lies close to the peak of the control pulse. However, the control pulse should be constrained within the bit period (25 ps) to eliminate the possibility of crosstalk. In this instance, crosstalk refers to the partial switching of a soliton pulse due to the presence of a control pulse in

an adjacent time slot.

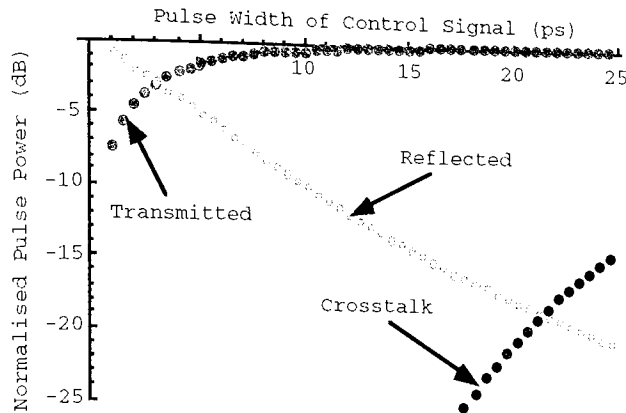


Figure 3-48 ; Variation of through signal attenuation (red), reflected power (light blue) and adjacent channel crosstalk (dark blue) of NOLM based 40 Gbit/s optical modulator as a function of control pulse width.

It is thus easy to conclude that in the non-inverting state (soliton output pulse when control pulse applied), with zero walk off, either severe pulse distortion will occur (short control pulses), negating the benefit of a pure soliton source, or unacceptably high levels of crosstalk will occur (long control pulses). If on the other hand, the normal bias point of the NOLM is adjusted to give transmission in the absence of control pulses (the inverting state) then the action of the control pulses is meagrely to remove power from unwanted pulses. In this case, the signal throughput comprises relatively undisturbed pulses for data 1's, but incomplete switching by the control pulses (light blue curve of Figure 3-48) implies that the extinction ratio of the output signal will be poor (< 15 dB).

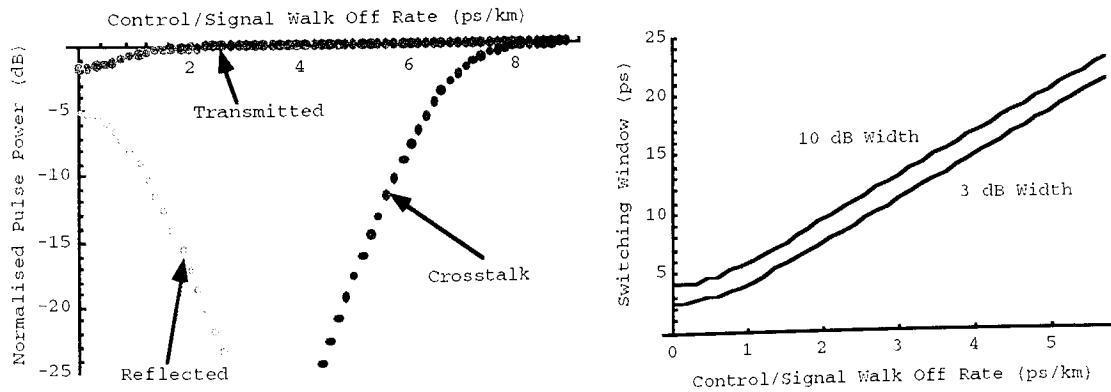


Figure 3-49 ; Anticipated Performance of 40 Gbit/s NOLM modulator as a function of walk off rate between 5 ps signal and 6.4 ps control pulses, with a fixed fibre length and a signal power adjusted for a peak phase shift of π .

The performance of both inverting and non-inverting states is fortunately greatly enhanced by employing short pulses (for low crosstalk) and a significant degree of walk through (for low pulse distortion). This is illustrated in Figure 3-49, where an optimum performance in terms of transmitted energy and crosstalk is achieved for walk off rates between 3 and 4 ps/km, provided that the control pulse amplitude is increased to induce a peak phase shift of π in the signal pulse for each value of walk off rate.

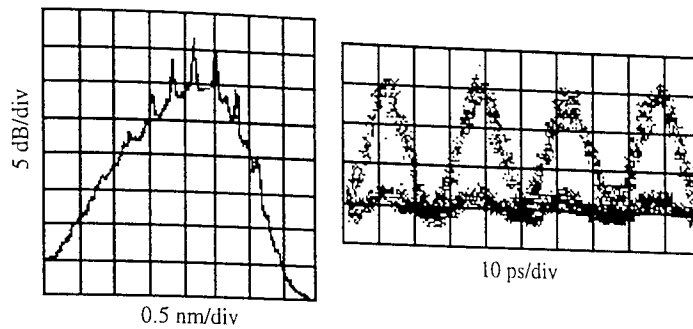


Figure 3-50; Output eye diagram (right) and spectra (left) of beat frequency source modulated at 40 Gbit/s using a NOLM modulator.

The performance of the NOLM for modulation of the beat frequency source (arranged as Figure 3-45 above but with the NOLM replacing the Kerr gate) is illustrated in Figure 3-50, where the 5 ps pulses from the 1557 nm beat frequency source were switched to the NOLM output by a 40 Gbit/s data stream comprising 6.4 ps, 1545 nm pulses derived from a jitter suppressed gain switched DFB. Clearly although an adequate eye diagram was achieved, with no observable degradations, the optical spectra is strongly distorted. This may be due to the residual chirp imposed by the data sequence¹⁸⁴, nevertheless, this poor spectral quality, coupled with the dubious environmental stability of a NOLM constructed from standard dispersion shifted fibre¹⁸⁵ results in an unsatisfactory pulse source.

3.4.2.2 All optical modulation with a Kerr rotation gate

For these reasons, the use of a Kerr rotation gate for the all optical modulation was favoured over the NOLM. Whilst theoretically of a fundamentally more complex nature, the overall characteristics of a Kerr gate are, in principle, the same as for a NOLM gate. That is the switching window is governed by the cosine of the induced phase shift, which in turn is determined from the walk of rate and the control signal pulse width. A schematic diagram of the Kerr gate is shown in Figure 3-51, where non-linear polarisation rotation along the dispersion shifted fibre is converted into intensity modulation via the output polariser. The input polariser is used to ensure a linearly polarised signal after pulse generation in the DDF and consequently ensures that the maximum 30 dB extinction ratio may be achieved.

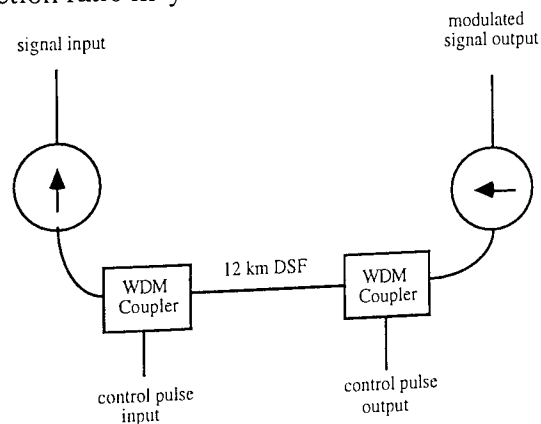


Figure 3-51; Schematic diagram of Kerr gate

Figure 3-45 illustrates the experimental arrangement, incorporating the soliton source

described above and an electronic clock recovery circuit to ensure that the modulating data is synchronised to the generated pulse stream. 6.4 ps pulses from a 10 GHz, 1545 nm semiconductor mode locked external cavity laser, modulated with a 10 Gbit/s 2^7-1 PRBS was input to the optical modulator via a 4 to 1 passive multiplexer to generate a 40 Gbit/s test signal. The all optical modulator itself comprised a 12.6 km length of dispersion shifted fibre ($\lambda_0 = 1551$ nm). With the two polarisers initially crossed the action of the 1545 nm data signal is to open the gate (non-inverting modulation). The output of the all optical gate when the soliton stream is modulated by the 1545 nm data sequence is shown in Figure 3-52. In this mode, the finite switching window of the all optical modulator (measured to be 19 ps) imposed a slight degree of pulse shaping, decreasing the pulse width from 4.5 ps to 4 ps. However, despite this slight corruption of the pulse profiles, a highly uniform 40 Gbit/s pulse train is generated (as shown by the autocorrelation) with a clearly open eye.

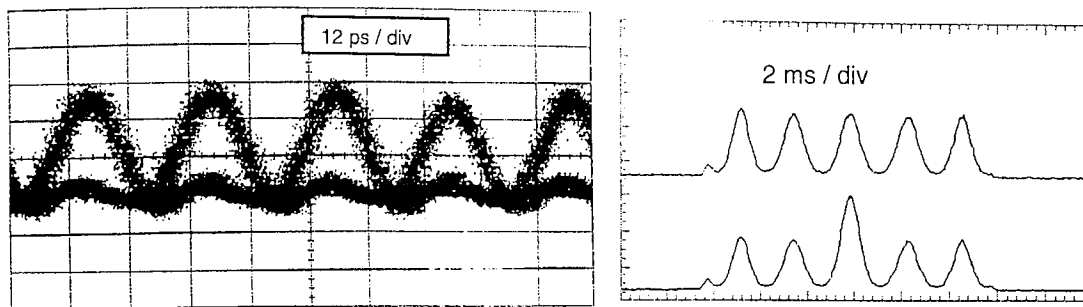


Figure 3-52 ; Modulated output of beat frequency source using Kerr gate. Showing eye diagram (left) and autocorrelation (right). The upper trace on autocorrelation represents modulation by all ones and the lower trace by a PRBS data sequence.

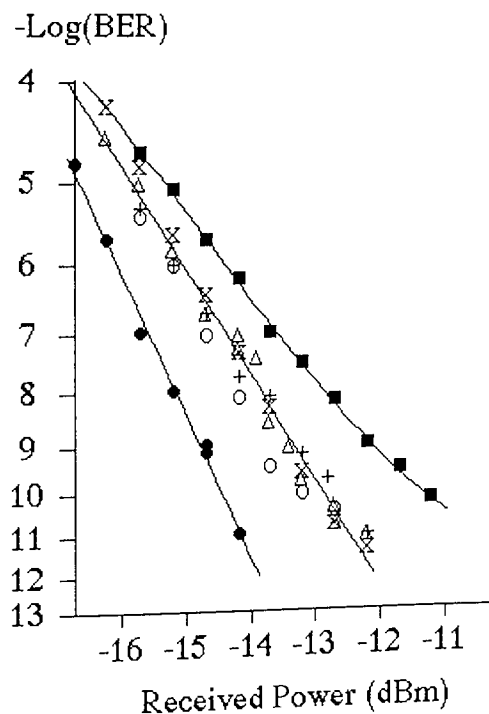


Figure 3-53; BER characteristics for 40 Gbit/s modulation of a beat frequency source, showing 1545 nm back to back at 10 Gbit/s (filled circles) and 40 Gbit/s (filled squares) along with all four channels of the modulated beat frequency source at 1557 nm. Signal powers are measured at the input to the photodiode.

In order to thoroughly assess the performance of this modulation scheme, error ratio measurements were performed for non-inverting modulation at 40 Gbit/s after the signal was demultiplexed to 10 Gbit/s using an electroabsorption modulator. As can be seen from Figure 3-53, error free operation was easily achieved for the modulated beat frequency signal, however, the 1545 nm 40 Gbit/s back to back signal demonstrated a significant error floor due to the finite extinction ratio of the electroabsorption modulator (22.0 dB) at that wavelength. Consequently, the apparent performance of the modulated beat frequency signal will be partly obscured by the extinction ratio at 1557 nm (25.3 dB), but clearly demonstrates a penalty of less than 1.5 dB when compared to a simple 1545 nm 10 Gbit/s signal.

3.5 Chapter Summary

In this chapter, we have discussed the construction and interconnection of OTDM transmitters. Of critical importance is the pulse source, requiring a sufficiently low duty cycle, whilst maintaining an extremely high extinction ratio. These requirements are readily achieved using mode locked fibre ring lasers. Whilst many other sources appear promising, the demanding constraints of OTDM systems reduce the areas of applicability of such sources. Suitable alternatives include EC-MLL, offering the advantage of simple wavelength and repetition rate tunability, at the expense of pulse quality. Similarly, electroabsorption modulators produce high quality pulses, but with reduced extinction ratio, necessitating the use of cascaded modulators. However, the unique properties of electroabsorption modulators has enabled the demonstration of a unique single modulator based source of data encoded solitons, suitable for simultaneous operation over a large number of wavelengths.

Having selected a suitable pulse source (in this thesis a mode locked laser or multiple electroabsorption modulators) - it remains to construct the modulator array to encode N copies of the pulse train with N independent data signals. Ideally, an integrated array of modulators would be used, however, in the medium term, fibre based multiplexers offer a more readily available alternative. This should be borne in mind when simplified experimental transmitters (based on a single modulator and passive interleavers) are constructed. In particular, the incoherent interference penalties of long fibre based interleavers differ significantly from short, integrated passive interleavers. Similarly sufficient delay should be present in any passive interleaver to decorrelate the test patterns and avoid masking pattern dependant and demultiplexer penalties.

The chapter was concluded with a comprehensive investigation of beat frequency conversion sources. Such sources relax the demanding constraints of OTDM pulse sources by eliminating the need for interleavers and offer the potential for ultra high repetition rate operation. However, the practical deployment of these sources requires the development of suitable all optical modulators. The world's first complete assessment of an OTDM data source based on this technology was successfully completed, and offers an interesting alternative to traditional OTDM multiplexers. Similarly, pulse shaping and multiplexing of NRZ signals may be used to form an alternative OTDM source^{361,186}.

4. OTDM Receivers

In the previous chapter, the construction of picosecond pulse sources and OTDM multiplexers to allow the generation of OTDM signals were examined. Following the transmission and routing of these signals (covered in chapters 5 and 6 respectively) it is the function of an OTDM receiver to recover one or more base rate electrical data signals from the serial OTDM data stream. In addition to components traditionally used in optical communications systems (which will not be covered in detail here) such as optical pre amplifiers and opto electronic converters, an OTDM system requires an active demultiplexer in order to separate out the individual channels, and a clock recovery circuit to provide the appropriate synchronisation on a picosecond timescale. These two functional blocks are discussed in this chapter. Electronic clock recovery is introduced as the natural choice for OTDM synchronisation, whilst optical clock recovery is discussed with regenerative applications in mind. For the demultiplexer function, the discussion is restricted to electro-optic devices, offering the potential of 160 Gbit/s operation using existing commercial technology.

4.1 Clock Recovery

In order to separate the individual OTDM channels, an active processing device is required, driven by optical electrical signals in precise synchronism with the incoming data. This requires the development of low jitter clock recovery circuits. Several options for the deployment of OTDM clock recovery exist, and these are illustrated in Figure 4-1 (expanding the detail for figure 1.1) for a typical OTDM node.

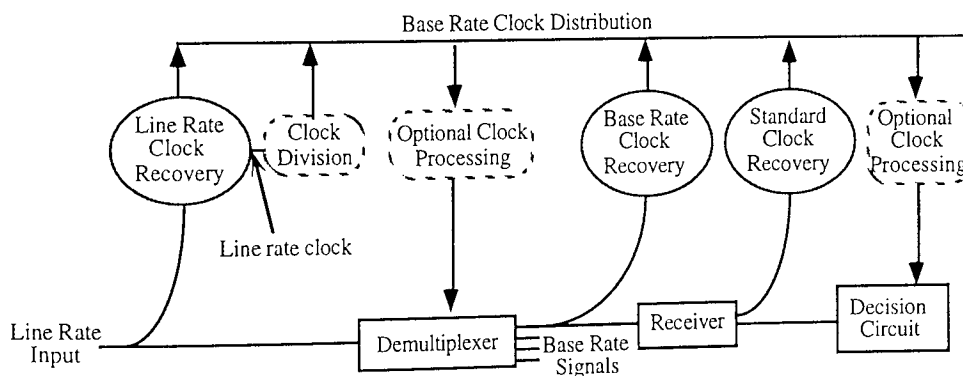


Figure 4-1 Options for the location of an OTDM clock recovery circuits.

Typically only one of the clock recovery circuits shown would be employed for any given system, providing synchronisation for all required functions within the node (the diagram illustrates demultiplexing and the decision circuit). The optional clock processing elements shown may include functions such as conversion between optical and electrical signals, optical or electrical pulse compression or wavelength conversion. Recall that a properly interleaved OTDM data signal does not contain a distinct RF spectral component at the base rate clock frequency, only at the higher line rate. Whilst it has been proposed that a system with deliberately mis-aligned interleaving may be used for clock distribution¹⁸⁷, this condition cannot always be guaranteed, especially

after traversing an optical network, or a transmission line employing soliton control. Consequently, timing extraction prior to the demultiplexer is not generally possible at the base rate. Clock recovery may also be achieved by recovering a line rate clock signal and performing an optical or electrical clock division process to obtain the necessary base rate clock signal. Whilst this approach has proved successful, the process of clock division becomes increasingly difficult for increasing line rates^{188,189}. One alternative is to perform base rate clock recovery (optical or electrical) following the demultiplexer where an appropriate RF component exists¹⁹⁰. However this approach is often troublesome with the possibility of start up ambiguities and "self pulsation"¹⁹¹. Clock extraction at the full line rate prior to demultiplexing, but with a clock output at the system base rate is clearly the most favoured option, allowing the development and optimisation of components in isolation, and the operation in logical sequence through an OTDM node.

4.1.1 Electronic Clock Recovery

Electronic clock recovery has previously been achieved using a 40 GHz phase lock loop (PLL) in which the phase comparison was performed at 40 GHz but the VCO ran at the base rate of 10 GHz⁷³. Following the VCO two stages of frequency doubling and narrow band amplification at 20 GHz and 40 GHz were used to derive a 40 GHz local oscillator. This is illustrated in the upper circuit diagram of Figure 4-2, and may be constructed entirely from commercially available components. The circuit recovers a stable 10 GHz clock signal from 10, 20 or 40 Gbit/s data signals with rms jitter levels well below the available measurement resolution of 300 fs for input signal powers above -22 dBm.

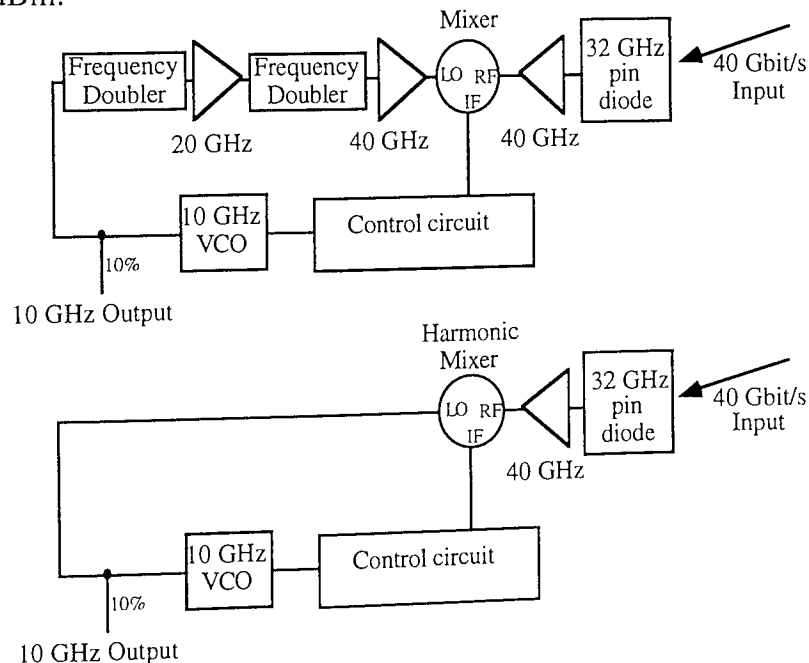


Figure 4-2 Schematic diagram of electronic clock recovery circuits

This sensitivity level has recently been improved to -28 dBm by decreasing the VCO sensitivity from 17.6 MHz/V to 6.67 MHz/V (allowing higher gain within the control circuit). In an alternative configuration (the optical phase locked loop), the frequency

multiplication process occurs during the generation of a short optical pulse, whilst mixing is performed via cross gain modulation¹⁹² or four wave mixing in a semiconductor amplifier¹⁹³. In this thesis, a new electronic circuit has been designed that utilises a harmonic mixer in which the local oscillator input is at 10 GHz realising a much more practical solution. This is illustrated in the second schematic diagram of Figure 4-2. The phase comparison is still performed at 40 GHz since the non-linear properties of the harmonic mixer are used to derive the appropriate harmonics from the local oscillator with high efficiency. The conversion efficiency of the mixer decreases with harmonic number and in this case was -14 dB for operation at 40 GHz with a local oscillator of 10 GHz. The new circuit was able to recover a stable clock signal at a data signal power of -18 dBm input to the *pin* and for input powers above -15 dBm the measured jitter was below that of the 10 GHz synthesiser used in the source (≈ 300 fs). Both measurements were performed with a 2^7-1 PRBS data pattern but no noticeable degradation was observed on a high speed scope for pattern lengths up to $2^{31}-1$, or with error rate measurements made using the longer pattern lengths (for which penalties as small as 1 dB were recorded).

Mature RF technology suggests that similar operation would be achieved for bit rates of 100 Gbit/s, using a Waveguide 27 (75-110 GHz) based harmonic mixer (optimised for the 10th harmonic). With a measured conversion loss of 20 dB at 92 GHz using Millitek MSH-10 mixer, satisfactory operation may be anticipated for input 100 Gbit/s signal powers of a few mW. Recent advances in device technology suggest that the only constraining in this conversion factor is the device packaging¹⁹⁴.

4.1.2 All Optical Clock Recovery

Clock recovery may also be performed all optically using a number of techniques, however, unlike phase locked loop techniques (either optical or electrical), optical clock recovery techniques usually derive clock signals at the same frequency as the input data stream. It is well known that a simple FM mode locked ring laser may be used perform clock recovery, if the driving signal is replaced by an optical data stream^{195,112}. The data copropagating along a length of dispersion shifted fibre causes a periodic modulation of the laser cavity through cross phase modulation. Modelocking occurs provided that the round trip delay of the laser cavity is equal to an integer multiple of the bit period of the input data stream. In the case of a simple FM mode locked ring laser, data ones serve to mode lock the laser, whilst a data zero simply has no effect, allowing the circulating pulses to propagate undisturbed. Unwanted spontaneous emission noise is either incorporated into the pulse, or chirped by the wings of the incoming data to be attenuated by the cavity filter. Consequently, although little difference is anticipated between mode locked and clock recovery operation of an FM mode locked laser (slight change in the required signal powers) quite high launch powers are required (to give XPM phase shifts of a few π). However, we have seen above that the simple addition of a polariser to a mode locked fibre ring laser greatly reduces the required peak phase shift by adding a synchronous amplitude modulation to the system. The reduced phase shift requirement of this configuration allows the construction of relatively short ring

laser cavities. We now examine the clock recovery performance of such a cavity, paying particular attention to the effects of the amplitude modulation. The laser cavity investigated is shown in Figure 4-3, the basic characteristics of which were described in chapter 3 for a 12.6 km fibre length.

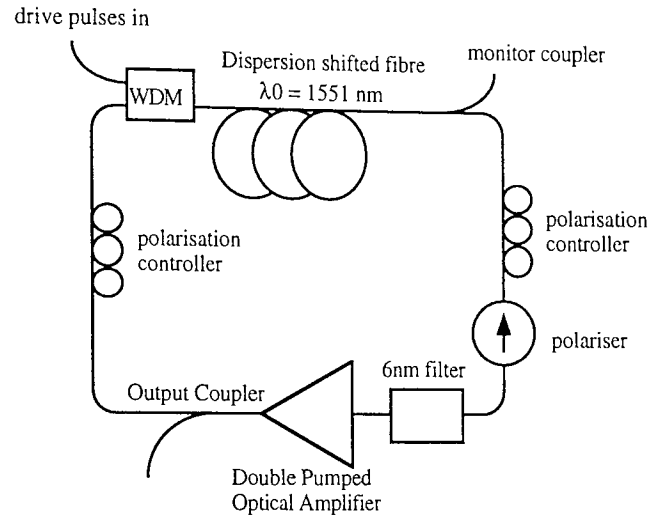


Figure 4-3 : Erbium fibre ring laser clock recovery

The laser, constructed with 12.6 and 1 km fibre lengths was driven with 10, 20 and 40 Gbit/s OTDM signals derived from a harmonically mode locked external cavity laser, modulated with a 2^7-1 PRBS data sequence and interleaved using MUX-3. The pulse source had a central wavelength in the region of 1545 nm, and following linear compression, generated ≈ 7 ps pulses. The ring laser was nominally tuned to a central wavelength of typically 1554 nm, giving a typical walk off rate of 0.67 ps/km in the 1550.5 nm dispersion zero fibre, however, slight variations to this central wavelength occurred during day to day optimisation of the cavity without significant degradation in performance. The cavity round trip times corresponded to a fundamental frequency of 9.167 kHz for the 12.6 km modulator fibre, and 188 kHz for the 1 km fibre, and could be directly observed as periodic resonant noise spikes in the RF spectrum (see Figure 4-7). Thus 40 Gbit/s clock recovery corresponds to modelocking on approximately the 4.3 millionth and the 200 thousandth harmonic of the fundamental for each laser. In all cases the drive frequency was matched to a harmonic of the cavity round trip by manually or automatically adjusting the drive frequency of the source laser. Typical clock recovered pulse streams, at 10 and 40 GHz are shown in Figure 4-4 obtained using the 1 km fibre length.

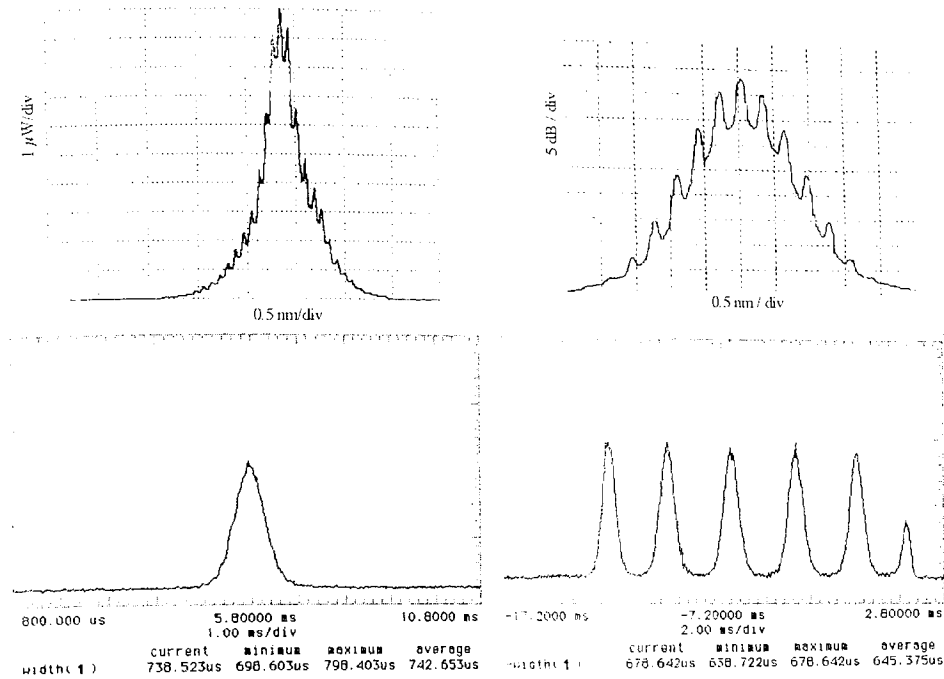


Figure 4-4 Output of 1 km clock recovery circuit, driven by 10 Gbit/s (left) and 40 Gbit/s (right) data signals, showing spectra (top) and autocorrelations (bottom).

During the assessment of the laser driven by a continuous sequence of pulses (mode locked operation), it was observed that the quality of the mode locking could easily be deduced from the optical spectrum, via the visibility of the individual spectral modes. This spectral mode contrast ratio (SMCR) is defined as the ratio between the peak intensity of the modes and the background level between the modes. The variation in SMCR for mode locked and clock recovery modes of operation for this ring laser (12.6 km fibre length), with a 40 GHz output signal is shown in Figure 4-5.

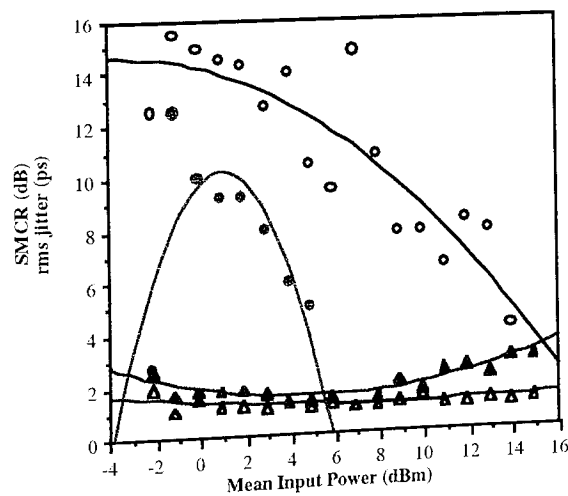


Figure 4-5 Variation of jitter (triangles) and spectral mode contrast (circles) for 40 Gbit/s clock recovery in a 12 km mode locked ring laser with data (filled) and clock (open) inputs. Solid lines represent parabolic data fits to guide the eye.

Whilst it is apparent that broadly similar performance may be achieved for a data input signal, the operating range of the ring laser is dramatically reduced. On the low power side, the clock recovery simply fails due to insufficient modulation strength,

exacerbated by the net reduction in strength due to the data zeros. On the high power side, the situation is more complex, and relates to competition between active and passive mode locking. In the case of normal modelocking (driven by a continuous clock signal), it is possible to align the cavity such that the transmission through the polariser is maximised during the presence of a drive pulse. In this way the phase modulation (XPM) and amplitude modulation (via non-linear polarisation rotation) act cooperatively to produce strong mode locking. In the case of clock recovery (ring laser driven by a data sequence), if the cavity alignment remains unchanged, pulses recirculating within the cavity will be somewhat attenuated by the polariser in the presence of a data zero, and the amplitude modulation acts to destroy the mode locking imposed by the XPM. However, provided that the polarisation rotation is small, a slight adjustment of the cavity will ensure that the attenuation of the recirculating pulses is the same in the presence of one's or zero's, with the unwanted spontaneous emission being dissipated by virtue of a slight intensity dependant polarisation rotation within the cavity (through SPM). A recent study has further investigated these dual effects of amplitude and phase modulation in a clock recovery circuit based on a figure 8 laser¹⁹⁶.

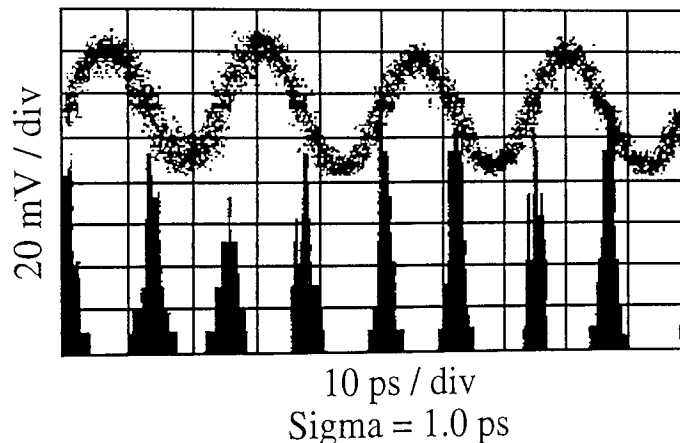


Figure 4-6; Jitter measurement of 12.6 km fibre ring laser 40 GHz clock recovery

Figure 4-6 illustrates the extremely low jitter (resolution limited) obtained for the clock recovery circuit after careful optimisation of signal powers and polarisations using the 12.6 km fibre. In this example, a mean 1546 nm, 40 Gbit/s signal power of 1.1 mW (giving a peak XPM phase shift of less than 0.08π , neglecting walk off) was used to give a recovered clock of 5.8 ps pulse width with a peak wavelength of 1555.2 nm. Further results are summarised in Table 8, including, for reference, the previously published result in the absence of a fibre polariser¹⁹⁵ (denoted *).

Bit Rate (Gbit/s)	Cavity Length (km)	Peak XPM Phase Shift (rads)	Data Wavelength (nm)	Pulse Width (ps)	Clock Wavelength (nm)
40	12.6	0.08π	1546.0	5.8	1555.2
10	1	0.02π	1545.2	4.5	1553.1
40	1	0.06π	1543.7	4.1	1554.1
40 *	11	π		5	

Table 8 Summary of clock recovery experiments using a mode locked fibre ring laser

Note the increased peak phase shift required for 40 Gbit/s operation (between 3 and 4 times), indicating either a reduction in beneficial intra-cavity effects such as non-linear polarisation rotation due to reduced peak powers, or the necessity to reduce interactions between the recirculating pulses due to the reduced pulse spacing¹⁹⁷.

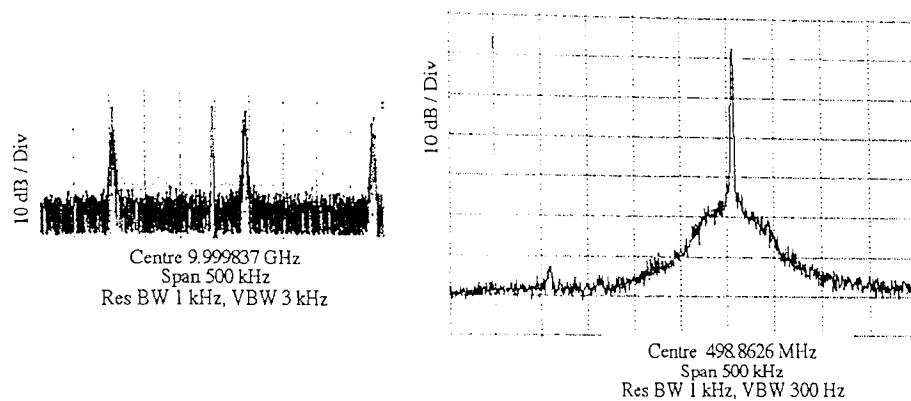


Figure 4-7 RF spectra of 40 GHz clock recovery, showing lock condition (left) and the downconverted 40 GHz harmonic (right)

Figure 4-7 illustrates two experimental RF spectra of the laser. The right hand spectrum illustrates the heterodyne spectrum of the 40 GHz component of the recovered clock, obtained by mixing the output of the laser with the output of a second RF source tuned to 9.875 GHz in a harmonic mixer. Whilst the observed phase noise dominated by the mixing process, this figure serves to illustrate the excellent suppression of the cavity mode harmonics and verifies that the laser is well mode locked. The left hand spectrum also illustrates a stable mode locking condition, with the residual 10 GHz data component located 3/4 of the way between the cavity mode harmonics at 10 GHz. This corresponds to the 40 GHz fundamental frequency of the drive signal matching an ODD harmonic of the cavity round trip and ensures that any given pulse recirculating within the cavity is mode locked by pulses from all four OTDM data channels. If on the other hand, the residual 10 GHz component is aligned exactly with a cavity harmonic, then each pulse within the cavity is mode locked by only ONE of the data channels, and consequently the recovered clock signal comprises four independent 10 GHz clock streams (or two 20 GHz streams). Unfortunately due to slight differences between the input OTDM data channels, one channel tends to become dominant, and the recovered clock exhibits a strong 10 GHz component. Similarly, a strong 20 GHz component in the recovered clock is evident when the residual 10 GHz component falls halfway between the cavity harmonics¹⁹⁸.

4.1.3 Alternative OTDM clock recovery techniques

Technique	Location	Output	Max Frequency / Highlights	Ref
Self Pulsating Laser Diode	post demux	Optical	18 GHz	199
			5 GHz in 20 Gbit/s OTDM	190
SAW filter	post demux	Electrical	20 GHz	200
	pre demux		2.5GHz in 10 Gbit/s OTDM	188
Electronic PLL	pre demux	Electrical	40 GHz	73
Optical PLL	pre demux	Optical or Electrical	400 GHz	201
FM ring laser	post demux	Optical	40 GHz	195
Programmable Fibre Ring Laser	pre demux	Optical	2 GHz	189
Semiconductor ring laser	post demux	Optical	20 GHz	202
TWSLA-NOLM ring laser	post demux	Optical	40 GHz	203
Injection locked semiconductor MLL	post demux	Optical	10 GHz	204
	pre demux		40 GHz	205
Optical Tank Circuit	post demux	Optical	2 GHz	206
Optical Mixer	post demux	Optical or Electrical	1 GHz	207
			40 GHz	208
WDM	pre demux	Optical or Electrical	20 GHz	209

Table 9; Summary of alternative OTDM clock recovery techniques

Various alternative clock recovery schemes have been investigated worldwide for high speed transmission systems, and have been categorised above (Table 9) according to their output signal and their location within Figure 4-1. Whilst many of these techniques are promising, only the two PLL based options demonstrate the levels of performance and stability for deployment in the logical pre-demultiplexer location. Indeed, the alternative schemes have been sparsely deployed in systems demonstrations, and remain proof of principle investigations. However, for all optical processing systems²¹⁰, optically mode locked lasers show great promise where base rate signals are not necessarily required. Given the simplicity of operation, and excellent performance, PLL techniques are certainly the most promising techniques reported to date. In particular, where commercial photodiodes are available, the ready availability of suitable electronic components suggests that electronic PLL's should be favoured.

4.2 Demultiplexers

In order to separate out the individual base rate channels from an OTDM data stream, some form of active demultiplexer is required (Figures 1-1, 1-34 & 4-1). A wide variety of optical demultiplexers have been demonstrated (see Table 10), falling into three broad categories;

- All optical switching - relying on a χ^3 mediated interaction between optical pulses.
- All optical switching - mediated by free carriers in a semiconductor material.
- Electro-optic switching - where optical pulses are switched by electrical signals.

Type	Technology	Configuration	Line Rate (Gbit/s)	Ref
Electro Optic	Sinusoidal Polarisation Switch	Multistage	6.7	68
	"Velocity Matched Gate"		Proposal	211
	Mach Zehnder Modulators	Integrated Multistage <i>Single Stage</i>	4	212
			40	213
		Multistage	40	73
		Single stage	40	118
	<i>Electroabsorption modulators</i>	<i>Single stage</i>	80	121
χ^3	NPR	DS fibre	40	182
		SLA	20	214
	XPM	DS fibre	40	182
		<i>PM fibre</i>	100	215
	FWM	DS-PM fibre	500	216
		SLA	200	217
	PALM	FWM Loop mirror	6.3	218
	NOLM	DS fibre	100	219
		<i>DS-PM fibre</i>	100	220
Free Carrier	Loop Mirror	TOAD	160	86
		<i>Data Driven</i>	40	81
		Integrated	20	221
	Mach Zehnder	Integrated	40	222
	Michelson	Integrated	20	223
	Cross Gain Modulation	Pump Probe	40	224

Table 10 Summary of successful OTDM demultiplexing technologies.

Whilst the earliest OTDM demonstrations necessarily incorporated electro-optic switches, considerable recent attention has focused on weak χ^3 mediated interactions lured by the potential of ultra fast operation²¹⁶. However, the most promising demultiplexers reported to date incorporate interaction between electrons and photons rather than between two photons, either within an electro optic modulator, or within a semiconductor amplifier. These two technologies offer maturity and compactness and

low switching energies. Table 10 summarises recent progress in optical demultiplexing for OTDM systems. The majority of the systems reported are sensitive to the input signal polarisation. However, results where polarisation insensitive operation has been confirmed are indicated in italics.

4.2.1 Mach Zehnder Modulators

Consider now the operation of a Mach Zehnder modulator based demultiplexer in a 4 channel OTDM system. The first modulator is biased at a transmission null and driven with a 10 GHz sine wave of $2V\pi$ amplitude to demultiplex a 40 Gbit/s signal into two 20 Gbit/s signals. The second modulator is driven by the same 10 GHz sine wave, but with only $V\pi$ amplitude to demultiplex the 20 Gbit/s signal into a 10 Gbit/s base rate signal (Figure 4-8). Note that the entire demultiplexer is deployed only using components suitable for use at the system base rate. Consequently using this approach, once systems are deployed at the base rate, four fold capacity upgrades via OTDM should only require the development of suitable pulse sources.

Two factors influence the overall extinction ratio of a switch (and hence its performance); the maximum device extinction ratio and the overlap of the switching window with the tails of adjacent pulses. Whilst the former relies solely on the device specification, the exact nature of the drive signals and optical pulses may have a profound influence on the net achieved extinction ratio and consequently the system performance.

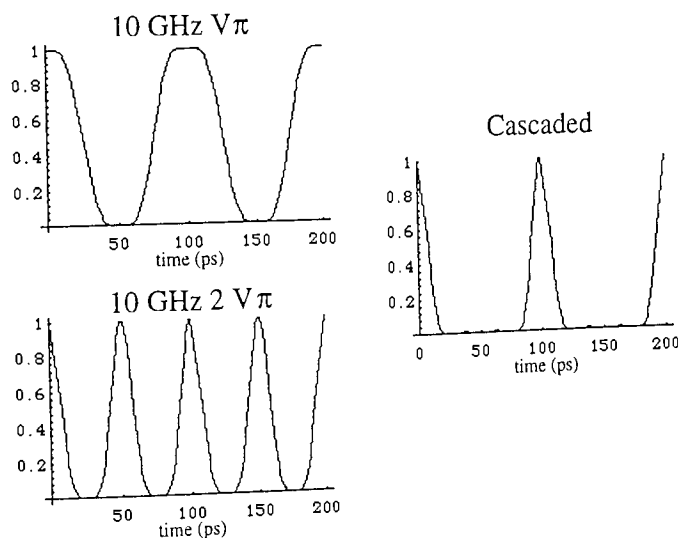


Figure 4-8 Switching windows of Mach Zehnder modulators driven by a 10 GHz signals;
 top left - modulator driven by peak to peak amplitude of $V\pi$.
 bottom left - modulator driven by peak to peak amplitude of $2V\pi$.
 right - response of these modulators cascaded together.

The amplitude response of each of the two modulators (as calculated from Equation 3-52), and of the cascaded pair is shown in Figure 4-8. Clearly, a well distinguished gating period of less than 25% of the bit period is established with good extinction in-between the wanted channels. The critical performance indicator of the demultiplexer is the crosstalk level, determined from the throughput of the demultiplexed channels and the total throughput of the rejected channels. For arbitrarily narrow pulses, cascaded modulators would completely reject the unwanted channels. However, for pulses of

finite size, the overlap of the pulse tails and the sine waves will necessarily lead to a finite level of crosstalk. This is illustrated in Figure 4-9, where the output signals for wanted and interfering channels are shown simultaneously for an input pulse train of 8 ps pulses. From this figure we confirm that the most significant penalty should arise from the tails of the channels immediately adjacent to the demultiplexed channel, the actual pulse peaks being attenuated by over 30 dB.

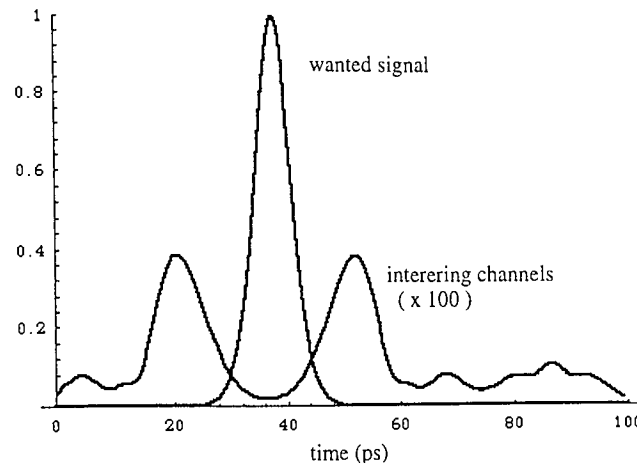


Figure 4-9 Output of cascaded Mach Zehnder modulator demultiplexer for an 8 ps input pulse train at 40 GHz.

In Figure 4-10 the output signal to crosstalk (SXR) ratio for this system is illustrated as a function of signal pulse width with an extinction ratio of 30 dB per modulator. As anticipated the performance increases monotonically with decreasing pulse width down to a pulse width of 2 ps, below which the performance is dominated entirely by the modulator extinction ratio. Significantly however, the performance degrades rapidly above 4 ps, reaching unacceptable levels for a pulse width of ≈ 8 ps. This value may thus be taken as the maximum allowed pulse width for a 40 Gbit/s OTDM system employing this type of demultiplexer.

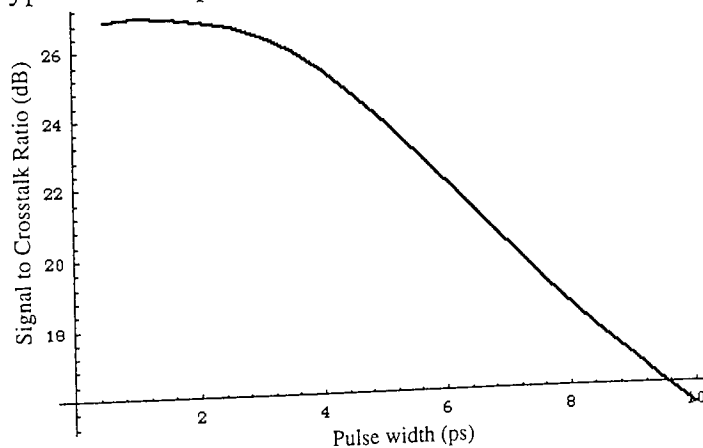


Figure 4-10 Signal to crosstalk ratio of cascaded Mach Zehnder modulator demultiplexer as a function of input 40 Gbit/s pulse width.

The system described above provides a four fold demultiplexing but clearly, lower frequency RF signals could be applied to subsequent modulators to increase the degree of demultiplexing. This requires a minimum of $\text{Log}_2 N$ modulators to demultiplex 1

channel from N , and gives the maximum line rate of four times the maximum drive frequency (40 Gbit/s for $2 V\pi$ 10 GHz drive in this case). Alternatively broadband modulators may be employed with more complex drive signals. Consider for example, a drive signal comprising a 20 GHz sine wave, amplitude modulated by a 10 GHz sine wave.

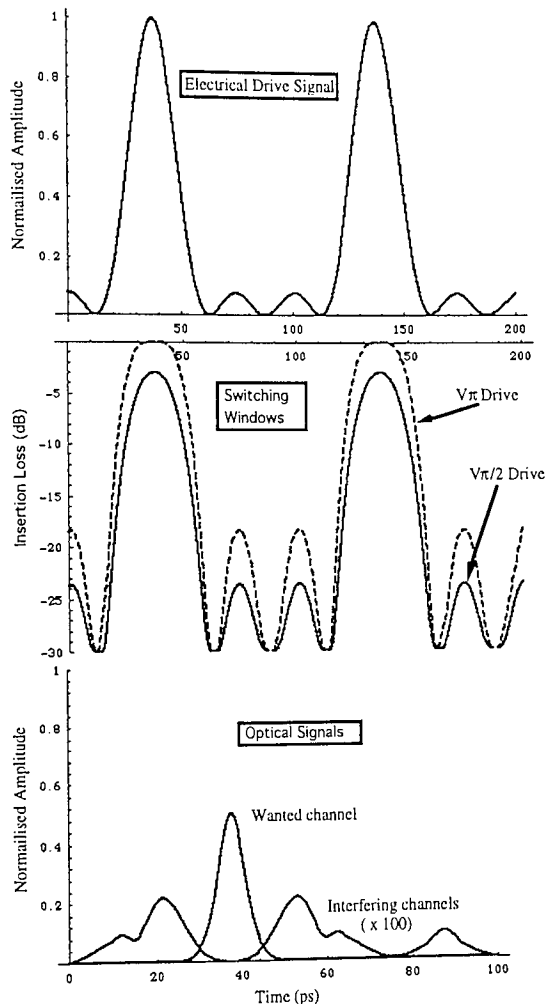


Figure 4-11 Illustration of the operation and performance of Mach Zehnder modulator based demultiplexer driven by a pulsed electrical drive (final diagram assumes 8 ps pulses at 40 Gbit/s).

Simplistically, we may argue that a 20 GHz sine wave applied to a Mach Zehnder modulator would attenuate alternate pulses in a 40 Gbit/s data stream, or allow every other pulses to pass. If the cycle is interrupted then the corresponding pulse would not pass through the modulator. In this way, the 10 GHz signal eliminates alternate cycles of the 20 GHz sine wave, allowing a single pulse within the 40 Gbit/s data stream to be transmitted through the modulator. As in the case of the cascaded modulators, the exact switching window obtained in this fashion, along with the finite data pulse width will determine the cross talk performance. Using this pulsed electrical drive signal, an additional degree of freedom is afforded by the amplitude of the electrical drive pulse. The sinusoidal transfer function of the modulator will tend to square off the switching window for a drive signal of $V\pi$ amplitude, whilst signals with amplitudes less than $V\pi/2$ would tend to produce shorter switching windows at the expense of a diminishing extinction ratio.

This is illustrated in Figure 4-11 where the electrical drive signal is shown along with the resultant switching windows for both $V\pi$ and $V\pi/2$ amplitudes and the pulse waveforms of the demultiplexed and interfering channels after the modulator (driven at $V\pi/2$). With full $V\pi$ drive, the overshoots present in the drive signal are transferred to the optical switching window resulting in unacceptable performance, however, for the reduced drive level of $V\pi/2$ we observe that the sinusoidal transfer function of the modulator has significantly attenuated the overshoots with respect to the wanted signal. The lower trace of Figure 4-11 illustrates the effect of this configuration on a 40 Gbit/s OTDM signal comprising 8 ps pulses. Again we observe that the main crosstalk terms arise from the pulse wings rather than the actual pulse peaks. In addition to modulating the amplitude of the 20 GHz sine wave with a 10 GHz signal, further electronic processing may be used to eliminate further electrical pulses, allowing demultiplexing down to an arbitrarily low base rate.

In summary, we have seen how Mach Zehnder modulators may be used as efficient demultiplexers, either driven with narrow band signals at the base rate clock frequency, or with broadband signals where component count and overall insertion loss are of importance. It is interesting to note that demultiplexing at four times the RF signal rate is possible, suggesting that 160 Gbit/s demultiplexers may be constructed from the latest commercial modulators, as shown in Figure 4-12. Note that with the exception of the pin¹⁹⁴, all the required components are readily available commercially.

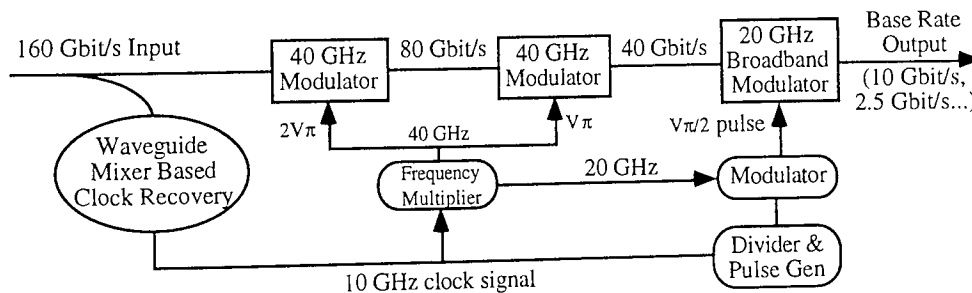


Figure 4-12 Schematic diagram of proposed 160 Gbit/s demultiplexer

4.2.2 Electroabsorption modulators

Clearly, any optical modulator capable of generating pulses for use in OTDM networks may also be used as a demultiplexer. In general the demultiplexer may tolerate a somewhat reduced extinction ratio, and is often designed to produce slightly broader pulses (switching window) to avoid attenuation of the wanted channel. Indeed many potential pulse sources were originally demonstrated as demultiplexers because of this relaxed requirement. During this thesis, electro absorption modulators have been widely used to provide a demultiplexing function due to the simple operation of the compact device and its day to day stability.

4.2.2.1 Theoretical Performance at 40 Gbit/s

The demultiplexing operation of an electroabsorption modulator is well understood and operates in the same manner as a pulse source, with the RF signal derived from the

local clock recovery circuit. For a 10 V peak to peak drive signal, the achievable switching windows for Mod#1 and Mod#2 modulators is shown in Figure 3.20. Note that when deployed as a pulse source, the modulator chirp enables some degree of additional pulse compression. Consequently, the same modulator may be used to firstly generate signal pulses, and then demultiplex them with an acceptable switching window¹²¹. At 10 GHz, an acceptable window width of ≈ 15 ps is achieved for a reverse bias of ≈ 8 V, whilst the linearly compressed pulses at the same operating point would be ≈ 6.3 ps. Figure 4-13 illustrates the signal to cross talk ratio of an electroabsorption modulator demultiplexer described by Equation 2-40 as a function of the reverse bias for a 40 Gbit/s OTDM signal comprising these 6.3 ps pulses.

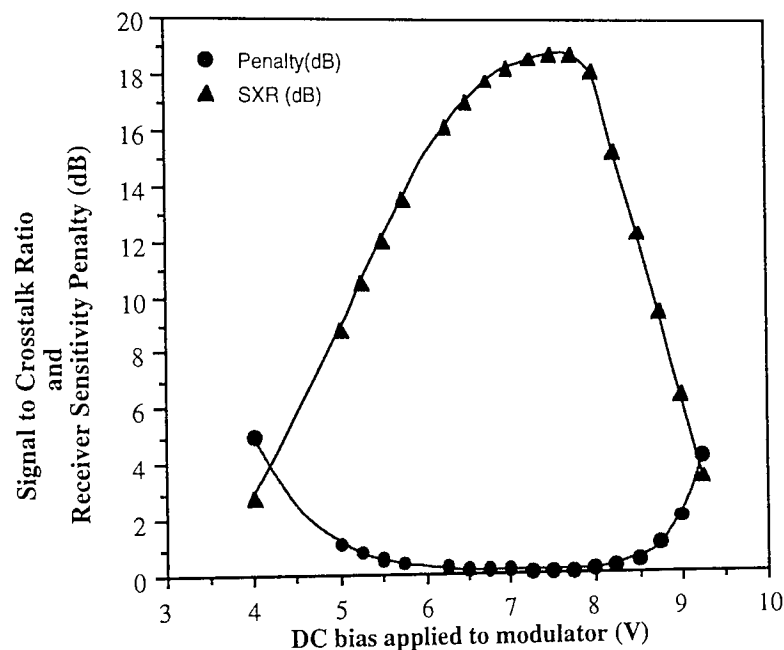


Figure 4-13 Signal to crosstalk ratio of electro-absorption modulator demultiplexer with 6.3 ps 40 Gbit/s input signal, 24 dB extinction ratio, 11.8 dB/V absorption slope and a 10 V peak to peak 10 GHz drive signal.

This figure illustrates both the signal to crosstalk ratio, used to derive the change in error floor, and the direct reduction in receiver sensitivity due to simple eye closure. The optimum shown results from a reducing net extinction ratio at high reverse bias and excessively broad switching windows at low reverse bias. It can be seen that the 8 V bias condition suggested corresponds closely with this optimum. This device was used in many of the 40 Gbit/s systems demonstrations reported below.

4.2.2.2 80 Gbit/s systems based on electroabsorption modulators

80 Gbit/s transmission systems are readily constructed from electroabsorption modulator devices. This may be achieved either by increasing the system base rate to 20 Gbit/s, or by increasing the degree of multiplexing to 8×10 Gbit/s. This is illustrated in Figure 4-14 and Figure 4-15. In Figure 4-14, the simple electroabsorption modulator pulse source is modified by adding a second pulsed modulator to enhance the extinction ratio and reduce the pulse width. Frequency doublers are also added to the inputs to 20 GHz drive amplifiers to provide the modulators (similar to Mod#1) with simultaneous,

in phase, 10 and 20 GHz components. Following subsequent compression through a suitable length of dispersion compensating fibre, 4.5 ps pulses are obtained, modulated with a third electroabsorption modulator, and interleaved (MUX-3).

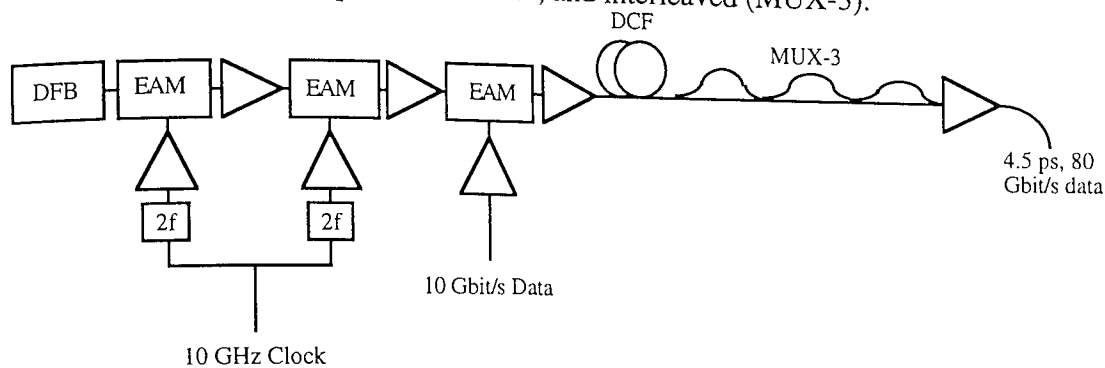


Figure 4-14 Schematic diagram of electroabsorption modulator, 80 Gbit/s data source.

The demultiplexer for this system (Figure 4-15) again comprises an electroabsorption modulator driven at 10 GHz via a narrow band electrical amplifier. In this case, the modulator (Mod#5) was polarisation insensitive, and gave a minimum uncompressed pulse width of approximately 8 ps for acceptable extinction ratio's.

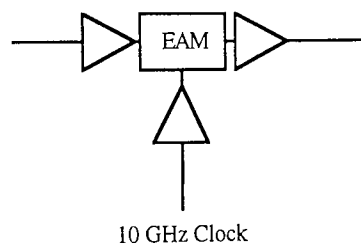


Figure 4-15 Schematic diagram of polarisation insensitive electroabsorption modulator based 80 Gbit/s demultiplexer.

The entire system was tested, giving a preamplified receiver sensitivity, at the input to the demultiplexer, of ≈ -23 dBm, and a variation of less than ± 0.7 dB across all 8 channels and all polarisation states. The stability and uniformity of the system is verified by the bandlimited eye diagram and autocorrelation (Figure 4-16). Note that the 80 Gbit/s RZ signal is displayed as an equalised NRZ eye diagram using the 32 GHz photodetector. Coupled with harmonic mixer based clock recovery, this represents a particularly simple implementation of 80 Gbit/s OTDM terminal equipment, offering single stage sine wave driven 8 fold demultiplexing, and an integrable pulse source of high quality, low background 4.5 ps pulses.

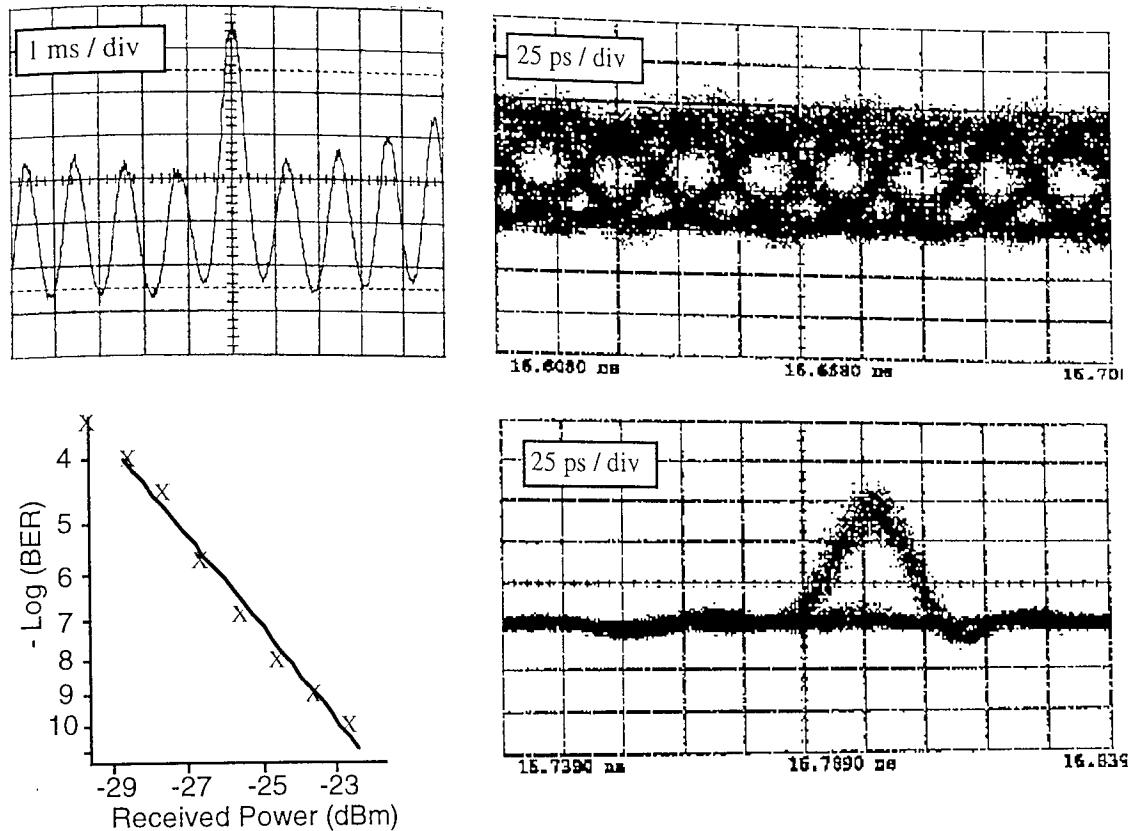


Figure 4-16 80 Gbit/s OTDM system employing four electroabsorption modulators. Showing autocorrelation (top left) and eye diagram (top right) of 80 Gbit/s data signal, and BER measurements (bottom left) of demultiplexed signal (bottom right).

4.2.2.3 Simultaneous photodetection and demultiplexing

The unique properties of electroabsorption modulators also allow the possibility of simultaneous photodetection and demultiplexing with a single modulator^{225,226}. Consider a modulator biased normally transmissive with the usual sine wave drive. For the majority of the drive cycle, the modulator is transparent, allowing pulses to pass undisturbed. At the peak of the cycle however, the modulator is driven into absorption and would remove power from the unwanted time slot. Now, if the OTDM data channel and would remove power from the unwanted time slot contains a data one, this absorption will generate carriers corresponding to this time slot contains a data one, this absorption will generate carriers within the active region of the modulator, the presence of which may be detected as a voltage across the device²²⁷.

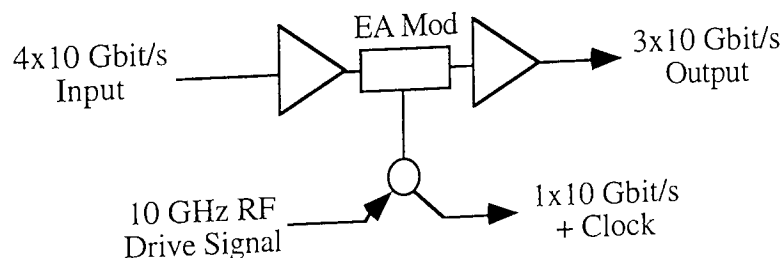


Figure 4-17 Schematic diagram showing simultaneous switching and detection of OTDM data channels using an electroabsorption modulator.

In this way, a single electroabsorption modulator may be used to simultaneously remove an OTDM channel from the optical pulse stream and detect it locally (Figure 4-

17). Unfortunately, a residual component of the RF drive signal applied to the modulator will also be present and so the detected signal will comprise a large 10 GHz RF signal and a small return to zero 10 Gbit/s data sequence. Separation of these signals is possible using a suitably designed electrical filter, an example of which is shown in Figure 4-18. The remarkable performance of this simple filter circuit is illustrated by the eye diagrams, where a clear 10 Gbit/s eye is extracted from a signal where apparent data signal is present. Electrical error ratio measurements suggest that error free operation is possible for data signals greater than ≈ 7 mV (noise floor of the circuit) provided the data power is no lower than ≈ 40 dB below the detected residual clock power. For a typical residual detected clock signal of 2V, this results in a minimum detected photocurrent of $400\mu\text{A}$ (assuming a $50\ \Omega$ load), or an optical input power of around 1 mW (assuming $> 90\%$ absorption and 4 dB coupling loss). This encouraging result is perfectly within the power handling capabilities of current electroabsorption modulators studied in this thesis ($\approx +5$ dBm).

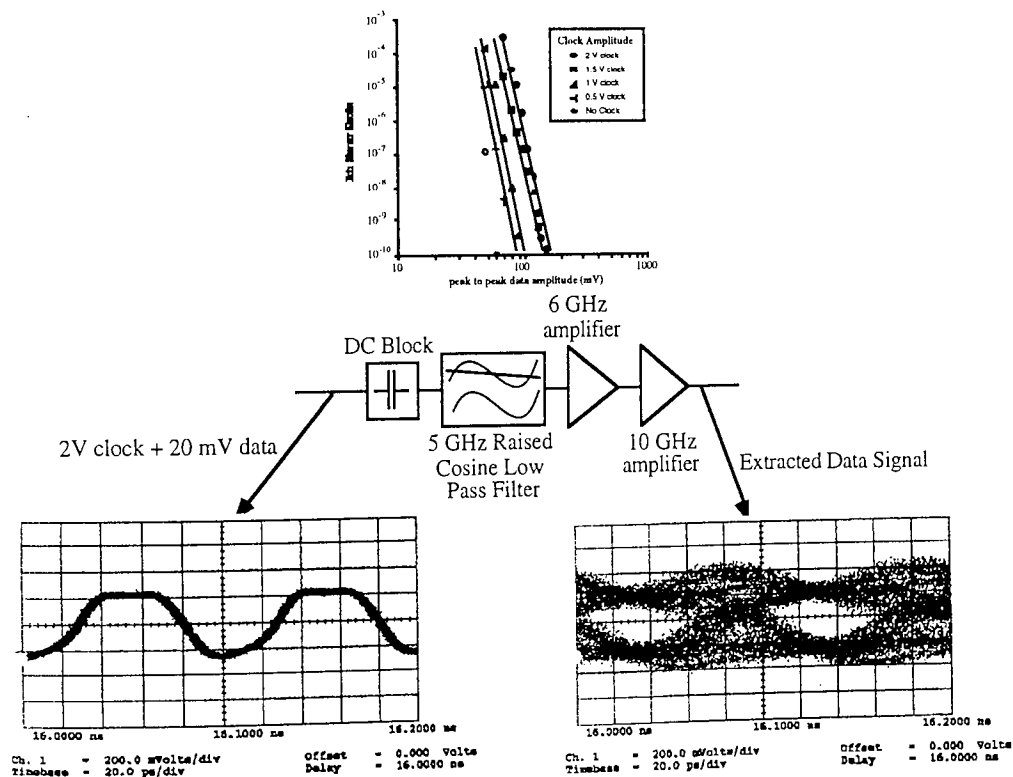


Figure 4-18 Electrical extraction of a weak data signal from a mixture of clock and data

Unfortunately the background absorption of the electroabsorption modulators was around 10%, leading to a significant absorption of the unwanted (through) channels and a corresponding high level of crosstalk. This precluded a full demonstration of the technique. However, along with the potential for dark pulse generation, this work has led to the design and fabrication of a new "blue shifting" electroabsorption modulator²²⁸. This device is designed to have a low background absorption state, and to avoid the need for high forward bias levels (giving current leakage and high capacitance) when generating dark pulses (or short pulse absorption windows) by inverting the absorption characteristic. Preliminary samples have been grown by

colleagues at BT laboratories showing the potential for blue shifts of up to 90 nm, suggesting that operational blue shift modulators may be developed.

4.3 Chapter Summary

In this chapter, we have examined options for OTDM clock recovery and demultiplexers. Phase locked loop clock recovery circuits are proposed as the natural choice for OTDM synchronisation, although the precise implementation of the high frequency mixer remains open to debate. The two main candidates are electronic waveguide based harmonic mixers, proposed in this thesis, and ultra fast all optical mixers coupled with generation of high frequency clock components via short pulse generation proposed by NTT. Both of these techniques are likely to produce low jitter electronic base rate clock signals from an incoming OTDM data signal, irrespective of the quality of the interleaving. Furthermore, the electronic version is fundamentally wavelength and polarisation insensitive. In terms of demultiplexers, attention has been restricted to electro-optic based modulators. It has been shown that operation to 80 Gbit/s and even 160 Gbit/s is perfectly feasible given state of the art modulator technology. In particular the use of polarisation insensitive electroabsorption modulators is particularly promising for the implementation of OTDM systems in the region of 100 Gbit/s.

5. OTDM Transmission

In the previous chapters, the key issues associated with the generation and detection of OTDM data signals were discussed. Particular attention was focused on the key issues of pulse generation, timing synchronisation and demultiplexing, concentrating on techniques employed in this thesis. In this chapter, the transmission of OTDM signals, a key element of optical communications networks, is discussed. Of particular importance is the use of standard fibre, where the dispersion limited transmission distance is less than 5 km. Following demonstrations of how this may be overcome, attention is focused on dispersion shifted and novel fibre types for soliton transmission. Finally, the chapter is concluded by a demonstration of all optical regeneration.

5.1 Standard Fibre Systems

In order to provide a low cost evolution strategy to upgrade the existing network, it is imperative that any multiplexing techniques (optical or electrical) exploit the existing fibre plant. Whilst in Japan this translates to simply accommodating a wide variation in the dispersion zero of dispersion shifted fibres²²⁹, within Europe and the United States the key issue is the prevalence of standard step index fibre²⁸. Several techniques have been proposed to overcome the chromatic dispersion inherent in this fibre base when used in the 1.55 μ m window. The proposed techniques include dispersion tolerant²³⁰ and dispersion supported²³¹ transmission formats, optical²³² and electrical²³³ dispersion compensation and mid span spectral inversion²³⁴ (MSSI). Many of these techniques involve precise manipulation of the optical data format, a degree of freedom already exploited within an OTDM system to produce a high aggregate capacity. However, optical dispersion compensation and mid span spectral inversion show great promise for completely removing penalties from chromatic dispersion in OTDM systems^{232,128,19}, and in the case of MSSI, alleviating non-linear impairments in certain circumstances²³⁵. Correctly designed, these techniques are not only suitable for high speed OTDM systems, but may be "downgraded" and initially deployed for 10 Gbit/s NRZ system.

Optical dispersion compensation of OTDM signals may also be achieved using either dispersion compensating fibre^{232,236}, planar components²³⁷, or chirped fibre gratings²³⁹. Dispersion compensating fibre is now readily available, and is easily adapted to ultra high speed operation by adjusting the fibre length. On the other hand chirped fibre gratings offer the advantages of a simple and compact device with low non-linearity. Preliminary measurements of such techniques for short pulses show great promise, with recent increases in overall grating length²³⁸ allowing impressive system demonstrations²³⁹. Once developed, such gratings may usefully act to partially dispersion compensate a fibre link, allowing soliton transmission³⁷, with the chirped grating simultaneously acting as a guiding filter.

5.1.1 Mid Span Spectral Inversion

Recent demonstrations of mid span spectral inversion (MSSI), or optical phase conjugation (OPC), show great promise for completely removing penalties from first order chromatic dispersion in the transmission fibre²⁴⁰, and alleviating many of the non-linear impairments of appropriately designed long haul transmission systems²³⁵. This technique has been demonstrated even using signals of relatively high spectral width, and should thus be eminently suited for use in an OTDM network. The basic principle of operation is shown in Figure 5-1. A pulse temporally broadens in the optical fibre, with the long wavelength components trailing the shorter. At the mid point of the transmission link, the spectrum is inverted, such that the short wavelength components now trail the longer. During subsequent propagation, the shorter wavelengths propagate with a higher velocity, and the pulse reforms at the fibre output.

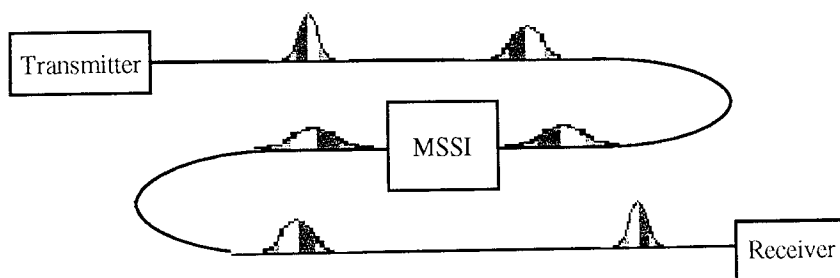


Figure 5-1 Operating principle of mid span spectral inversion, showing pulse broadening in the first fibre link, and restoration in the second, symmetric fibre link.

This process is highly analogous the phase conjugate reflection where, in the absence of loss, a pulse unwinds all distortions (temporal, spectral and spatial) as it propagates back towards the transmitter through an effective mathematical time reversal. Consequently, provided the two transmission links are sufficiently symmetric, and the amplifier spacing short enough, then we may expect compensation of self phase modulation and four wave mixing in addition to chromatic dispersion. Previously the technique has been used to provide dispersion compensation for bit rates of up to 10 Gbit/s with directly²⁴⁰ and externally modulated transmitters, for ≈ 5 ps pulses²⁴¹ and for multiple wavelength systems²⁴². Similarly, the cancellation of self phase modulation²³⁵ and four wave mixing²⁴² have been effectively demonstrated. In this thesis, the extension of this technique to higher bit rates is discussed.

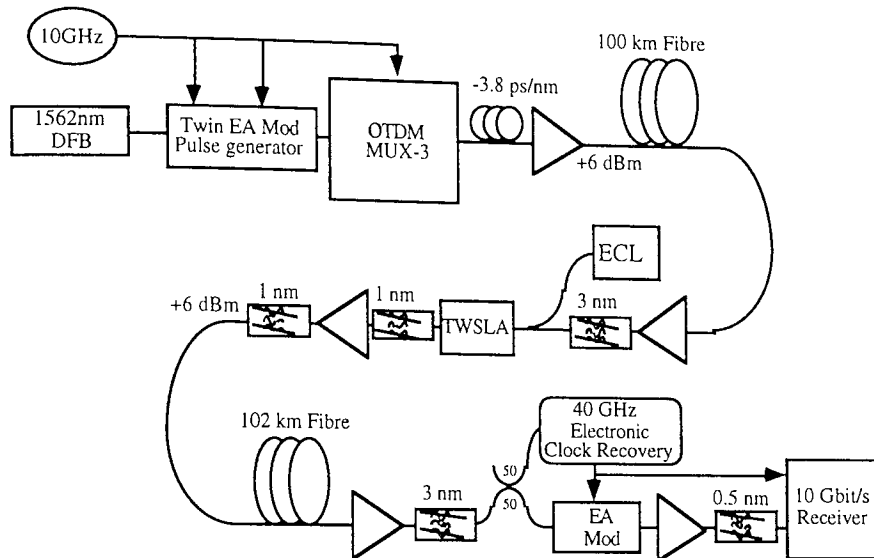


Figure 5-2 Schematic diagram of 202 km transmission system employing MSSSI

Figure 5-2 illustrates the 202 km OTDM transmission system used to demonstrate the worlds first application of MSSSI to a high speed OTDM formatted signal. Near transform limited 7 ps pulses at 1562 nm & 10 GHz repetition rate are derived from a cw DFB, a pair of sine wave driven electro absorption modulators and linear compression. The second modulator is used primarily to enhance the contrast ratio of the pulses and consequently improve the stability of the subsequent interleaving. A 40 Gbit/s data sequence (2^7-1 pattern lengths) is derived from this pulse train before amplification to +6 dBm and transmission over a 100 km length of standard Sumitomo fibre (with a dispersion length for these pulses of ≈ 2 km). Upon entering the MSSSI node, the signal was amplified and combined with a copolarised 1559.8 nm, cw pump before amplification by a bulk InGaAsP semiconductor amplifier (SLA). In the SLA four wave mixing between the incoming signal (<+3dBm) and the local pump (+13 dBm) generates the spectrally inverted phase conjugate signal. Note that the four wave mixing process also produces a wavelength shift in addition to the wanted spectral inversion.

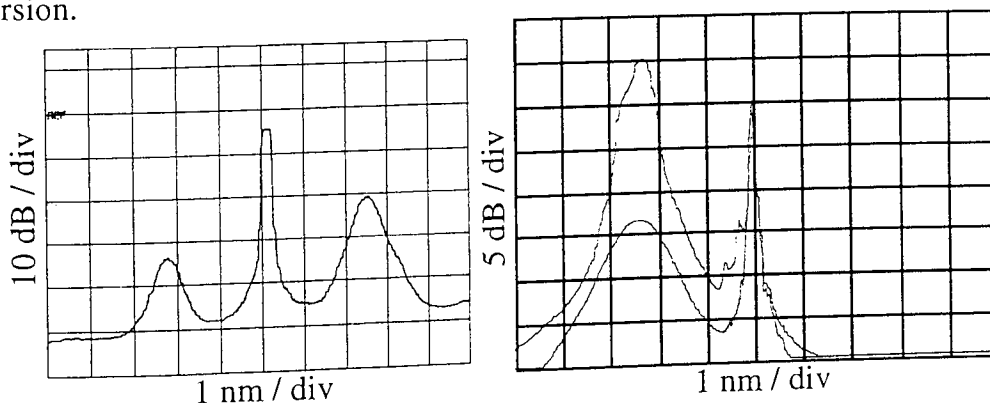


Figure 5-3 Optical spectrum of 40 Gbit/s MSSSI experiment. LEFT - Output of SLA showing input signal, pump, and phase conjugate signal. RIGHT - Output of final filter with and without input data signal, illustrating the achieved signal to noise ratio.

The wavelength shifted phase conjugate signal was isolated from the input signal and the residual pump using two cascaded 1.3 nm bandpass filters and the signal power boosted to +6 dBm before onward transmission from the node (Figure 5-3). Following

transmission through a further 102 km, the restored 40 Gbit/s OTDM signal is demultiplexed using another electroabsorption modulator, driven via a 40 GHz clock recovery circuit and providing a 15 ps switching window and 22 dB extinction ratio. As can be seen from Figure 5-3, the finite conversion efficiency (≈ -14 dB neglecting amplifier gain) of the four wave mixing process and spontaneous emission from the SLA results in a degradation in the optical signal to noise ratio (to ≈ 20 dB), and it is critically important to optimise the FWM efficiency. The spectral variation in conversion efficiency is well understood in terms of inter and intra band carrier transport effects and carrier heating²⁴³. In Figure 5-4, the observed variation in 40 Gbit/s conversion efficiency is plotted against the wavelength detuning between pump and signal (pump wavelength minus input signal wavelength). These results reproduce the anticipated deterioration in efficiency as the wavelength separation increases, and also illustrate the higher efficiency achieved when the pump wavelength is shorter than the signal²⁴⁴. The spectral asymmetry in the efficiency characteristic relates to interference between four wave mixing signals generated by inter and intra band carrier transport processes, adding constructively for negative wavelength differences, and destructively for positive differences^{245,246}.

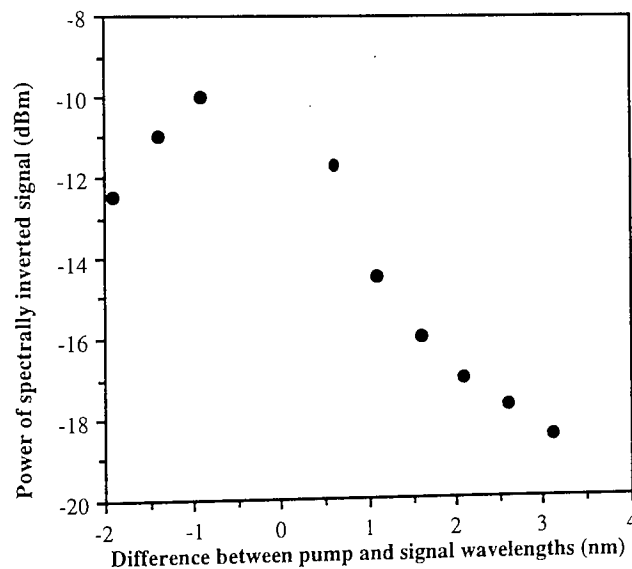


Figure 5-4 Peak signal power of phase conjugate signal as a function of signal/pump detuning.

With this in mind the pump signal was located to the short wavelength side of the input OTDM signal, and the effect of this efficiency variation on the system performance was investigated (Figure 5-5) by replacing the 202 km transmission fibre with 23 dB attenuation (ensuring equivalent or worse signal to noise ratio performance throughout the system). For each pump wavelength investigated (with a fixed input signal wavelength), the MSSI node itself was optimised in terms of signal powers and polarisations. It is observed that severe error floors are encountered for large wavelength shifts (greater than 3 nm) mainly as a result of reduced MSSI efficiency leading to signal-to-noise degradation at the output of the SLA. While the phase-conjugate signal-to-noise could be increased simply by increasing the signal input power, this also increased the degree of distortion in the received signal due to carrier

density modulation. For small differences between pump and signal wavelengths, a net receiver sensitivity degradation is encountered due to residual pump leakage through the cascaded filters, although no specific error floor was encountered. It was thus determined that a finite window of some 1.2 nm exists over which successful MSSI may be performed using this particular SLA and these filters. It is anticipated that this window will become narrower for higher bit rates. This is due the requirement for broader optical filters to pass the OTDM signal which would increase the pump breakthrough, and the increased total power for a given signal to noise ratio of a base rate channel impacting on the trade off between FWM efficiency and signal distortion in the SLA. Subsequent work has shown that the pump signal detuning and the conversion efficiency may be simultaneously increased by the use of longer SLA devices²⁴⁷, and should in principle allow the operation of MSSI at bit rates up to at least 100 Gbit/s and perhaps beyond.

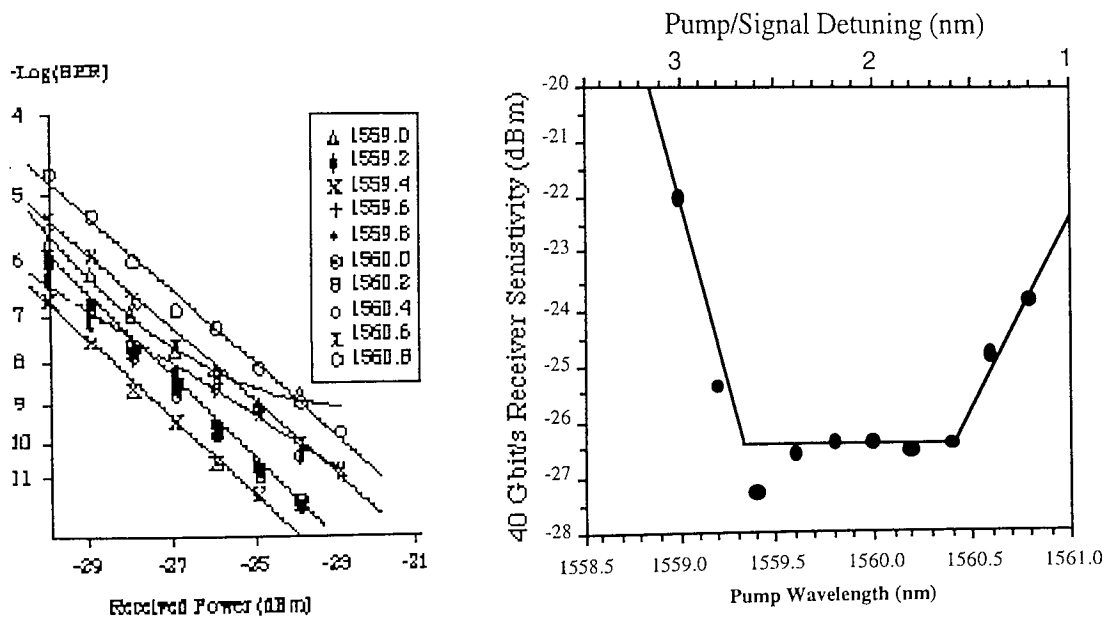


Figure 5-5 BER performance of MSSI without fibre as a function of signal-pump detuning

Figure 5-6 illustrates the excellent performance of the overall 202 km system for a wavelength difference of 2.5 nm. The excess length (2.2 km) of the second fibre link was determined simply by calculating the relative total dispersions of the two links, taking into account the overall wavelength shift of ≈ 5 nm and the dispersion slope. It is interesting to note that in this experiment this relatively small excess length corresponds approximately to the dispersion length. The pulse width was almost exactly restored (to ≈ 7.5 ps) using this fibre length, whereas with precisely equal fibre lengths a significantly broader 14 ps pulse was observed, giving rise to error floors due to incomplete demultiplexing. The overall preamplified receiver sensitivity of -25.1 dBm included a small 0.4 dB penalty for the use of MSSI and 23 dB attenuators, and a further 0.8 dB transmission penalty from residual dispersive effects (through the transmission fibre and optical filters) and non-linear crosstalk. However, the overall penalty (1.2 dB) remains comparable to previous demonstrations of 40 Gbit/s soliton transmission over 205 km at 1557 nm, where signal depolarisation gave rise to a net 2

dB penalty²⁴⁸. This result represents the first experimental demonstration of MSSSI compensated transmission of a 40 Gbit/s OTDM signal over standard fibre. The achieved bit rate distance product of 8.1 Tbit/s/km represented the highest reported value for a single wavelength using any dispersion compensation technique when initially reported.

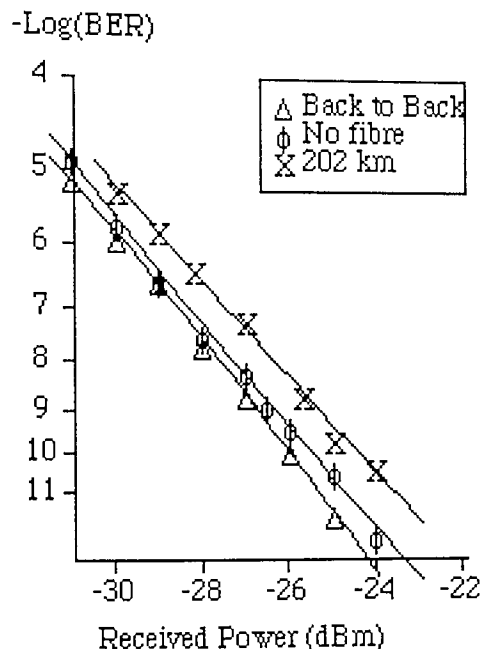


Figure 5-6 Overall performance of 202 km transmission of a 40 Gbit/s OTDM signal over standard fibre using MSSSI.

Whilst the measurements reported here indicate the limitations in bit rate, numerical simulations by others has suggested that transmission distances of up to 3,000 km should be possible using a single MSSSI node²⁴⁹, limited by a combination of third order dispersion and amplifier noise. Indeed, in a recent demonstration, a 40 Gbit/s OTDM signal has been transmitted over 400 km using a 2 mm long MQW SLA²⁵⁰. Whilst MSSSI clearly offers remarkable performance, and may allow the deployment of long haul systems with a single dispersion compensating element. However, outside the realm of simple point to point systems, the simplicity of span by span passive optical dispersion compensation would alleviate difficulties associated with different optical path lengths for each channel. In both cases however, upgrades to higher bit rates are likely to be restricted by polarisation mode dispersion and uncompensated higher order dispersion²⁵¹. Similarly, for bit rate transparent systems, with a target upgrade capacity of 40 Gbit/s, particular attention must be paid to the short dispersion length of the OTDM system (≈ 2 km), precluding the use of partially compensated systems at lower bit rates.

5.2 Soliton Systems

In chapter 2, we introduced the concept of optical solitons where, for certain pulse profiles, the phase shifts due to dispersion of an optical pulse are balanced by phase shifts from the fibre non-linearity (SPM). Whilst the use of transmission format to provide optical multiplexing in an OTDM system precludes the use of many dispersion accommodation techniques (Section 5.1), RZ pulses are perfectly suited to soliton communication. Indeed the proposed OTDM pulse sources often produce either sech squared pulses ideally suited to soliton communications systems or pulses close to a gaussian profile, which may be converted on transmission into solitons with negligible loss of energy. Thus, where new systems are commissioned, or dispersion shifted fibre exists, soliton transmission of OTDM data signals may be considered a particularly attractive option.

As this thesis is nearing completion, soliton transmission at bit rates of up to 20 Gbit/s has reached an encouraging state of maturity²⁵², however, at the outset of this thesis little work on soliton transmission above this bit rate had been reported^{253,248}. Indeed the single report of long haul 40 Gbit/s transmission utilised the additional degree of freedom of polarisation multiplexing to allow the use of broader pulses (≈ 9 ps) simultaneously reducing jitter and soliton-soliton interactions²⁵⁴. This thesis reports the worlds first experimental demonstration of long haul soliton transmission of a single polarisation 40 Gbit/s OTDM data sequence, and the use of active soliton control techniques and novel fibre types to enhance the system performance. For the later techniques, the emphasis is on overcoming the potential limitations of ultra high capacity soliton systems. In the following chapter, it will be shown how the transmission techniques illustrated here allow for the construction of truly global OTDM networks.

5.2.1 40 Gbit/s soliton transmission

Many recent transmission experiments have demonstrated the striking potential of OTDM transmission over moderate distances using either soliton or linear transmission techniques. However as system capacities have been increased, the distance has reduced, closely following (with few exceptions²⁵⁵) a fixed maximum bit rate distance product of approximately 40 Tbit/s.km for soliton OTDM systems^{187,103} and ≈ 20 Tbit/s.km for dispersion managed OTDM systems²⁵⁶. Soliton control in frequency²⁵⁷ and time domains²⁵⁸ have increased these limits dramatically. Here, the transmission of a 40 Gbit/s OTDM data stream over 2,200 km without transmission control is reported (bit rate distance product of 88 Tbit/s.km) using a substantially unaltered transmission line previously reported for 2.5 Gbit/s soliton transmission^{103,258}, and with a near uniform dispersion map.

Figure 5-7 illustrates the experimental configuration of the various soliton transmission experiments reported in this thesis. The main loop differs only slightly from previously reported experiments¹⁰³ through the inclusion of an optional in line electro-optic modulator and a second inject port at the "origin" of the loop. The particular configuration used is more complex than is reasonably required for any given

transmission experiment, however, it allows simple reconfiguration of the experiment. In the figure, the timing signals used to determine inject and measurement windows, and the overall transmission distance are omitted for simplicity. However, those components switched by these timing signals are outlined in orange.

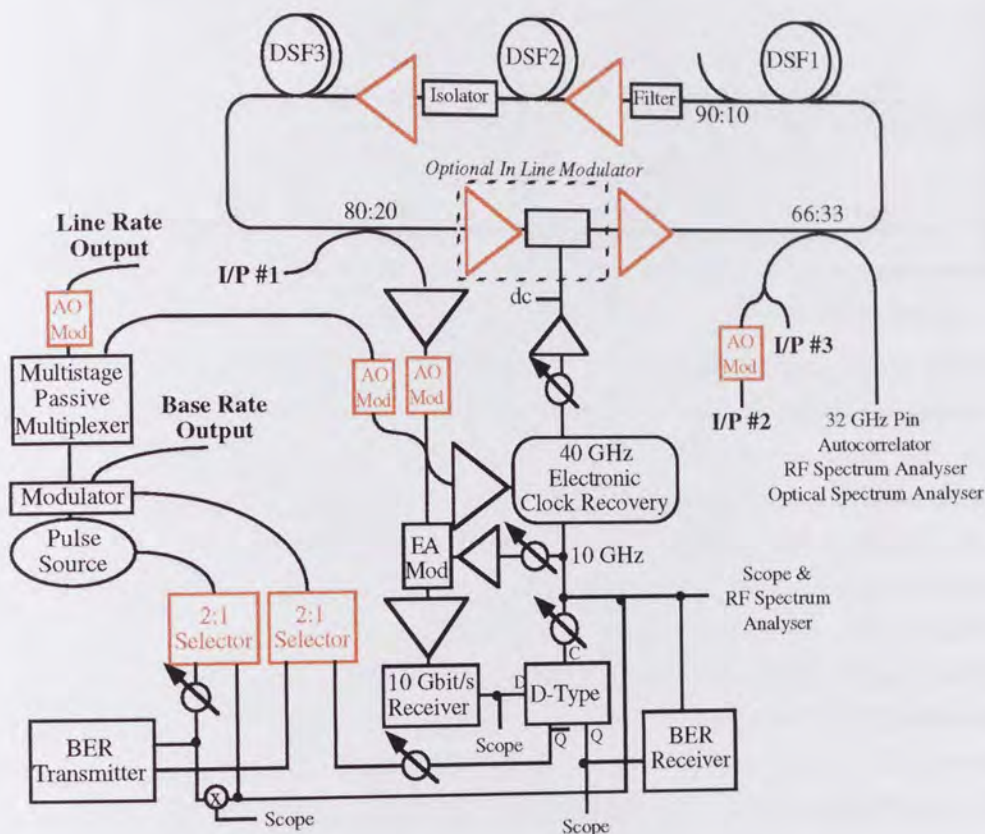


Figure 5-7 Schematic diagram of OTDM recirculating loop.

Two alternative 10 GHz pulse sources were employed producing pulses between 4 and 7 ps in duration. Transform limited sech squared pulses were obtained from a phase locked erbium doped fibre ring laser, with a small degree of repetition rate tunability available via the piezo electric drum on which was mounted the erbium doped fibre. Alternatively, closely transform limited gaussian pulses could be obtained from a harmonically mode locked semiconductor external cavity laser, with repetition rate tunability over several megahertz. Following modulation with a 2^7-1 PRBS pattern via a low chirp lithium niobate modulator, the pulses were passively interleaved (MUX-3) to the appropriate bit rate. The signal was normally injected into the recirculating loop at port #1 via an acousto-optic modulator. The recirculating loop comprised three 1480 nm counter pumped erbium doped fibre amplifiers (7 dB noise figure), spaced by 33 km of dispersion shifted fibre whose characteristics are listed in Table 11. Full details of the fibre are provided to assist any subsequent analysis of the system taking into account the exact dispersion profile. In this thesis however, a constant mean dispersion zero of 1548.5 nm is used throughout according to the average soliton model.

Link	Reel ID	Length (km)	Dispersion Zero (nm)	Loss (dB/km)
1	2	17.65	1548	.214
1	7	15.44	1549	
2	6	18.31	1549	.223
2	12	12.73	1549	
2	17b	2.00	1548	
3	11	8.84	1545	.217
3	17	11.03	1550	
3	10	8.84	1550	
3	17c	4.00	1548	

Table 11 Dispersion map of 100 km recirculating loop with 33 km amplifier spacing.

For the 40 Gbit/s transmission experiment, the 100 km recirculating loop contained a single 2.7 nm tuneable optical bandpass filter and a single premium grade optical isolator. For this simple experiment, the in line modulator was removed. After an appropriate number of recirculations, timing synchronisation was achieved using a 40 Gbit/s electronic phase locked loop clock recovery circuit, and a single 10 Gbit/s channel was extracted using an electroabsorption modulator, detected and regenerated. In contrast to previous experiments, the lock condition of the PLL was maintained in the absence of recirculating data (i.e. between the measurement and inject periods) by switching between the loop output and a spare output of the passive multiplexer using a pair of acousto-optic modulators. Note that by varying the loop length (in bit periods), the clock recovery may be forced to demultiplex either the same, alternating or random channels within the OTDM multiplex. The current demultiplexing state is monitored by comparing the phase of the recovered 10 GHz clock with the transmitted clock as a function of transmission distance, whilst the relative loop length (in bit periods) is adjusted by fine tuning the source frequency. The evolution of the pulses as a function of distance was monitored using optical (0.1 nm resolution) and electrical (40 GHz component) spectrum analysers, whilst a sampling scope and 32 GHz pin were used to temporally analyse the received signals. Error ratio measurements were taken on the regenerated data using a burst mode enabled 10 Gbit/s error rate test set. In all cases, the instrument triggers were controlled via the appropriate loop timing signals with a continuous optical input from the recirculating loop. In this experiment the second and third loop inputs and the 2:1 selectors were unused.

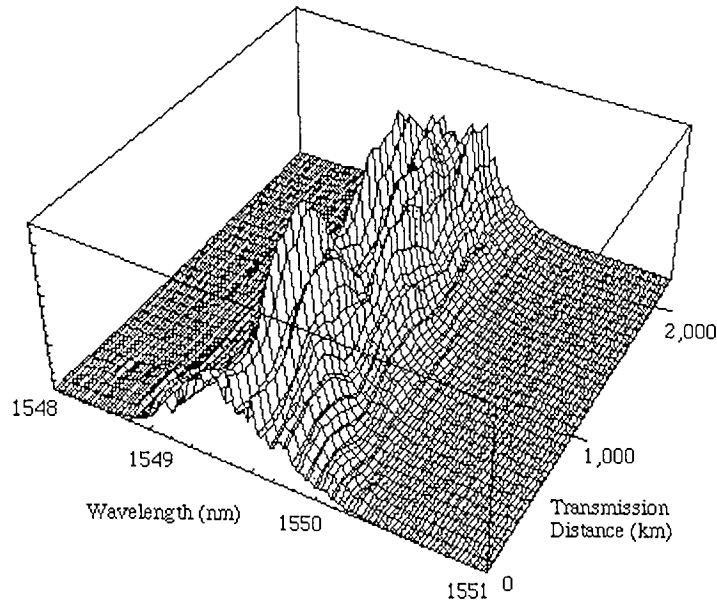


Figure 5-8 Spectral evolution of pulses during 40 Gbit/s soliton transmission experiment with a centre wavelength of 1549.2 nm.

With the erbium doped fibre ring laser tuned to give 6 ps pulses at a centre wavelength of 1549.2 nm (corresponding to 0.05 ps/nm/km dispersion in the transmission line), error free transmission was obtained for transmission distances up to 2,200 km. The spectral evolution of the pulses is shown in Figure 5-8, clearly illustrating that following an initial evolution, the spectral width propagates largely unchanged after propagation over 8 soliton periods, confirming soliton like propagation. The received eye diagram and the evolution of the 40 GHz RF component (Figure 5-9) similarly confirms that negligible temporal distortion has been experienced on propagation.

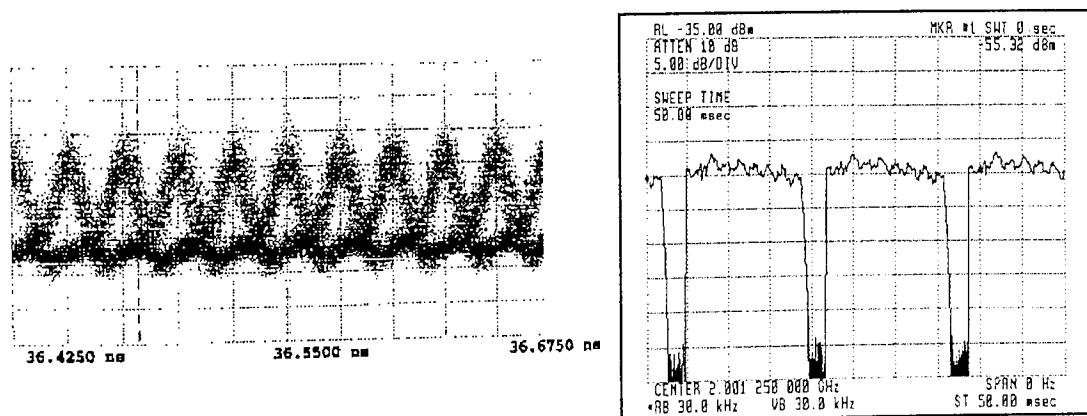


Figure 5-9 Eye Diagram after 2,200 km and evolution of 40 GHz RF component with distance (right) for 40 Gbit/s soliton transmission at 1549.2 nm.

As the signal wavelength was detuned to higher dispersions, an increased degradation in the 40 GHz component of the RF spectrum indicates that pulse to pulse jitter gradually degrades the performance to an error free transmission distance of 1,100 km at 1550.2 nm ($D = 0.13$ ps/nm/km). This is illustrated in Figure 5-10, which summarises the observed error free distances ($<10^{-9}$ BER), along side a theoretical plot of the anticipated error rate performance. It is apparent that the experimental error free

distances follow qualitatively theoretical error free distances ($< 10^{-15}$ BER) for Gordon Haus jitter, but the actual transmission distance is somewhat degraded.

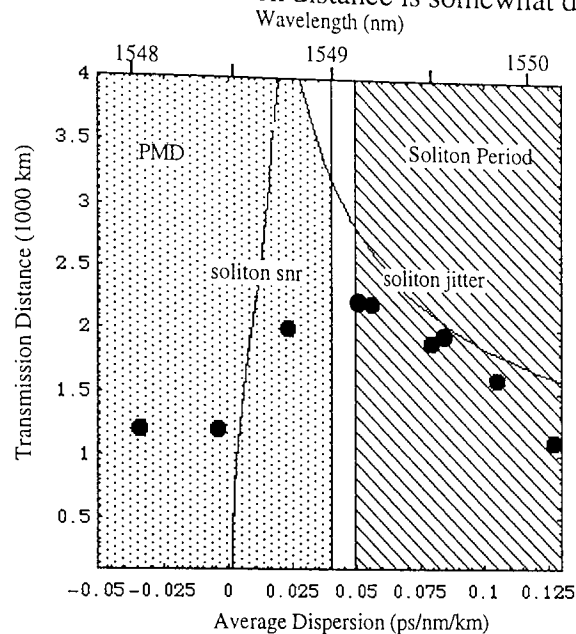


Figure 5-10 Theoretical and experimental performance of 40 Gbit/s transmission system.

Dots - experimentally measured error free distance ($< 10^{-9}$)

Solid curves - theoretical error free distance ($< 10^{-15}$)

Dotted region - pulse not stable against PMD

Shaded region - soliton period less than 6 amplifier spacings

Theoretical predictions of soliton soliton interactions in the presence of the weak guiding filter (2.7 nm every three fibre spans) suggest that the collapse length tends to infinity provided the system dispersion remains below $0.13 \text{ ps/nm/km}^{259}$. However, whilst penalties from interactions alone should not be responsible, the observed performance degradation may be due to soliton interactions between pulses experiencing Gordon Haus jitter²⁶⁰. This was verified in principle by eliminating alternate pulses (to give a 20 Gbit/s signal) whilst maintaining the same demultiplexer switching window (to demonstrate the same jitter tolerance), where significantly enhanced transmission performance was established (2,700 km at 1549.1 nm and 2,500 km at 1549.7 nm). Degradations due to dispersive wave radiation generated from violations of the average soliton model are also anticipated for dispersions above 0.05 ps/nm/km .

Below the optimum transmission wavelength, polarisation mode dispersion was anticipated to have a major effect on pulse stability (theoretically within the dotted region of Figure 5-10) and the error free distance rapidly degraded to $\approx 1,100 \text{ km}$, even for 20 Gbit/s signals. However, this transmission distance was maintained even for propagation within the normally dispersive region of the fibre. The experiment was repeated using the EC-MLL, where quantitatively similar performance was observed for dispersions above 0.06 ps/nm/km , however, at the previous optimum wavelength of 1549.2 nm the transmission distance was reduced to 1700 km, confirming previous comparisons of the performance of pulse sources for theoretically optimised soliton transmission⁷⁴.

In this experiment, it has been shown that pseudo-linear transmission of 40 Gbit/s data sequences over 1,000 km is possible over a range of signal wavelengths in excess of 2.3 nm, confirming previously reported results. However, the system performance is significantly enhanced to over 2,000 km for a narrow range of wavelengths (0.7 nm) where soliton transmission is possible. The performance of the soliton system appears to be restricted primarily by the soliton period and interplay between jitter and soliton interactions. We may anticipate somewhat enhanced performance by employing alternating amplitude or polarisation to suppress the interactions, and guiding filters to reduce jitter. Clearly however, in order to increase the system line rate, strong control of both jitter and interactions is required, along with techniques to alleviate dispersive wave penalties from violations of the average soliton model. The following experimental investigations into soliton control and novel fibres were carried out with these aims in mind.

5.2.2 Theory of Soliton Transmission Control

We have seen that the Gordon Haus effect arises when a soliton passes through an amplifier and consequently experiences the addition of noise. The effect of the noise is to randomly shift the central frequency of the soliton, which in combination with the chromatic dispersion of the fibre, gives rise to a velocity shift and arrival time errors. However, the original analysis used to predict the jitter levels did not account for the filter curvature, which will naturally resist variations in the soliton centre frequency by presenting lower losses to those frequency components closer to the filter maxima^{261,262,263,259}. That is to say, an amplified soliton, shifted to slightly longer wavelengths, is preferentially attenuated on the long wavelength side by any subsequent filters centred on the unperturbed soliton central wavelength (Figure 5-11). On subsequent transmission the new pulse will reform into a soliton whose centre wavelength is closer to the filter peak, provided the spectral distortion is not to extreme. During this process, the slight temporary wavelength offset will, through chromatic dispersion, result in some timing jitter, but since the central wavelength is always restored, the accumulation of jitter is no longer cubic (as in Equation 2-34 above).

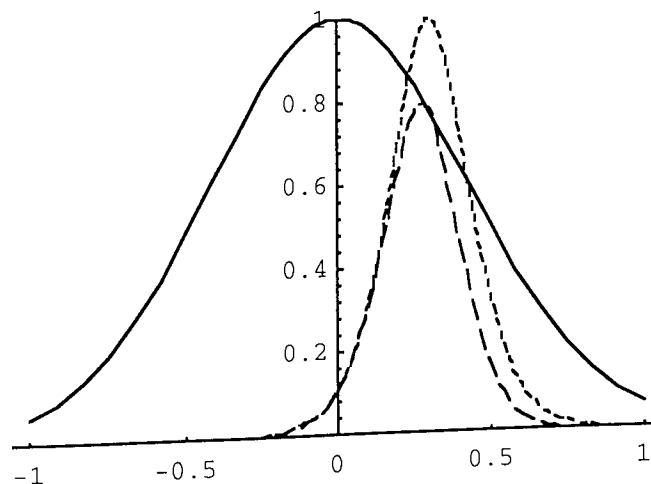


Figure 5-11 Illustration of the effect of guiding filter (exaggerated) showing the spectral profile of a jittered pulse (dotted), a gaussian filter (solid) and the resultant output pulse (dashed).

Defining a dimensionless parameter x , related to the ratio of the filter curvature to the soliton bandwidth (assuming a Gaussian filter inserted with each amplifier), and given by :

$$x = 2N_{\text{amps}} \Delta G$$

$$\Delta G = \frac{2.86}{(2\pi c)^2} \frac{\lambda_0^4}{\tau_{FW}^2 \lambda_{3dB}^2} \quad \text{Equation 5-54}$$

allows us to determine that the resultant mean squared arrival time jitter is reduced by a factor of

$$f = \frac{3}{2x^3} (2x - 3 + 4e^{-x} - e^{-2x}) \quad \text{Equation 5-55}$$

where N_{amps} represents the total number of amplifiers, each with an associated filter, λ_0 the centre wavelength of the soliton and λ_{3dB} the 3 dB width of the guiding filter²⁶³. If filters are located more sparsely, then the number of amplifiers should be replaced by the number of filters. For $x \gg 1$ (strong guiding), the jitter accumulates linearly with distance. By way of example, in the case of the above 2,200 km 40 Gbit/s transmission experiment, we find that the rms Gordon Haus jitter is only reduced to 76 % of its uncontrolled state by employing a single 2.7 nm filter every three amplifiers, and the soliton control could be said to be weak.

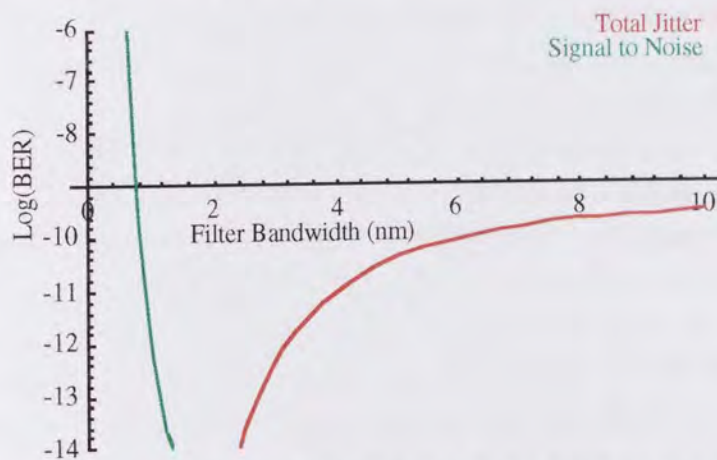


Figure 5-12 Typical variation in error rate for a 40 Gbit/s, 3000 km transmission system as a function of guiding filter width using parameters from experimental demonstration above.

Since a certain degree of spectral loss is imposed on the solitons by the guiding filters, in order to restore the correct central frequency, additional gain must be provided by the amplifiers in order to overcome this excess loss (ΔG in Equation 5-54). This additional gain is of course accompanied by increased spontaneous emission at the peak of the filter and we would expect the signal to noise ratio of the system to be degraded, the degradation increasing as the degree of guiding is increased^{261,263}. This leads to an optimum filter bandwidth (≈ 2 nm), as illustrated in Figure 5-12, for the 40 Gbit/s transmission system studied above. This optimum bandwidth would give a reduction in jitter to 22 % of its unconstrained value at 2,200 km. A further constraint on the filter

bandwidth arises from the spectral distortions imposed on the pulse by the filters²⁶², and the consequent dispersive wave radiation generated on subsequent propagation. In addition to suppressing jitter from the Gordon Haus effect, it has also been shown that by restricting the signal wavelength, guiding filters reduce the detrimental effects of soliton interactions^{259,264}, the acousto-optic effect²⁶⁵ and collisions in a WDM system²⁶⁶. For example the interaction force attracting two solitons together produces a change in the soliton velocity, which, in a dispersive fibre, must correspond to a change in wavelength. If this wavelength variation is restricted, the interaction force must be resisted and the collapse period increased. Taking this reduction in strength of the interaction force into account, it may be shown^{259,267,268} that the collapse length is now given by

$$L_{coll} = -\frac{L_{rep}}{4\Delta G} \ln \left\{ 1 - \frac{2\pi L_{sol} \Delta G}{L_{rep} \operatorname{sech} \left[\frac{1.76T}{2\tau_{FW}} \right]} \right\} \quad \text{Equation 5-56}$$

Which, in the limit of $\Delta G \rightarrow 0$, reduces to equation 2-31, which in turn reduces to the familiar exponential form for well separated pulses. Furthermore, for sufficiently strong guiding, the collision length tends to infinity, and the collision is completely suppressed.

The accumulation of spontaneous emission down the transmission line can be greatly reduced by slightly offsetting the centre wavelength of each guiding filter^{269, 270} (a technique known as "sliding guiding"). The non-linear, quasi particulate nature of the soliton pulses enables them to follow the shift in gain peak of the system but linear signals, such as noise from amplifiers earlier in the link and dispersive wave radiation will be attenuated by subsequent filtering. Equivalent performance is achieved by periodically frequency shifting the optical signal in a fixed filter transmission line^{271,276}. In this case, the fixed filters enable the soliton pulses to resist the frequency shift, whilst linear pulses are frequency shifted and attenuated by subsequent filters. In both cases, the transmission line only supports long haul transmission of soliton pulses. Indeed, it has been shown that the such systems reduce intensity noise, efficiently shed non soliton components from non ideal sources, and stabilise the soliton amplitude and pulse width. Particularly impressive results using these technique have been reported, with transoceanic distances achieved for bit rates up to 20 Gbit/s²⁷⁹, and the transmission span at 40 Gbit/s is increased by almost a factor of 2 using a combination of sliding guiding and adiabatic pulse compression²⁸⁰. Due to the excellent progress reported openly by other laboratories (see for example Table 12), the use of guiding filters alone has not been specifically investigated in this thesis.

Bit Rate (Gbit/s)	Transmission Distance (km)	Additional Features Demonstrated	Ref
5 (2λ)	6,000	Used UV written fibre grating based Fabry-Perot filter	272 273
10	1,000	Reduction of soliton interaction	274
10 (2λ)	13,000	Sliding filters used in WDM system	275
10	27,000	Signal frequency sliding	276
10 (7λ)	9,400	Stabilisation of pulse amplitude	277
10	10,000	Shedding of non soliton component	278
20	19,000	High speed OTDM operation	279
40	4,000	Simultaneously used to vary mean dispersion giving adiabatic compression	280

Table 12 Recent progress in sliding guiding filter based soliton systems

These ideas for soliton control are further expanded by the idea of active soliton control²⁸¹. With active soliton control, a simple fixed frequency guiding filter provides mild spectral and intensity management of the signal, as described above, but the jitter and noise accumulation are strictly restricted by applying a synchronous modulation in either amplitude²⁸² or phase²⁸³ periodically along the system. One clear drawback of the technique is the requirement to extract timing information from the pulse stream each time synchronous modulation is required, however, using the clock recovery techniques described above (Section 4.1.1), little difficulty is anticipated in this area.

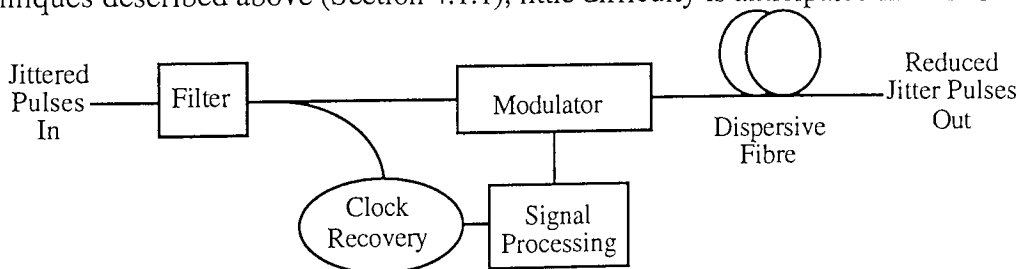


Figure 5-13 Schematic diagram of a generic active soliton control module.

In the case of amplitude modulation, a pulse which through some mechanism (for example; Gordon Haus jitter, soliton interactions or acousto-optic effect) has drifted from the mean arrival time will experience a differential loss along its length when it passes through the modulator and the centre of gravity of the pulse is pulled back towards the middle of the time slot, in much the same way that guiding filters restore the mean wavelength of a pulse. Any non-soliton components (including noise and dispersive wave radiation) which are not incorporated into soliton pulses are subject to the periodic attenuation of the synchronous modulator. These components propagate at different velocities to the soliton, due to chromatic dispersion and non-linear changes in the refractive index. On arrival at subsequent modulators therefore those parts of the noise passing through the peak of one modulator, will be attenuated by subsequent modulators. It has been shown²⁸² that the noise level rapidly saturates to;

$$P_{\text{spont}}(\infty) = P_{\text{spont}}(\text{mod})(1 + \Delta G) \left[\frac{1}{1 - \frac{(1 + xr)(1 + \Delta G')}{2}} \right] \quad \text{Equation 5-57}$$

where $P_{\text{spont}}(\text{mod})$ is the spontaneous emission generated between modulators in the absence of soliton control, xr the achieved modulator extinction ratio, ΔG the excess gain due to filtration and $\Delta G'$ the required excess gain due to modulation given by ;

$$\Delta G' = \frac{1 - e^{-\frac{\pi^2 \tau_{FW}^2}{4 \ln 2 T^2}}}{\left\{ \frac{1 + xr}{1 - xr} \right\} + e^{-\frac{\pi^2 \tau_{FW}^2}{4 \ln 2 T^2}}} \quad \text{Equation 5-58}$$

In the reduction of timing jitter, and the suppression of soliton interactions, it can also be shown²⁸⁴ that for a given temporal deviation δt_{in} from the peak of the middle of the time slot, the output deviation δt_{out} is given by;

$$\delta t_{\text{out}} = \frac{\delta t_{\text{in}}}{1 + (1 - xr) \left(\frac{\pi \cdot \tau_{FW}}{1.76 T} \right)^2} \quad \text{Equation 5-59}$$

for a purely sinusoidal modulator function, and is clearly non zero. Consequently, although strictly restrained, a finite level of timing error will remain at the output of the transmission line. In particular, interacting pulses will tend to be pulled together slightly. Clearly, transmission errors will occur if a pulse jitters beyond its time slot (or the influence of the modulator) between modulation stages, placing an upper bound on the spacing between modulators, however, it is possible to significantly increase the spacing of optical amplifiers over that normally required²⁸⁵. The reduction in timing jitter achieved using an amplitude modulator can be viewed as a phase to amplitude noise conversion, jittered pulses experiencing greater loss. Consequently, amplitude modulators are deployed *in addition* to guiding filters, the later stabilising the pulse amplitude^{282,277}. The significant benefits of soliton retiming are demonstrated in this thesis and have enabled the worlds first demonstration of 20 Gbit/s transmission over global distances^{258,286}.

Phase modulation has been proposed as an alternative to amplitude modulation²⁸³ and offers the potential for superior suppression of Gordon Haus jitter. In this scheme, phase modulators are arranged such that correctly timed pulses experience little phase modulation, whilst jittered pulses are chirped by the modulator. Subsequent chromatic dispersion then imposes the necessary delay on the pulse to restore the correct position. Note that this is a continuous process, enabling the pulse to return exactly to the correct temporal position, in contrast to the discrete time shifts imposed by amplitude modulators. Furthermore, since the control technique imposes no direct energy loss, guiding filters are not explicitly required to stabilise the pulse amplitude, and excess gain may be avoided. Unwanted spontaneous emission between pulses is chirped away from the soliton central frequency, to be eventually attenuated in the wings of the transmission filters. Unfortunately, as observed in the case of optically mode locked

ring lasers, this noise suppression technique is somewhat inefficient and large XPM phase shifts are required to eliminate noise completely¹¹², unless the XPM is accompanied by a degree of simultaneous amplitude modulation¹¹³.

Remarkably small phase shifts are required to stabilise the transmission of soliton pulses against both jitter, and nearest neighbour interactions^{197,287} (typically less than 0.1 radians) using regularly spaced modulators. Given that such small phase shifts are required, it has been proposed that the phase modulation may be carried out all optically through cross phase modulation. A preliminary demonstration of the technique²⁸⁸ demonstrated the doubling of the transmission span of a 2.5 Gbit/s soliton system with a peak phase shift of only ≈ 0.01 radians imposed via cross phase modulation along 13 km of the transmission fibre every 100 km. The technique has been called soliton shepherding since clock pulses accompany, or shepherd, the data pulses. Since the technique is all optical, an appropriate shepherding signal may always be generated using the same techniques used to generate the OTDM data sequence itself.

It has been proposed²⁸⁹ and experimentally demonstrated⁷⁰ that particularly stable transmission will be obtained by combining the jitter suppression of phase modulation with the noise suppression of amplitude modulation. This is achieved by carefully controlling the chirp of the amplitude modulator to produce co-operative rather than competitive soliton control effects. The importance of this fine control will be further demonstrated below. It has also been proposed¹, and theoretically confirmed²⁹⁰ that active retiming, may also be applied to a correctly designed WDM system with a single modulator at each retiming stage, and experimental demonstrations of active retiming with a modulator per wavelength are now well under way^{291,292}.

5.2.3 20 Gbit/s soliton control

Figure 4-7 illustrates the experimental arrangement used to demonstrate active soliton control at 20 Gbit/s using synchronous amplitude modulation. 10 GHz, 1553nm pulses from the external cavity laser were modulated with a 2^7-1 PRBS data stream by a LiNbO₃ Mach-Zehnder interferometer and compressed down to 6 ps in a 300 m length of dispersion compensating fibre before passive interleaving and injection into the loop. Transmission control was achieved by a balanced 26 GHz GaAs Mach Zehnder amplitude modulator whose polarisation sensitive waveguide necessitated the use of a polarisation controller within the loop. The soliton amplitude was stabilised using a single 1 nm bandwidth filter. At the receiver timing recovery was performed by a 20 GHz electronic phase locked loop (PLL) as described in section 4.1.1. The 10 GHz output of the VCO was used to drive the error detector and the electroabsorption modulator demultiplexer whilst the retiming modulator was driven from the PLL via a frequency doubler to give a phase locked 20 GHz RF signal. Note that it was essential to perform timing extraction at the full line rate since the component at the base rate of 10 GHz was negligible, especially under transmission control where any residual 10 GHz RF component was eliminated. Note also that the data stream is injected into the loop via input #1, *through* the retiming modulator, correct phasing being ensured by performing clock recovery whilst the data is injected into the loop.

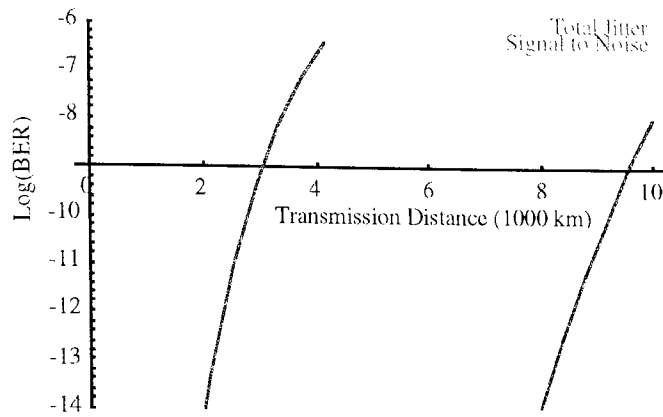


Figure 5-14 Theoretical error ratio performance as a function of transmission distance for the 20 Gbit/s transmission experiment described below.

With transmission control disabled error free operation (defined as a BER $< 1 \times 10^{-9}$) was limited to a distance of $\approx 2,000$ km by the accumulation of timing jitter, in reasonable agreement with previously published results^{293,254}, a recent field demonstration in the Tokyo area²⁹⁴ and theoretical predictions (Figure 5-14). This was achieved with a path average fibre dispersion at the operating wavelength of 0.33 ps/nm/km and a source time bandwidth product 0.6. The 1 nm filters deployed ever 100 km would be expected to reduce the rms timing jitter at 2000 km to $\approx 30\%$ of its unconstrained value. Given the strong influence of the filters in this experiment, and the relatively large excess gain ($\Delta G = 0.13$), the use of sliding filters would be of considerable benefit²⁵⁷. Note that the filter width was determined by the requirement to stabilise the soliton amplitude with the retiming signal applied rather than an optimisation of the filtered transmission performance. This resulted in a non optimal system performance in the absence of active control. Also, with a soliton period of only 43 km (compared to an amplifier spacing of 33 km and a filter spacing of 100 km) a performance degradation from dispersive wave radiation would be anticipated.

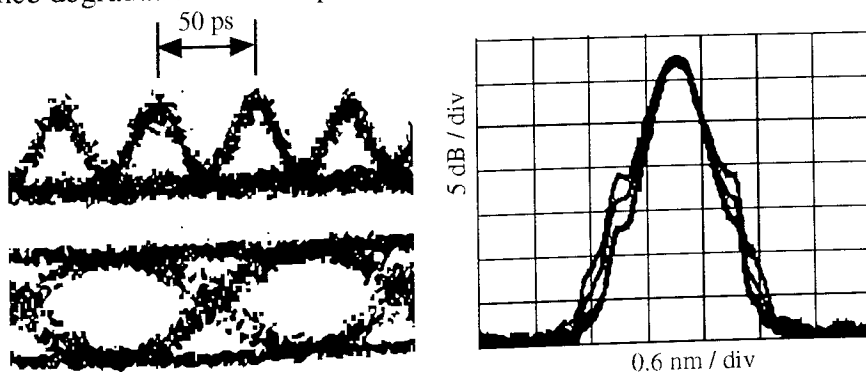


Figure 5-15 Transmission of 20 Gbit/s soliton signal over 125,000 km showing path averaged optical spectrum for pulse widths of 5.65 and 8 ps (right), the received 20 Gbit/s eye diagram (top left) and the demultiplexed and bandlimited eye diagram (bottom right)

When the retiming signal was correctly applied to the modulator the data stream propagated a distance in excess of 125,000 km error free. Figure 5-15 details the 20 Gbit/s eye diagram detected on a 20 GHz pin at this distance and also the demultiplexed and bandlimited eye. No evidence of degradation is observed, indeed for slight intentional misalignments of the transmitter interleaver, the 20 GHz soliton control

restores the pulses to their correct positions. This was confirmed by the reduction of the residual 10 GHz RF component. Further stable transmission beyond 125,000 km appeared to be limited only by the state of signal polarisation drifting out of alignment with the modulator axis during the elongated measurement cycle. This polarisation sensitivity may be eliminated by the use of polarisation insensitive electro-absorption modulators⁶⁶, or cross spliced lithium niobate modulators²⁹⁵. These results were achieved with a 1.4 V_{p-p} 20GHz RF signal applied to the modulator, resulting in a 66% optical modulation depth ($\Delta G' = 0.008$), suggesting that increases in the spacing between modulators is perfectly feasible.

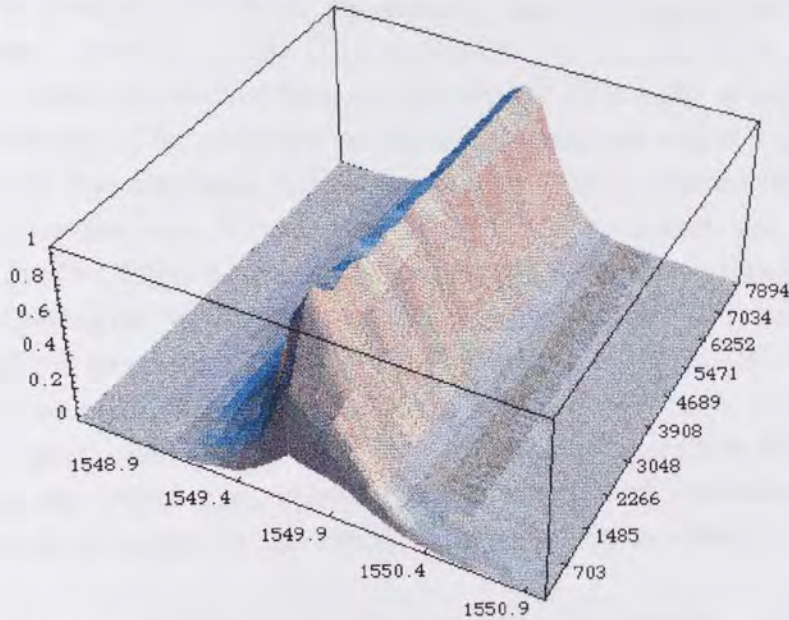


Figure 5-16 Spectral evolution of 20 Gbit/s data under active retiming soliton control.

The path averaged pulse width of the recirculating solitons was measured on an auto-correlator to be 6 ps giving a ratio of soliton period to amplifier spacing of only 1.3, violating the general guidelines of the average soliton model and resulting in resonance's occurring in the spectrum of the solitons^{296,296,49}. Variation in loop pump power allowed the width of the propagating solitons to be adjusted between 8 ps and 5 ps through the stabilising effects of the soliton control. This was observed to vary the amplitude of the sidebands in the spectrum, as shown in Figure 5-15. However, the spectral positions of the n th resonance, δv_n (Hz), did not vary significantly with pulse width as predicted empirically by theoretical studies⁵⁴ and confirmed analytically²⁹⁷ (Equation 2-33) In this experiment the first sideband is predicted to be ≈ 0.7 nm away from the peak, comparing favourably with the measured value of 0.65 nm (0.1nm resolution). By operating with such distinct sidebands, it is confirmed that soliton control eliminates not only jitter and amplitude noise, but degradations due to dispersive wave radiation. This experiment has demonstrated error free operation of 20 Gbit/s soliton propagation over global distances with the soliton period to approaching the amplifier spacing. Such performance will be crucial in minimising the cost of high speed soliton systems, particularly at higher capacities where it becomes difficult to increase the soliton period by reducing the mean dispersion coefficient.

5.2.4 Soliton control using electro-optic frequency doubling.

One of the advantages of OTDM systems is the ability to operate at bit rates beyond the capacity of state of the art electronics. Consequently it is important to establish soliton control techniques for global transmission of high bit rate OTDM systems. As we have seen above (Section 4.2.1), frequency doubling may be achieved by dc biasing a Mach Zehnder modulator at an optical null and applying RF signals with peak to peak amplitudes up to $2\sqrt{\pi}$. In this way, 40 Gbit/s transmission control may be established using a 20 GHz RF drive signal.

The above experimental set up was modified by adding a second interleaver stage in the transmitter to produce a 40 Gbit/s data sequence, and by changing the 20 GHz PLL clock recovery circuit for its 40 GHz equivalent. The 20 GHz drive signal to the retiming modulator was derived from the recovered 10 GHz clock in the same manner as above. Inclusion of the polarising modulator, its associated optical amplifier and the filter required for amplitude stabilisation under control reduced the 40 Gbit/s uncontrolled transmission distance from 2,000 km to somewhat less than 800 km (Figure 5-17). Two filters were used in turn to stabilise the soliton transmission, the 1 nm filter employed for the 20 Gbit/s soliton control experiment, and a broader 2.1 nm filter. Whilst the increased excess gain due to filtering (0.13 and 0.03 respectively) is cause for some concern, the degraded signal to noise ratio alone is insufficient to explain the deteriorated performance, although a subtle interaction between several degradations (eg excess gain, sideband instabilities, soliton interactions, dispersive wave radiation generated by the filters) may adequately describe the uncontrolled system.

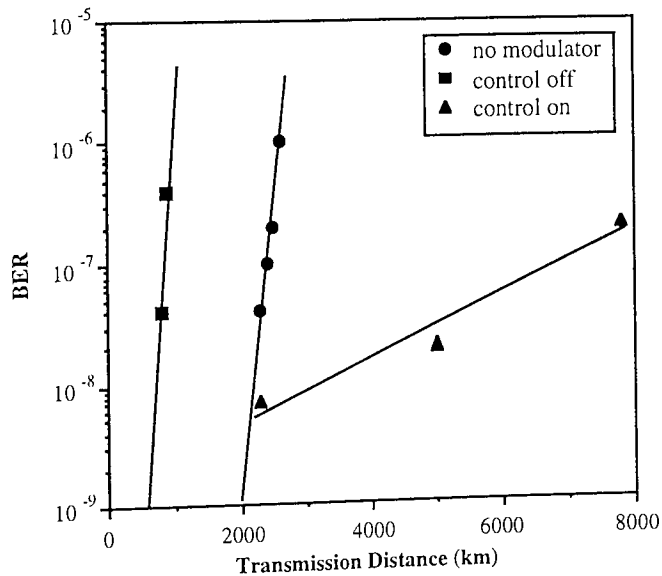


Figure 5-17 Error ratio performance of 40 Gbit/s transmission in the absence of soliton control (circles), with control elements in place (squares) and with soliton control applied (triangles)

Using the 1 nm filter, soliton control allowed the transmission distance of the system to be improved to 1,500 km for an error ratio of 2×10^{-8} . Whilst perfectly suitable for 20 Gbit/s soliton transmission, such strong filtration clearly compromised the transmission control, potentially through increases in the soliton interactions due to the dispersive wave radiation generated by the filter. Increasing the filter width to 2.1 nm, improved

the system performance (error rate of less than 10^{-6} at 8,000 km, Figure 5-17) by reducing the dispersive wave radiation at the expense of amplitude stability. For the high modulation depth required to minimise the insertion loss of the retiming modulator biased at a null, the excess gain due to the amplitude modulation is ≈ 0.10 (Equation 5-58). Consequently, we anticipate a maximum spontaneous emission noise level equivalent to only 2.3 times the noise generated between modulators (≈ 230 km), whilst the jitter is reduced by $\approx 15\%$ per modulator, theoretically giving a well controlled system, as illustrated by the stability of the 40 GHz RF component (Figure 5-18).

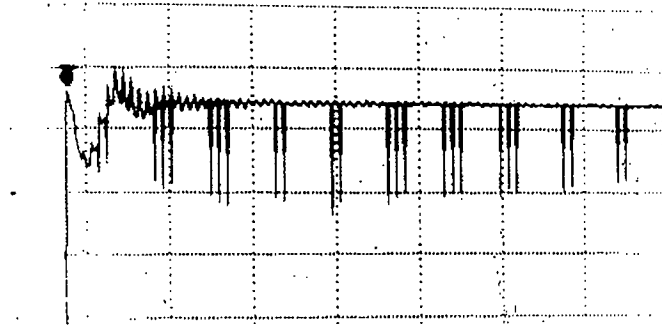


Figure 5-18 Evolution of 40 GHz RF spectral component for 40 Gbit/s soliton control (horizontal scale 5 ms/div, vertical scale 5 dB/div)

The evolution of the pulse spectrum is illustrated in Figure 5-19, and allows some insight into the performance. A significant evolution of the pulse spectrum is observed as the launched gaussian pulses reform into the appropriate soliton pulses. This evolution is accompanied by a distinct wavelength shift towards the optimised filter centre frequency, suggesting that the system is attempting to shed non soliton components in analogy with sliding guiding or signal frequency sliding techniques. Furthermore, analysis of the spectral width and autocorrelations suggests that the output pulse width is reduced to ≈ 4 ps. The stabilisation of the pulse width is to be anticipated by the stability criteria of the controlled system, and we would expect significantly improved performance by launching transform limited pulses of this optimum width and consequently reducing dispersive wave radiation.

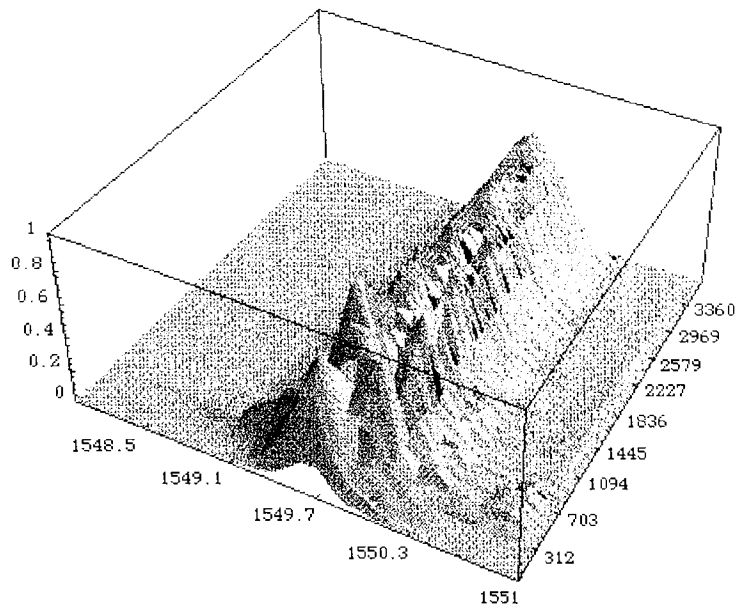


Figure 5-19 Spectral evolution of 40 Gbit/s soliton data under transmission control.

Significantly, this performance was only possible with the loop length equal to a non integer (or odd) number of bit periods, and the clock recovery adjusted to demultiplex a random (or alternating) signal channel. Unless this condition was maintained, the signal rapidly degraded, accompanied by a distinct increase in the 20 GHz RF component. Continuous drifts away from this optimum made global optimisation of the transmission system particularly difficult. This performance is not unexpected, and may be explained as follows. The balanced Mach Zehnder modulator employed was subsequently found to have a minimum chirp parameter α_m of ≈ 0.08 , measured using a frequency domain technique²⁹⁸, giving rise to a small degree of phase modulation accompanying the amplitude modulation. Due to the frequency doubling technique applied, the sign of the phase modulation alternates regularly between passbands originating from the maximum and minimum of the 20 GHz RF signal, whilst the peak amplitude is of the order 10 mrad. This level of phase shift is anticipated to be sufficient to control the soliton independently of the amplitude modulation²⁸³ for the appropriate sign, whilst serious instabilities are anticipated for the opposite sign²⁸⁹. Thus, if the relative phase of the 20 GHz control signal with respect to the base rate channels within the 40 Gbit/s data signal is the same for each successive retiming modulator, only half of the channels will be correctly controlled, whilst if the phase regularly alternates so that each base rate channel experiences an equal number of positive and negative chirps, all channels will be stably controlled with zero net phase modulation. This has a close analogy with the operation of harmonically mode locked fibre ring lasers^{299,300,301} where stable operation is only obtained for odd numbered harmonics (section 4.1.2).

5.2.5 Soliton shepherding

As discussed above, soliton shepherding is a particularly attractive technique that allows the phase modulation of any OTDM data sequence by exploiting non-linear interactions in the transmission fibre itself²⁸⁸. At a repeater station, an optical clock signal is generated in synchronism with the OTDM data signal and propagated along the subsequent transmission fibre. Ideally the shepherding signal propagates at a velocity matched wavelength (eg symmetrically about the dispersion zero). Cross phase modulation via the non-linear refractive index then provides the appropriate phase shifts to control the position of the solitons, each data pulse being temporally attracted to a shepherding pulse.

The recirculating loop configuration used in the soliton shepherding experiments is also shown in figure 5-7. In this case, a 10 Gbit/s data signal comprising 1550.9nm, 6 ps EC-MLL pulses was inserted via input #1, whilst shepherding pulses were continuously derived from the electronic clock recovery circuit and injected via input #3. The shepherding pulses co-propagated along the first fibre link, and were rejected by the 3 nm optical filter, whilst the 90:10 coupler was used to ensure that the two signals are velocity matched. The shepherding signal itself was generated using a cw DFB and the GaAs device previously used for amplitude modulation based retiming above, driven at 20 GHz.

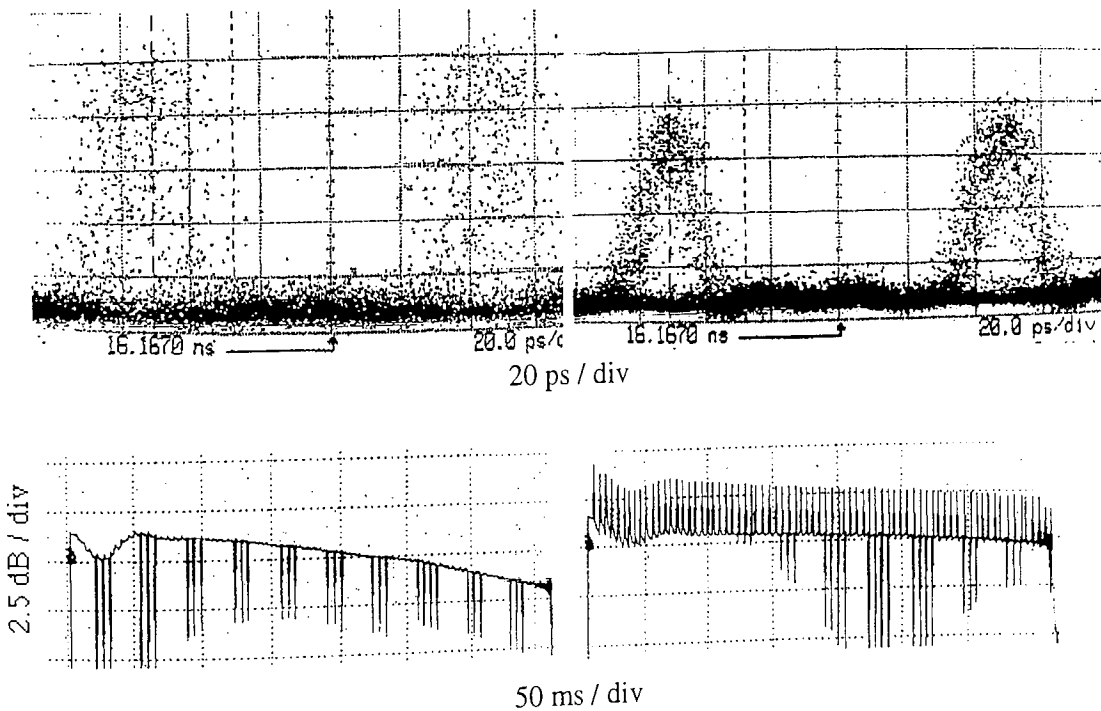


Figure 5-20 20 GHz RF component (bottom) and eye diagrams (top) for 10 Gbit/s soliton transmission over 7,500 km, with (right) and without (left) soliton shepherding.

Figure 5-20 details the evolution of power in the 20 GHz RF component of the 10 Gbit/s soliton data stream with distance with and without soliton shepherding. Without retiming the harmonic rapidly diminishes in amplitude as a consequence of timing jitter, as confirmed by the output eye diagram. With the presence of a weak shepherding

beam ($\approx 50\%$ of the data amplitude) the jitter is almost completely suppressed. In this case the 20 GHz component of the microwave spectrum has dropped by less than 2 dB at 7,000 km, indicating the effectiveness of the technique in constraining the solitons to their correct time slots.

In the absence of shepherding the combination of jitter and degraded signal to noise ratio resulted in a BER of $\approx 10^{-4}$, in reasonable agreement with published results in the absence of sliding guiding filters or retiming modulators^{302,303}. Soliton shepherding almost completely removes the jitter from the received signal, however, the BER is only marginally improved to $\approx 10^{-5}$. That this system is noise limited is confirmed by the unchanged noise level in the absence of data pulses in both shepherded and un-shepherded cases. Further confirmation is found by inserting the electro-absorption modulator demultiplexer, driven as if to demultiplex a 20 Gbit/s data signal, whereupon a factor of 2 improvement in BER is observed. Similar results were obtained at 20 Gbit/s, with a signal wavelength of 1553 nm (to give a higher soliton power), and the noise growth is illustrated in Figure 5-21 following transmission over 5,000 km with negligible jitter.

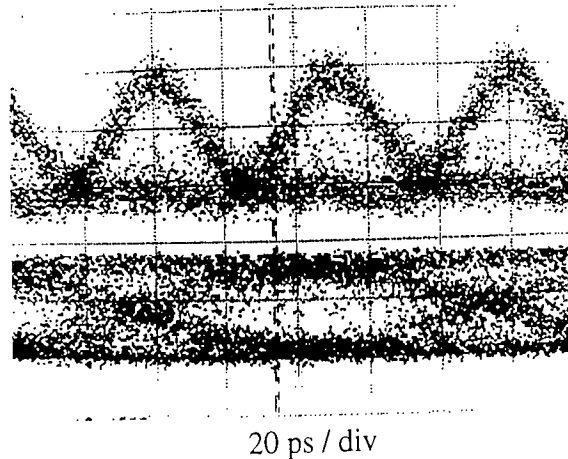


Figure 5-21 Eye diagram of 20 Gbit/s soliton data transmission over 5,000 km with soliton shepherding (top), along with the corresponding demultiplexed and bandlimited 10 Gbit/s base rate signal (bottom).

Previous experiments on soliton shepherding²⁸⁸ tackled the problem of noise growth simply by increasing the fibre dispersion, giving an improved signal to noise ratio at the expense of increased jitter, which is controlled by the shepherding beam. Equivalently, the soliton pulse width may be reduced. At higher capacities, the extent to which the signal to noise ratio may be increased in this manner is somewhat restricted by the average soliton model. Alternative techniques for improving the signal to noise ratio include several forms of dispersion management^{65,304,305,306}, whilst noise accumulation may be restricted using sliding guiding filters or saturable absorbers^{307,308}. These may be realised from semiconductor optical amplifiers³⁰⁹ or non-linear loop mirrors^{310,311,312}. Clearly, all-optical amplitude modulators may also be used to simultaneously gain the benefits of noise rejection and high capacity^{184,313}. Indeed, it may be possible to combine the beneficial effects of all-optical amplitude modulation and saturable absorption by utilising two wavelength non-linear amplifying loop mirrors⁵⁰.

5.2.6 Novel Transmission Fibres for Soliton Transmission

We have seen above, that at 40 Gbit/s and above, violations of the average soliton model³¹⁴ pose a significant performance limitation for long haul soliton transmission systems^{258,315,54}. These violations occur when no further scope for reducing the mean dispersion exists (due to for example higher order dispersion or PMD) and when economic constraints prevent further reduction in repeater spacing to ensure compliance. Furthermore, in soliton controlled systems, excellent control of timing jitter favours high dispersion or short pulse width systems to enable high signal to noise ratios. However, once again, violations of the average soliton model restrict the degree of flexibility available at high capacities unless repeater spacings are reduced. Two techniques have been proposed to alleviate this downward pressure on the repeater spacing. Distributed amplification^{316,317,318,319,320} aims to eliminate the actual power fluctuations, whilst loss compensating dispersion shifted fibre (LCDDF) ensures a continuous balance between dispersive and non-linear chirp by reducing the dispersion in proportion with the signal power^{157,152,176,321}. In this section, the feasibility of these two techniques for overcoming the limitations of the average soliton model is investigated.

5.2.6.1 Distributed Amplification³²²

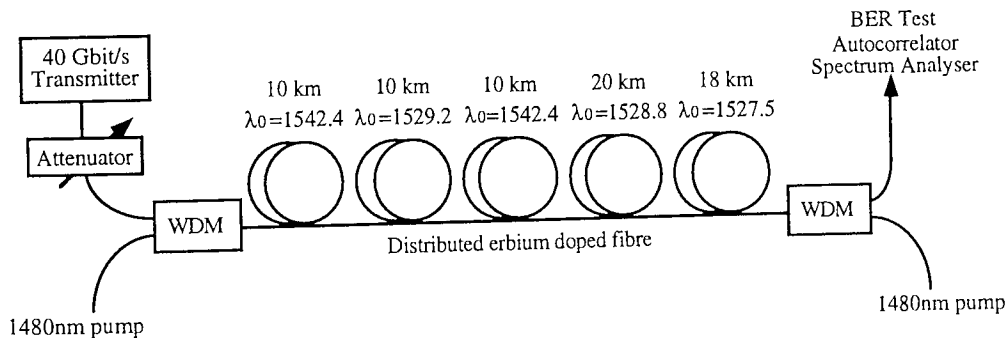


Figure 5-22 Schematic diagram of distributed erbium fibre link with low signal power excursion used for 40 Gbit/s transmission experiments.

Distributed amplification has been widely investigated as a technique for extending the transmission range on unrepeated systems at a variety of bit rates³²³ with gain coefficients of a few dB/km. However, this has recently been supplanted by the equally efficient technique of remotely pumped amplification³²⁴. The distributed erbium doped fibres used during these experiments (typically optimised in terms of gain per mW of pump power³²⁵) are unlikely to allow a significant improvement in high speed soliton transmission for two important reasons. Firstly, because of the high intrinsic gain coefficient, an amplified link is likely to give rise to power fluctuations of equal or greater magnitude as a simple dispersion shifted fibre link. Secondly, when deployed in long lengths, the fibres are prone to instabilities due to Rayleigh scattering³²⁶. Consequently, for high speed soliton applications, a new distributed erbium fibre amplifier was designed to allow the longest possible repeater span in the presence of Rayleigh scatter, with the dispersion zero targeted just below the amplifier gain peak at

1535 nm. Similar fibres were previously reported for pseudo linear transmission with a dispersion zero around 1545 nm³²⁷.

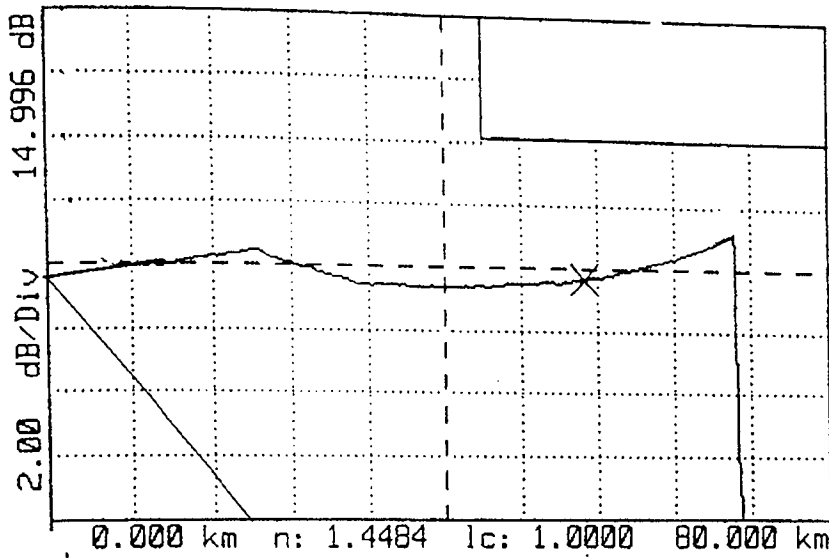


Figure 5-23 Gain variation along a 68 km distributed erbium doped fibre amplifier directly observed using an OTDR, standard fibre also shown for reference.

Figure 5-22 illustrates the experimental set up used to investigate soliton transmission over a low gain distributed erbium doped fibre amplifier. The 1535 nm signal was derived from a linearly compressed harmonically mode locked external cavity laser giving 7.8 ps pulses. The pulse train was modulated with a 2^7-1 PRBS and passively interleaved to 40 Gbit/s before launching into the fibre link. The 68 km transmission link comprised five lengths of lightly doped Er-doped dispersion shifted fibre with nearly equal unpumped attenuation coefficients of ≈ 0.68 dB/km, giving an estimated net maximum gain coefficient of ≈ 0.12 dB/km. The mean dispersion zero wavelength and the dispersion slope of the total link were as 1532.6 nm and 0.07 ps.nm².km⁻¹, respectively. Consequently, the average dispersion of the fibre was 0.165 ps/nm/km at the signal wavelength of 1535 nm. Full measurement data for the constituent fibres, performed by the manufacturer, Corning Inc., is given in Table 13. The fibre was bidirectionally pumped with a total of only 100 mW of 1480 nm pump power. For an input signal power of -3 dBm a net intrinsic fibre gain of 2 dB was achieved compensating for the loss of the two WDM couplers.

Fibre	Attenuation (dB/km) @ 1530 nm	Attenuation (dB/km) @ 1540 nm	Attenuation (dB/km) @ 1600 nm	Mode Field Diameter (μ m)	Dispersion Zero (nm)	Dispersion Slope (ps/nm ² /km)	Length (km)
1	.64	.72	.30	7.7	1542.4	.073	10
2	.67	.77	.25	7.5	1529.2	.069	10
3	.65	.70	.30	7.7	1542.4	.0724	10
4	.64	.71	.35		1528.8	.069	20
5	.73	.72	.28	7.4	1527.5	.069	18

Table 13 Fundamental parameters of constituent fibres in 68 km, low power excursion, distributed erbium fibre amplifier link.

Measurements of the gain and noise figure of the amplifier³²⁸ confirm that stable oscillation free amplification over a wide dynamic range of signal powers is possible using these low gain distributed erbium fibres with close to the theoretical minimum noise figure. This is of course at the expense of the transparency pump power, the usual figure of merit for distributed amplifier. The gain distribution along the 68 km DEDFA for small mean signal powers was obtained by an OTDR equipped with a ~1535 nm DFB laser confirming a negligible signal power excursion along the entire fibre length (Figure 5-23).

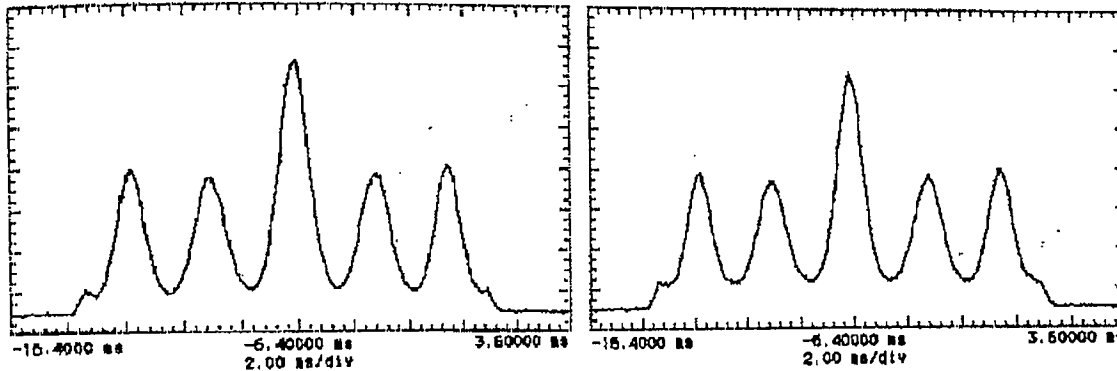


Figure 5-24 Autocorrelation trace before and after 68 km transmission at 40 Gbit/s.

For a mean signal launch power of ≈ -2 dBm, the received pulses at 40 Gbit/s had a pulse width of 7.2 ps with a time-bandwidth product of 0.38, showing a small degree of adiabatic pulse compression³¹⁶, in line with previous pulse compression experiments on a similar 60 km distributed amplifier (Section 3.2.1).

Figure 5-24 shows the autocorrelator traces of the pulses obtained before and after 40 Gbit/s transmission confirming that negligible change in pulse width was observed, in contrast to small signal measurements where 57.5% dispersive broadening was observed. Thus, although the pulses only traversed ≈ 0.4 of a soliton period, it is clear that soliton like propagation dominates the transmission characteristics of the line. Following transmission, the received OTDM data stream was demultiplexed using two electroabsorption modulators. The second modulator was necessary to compensate for the reduction in extinction ratio away from the designed operating region of ≈ 1550 -1560 nm. Not surprisingly Figure 5-25 shows negligible penalty for 10 and 40 Gbit/s soliton transmission over this fibre, measured at the input to the opto-electronic receiver. Note that a large back to back demultiplexing penalty is present at 40 Gbit/s system despite the use of two electroabsorption modulators.

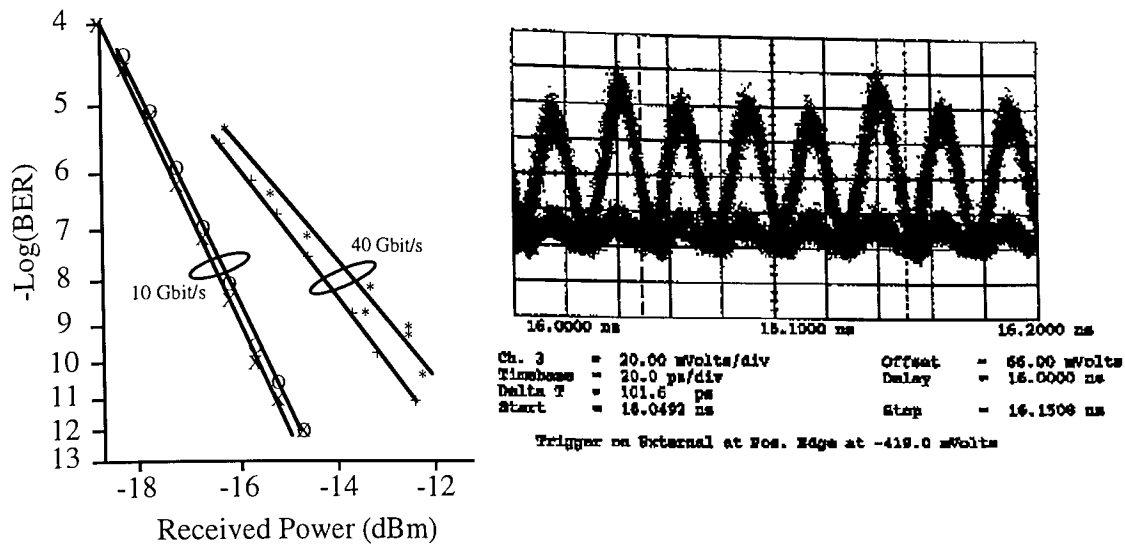


Figure 5-25 BER performance of a 68 km distributed amplifier at 10 and 40 Gbit/s (left) and received 40 Gbit/s eye diagram (right).

These results confirm, for the first time, that high capacity data sequences may be transmitted error free over relatively long distances of distributed erbium fibre with negligible penalty. The exceptionally low (<0.03 dB/km) variation in signal power obtained during this experiment shows great promise for future high capacity long haul soliton transmission systems. In particular, the system is designed with a small net gain to overcome coupler and isolator losses, allowing the cascability of the amplifiers without necessity to insert additional discrete amplifiers. Furthermore, in addition to simply increasing the repeater spacing for 40 Gbit/s soliton systems, the relaxation of the average soliton model should provide increased scope for active soliton control. It is also confirmed that dispersion management may be used in a distributed amplification system, with positively and negatively dispersive fibres used along the transmission line^{280,329}.

5.2.6.2 Loss Compensating Dispersion Decreasing Fibre^{330,331}

The distributed amplification scheme described above provides an artificial lossless transmission line, and the concept of repeater spacing becomes irrelevant as far as soliton dynamics are concerned since the balance of non-linearity and dispersion is exact at any given point, rather than as a path average. This allows access to ultra high repetition rates with reasonable amplifier spacings³¹⁶. The alternative technique is to employ a dispersion decreasing fibre (DDF), where an exact balance is obtained by reducing the dispersion in line with the signal power¹⁵⁷ provided the dispersion decays exponentially. Fabrication techniques for such fibres are now well established¹⁵³, and early fibres were used to demonstrate pulse generation^{166,175} and compression^{332,154,162}. Recently, the application of DDF's to soliton transmission over many soliton periods has been demonstrated³²¹, along with the demonstration of near distortion free transmission over 19 soliton periods with an exponentially varying DDF³³³. This later fibre, and a subsequently produced fibre of lower mean dispersion were assessed for long haul soliton transmission using the recirculating loop in order to

verify that stable soliton transmission may indeed be obtained in a periodically amplified system comprising concatenated DDF's.

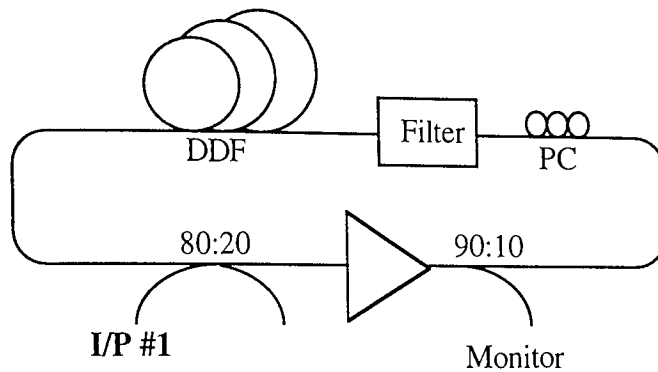


Figure 5-26 Transmission line section of recirculating loop used for dispersion decreasing fibre based transmission experiments

The modifications to the recirculating loop are shown in Figure 5-26. The major change is the reduction on loop length from three spans to one, with a consequent increase in the impact of loop specific losses (input coupler). The 10 GHz, phase-locked, erbium doped fibre ring laser, modulated at 10 Gbit/s was used as the pulse source, giving pulse widths between 4.1 and 11 ps. The three DDF's used (more fully described in ³³³) had exponential dispersion profiles at $\approx 1550\text{nm}$ that matched well to the average fibre loss. The specific properties of each fibre, and the characteristics of the recirculating loop are summarized in Table 14, showing in particular the variation in mean and root mean squared dispersion.

Configuration	1	2	3
Length (km)	38	18	20
Input Dispersion (ps/nm/km)	6	1.75	0.22
Output Dispersion (ps/nm/km)	0.65	0.65	0.10
Mean Dispersion (ps/nm/km)	2.4	1.1	0.17
RMS Dispersion (ps/nm/km)	3.7	1.4	
Dispersion Slope (ps/nm ² /km)	0.053	0.053	0.07
Loss (dB/km)	0.265	0.26	0.21
Filter bandwidth (nm)	2.7	2.7	5.1
Input Pulse Width (ps)	4.1	11	4.7
Fibre Length / Soliton Period	5.4	0.4	0.4

Table 14 Summary of basic parameters of dispersion decreasing fibres investigated in this thesis.

For the first configuration, with a DDF length of 38 km, the quality of the loss compensation process was examined in the spectral domain. The result of one such measurement is shown in Figure 5-27 for a launched pulse width of 6.5 ps, where we observe that after an initial stage of spectral narrowing on the first recirculation due to the intra loop filter, the spectrum remains stable over 300 km, or 43 soliton periods.

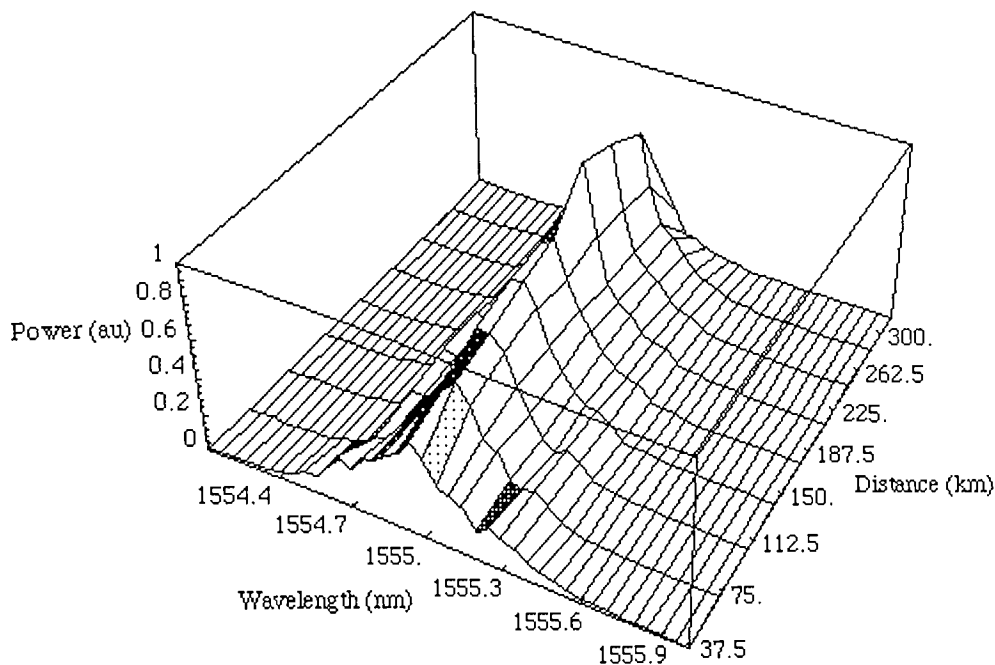


Figure 5-27 Spectral evolution of 6.5 ps pulses along a transmission line comprising concatenated 38 km DDF's.

This demonstrates the excellent loss compensation characteristics of the fibre, even when the system is operated up to 5 nm away from the design wavelength of 1550 nm. Unfortunately, due to the high mean dispersion of the system, the error free distance at this wavelength was limited to ≈ 260 km, and ≈ 300 km at the optimum wavelength. It is believed that the major limitation at the optimum arises from the soliton acousto-optic effect, in which the jitter scales as the square of the dispersion^{62,265}. A simple theoretical treatment, neglecting the effects of guiding filters, suggests a maximum transmission distance for this experiment of around 3-400 km.

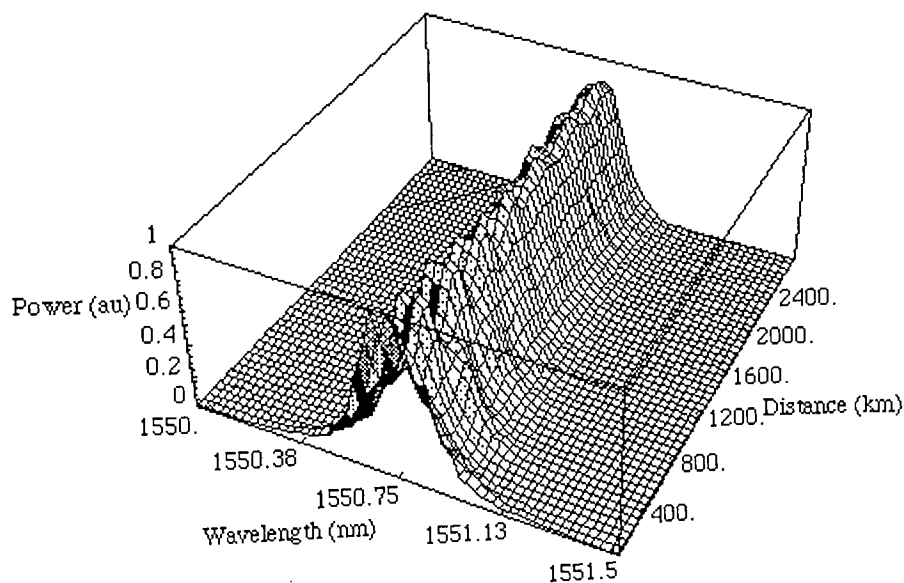


Figure 5-28 Spectral evolution of pulses along a transmission line comprising concatenated 18 km DDF's.

To verify this hypothesis, the fibre length was shortened to 18 km (≈ 2 soliton periods) using the second half of the DDF, reducing the mean dispersion from 2.4 to 1.1

ps/nm/km³³⁴, and the pulse width increased to 11ps. In this case, the spectrum remained stable for transmission distances in excess of 8,000 km, as shown in Figure 5-28, albeit with a slight undulation in the spectral amplitude with a period of ≈ 300 km. No evidence of side band generation, or energy shedding to the continuum is observed, in contrast to the expected performance of an equivalent uniform dispersion system with the same ratio of amplifier spacing to soliton period.

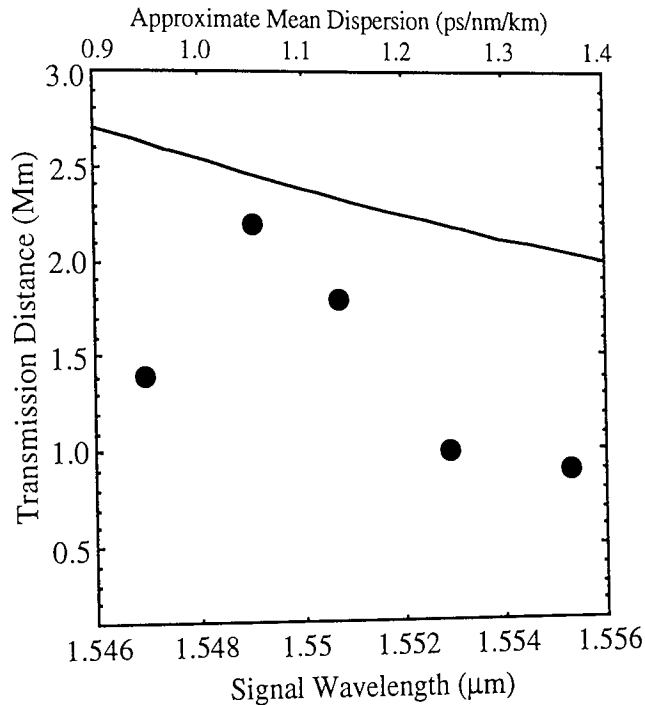


Figure 5-29 Theoretical and experimental performance of 18 km DDF system for 11 ps pulses.
Theoretical performance calculated jitter from appropriate mean dispersion values

In terms of error ratio performance (Figure 5-29), the optimum transmission distance of 2,200 km occurred at a wavelength of 1549 nm. This result is in good agreement with both the design wavelength for loss compensation (1550 nm) and theoretical maximum transmission distance for the acousto-optic effect ($\approx 2,500$ km). However, away from the optimum dispersion, the error free distance is rapidly degraded as the system transfers from a continuously balanced system to a path averaged balance (average soliton model). This is verified in Figure 5-30, where the undulations are becoming more exaggerated, to a level comparable to those observed for a uniform dispersion system close to the limit of average soliton dynamics (Figure 5-8).

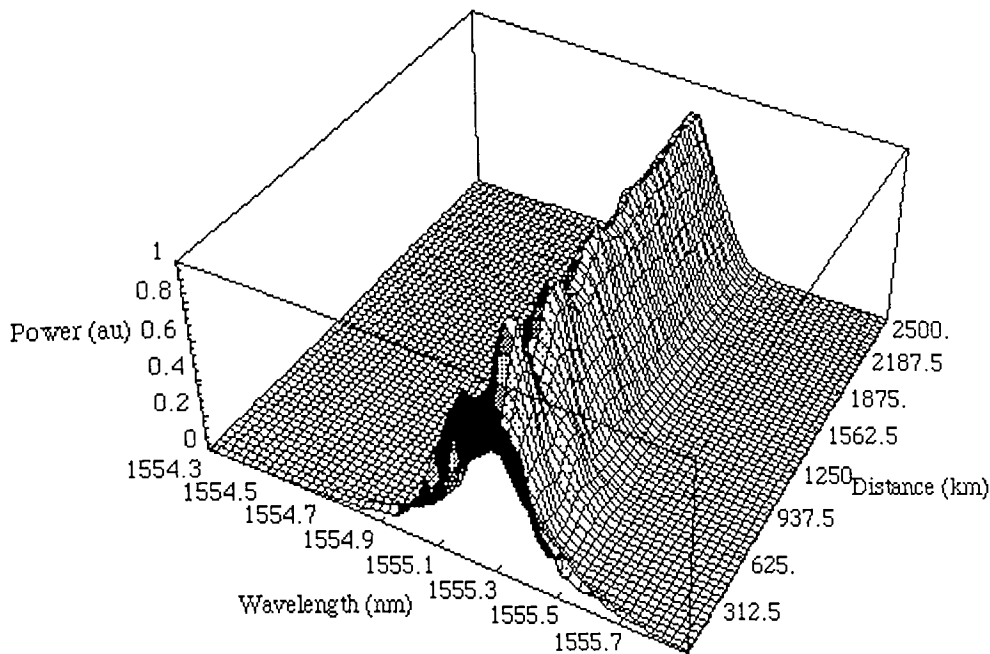


Figure 5-30 Spectral evolution of pulses along a transmission line comprising concatenated 18 km DDF's for a signal injected ≈ 5 nm above the design wavelength.

In order to further increase the transmission distance a third fibre (configuration 3) was fabricated from a dispersion shifted preform with a mean dispersion almost an order of magnitude lower (0.17 ps/nm/km). With this fibre however, manufacturing tolerances of $\approx \pm 0.1$ ps/nm/km resulted in a significant deviation from the ideal dispersion profile. The same errors in the dispersion zero wavelength were observed in the higher dispersion fibres, however, the impact was reduced in proportion with the mean dispersion. This fibre was again tested using the recirculating loop, however, in order to allow the propagation of short optical pulses over long distances, the filter bandwidth was increased to 5 nm with a flat topped profile. The soliton period was held constant in this reduced dispersion fibre by decreasing the pulse width to ≈ 4.7 ps.

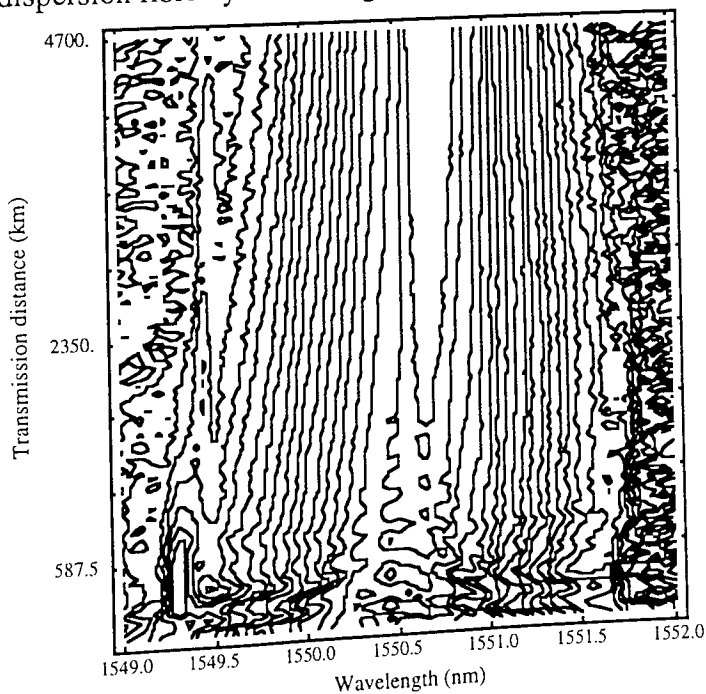


Figure 5-31 Spectral evolution of 4.7 ps pulses through a 20 km DDF (1.5 dB / contour).

Again, excellent spectral stability is achieved over the full propagation distance, with a change in the spectral bandwidth of less than 5 % and no evidence of sideband or continuum generation. However, we do observe a drift in the central wavelength of the pulse of around 5 MHz/km, partly due to the soliton self frequency shift. For a uniform fibre with the same mean dispersion, we theoretically predict^{335,28} a frequency shift of ≈ 1 MHz/km, whilst for a uniform fibre of the input dispersion, we predict a shift of 1.3 MHz/km. This is clearly illustrated in Figure 5-31, where we also observe that the pulses initially adjust themselves to suit the transmission line over the first 1,000 km, accompanied by the generation of a small side band around 1549.3 nm the position of which is in quantitative agreement with theoretical predictions⁵⁴. Similarly, the induced frequency shift appears constrained on the long wavelength side (by the edge of the 5.1 nm filter), resulting in the slight spectral narrowing (5%). That the observed rate of spectral shift is slightly greater than anticipated could be explained by the proximity of the system to the dispersion zero, allowing the effects of higher order dispersive terms^{336,337,332}, which tend to repel the soliton away from the dispersion zero, or a slight tilt on the filter profile.

In terms of error ratio performance, at the optimum launched signal wavelength of 1549.3 nm, an error free transmission distance in excess of 4,000 km was achieved, confirming the benefits of reducing the mean system dispersion. However, as the wavelength was detuned from the optimum by ± 1 nm, the error free distance rapidly degraded. On the short wavelength side the system was limited by signal to noise ratio, due to the reduced soliton power, whilst for longer wavelengths, deviations from ideal loss compensation degrade the transmission characteristics.

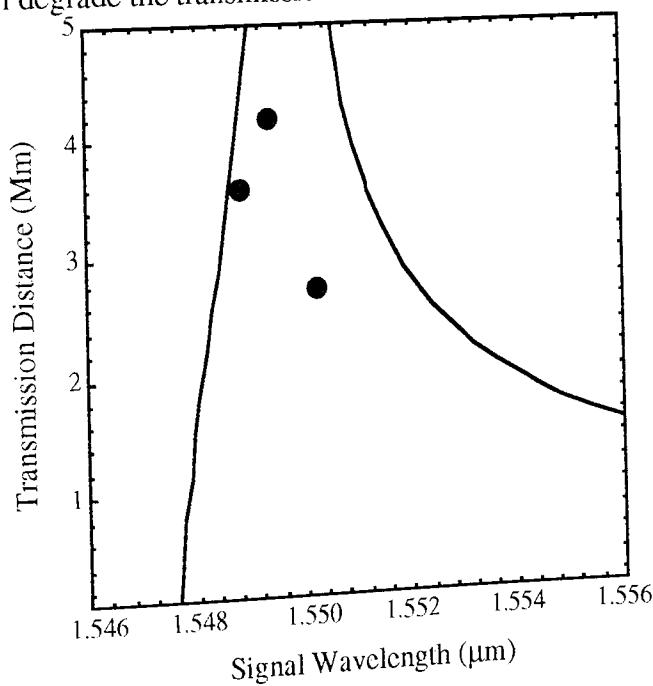


Figure 5-32 Theoretical and experimental error ratio performance of 20 km low dispersion DDF using 4.7 ps pulses.

These results serve to illustrate the powerful advantages of loss compensating dispersion decreasing fibres for operation of high speed soliton systems without the restrictions of the average soliton model. It is confirmed that the system performance is

limited by the high average dispersion of the fibres, and that for 4.7 ps pulses, current manufacturing tolerances are sufficient to give noise limited transmission distances. It is interesting to note that the total number of soliton periods traversed using low dispersion DDF's (86) far exceeds those achieved using conventional soliton systems in the absence of strong soliton control (≈ 40 soliton periods), and is comparable to strongly controlled systems^{338,279}. The excellent stability of the transmitted solitons makes this transmission medium particularly suitable for high speed soliton control techniques, for example by using a high dispersion DDF to allow the transmission of high power solitons with large repeater spacing coupled with soliton shepherding to eliminate jitter and interactions. The jitter may also be controlled through the use of phase conjugation^{339, 340}, or through the use of an appropriate dispersion map³⁰⁵ (recalling that pulse compression may also be achieved using the DDF). Note also that these results were obtained using a single amplifier recirculating loop, and that improvements in signal to noise ratio may be anticipated for a real system (or a multi-amplifier loop).

5.3 All Optical Regeneration

As we have seen above, whilst showing remarkable enhancements to system performance, optically amplified transmission systems are restricted by their essentially analogue nature and the consequent accumulation of transmission impairments. This can be overcome by the employment of digital technologies, such as active soliton control. To date, all such systems have employed electronic clock recovery with consequent uncertainties over upgradability and system reliability. Whilst the existence of RF components suitable for clock recovery at bit rates in the region of 100 Gbit/s is well known, it has long been envisioned that all optical regenerators will provide greater flexibility and higher capacities than partial or fully electronic regenerators.

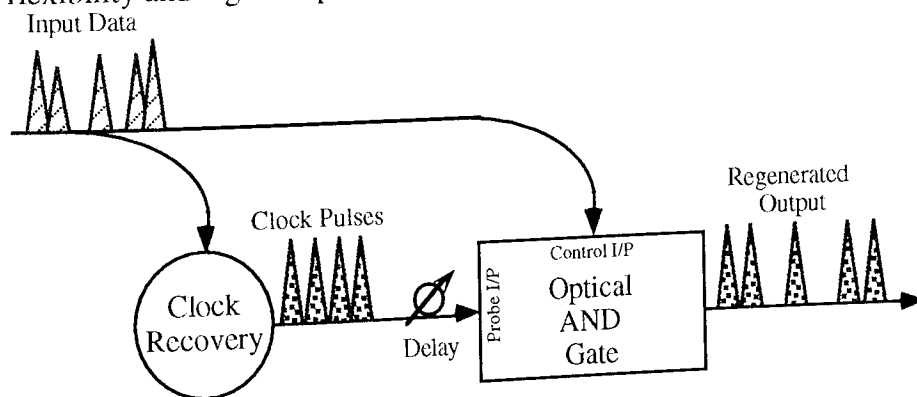


Figure 5-33 Schematic diagram of all optical regenerator

Optical regenerators generally comprise two distinct stages, a clock recovery stage, where a low jitter stream of pulses at a single wavelength is derived from the incoming data, and a decision gate stage, where these clean pulses are encoded with the appropriate information from the incoming data (Figure 5-33). Whilst progress on optical clock recovery is summarised in Table 9 above, the relatively slow progress on full optical regeneration and suitable optical gates is illustrated in Table 15.

Year	Clock Recovery	Decision Gate	Bit Rate	Ref
88	Self Electro-Optic Effect	Self Electro-Optic Effect	5 kbit/s	³⁴¹
92	Not implemented	NALM	10 Gbit/s	³⁴²
92	Not implemented	NOLM	5 Gbit/s	³⁴³
93	Not implemented	SLALOM	1 Gbit/s	³⁴⁴
93	FM Ring Laser	NOLM	1 Gbit/s	³⁴⁵
94	Not implemented	Bistable Fabry Perot	10 Gbit/s	³⁴⁶
95	Not implemented	SLA-NOLM	20 Gbit/s	³⁴⁷
95	Electronic + Pulse Source	NOLM	10 Gbit/s	³⁴⁸
95	Not implemented	Kerr gate	40 Gbit/s	³⁴⁹
95	FM/AM Ring Laser	Kerr gate	10 Gbit/s	³⁵⁰
96	Injection locked EC-MLL	Fabry Perot	5 Gbit/s	³⁵¹
96	FM/AM Ring Laser	Kerr gate	40 Gbit/s	²¹⁰
97	Optical PLL	SLA-NOLM	2.5 Gbit/s	³⁵²

Table 15 Summary of optical regeneration experiments

As can be seen, following initial research into optical regeneration based on electro-optic devices (SEEDS, or Self Electro optic Effect DeviceS), few distinct experiments have been reported on full optical regeneration, the majority of interest being devoted to the development of suitable data driven optical gates. This is not unreasonable, since the major benefits of all-optical regeneration are obtained from the transfer function of the optical gate. The particularly important features are temporally square switching windows for jitter tolerance and sinusoidal intensity responses for noise suppression^{343,345}. These features are illustrated by the theoretical switching windows illustrated in Figure 5-35. These features are easily obtained using cross phase modulation in optical fibres with walk-off (section 2.1.2) and travelling wave semiconductor laser amplifier non-linear optical loop mirrors³⁴⁷. A hybrid electronic/"all-optical" regenerator has recently been reported, where clock recovery was performed electronically and remodulation all-optically at 10Gbit/s³⁴⁸. In this paper it was also demonstrated that a degree of pulse distortion due to dispersion or non-linearity may be eliminated by the optical regenerator. The hybrid approach described may easily be extended to high speed OTDM systems using electronic clock recovery circuits to extract a base rate electrical clock signal, and a passive interleaver to multiply the optical clock frequency back up to the line rate. The usual difficulties associated with low duty cycle pulse generation and interleaving are of course avoided for all optical regenerators employing full line rate clock recovery.

5.3.1 Two stage all-optical regenerator

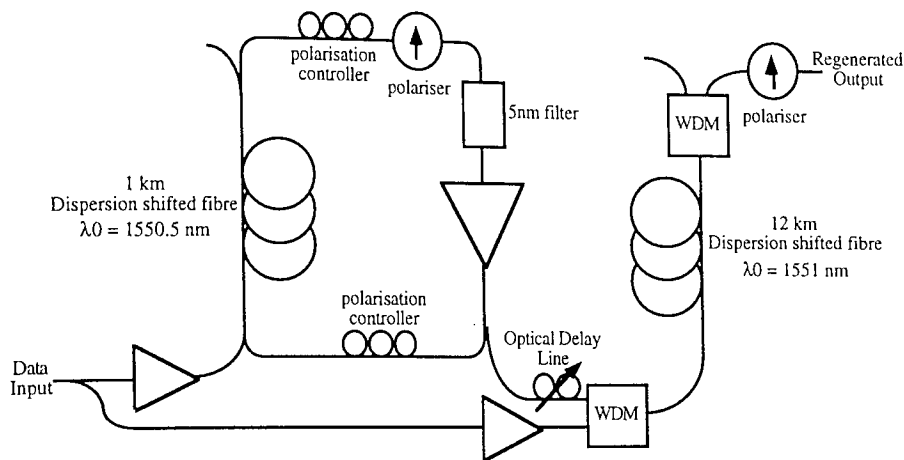


Figure 5-34 Schematic diagram of NPR based all optical regenerator.

In this thesis we describe the first error ratio characterisation of a fully all-optical regenerator. The regenerator, based on non-linear polarisation rotation is operated at 10 and 40 Gbit/s simply by varying the amplifier pump powers in accordance with the incoming optical signal. A schematic diagram of the regenerator is shown in Figure 5-34. A full line rate clock is recovered from the incoming data stream with a fibre ring laser actively mode-locked by a combination of cross-phase modulation and non-linear polarisation rotation (Section 4.1.2); this clock is modulated with the incoming data stream in a Kerr rotation gate (Section 3.4.2.2). Both of these components are fully described above, and we note that although the configuration is polarisation sensitive, commercially available automatic polarisation controllers may be included at the regenerator input to compensate for long term drifts.

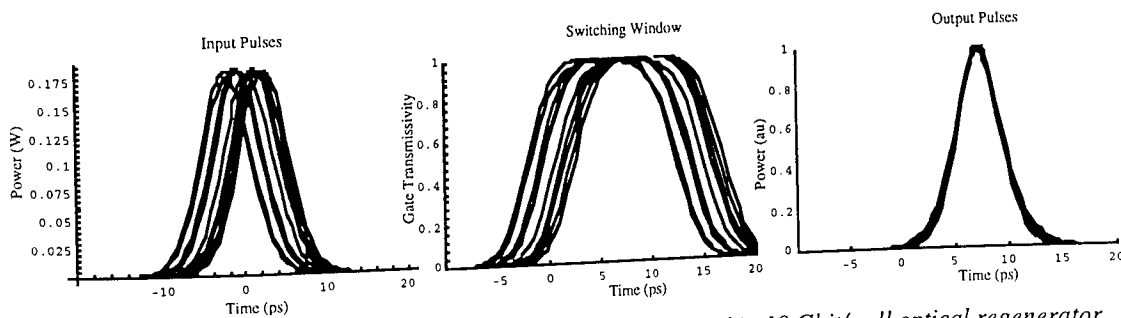


Figure 5-35 Theoretical switching performance of Kerr gate used in 10 Gbit/s all optical regenerator with input signal having 5% amplitude noise and 5 ps peak to peak timing jitter. Showing the input signal with noise and jitter (left), the resultant switching window (centre) and anticipated output pulse train following modulation of an ideal clock (right). Other parameters detailed in column 1 of Table 16.

The experimental details are summarised in Table 16. In the case of 10 Gbit/s all optical regeneration, the data stream bit period was matched to a subharmonic of the $1.553\mu\text{m}$ ring laser cavity round trip time for stable mode locking by manually fine tuning the source frequency synthesiser. Twenty percent of the cavity light was coupled out to form the recovered clock pulse stream which was remodulated in the Kerr gate with a switching window of ≈ 19 ps (neglecting effects of fibre loss and dispersive pulse broadening). The gate was polarisation biased to maximally (30 dB) attenuate the

recovered clock pulse in the absence of a data pulse. With the optical delay line adjusted to place the clock pulses in the centre of the switching window opened by the data pulses, the clock pulses are coded with the data from the incoming signal (non inverting configuration).

Bit Rate (Gbit/s)	10	40	40 SS
Pattern Length	2^7-1	2^7-1	2^7-1
Input Pulse Width (ps)	7.4	7	8.4
Input Wavelength (nm)	1545	1544	1545
Mean Drive Power for Ring Laser (dBm)	-0.7	+6.6	+7.7
Mean Drive Power for Kerr Gate (dBm)	+8	+16.8	+17.2
Clock Wavelength (nm)	1553	1553	1556
Walk Off Rate in Ring Laser (ps/km)	0.9	0.7	0.0
Pulse Width of Recovered Clock (ps)	5.5	3.8	4.8
Walk Off Rate in Kerr Gate (ps/km)	1.2	1	0.7
Estimated Switching Window (ps)	19	14	11.5
Output Pulse Width (ps)		3.3	3.4

Table 16 Operating conditions for experimental demonstrations of 10 and 40 Gbit/s all optical regeneration. First two columns represent traditional regenerator configurations, whilst the final column represents a novel self synchronising configuration (section 5.3.2).

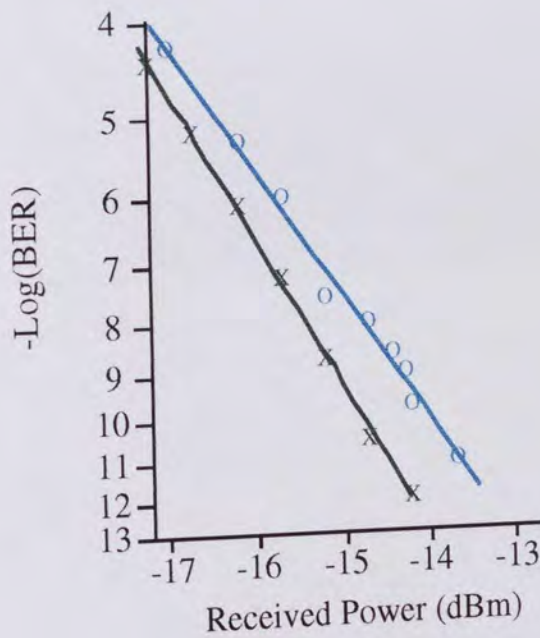


Figure 5-36 Error rate performance following 10 Gbit/s all optical regeneration (circles) and back to back (crosses).

The error ratio measured for back-to-back and for regenerated data is shown in Figure 5-36. A negligible 1dB penalty from the regenerator is observed, along with a slight change in slope. This small penalty is attributed solely to the thermal stability of the ring laser cavity, requiring manual fine tuning of the source frequency for stable operation. These results represented the worlds first error rate measurements of an *all-optical* regenerator, and confirmed the excellent potential of the technique.

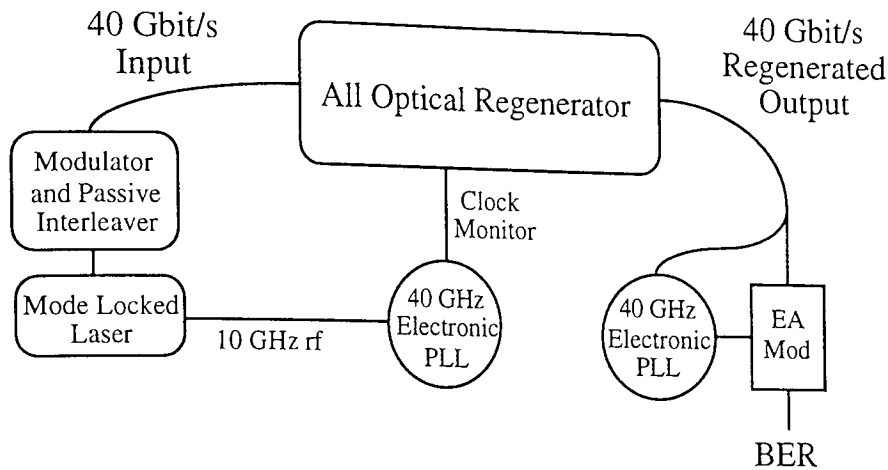


Figure 5-37 Schematic diagram of the experimental demonstration of 40 Gbit/s all optical regeneration.

In the case of 40 Gbit/s all optical regeneration, the same 10 Gbit/s data was passively multiplexed to 40 Gbit/s and minor modifications were made to the regenerator configuration. As with all fibre ring lasers, it is important to match the drive frequency of the incoming signal with the cavity length. Ideally this would be carried out using active cavity length control based on relaxation oscillations¹⁰⁴, supermode strength¹⁰⁶ or spectral shifts³⁵³. For experimental convenience however, the transmitter drive frequency was varied to match the cavity length using a 40 GHz phase locked loop connected to the ring laser output (giving performance similar to a phase locked ring laser). Following non-inverting regeneration, as described above, a 10 GHz clock was recovered from the regenerated data using a second 40 GHz phase locked loop, and used to drive an electro absorption modulator to demultiplex the data back down to 10 Gbit/s for error ratio measurements. This overall configuration is shown in Figure 5-37.

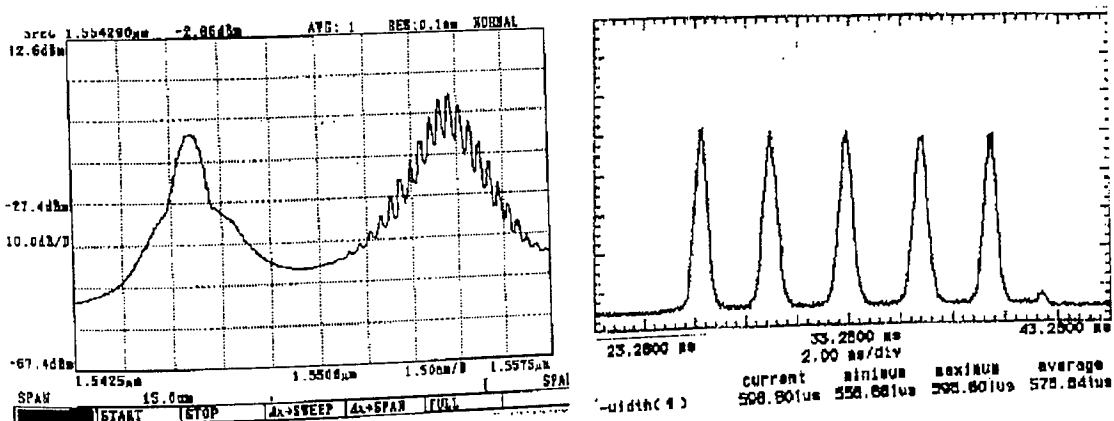


Figure 5-38 Output of the clock recovery section of a 40 Gbit/s all optical regenerator.

In this case, it was observed that it was critically important to ensure that the ring laser was mode locked to an odd numbered harmonic of the fundamental cavity mode of 188 kHz (1.064 km). This ensured that each supermode was modulated from data from all four OTDM channels. If the laser was modelocked to an even harmonic small differences in the individual OTDM channels resulted in strong amplitude modulation of the recovered clock at either 10 or 20 GHz. The output of the clock recovery section is shown in Figure 5-38 illustrating the spectral and temporal uniformity of the recovered

pulse train. Within the decision gate, in the absence of a data pulse, the output polariser was aligned to attenuate the recovered clock signal, consequently, the action of the data pulses was to switch the pulses ON, producing a non inverting modulator and giving rise to some degree of pulse shaping. Figure 5-39 shows an autocorrelation and eye diagram for the regenerated data, showing a modulated pulse width of 3.3 ps, whilst the excellent error ratio performance is illustrated in Figure 5-40. A receiver sensitivity of -15.5 dBm for the regenerated and demultiplexed signal was observed with no evidence of error floor down to error ratio's of 10^{-12} comparing favourably with previous back to back measurements (eg Figure 5-36).

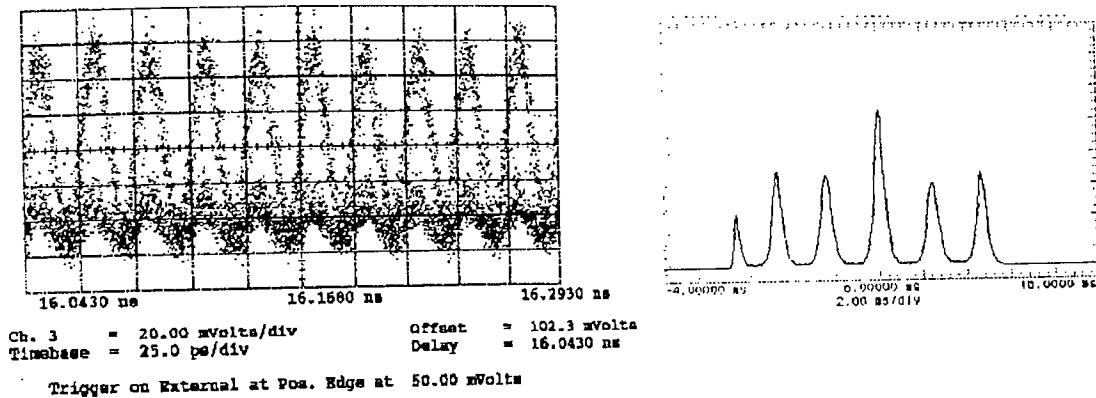


Figure 5-39 Eye diagram and autocorrelation of 40 Gbit/s signal following all-optical regeneration.

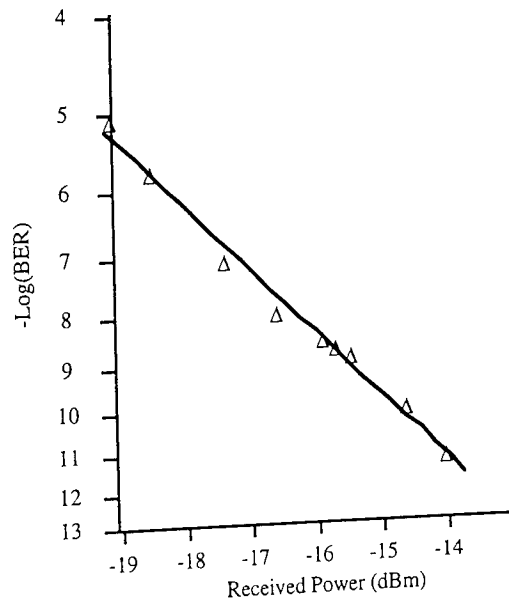


Figure 5-40 Error rate performance of a demultiplexed 10 Gbit/s channel following 40 Gbit/s all optical regeneration.

This experiment represents the highest reported repetition rate for a regenerator using any technology reported to date, and offers the significant advantage of simple bit rate flexibility through variations in the mean power levels to maintain the appropriate peak phase shifts. This indicates convincingly that this technology may be easily upgraded without expensive additional capital investment. Indeed the components employed in this demonstration are known to be capable of operation of even higher bit rates since the only known limiting features are the speed of response of the non-linearity,

dispersive effects within the modulator fibres, and the bandpass filter within the loop. Thus whilst many of the required research components now exist for the construction of opto-electronic regenerators at 40 Gbit/s^{354,194,355,356}, we may look forward with confidence to the demonstration of all optical regenerators beyond even the capabilities of current state of the art electronics. Clearly commercial deployment of 10 Gbit/s all-optical regenerators is unlikely given the maturity of opto-electronic technologies at these capacities, however, given a jitter tolerance equivalent to a typical demultiplexer switching window (around 10 ps) the eventual deployment of 40 Gbit/s all optical regenerators, spaced by up to $\approx 1,000$ km in soliton or dispersion managed transmission lines is not an unreasonable proposition.

5.3.2 Self Synchronising All Optical Regeneration

The previous section highlighted the remarkable potential of all optical regeneration for application to all-optical networks. In the regenerator described (and indeed in all reported optical regenerators to date), the incoming data signal propagates along two distinct optical paths to drive the clock recovery and decision gate circuitry respectively, with the recovered clock generally requiring a third path. This necessitates the use of optical delay lines to synchronise the recovered clock to the data signal. In the case of the regenerators described within this thesis however, it is known that the clock and data pulses are automatically temporally aligned within the modulation section of the ring laser cavity. Thus, for a correctly designed system, discrete optical synchronisation of data and recovered clock streams should not be necessary. Consider for example the circuit shown in Figure 5-41, the incoming data signal is divided by an asymmetric power splitter into the two lengths of dispersion shifted fibre, with the peak power in each fibre independently adjusted through a combination of the total input power and the coupler ratio. A 40 GHz clock is recovered from the incoming data signal in the usual way, however, the clock output is taken *from the same coupler* and so enters the modulation fibre along the same path as the second data signal. In the absence of walkoff in the ring laser, and chromatic dispersion in the asymmetric coupler, the two signals overlap exactly at the input to the modulator fibre *a-priorii*.

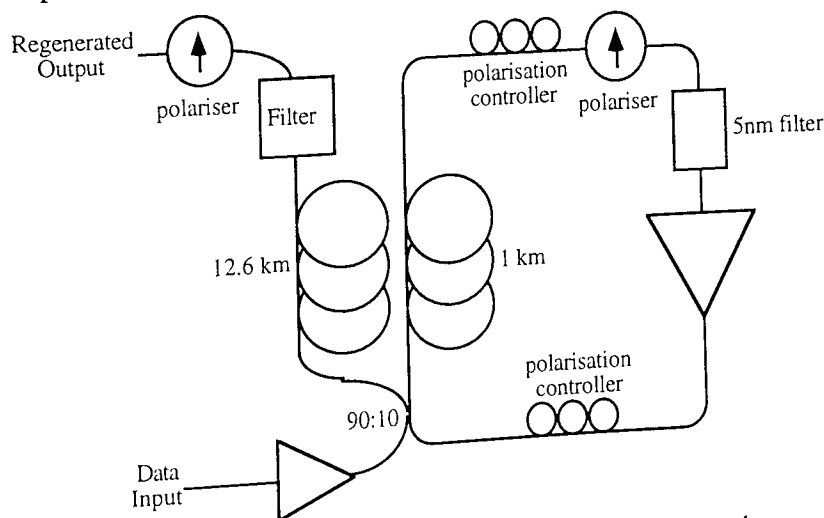


Figure 5-41 Schematic diagram of 40 Gbit/s self synchronising all optical regenerator.

An experimental demonstration of this concept was carried out using parameters listed in Table 16. As would be anticipated, there is no degradation in the recovered clock, an autocorrelation of which (Figure 5-33) illustrates a pulse width of ≈ 4.8 ps at 1556 nm. Whilst at first sight, the regenerated eye diagram appears satisfactory, following demultiplexing, amplitude noise on the data ones of the regenerated data results in error rate floors between 10^{-4} and 10^{-8} depending upon precise experimental configurations. The regenerated autocorrelation also shows some evidence of jitter between adjacent pulses in the resultant 3.4 ps data pulse train which was absent in the recovered clock. The origin of these degradations may of course be understood from the modulator switching window, as shown in Figure 5-43.

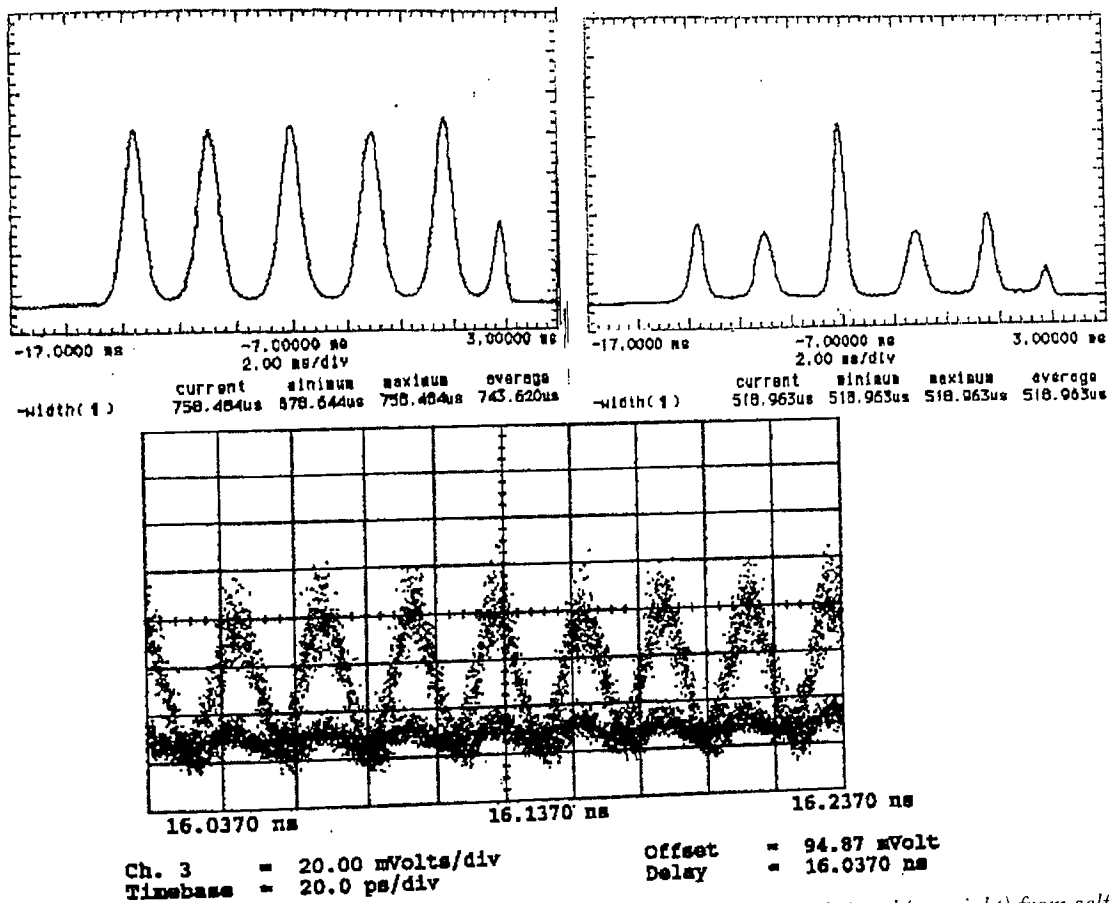


Figure 5-42 Autocorrelations of recovered clock (top left) and regenerated signal (top right) from self synchronising 40 Gbit/s all optical regenerator, along with eye diagram of regenerated data (bottom).

Now although the two pulse trains are initially temporally overlapped, the effect of walk-off in the modulator fibre is to move the switching pulse away from the data pulse. Consequently, the clock pulses are switched by the edge of the resultant switching window, and any small relative jitter is transferred to severe amplitude noise on the recovered pulse train. This problem should be readily overcome by the insertion of a short length of standard fibre at the input to the modulator fibre to induce the appropriate relative delay to ensure that the clock pulse is switched at the centre of the resultant switching window. In this case, a length of some 26 metres of standard fibre would be required to place the recovered clock pulses in the centre of the 11.5 ps switching window. Unfortunately time constraints prevented the experimental

verification of this simple modification. This section does however, indicate means in which traditional multi-path all optical regenerators may be simplified into a self synchronised architecture, offering enhanced reliability and simpler construction.

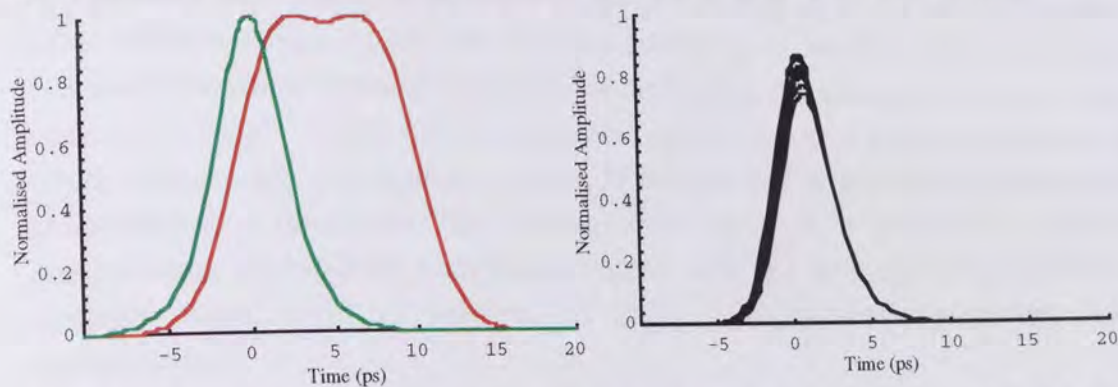


Figure 5-43 Illustration of the anticipated modulator switching window (red) and recovered clock pulse (green) along with resultant theoretical output pulse train for 1 ps peak to peak jitter (right) in a 40 Gbit/s self synchronising all optical regenerator.

5.4 Chapter Summary

In this chapter, the transmission properties of high speed OTDM signals have been investigated. The potential use of standard embedded fibre has been illustrated through the use of mid span spectral inversion. Whilst theoretical studies have indicated that the technique can easily be extended in transmission distance, it is apparent that increases in attainable conversion efficiencies are required in order to allow for increases in the transmission capacity. In comparison with passive dispersion compensation techniques, MSSI offers the significant advantage of relative simplicity and low component count for long haul point to point systems. However, in a more diverse network scenario, the complexities involved in identifying the mid point of all possible transmission systems tend to favour solutions based on a span by span dispersion compensation strategy. In the following section, soliton propagation of an OTDM data signal was investigated. Initial investigations focused on a dispersion shifted fibre link, with an almost uniform dispersion map and fixed frequency guiding filters (with excess gains between 0.02 and 0.13). In the absence of soliton control, transmission of a 40 Gbit/s data signal over 2,200 km was demonstrated, extending the maximum bit rate distance product of soliton systems from ≈ 40 Tbit/s.km to 88 Tbit/s.km. Using exactly the same transmission system, two forms of soliton control were demonstrated, based on electro-optic amplitude and all-optical phase modulation. In the case of amplitude modulation, the worlds first demonstration of retiming of an OTDM data sequence was performed, resulting in a transmission distance in excess of 125,000km, which remains the longest reported transmission distance at 20 Gbit/s. Furthermore, in a worlds first demonstration of 40 Gbit/s transmission control, we have demonstrated that soliton control of an OTDM is possible using electro-optic frequency doubling. However, residual chirp in the retiming modulator severely degrades the performance, and in implementation steps must be taken to ensure that retiming modulators are deployed either as matched pairs to cancel this chirp, or completely chirp free. For a 40 Gbit/s

system, comprising 6 ps pulses, the trade off between dispersive wave radiation (with narrow filters) and amplitude instability (broad filters) prohibits error free operation over transoceanic distances. The results suggest that shorter launched optical pulses (≈ 4 ps) should allow stable transmission without the generation of excessive dispersive wave radiation using a 2.1 nm filter. It is also interesting to note that whilst the current demonstration would normally be considered inadequate, the addition of forward error correction coding³⁵⁷ would result in acceptable performance of a single wavelength 40 Gbit/s transoceanic transmission system. Note also that a polarisation insensitive electroabsorption modulator has recently been used in a proof of principle demonstration of 40 Gbit/s transmission control, with the error floor at 10,000 km improved from $\approx 10^{-6}$ to between 10^{-9} and 10^{-8} depending upon the exact configuration³⁵⁸

In both this system, and soliton shepherding systems, it was concluded that modifications of the transmission line would be beneficial to both enhance the intrinsic signal to noise ratio and to avoid violations of the average soliton model. Preliminary work on novel fibre types has been presented, indicating that both distributed amplification and dispersion decreasing fibres can effectively eliminate violations of the average soliton model. Unfortunately, the large levels of timing jitter characteristic of DDF systems limits the transmission distance in the absence of active soliton control. It is interesting to note that several of the requisite techniques have also been demonstrated recently for soliton control systems at 20 Gbit/s³⁵⁹, and for the extension of the transmission distance at 40 Gbit/s^{280,360}. Together with the earlier results of this thesis, these results show great promise for ultra high capacity global scale soliton systems, however, it is apparent that carefully crafted transmission lines are required to meet this goal.

Finally, worlds first demonstrations of high capacity all optical regeneration have been described utilising non-linear polarisation rotation in a dispersion shifted fibre, including worlds first error ratio measurements of optical regeneration, and the highest reported bit rate for a regenerator employing any technology. Coupled with soliton or dispersion compensated transmission lines this technology may well provide a particularly simple route to high capacity global all-optical networks. An alternative vision would acknowledge the fact that all optical regenerators are constructed from the same components that would be used for an optical amplifier in a guiding filter based soliton system. This being so, there would be no reason why ALL of the optical amplifiers along a transmission line should not be replaced by all optical regenerators. When interconnected by long loss compensating dispersion decreasing fibres for ultra high capacity operation, the resultant system would represent a truly digital optical transmission system.

6. OTDM Networks

6.1 Network Concepts

Optically multiplexed systems currently offer access to aggregate capacities beyond the reach of commercial broadband electronics. However, in addition to providing very high capacity point to point optical pipes between any two given nodes, a particularly important functionality of an optical network is a “drop and insert” (D&I) capability^{361,11}, without recourse to complex and restrictive electronics. The addition of such optical networking functions makes the implementation of optical networks cost effective even in the absence of acute fibre shortages³. A particularly simple WDM bus network is shown in Figure 1-2, where local traffic for intermediate node is dropped from the main path between two major nodes. An OTDM implementation of this simple network is illustrated in Figure 6-1, where a 5 channel OTDM system provides 3 channels between the major switching centres and two channels between the main nodes and the intermediate stations. With the majority of the traffic bypassing the intermediate nodes, a considerable cost saving in terms of reduced line terminating equipment and electronic switching is ensured.

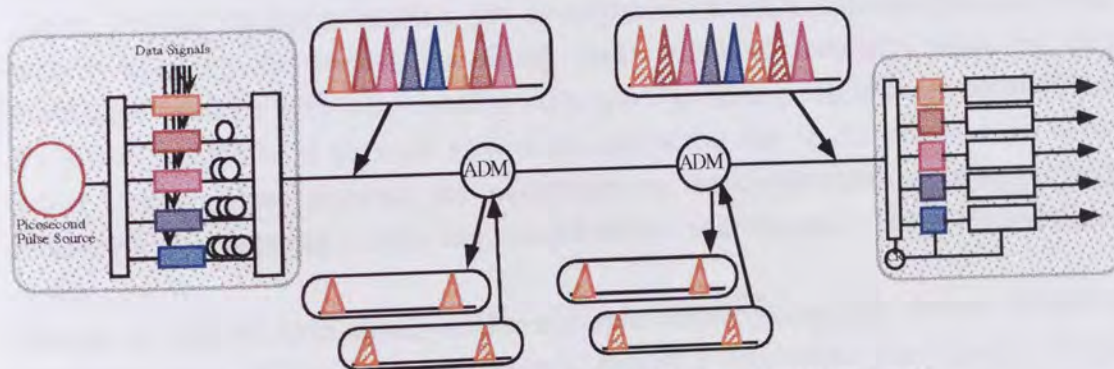


Figure 6-1 Illustration of a simple OTDM drop and insert network.

Many other network architectures exist, including rings, and mesh networks, where additional functionality is added to the network. For example, an optical ring provides protection for the entire aggregate capacity of the system in the event of a fibre outage. In all cases, the ability to remove and re-insert data within optical channels is critical in maintaining a high network utilisation. For example, in the network of Figure 6-1, without the option to re-insert local traffic into the vacant time slot, each intermediate station would require 2 time slots, reducing the available capacity between major nodes to a single time slot. Further enhancements in network utilisation occur with the introduction of time slot interchange (analogous to wavelength conversion in WDM networks), particularly for mesh networks, allowing greater flexibility in network planning and dynamic routing of signals. An OTDM time slot interchange is constructed simply from a pair of D&I nodes, with their drop ports cross connected to the insert ports via appropriate delays (Figure 6-2).

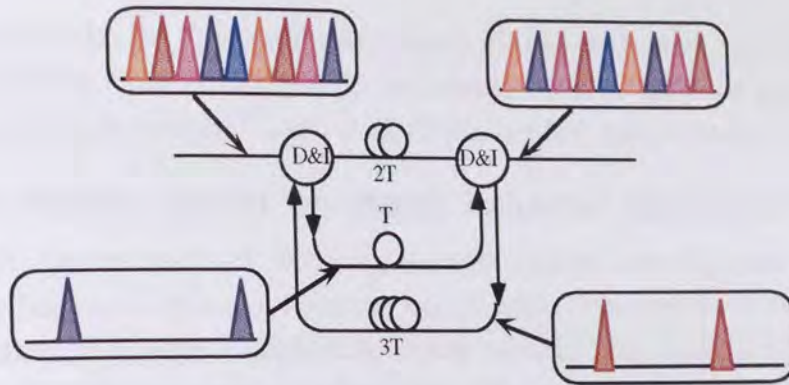


Figure 6-2 Schematic diagram of an OTDM time slot interchange constructed from a pair of add drop multiplexers

Having developed active demultiplexers for use in point to point systems, these components may be modified in similar ways to provide a multitude of advanced functional elements. With the ability to separate out any optical channel (or set of channels) the majority of required network functions may be provided using these simple components, full tunability being provided by readily available electrical (and perhaps optical) delay lines. These functions include drop and insert, time slot interchange and optical cross connects. This is in stark contrast to WDM networks; a fully flexible drop and insert requires either extensive space switching or tuneable filters; channel exchange requires the development of active wavelength converters, with a tendency to degrade the signal; cross connects generally being complex multistage designs with full demultiplexing, space switching and channel equalisation. So although OTDM is perhaps viewed as unattractive due to the requirement of an active demultiplexer element, the advantages in the construction of simple, fully reconfigurable network nodes are considerable, and require negligible additional development.

Within an OTDM D&I node, unlike a simple demultiplexer, the optical switch is configured in such a way as to *completely* remove a data stream (the “drop”), whilst leaving the remaining channels undisturbed. It is then a simple matter to insert a data stream generated locally at the node (or at some remote point) into the empty time slot (the “insert”). Both of these features are critical factors determining system performance. If the dropped channel is not completely removed, crosstalk between the local inserted signals and the remaining signals degrade the inserted channel performance, whilst pulse shaping and chirp may detrimentally affect the transmission properties of the through traffic. Currently, D&I functionality has been the almost¹¹ exclusive province of all optical techniques, with complete “drop” demonstrated in both fibre based devices^{362,363,182,364,189} semiconductor amplifier based interferometers^{365,146,366,367}, and a full D&I demonstration using a fibre loop mirror³⁶⁸. An alternative approach, recently demonstrated at 100 Gbit/s, demultiplexes each outgoing channel, using in this example four wave mixing, the wavelength translation avoiding crosstalk with residual light³⁶⁹. This technique is clearly applicable to any data driven optical switch where the output extinction ratio is determined by the probe signal⁸¹. However, with the exception of results presented in this thesis, error free operation of a full drop and insert node (measured after the insert) has only once been reported¹¹. In this

section, we consider the theoretical performance of drop and insert nodes based upon electro-optic Mach Zehnder modulators, and experimentally verify the performance at 40 Gbit/s in a 3 node network¹¹⁸, and at 20 Gbit/s in a 690 node network²⁰.

6.2 D&I Nodes based on Mach Zehnder Modulators

Two distinct options exist for providing a single channel demultiplexer using Mach Zehnder modulators. Figure 6-3 illustrates one possible arrangement of modulators for providing drop and insert functionality using simple sine wave driven base rate modulators. Clearly the switching performance of the dropped channel is identical to the simple demultiplexer described above (Section 4.2.1) being of a similar two stage design. However, for the through channel, the parameters of interest are the disturbance to the wanted signals (chirp, shaping and attenuation) which will govern the performance of onwards transmission for the through channels, and the achieved signal extinction ratio in the dropped time slot which will govern the signal to noise ratio of the inserted signals.

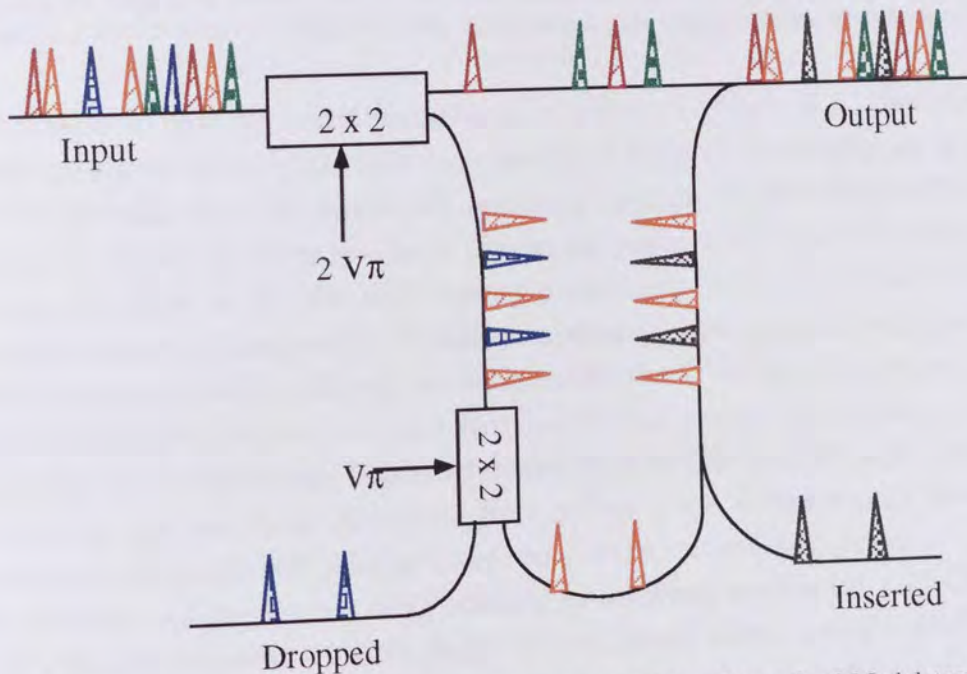


Figure 6-3: Schematic Diagram of D&I Node with Sine Wave Driven 2×2 Modulators

Transmission through a subsequent dispersive transmission line (using for example solitons) would impose severe timing problems, unless the wavelengths of the incoming and inserted signals are closely matched. In this case, the extinction ratio requirements are significantly sharpened by incoherent interference between the rejected signals and the inserted channel. The sinusoidal transfer function of the modulators may be used to calculate the node performance, considering the signal to cross talk ratio, and incoherent interference effects for the inserted channel. For completeness, the performance of the inserted signal is assessed following subsequent demultiplexing in an identical node.

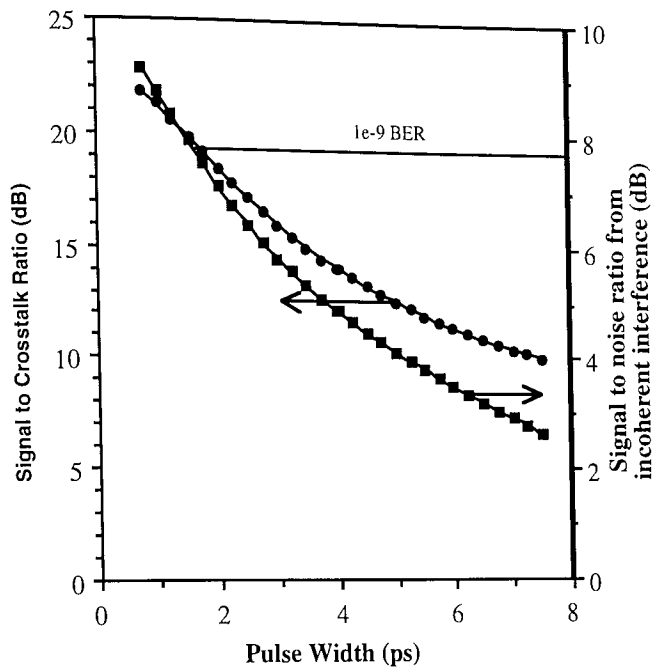


Figure 6-4 : Signal to crosstalk ratio (circles) and incoherent interference (squares) of a the inserted channel in a 4×10 Gbit/s, 2×2 Mach Zehnder switch based, D&I node, following demultiplexing in an identical node.

An example of this theoretical performance is shown in Figure 6-4. Unfortunately, whilst the signal to cross talk ratio confirms that in terms of demultiplexing alone the system operates well, the incomplete switching function of the sinusoidally driven modulators results in a large residue of unswitched power in this time slot (particularly towards the edges of the time slot), causing prohibitively severe interference with the inserted channel. Consequently, unless unreasonably short pulses (< 1.5 ps at 40 Gbit/s) are used this type of node is unsuitable for use in an OTDM network, unless signals are deliberately inserted at different wavelengths (giving rise to timing problems due to chromatic dispersion). This is of course an acceptable solution, however unless the system operates over dispersion flattened (or slope compensated) fibres, the wavelength difference will place an upper bound on the transmission distance.

Alternatively, a pulsed drive is easily obtained by amplitude modulating a 20 GHz sine wave with a synchronous 10 GHz signal. This technique allows a single modulator to be used to perform the demultiplexing function and with more complex drive signals, processing of the data stream to finer granularity is clearly possible (see Section 4.2.1). A schematic diagram of the necessary arrangement of such modulators to produce a drop and insert node is shown in Figure 6-5.

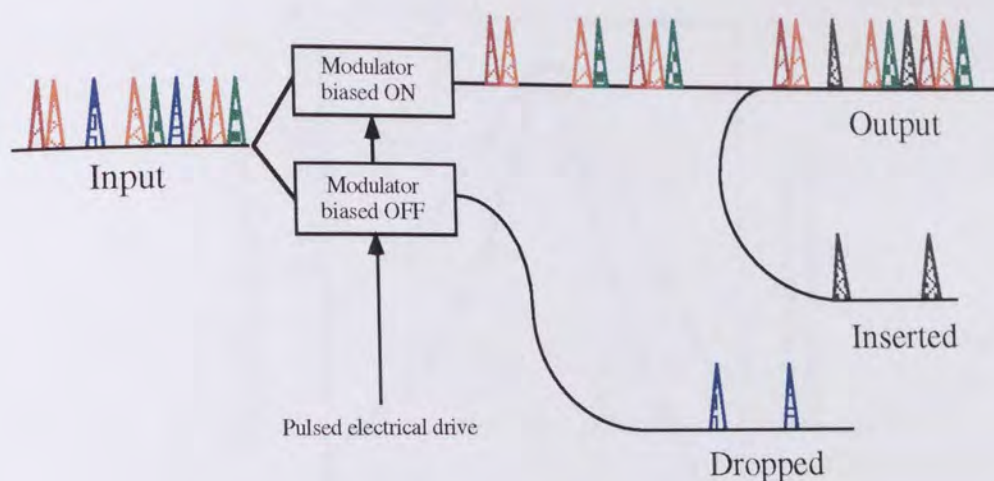


Figure 6-5 Schematic diagram of D&I node based on broadband modulators.

The demultiplexing function is carried out by a modulator normally biased OFF (maximum extinction), and ideally the modulator clearing that channel away is driven by exactly the same RF signal, but with a different d.c. bias condition. Whilst the nominal d.c. bias would be a fully transmitting state, the important criteria is that the modulator is biased for maximum extinction of the unwanted channel, giving rise to a complex optimisation of the required d.c. bias, RF drive level and signal pulse width. Consider for example, a 40 Gbit/s OTDM system, with a signal pulse width of 6 ps and a RF switching voltage with a peak to peak value of $V\pi / 2$, the conditions found to be favourable for demultiplexing. For this configuration, the performance of the inserted channel is dominated by the cross talk with the channel rejected by the "clear channel" modulator. In comparison with the two stage design discussed above, the broader switching window of this broadband system more efficiently rejects this unwanted signal reducing the worst case error floor from incoherent interference from $2 \cdot 10^{-2}$ to $3 \cdot 10^{-12}$. Further improvement may be obtained by fine tuning the system. By way of example, Figure 6-6 shows the performance of the inserted channel, as a function of the d.c. bias applied to the modulator used to clear the appropriate time slot, when the output of the D&I node is again demultiplexed by an identical node. Whilst acceptable performance is achieved for a d.c. bias of $V\pi / 2$, some degree of improvement is obtained if the modulator is tuned slightly lower. At the bias voltage of $V\pi / 2$, the modulator just extinguishes the peak of the pulse at the peak of the cycle. With the modulator slightly detuned, the sinusoidal transfer function ensures that whilst the signal extinction at the peak of the cycle is reduced, the resultant switching window is broadened somewhat, reducing the overall crosstalk by enhancing the attenuation of the wings of the rejected pulse.

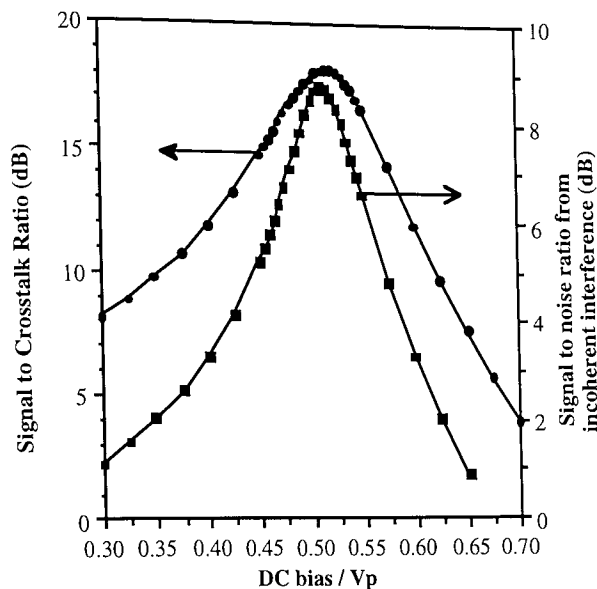


Figure 6-6 Signal to crosstalk ratio (circles) and incoherent interference (squares) of a 4 x 10 Gbit/s, Broadband Mach Zehnder switch based D&I node.

In the case of 6 ps pulses, the optimum detuning is about 2% of $V\pi$, a value which decreases rapidly as the pulse width is reduced. We find that the adjacent channels suffer a maximum of 0.3 dB excess loss due to signal shaping (over and above the insertion loss and 3 dB loss due to a d.c. bias of $V\pi/2$). Similarly the pulse spectrum of the channel adjacent to the cleared time slot suffers negligible chirp even with modulator chirp parameters $\alpha_m = \pm 1$. Consequently, the negligible degradation in the through channel pulses, low incoherent interference penalty (even for reasonable pulse widths), simplicity of implementation and adequate performance of the actively switched channels confirms this configuration as the natural choice for an OTDM network node. Furthermore by modulating the drive signal with an appropriate electrical NRZ signal using commercially available broadband mixers, finer granularity is readily available using broadband modulators. Similar performance is anticipated from pairs of electroabsorption modulators driven with base rate clock signals, one modulator biased normally transmissive, the other normally absorptive. Indeed it has been proposed that all of the required active operations may be performed with a single modulator (Section 4.2.2.3).

6.3 A 40 Gbit/s, 3 Node OTDM Network

To verify these simple D&I principles, a 3 node network is required. The first node generates a 40 Gbit/s test pattern, the second node performs a full D&I function, whilst the final node demultiplexes the four channels in order to assess the system performance. Without the third node, it is particularly difficult to assess the completeness of the channel rejection with an adequate dynamic range. A schematic diagram of the worlds first demonstration of high speed OTDM networking is shown in Figure 6-7. 8 ps pulses at 1554nm were derived from a 10 GHz harmonically mode locked external cavity laser and modulated to 40 Gbit/s with an array of four lithium niobate modulators (MUX-1). Following transmission over 20 km of dispersion shifted fibre (zero dispersion 1552 nm), the pulses were amplified and passed to two parallel

20 GHz lithium niobate modulators via a 3 dB coupler, and a 40 GHz electrical clock recovery circuit. The derived 10 GHz clock signal had an rms timing jitter of less than 0.1 ps (as assessed from the microwave spectrum).

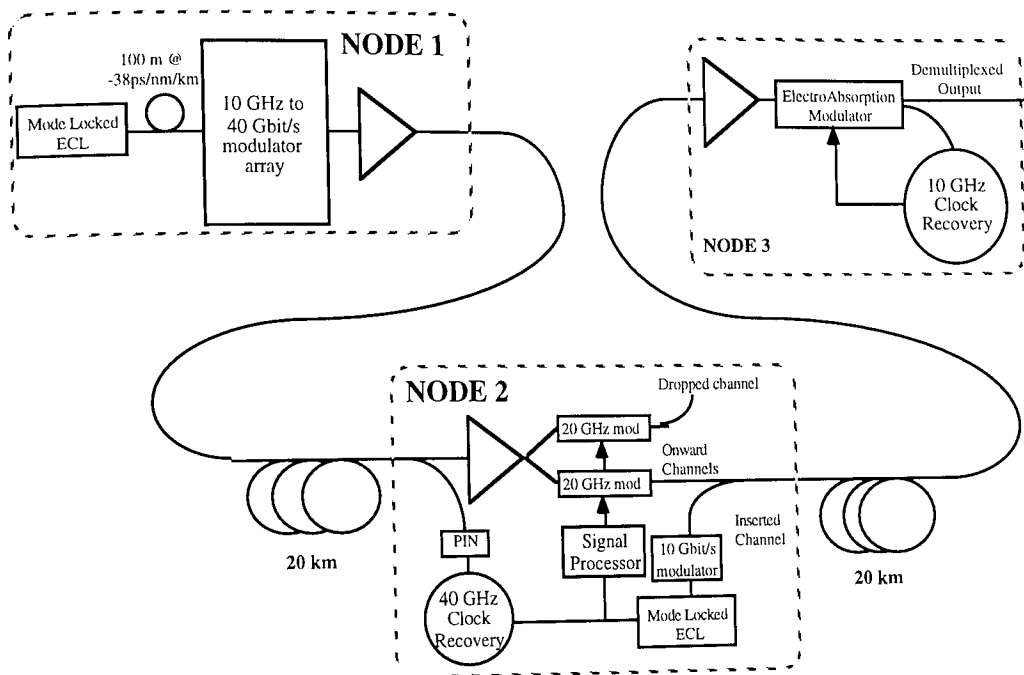


Figure 6-7 Experimental demonstration of 40 Gbit/s optical drop and insert using electro-optic modulators.

The two 20 GHz bandwidth modulators were driven with 10GHz, 23 ps electrical pulses derived by mixing 10 and 20 GHz clock signals from the clock recovery circuit, as shown in Figure 6-8. The demultiplex modulator was switched ON by this pulse, whilst second modulator was switched OFF in order to remove the demultiplexed channel from the data stream. The 1.3 V peak to peak electrical pulse amplitude represented 1/4 of the peak switching voltage of the modulators (5 V). A single RF drive signal was passed to each travelling wave modulator in series, via an RF delay line.

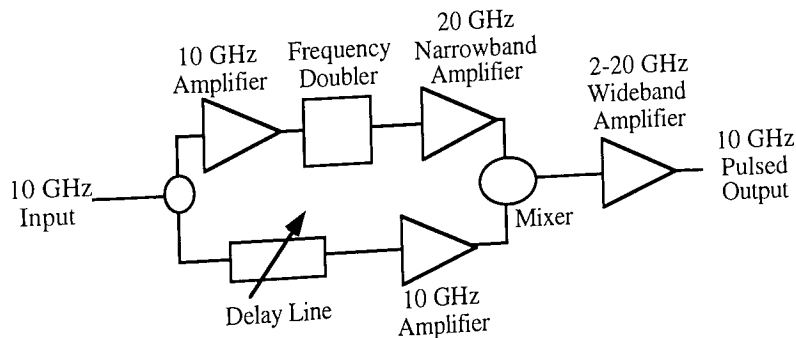


Figure 6-8 RF signal processing to derive pulsed signal from 10 GHz recovered clock

The actual drive signals and simultaneous outputs of the two modulators is shown in Figure 6-9, demonstrating a complete “drop” of the desired channel from the main through path onto the local path. Note that due to imperfections in the electronics, the anticipated ringing of the electrical pulse is absent, giving rise to a cleaner switching pulse. A second 10 GHz mode locked laser, giving 10 ps pulses, also at approximately

1554 nm was modulated with a separate test set (clocked from the locally recovered clock) and inserted with appropriate delay, amplitude and polarisation.

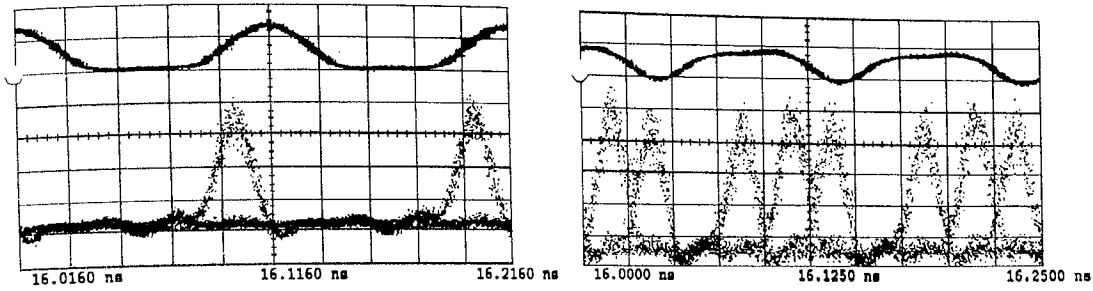


Figure 6-9 Eye diagrams of dropped (*left*) and through (*right*) signals at the intermediate node, along with the electrical switching signals (*upper traces*).

The performance of the D&I node was assessed after a further 20 km of transmission and demultiplexing using a 10 GHz electro-absorption modulator. This modulator gave an ≈ 20 ps wide switching window when a 1 Watt 10 GHz RF drive and 4.8 Volt dc bias were applied to the modulator. The clock signal for the final demultiplexer was derived using the alternative scheme of electrical clock recovery, where a circuit operating at the base rate (10 Gbit/s) is located *after* the demultiplexer. The received and demultiplexed eye patterns are shown in Figure 6-10, at the input to the final demultiplexer, following demultiplexing of a channel from the first node adjacent to the dropped channel, and the inserted channel itself. These figures illustrate the complete switching of the appropriate channels with an extinction ratio in excess of 18 dB. Finally, error ratio measurements are carried out with a simple PIN receiver on the inserted channel, and one of the two original channels adjacent to the dropped channel. It can be seen from Figure 6-11 that both signals operate error free over the whole transmission link, with the differing receiver sensitivities attributed to the number of nodes traversed and different electrical drive amplifiers.

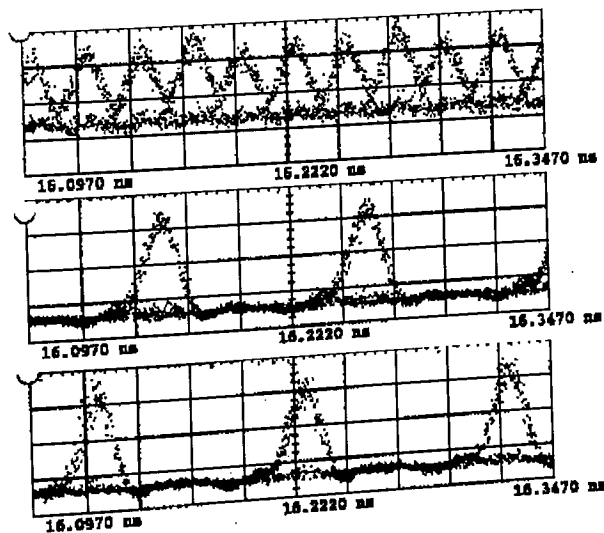


Figure 6-10 Eye diagrams of received signals at third node, showing the input comprising three channels from node 1 and one channel from node 2 (top) and a demultiplexed eye diagram of a channel from node 1 (middle) and the inserted channel from node 2 (bottom).

Note that the approximately 3 ps/nm dispersion of the final transmission line, along with the relatively broad switching window deliberately placed a tight restriction on the operating wavelength of the inserted signals.

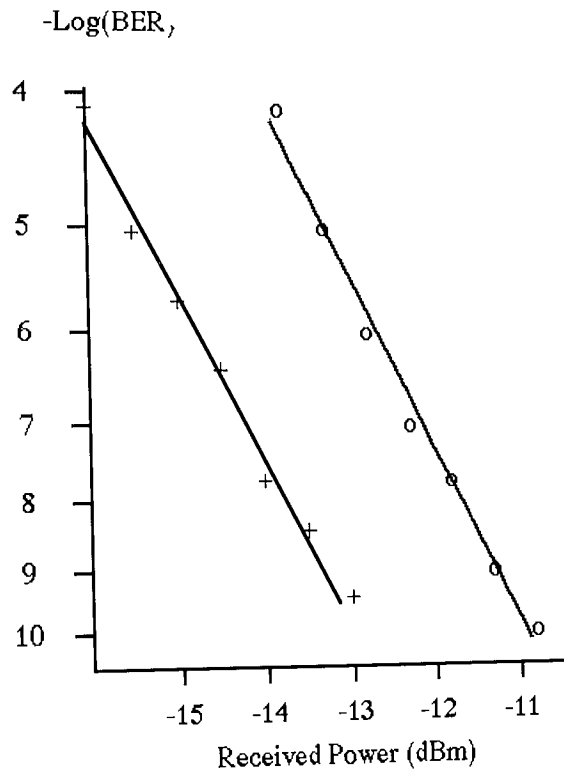


Figure 6-11 Error ratio performance of signals demultiplexed at node three, originating from node 1 (circles) and node 2 (squares).

This experiment clearly confirms that single electro optical modulators may be used to perform both demultiplexing and drop and insert functions in 40 Gbit/s OTDM networks. Such modulators require negligible integration, and may be rapidly deployed in any future OTDM network. Thus, in addition to the exploitation of fibre bandwidth between switching centres, OTDM has been shown to allow a reduction in the complexity and number of switches throughout the network. Two technologies for single stage demultiplexing were simultaneously operated within a single network for single stage demultiplexing, demonstrating the simplicity of approach for an OTDM system, where full interoperability of different technological solutions is a natural consequence of the synchronous nature of the technology. In contrast WDM technology offers many architectural solutions to a given networking problem in terms of, for example, wavelength plans, and thus requiring extensive standardisation to allow full interoperability between manufacturers and technologies.

6.4 OTDM Network Scalability

In this section, the almost infinite cascability of D&I network nodes is demonstrated using the recirculating loop described above (Section 5.2.1). At each node, one of two channels is chosen randomly, demultiplexed and passed to the node for electronic processing. Locally generated traffic (simulated by regenerating the detected signal) is re-injected into the vacant time slot and passed onto the remainder of the network.

Meanwhile, the channel passing through the node for onwards transmission is subject to a synchronous retiming signal, thus ensuring, for a soliton transmission line, that an arbitrarily large network may be constructed²⁵⁸.

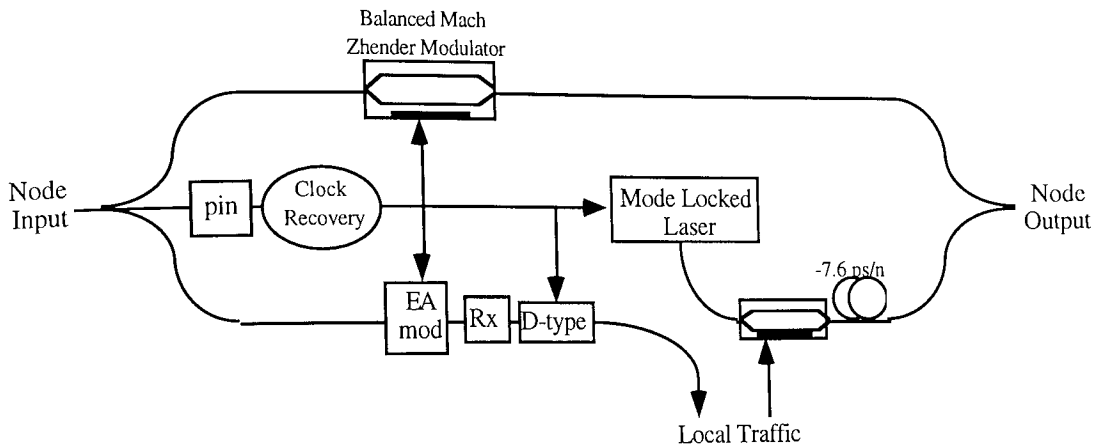


Figure 6-12 Schematic diagram of 20 Gbit/s D&I node.

The network node that was inserted into the recirculating loop is illustrated in Figure 6-12 (all stages of optical amplification and loop timing switches omitted). Close examination will reveal that this corresponds simply to arrangement of the recirculating loop (Figure 5-7) such that the main OTDM output is connected to loop input #3, whilst a base rate output is connected to input #2, the main functionality being derived from the dynamic configuration of the 2:1 selectors and acousto-optic switches. These devices ensure that the loop is initially loaded with a 20 Gbit/s data sequence from the pattern generator, but for subsequent recirculations, a suitable 10 Gbit/s signal is injected into the vacant time slot. For this initial injection of data, the 1553 nm external cavity laser and its external modulator are driven from the pattern generator (2^7-1 PRBS), and passed into a passive interleaving circuit (≈ 200 ns relative path delay) to produce a 20 Gbit/s OTDM signal comprising 12 ps pulses. Following modulation (but before interleaving), the pulses were optionally compressed by a length of dispersion compensating fibre (-7.8 ps/nm dispersion) giving a near transform limited 8 ps pulse train. A 100 km node spacing is achieved using two in line optical amplifiers, and three 33 km lengths of soliton supporting fibre (dispersion zero 1548.5 nm). Consequently, the mean fibre dispersion was ≈ 0.3 ps/nm/km, giving a soliton period of 85km and 190 km for the compressed and uncompressed pulse widths respectively. Timing synchronisation of the node to the incoming data signal is provided via a 20 GHz electronic clock recovery circuit providing a 10 GHz drive signal. In order to determine the channel selected for demultiplexing, the source frequency is adjusted such that the loop length corresponds to either an even number of bit periods (same channel always selected), an odd number of bit periods (alternating channels selected) or an intermediate value (random channel selection). The optical switching is provided by an electro-absorption modulator to demultiplex the desired channel in parallel with a balanced Mach Zehnder modulator to simultaneously clear that channel from the transmission line and retime the onwardly transmitted signals. The Mach Zehnder modulator is driven by a 10 GHz sine wave with a peak to peak amplitude of V_{π} , giving

a 100 % modulation depth. This suggests that the total noise level saturates to 2.11 times the noise generated by a single recirculation, and that the jitter is reduced by 2% per revolution (Equations 5-4 and 5-6). That is, the soliton pulse train is strongly controlled.

Following detection, the demultiplexed signal is regenerated and passed simultaneously to error ratio monitoring equipment, and to simulate locally generated traffic. To achieve this the signal is used to externally modulate the same 1553 nm harmonically mode locked external cavity laser used to generate the initially injected traffic, to ensure a worst case scenario in terms of incoherent interference. This "locally generated" signal is then re-injected into the loop with appropriate, amplitude, delay and polarisation. A total excess delay within the node of $\approx 1\mu\text{s}$ ensures that the transmitted pattern is de-correlated from the incoming signal to accurately simulate the injection of locally generated traffic. It should be noted that because each node is regenerative, errors are "frozen in" and the error ratio measured at the final node represents the accumulation of errors through the entire network.

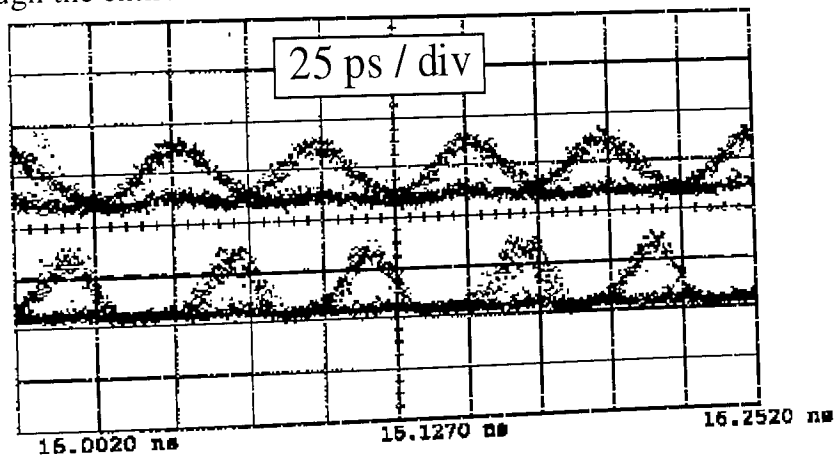


Figure 6-13 Eye diagram of input (upper) and output (lower) of the 244th D&I node with the same channel dropped at each node, measured using 15 and 32 GHz detectors respectively.

The loop was initially tested for transmission by biasing the Mach Zehnder modulator for transmission and turning the locally injected pulses off, giving an error free distance of $\approx 1,500$ km (15 nodes). This slight degradation in performance over previous measurements (Section 5.2.3) arises from the reduced effect of the guiding filters on the broader pulses (8-10 ps cf 5-8 ps) used in this experiment. When near transform limited pulses (time bandwidth product < 0.4) are used at each node, stable error free operation of the fully functional D&I system was achieved over 690 nodes (a total network length of 69,000 km), for both randomly alternating and same channel modes of operation. This level of cascability was limited solely by the differential propagation delay through the regenerator causing variations in the data arrival time of up to 50% of the measurement interval. Such remarkable performance was obtained by virtue of the retiming action of the 10 GHz driven Mach Zehnder modulator used to clear data from the appropriate time slot. This is verified in Figure 6-13, which illustrates the eye diagram after the same channel has passed through 244 nodes (limited by temperature fluctuations altering the loop length, and consequently the relative clock phase after each recirculation). A small, but constrained degree of timing jitter is clearly evident for the

channel passing straight through each node, due to the optimisation of the transmission control modulator for D&I functionality rather than retiming, however, error free performance is still maintained.

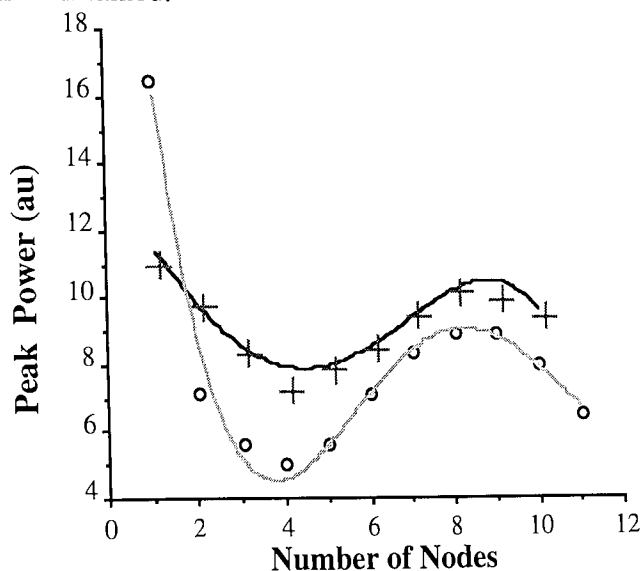


Figure 6-14 Evolution of the pulse peak power as a function of transmission distance for compressed (crosses) and uncompressed (circles) pulses.

As may be anticipated, the major limitation of this type of network is the degree to which the various pulse streams are matched (in terms of amplitude, width, wavelength and chirp). In this demonstration, wavelength (and consequently velocity) matching was assured by using the same laser at each node. However, if the dispersion compensating fibre is removed (increasing the time bandwidth product of the launched pulses by $\approx 50\%$), a significant pulse width and power evolution is observed as the launched pulses evolve into solitons (see Figure 6-14). In this case, it was only possible to cascade 6 network nodes, due to the extreme difficulty of matching the amplitude and width of the injected pulses at each node. This problem was sufficiently eliminated using the compression fibre to produce near transform limited pulses, and so reduce the initial evolution in pulse shape.

This experiment has demonstrated, for the first time, almost infinite cascading of D&I nodes within an OTDM network (>500 nodes). In this demonstration, the electronically driven switches may be easily, and rapidly reconfigured (eg³⁷⁰) to provide a flexible series of interconnections between the nodes for standard SDH/SONET circuit line rates, whilst synchronous retiming enables the 20 Gbit/s transport layer to be extended over essentially indefinite distances. In this simple demonstration, the demultiplexing and retiming functions were performed in a single component, however, for a more flexible network, with either a finer switched granularity (eg 2.488 Gbit/s) or a higher capacity transport layer (eg 40 or 100 Gbit/s), the separation of these functions into separate elements is not unreasonable. In particular, all optical demultiplexers and soliton shepherding offer particularly attractive implementations of these functions that will allow the deployment of ultra high capacity all-optical networks. It is worth noting however, that the theoretical transfer function of the broadband modulator used in the 3 node 40 Gbit/s network experiment described

above contains a periodic amplitude ripple, capable of providing a low amplitude soliton retiming signal (Figure 6-15).

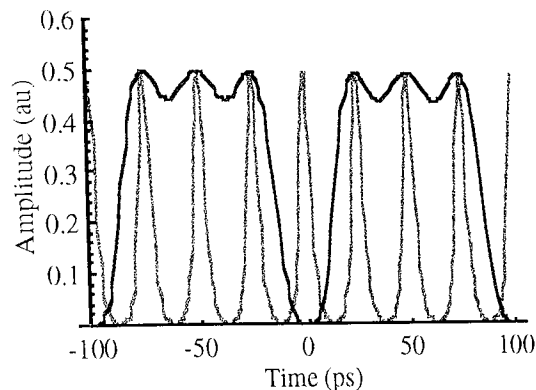


Figure 6-15 Illustration of the soliton control functionality of a broadband modulator based D&I node showing representative soliton train (grey) and the modulator switching window (purple)

This ripple produces an 11 % modulation depth, giving an extinction ratio of 0.5 dB. Consequently, for a typical 40 Gbit/s system, comprising 4 ps pulses and a 2 nm filter, we would anticipate a maximum noise accumulation equivalent to 20 times a single internode link and a jitter reduction of ≈ 1.8 % per node due to the amplitude modulation. Enhanced soliton control would be possible using an unbalanced modulator, giving simultaneous synchronous phase modulation of up to ≈ 1 mrad. Given the experimental transmission results of Chapter 5 this suggests that large scale 40 Gbit/s OTDM networks are feasible. This network would employ dispersion profiled fibre to overcome the limits of the average soliton model and allow increased launch powers and soliton control to constrain timing jitter.

6.5 OTDM Network Connectivity

Although the results presented above show great promise for OTDM networks, several issues remain unresolved. For example, it may be advantageous to allow an OTDM network to be branched. However, at the meeting of the two branches, the incoming data signals should be well matched. Whilst the optical properties of the signals (wavelength, pulse width, peak power) may be forcibly matched using an all optical regenerator, it is also necessary to ensure the time slots are appropriately aligned to less than a bit period, despite thermal fluctuations in the relative optical path lengths³⁷¹

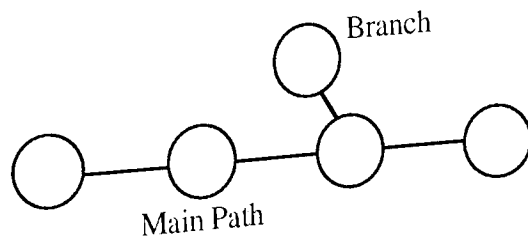


Figure 6-16 Schematic diagram of a branched OTDM network

An appropriate error signal may be obtained by comparing the phases of the recovered clock signals at the branching point using a mixer. This error signal may be used to drive a fibre optic delay line to counter the drifts in fibre length. However, the finite

physical dimension of the delay line typically precludes the endless operation required for continuous stabilisation under arbitrary conditions. Now for given a typical expansion coefficients of $10^{-6}/^{\circ}\text{C}$, changes in delay of $\approx 0.5\text{ns}/100\text{km}/^{\circ}\text{C}$ are to be anticipated. Thus even by sacrificing continuous tunability for a limited tuning range, variations of several ns are required.

Alternatively, endless control is available by using the error signal to control the signal frequency of one of the branches (the slave branch). A preliminary investigation of this technique was carried out by Terry Widdowson, illustrating successful stabilisation of relative phase between two 10 GHz pulse trains for slave branch lengths up to $\approx 12\text{ km}$. This demonstration was limited by the unlocked linewidth of the slave VCO, which introduced a degree of jitter proportional to the transit time of the branch. Optimal operation of this scheme would require the use of a narrow linewidth oscillator, or frequency synthesiser in place of the slave VCO.

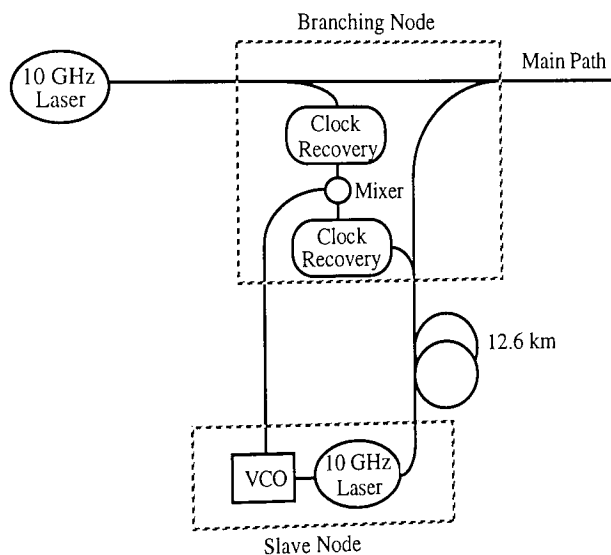


Figure 6-17 Schematic diagram of branched network synchronisation experiment of Widdowson.

For a mesh network, the situation becomes more complex, with a given node required to be synchronous with at least two remote branching nodes. Clearly the endless control described above may not be used to simultaneously meet these requirements, since the VCO may only be tuned to match one of the paths. Alternative techniques therefore are clearly required to allow mesh or ring networks to be implemented using OTDM techniques.

Possible techniques include;

- Optical delay lines with large tuning ranges (to constrain the total optical path length to a fixed value)
- All-optical variable buffer store or shift register based on all optical logic gates (analogous to buffer stores used in SDH networks).
- Switched fibre paths (to reduce the delay range required for optical delay lines)

Where discrete switching between delay paths is required, appropriate protocols should be established to signal switching events and prevent service interruption.

These timing issues are also of great importance when interconnecting SDH equipment into an OTDM network. Figure 3-34 illustrates how, in a terminal node, SDH equipment may be interfaced into an OTDM node. Of critical importance is the existence of a single, common master clock, either derived from one of the SDH terminals or the RF source used to generate the optical pulses. This master clock is then used to drive all of the terminals and pulse sources in the node. On the receive side, the buffer stores within the SDH terminals are used to interface with the incoming traffic of indeterminate phase, although a local OTDM clock recovery is required to drive the demultiplexer. For a simple bi-directional D&I node, the situation becomes more complex. Consider for example the node structure of Figure 6-12, with the local traffic either terminating on SDH line terminals or simply switched by a single SDH ADM.

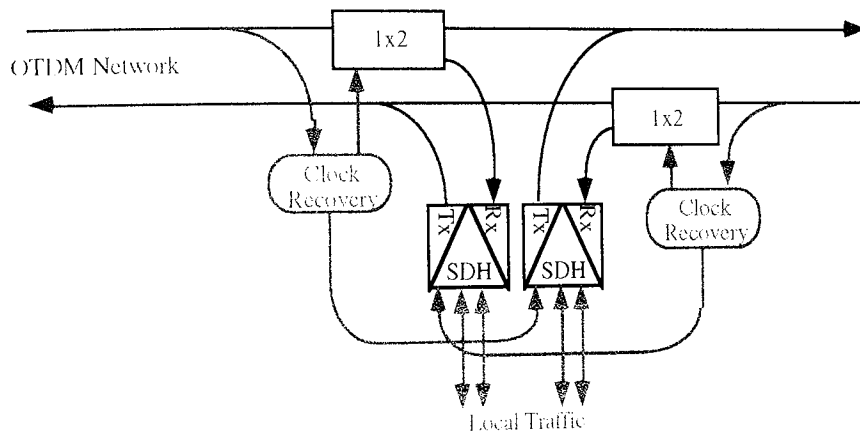


Figure 6-18 Schematic diagram of a bi-directional OTDM D&I node, with local traffic terminating on SDH terminals.

Note first that in establishing a *circuit* between two SDH line terminals through a D&I network, locally generated traffic is inserted into a separate counter propagating fibre path, not directly into the space created by the removal of the dropped channel. This space is used to establish circuits with downstream nodes using separate SDH terminals. This leads to the connection of terminals and OTDM systems illustrated in Figure 6-18 where a given terminal receives data from one OTDM line system, and inserts data into another. Now, a given terminal must inject data synchronously into an OTDM line system, whose clock source is remote. This terminal must therefore extract its clock from that line system via the OTDM clock recovery. Incoming data from the other line system, clearly of differing phase, is again received via the SDH buffer store. Thus the clock synchronisation strategy of an OTDM D&I node is similar to that of a terminal node (Figure 3-34), but with no option for the location of the master clock (which must be the incoming data stream).

However, although this argument suggests that interconnection between OTDM networks and SDH terminals is feasible, requiring only the evolution of appropriate clock distribution strategies, many SDH networks are based on SDH Add Drop Multiplexers (ADM's) where traffic passes *through* a node, with lower granularity traffic dropped as appropriate. One possible interconnection of ADM's into an OTDM network, based on Figure 6-18, would take two terminals (interconnected via the spare

aggregate outputs) each with a transmitter synchronised to the appropriate OTDM transmission line. The SDH buffer store between the interconnecting aggregates allowing for the variation between the two OTDM line systems. Alternatively, the use of a single ADM would avoid the unnecessary duplication of SDH aggregates. The appropriate connections for a single ADM are shown in Figure 6-19 with each aggregate interconnected to upstream and downstream paths in the OTDM network. Whilst the ADM inputs are synchronised via the SDH buffer stores as usual, the use of a single terminal prohibits the simultaneous synchronisation of *both* outputs to the appropriate OTDM line systems. It is thus necessary to allow an independent control of the second ADM output via an optical delay line. This delay line is adjusted according to the relative phases of the clock signals recovered from the OTDM line systems.

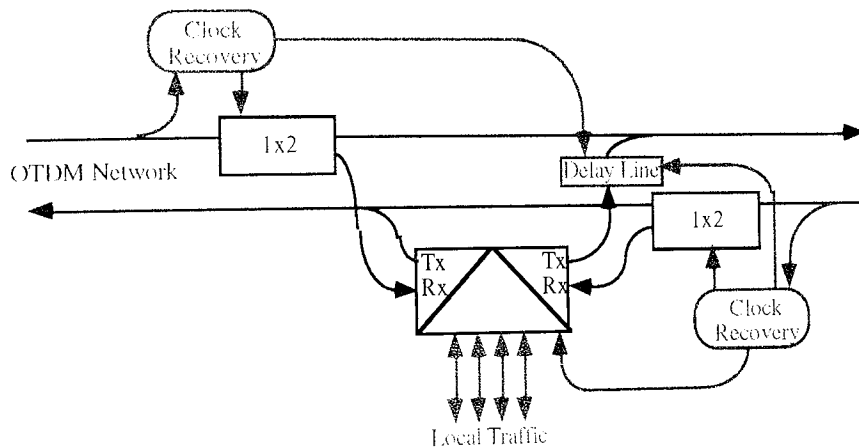


Figure 6-19 Schematic diagram of a bi-directional OTDM D&I node, with local traffic routed via a single SDH ADM.

Thus, provided sufficient delay range is available, the inclusion of optical delay lines allows the arbitrary interconnection of OTDM network nodes, and the interconnection of OTDM networks with existing and future SDH networks. The deployment of such delay lines is minimised by the adoption of appropriate clock distribution strategies.

6.6 Chapter Summary

In this chapter, it has been demonstrated how electro-optic demultiplexers may be deployed to allow a full drop and insert functionality within an OTDM network. In principle this allows OTDM systems to offer the same functionality as WDM systems, without the added difficulties of wavelength management and amplifier gain flatness. The network architecture proposed also allows the selection of any OTDM channel simply by adjusting the phase of the drive signals, unlike traditional WDM systems, where appropriate switchable filtration must be deployed for each optical channel. Consequently whilst OTDM nodes require active elements, a considerable overall simplification is anticipated with a vastly reduced component count. Equally significantly, a second network experiment demonstrated that, in combination with soliton control techniques, OTDM networks are almost infinitely cascable. This is in

stark contrast to recent WDM network demonstrations, where, in the absence of optoelectronic conversion, the maximum number of cascaded nodes reported to date is ≈ 10 . Thus, a truly all-optical, global scale OTDM network may be readily constructed using entirely commercially available components. Whilst additional complexities are encountered for the development of meshed and multipath network architectures, full interconnectivity is anticipated following the development of optical delay lines with large delay ranges (in the region of several ns).

7. Conclusions

In this thesis, we have discussed a detailed experimental investigation of OTDM networks at aggregate line rates of up to 40 Gbit/s using electro-optic modulators and fibre ring lasers. The key enabling technologies for this work are low jitter, transform limited optical pulse sources, and low jitter clock recovery circuits for network synchronisation. Appropriately therefore a large part of the thesis was devoted to the development of optical pulse sources at both the system base rate (10 GHz) and, to provide an alternative OTDM architecture, at the system line rate. Constraints pertaining to the multiplexing of signals over arbitrary path lengths imposed quite stringent limitations on the source extinction ratio and pulse width, suggesting that mode locked lasers are required. Consequently both fibre and semiconductor based mode locked lasers were employed in the majority of system demonstrations in this thesis (Chapter 3). For demanding soliton transmission applications however, the high pulse quality of mode locked fibre lasers represents the ideal source, with cascaded electroabsorption modulators (cascaded for enhanced extinction ratio) coming a close second due to their simplicity and flexibility.

Throughout this investigation, electronic clock recovery was found to provide excellent performance, producing recovered clocks with jitter levels well below measurement resolutions (300 fs). Recent improvements to the circuit include the inclusion of high efficiency (GHz/V) voltage controlled oscillators and harmonic mixers. Issues of multiplexing and demultiplexing OTDM systems were considered, and attention was focused on solutions based on discrete electro-optic modulators with simple drive signals. The electro-absorption modulator was found to be particularly suited to an OTDM demultiplexing function for bit rates up to (and perhaps exceeding) 80 Gbit/s.

Transmission of 40 Gbit/s OTDM data sequences on both standard and dispersion shifted fibres was investigated, and world record maximum transmission distances for each fibre type were extended to 202 and 2,200 km respectively. The requirements for high speed active soliton control were investigated for the first time, with attention focused on the development of control strategies applicable to OTDM systems operating at bit rates above the maximum electronic signal frequency. A combination of 20 and 40 Gbit/s transmission experiments were carried out, and revealed requirements for novel transmission fibres and/or dispersion management to allow a reasonable spacing between optical amplifiers and control elements. Subsequent preliminary investigations into such fibres revealed that both dispersion decreasing fibres and distributed erbium doped fibre amplifiers may be used for high speed OTDM systems and, in combination with active soliton control, offer a route to global transmission of ultra high speed OTDM data signals (Chapter 5).

As an alternative to long haul OTDM transmission, techniques for full all-optical regeneration were developed, and demonstrated with full error ratio measurements for the first time. The 40 Gbit/s OTDM regenerator developed in this thesis represents to the highest reported capacity regenerator using any technology. The simple construction of the regenerator (two optical amplifiers and some dispersion shifted fibre) suggests that

it would not be unreasonable to replace line amplifiers with all optical regenerators, giving a truly digital optical transmission line (Chapter 5).

Finally, worlds first demonstrations of optical networking using OTDM data signals revealed that the significant cost savings offered by course routing may be exploited using OTDM as an alternative multiplexing strategy to WDM. Significantly, the combination of OTDM networking and optical soliton control enables the infinitely cascability of OTDM network nodes and thus offers significant advantages over current all optical WDM networks of limited scalability (Chapter 6). The use of dispersion compensation to allow soliton propagation at 1550 nm over embedded standard fibre^{372,373} may allow the deployment of similar OTDM networks without additional cable investment. The network nodes investigated in this thesis comprised commercially available electro-optic modulators, and are thus suited to immediate deployment, however, it should be recalled that many all optical techniques may be used to provide similar routing functionality. Indeed certain configurations of optical switches give rise to a naturally regenerative performance, again offering infinite scalability.

It is interesting to compare this solution to WDM and electrically multiplexed network solutions. For transmission, electrically multiplexed systems and OTDM systems would be anticipated to demonstrate similar performance. Such systems are limited by signal to noise ratio and self phase modulation effects, such as jitter in soliton systems, and crosstalk in dispersion compensated systems. The ultimate transmission performance is anticipated for soliton transmission on dispersion profiled fibre. For WDM, on the other hand, major limitations arise from non-linear crosstalk, necessitating the use of dispersive fibres and strong dispersion management. Whilst WDM systems are further complicated by the requirements for gain flattened amplifiers, wavelength referencing and management, recent laboratory systems demonstrations have failed to reveal a significant long term advantage for either transmission technology.

In terms of optical networking, both OTDM and WDM offer the potential of course routing in the optical domain, performing switching operations only on the required channels. This is in contrast to electrically multiplexed systems, where the entire aggregate capacity signal must be detected and processed. Now, the nature of WDM and OTDM systems leads to different performances within an optical network. As we have seen above, the synchronous nature of OTDM allows infinite node cascability through optical regeneration or soliton control. Branched networks are possible by adjusting the source clock frequency for tributary branches, and mesh networks may be deployed following the development of wide tuning range optical delay lines. For a WDM system on the other hand, the asynchronous nature precludes simple regeneration at the aggregate line rate, limiting the network scalability. However, it is a simple task to construct complex mesh networks using WDM cross connects, offering restoration, path protection for individual wavelengths and transparent to signal format. We may imagine therefore that with current technology, WDM networks are highly suited to complex metropolitan networks with tens of multiply interconnected nodes,

whilst OTDM networks are suited to long haul backbone networks, offering high performance over a global scale. This division is illustrated in Figure 7-1, where the multi-layer model of Figure 1-3 is extended to include these features.

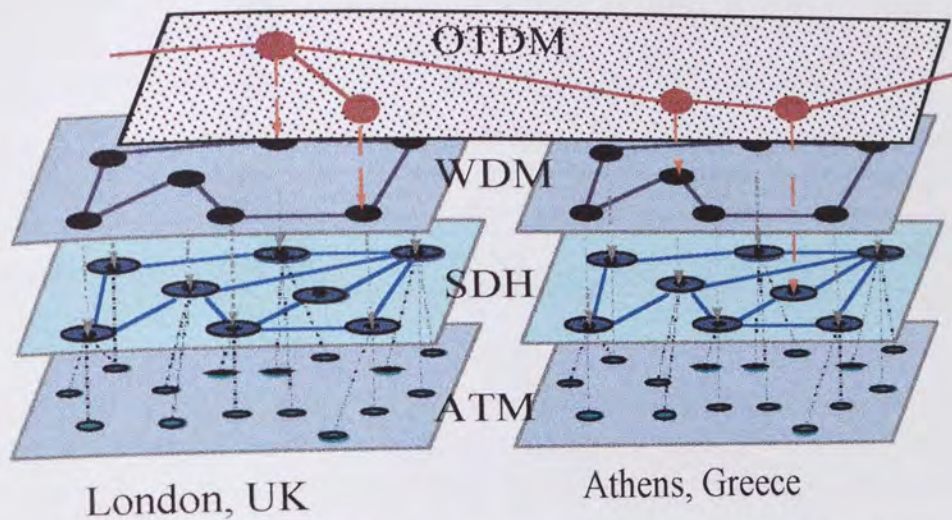


Figure 7-1 Multi Layer model of an optical network employing WDM for rich interconnectivity on a regional level, and OTDM for a global scale backbone network.

In order to remove one of these optical layers, it is necessary for it to adopt the features of the other. For example, an OTDM network should be able to be deployed in a complex mesh network. This clearly necessitates the development of techniques to stabilise the effective optical path length of all of the links within the network, through, for example, optical delay lines. For a WDM system, it is necessary to provide infinite scalability, through either regeneration of each individual wavelength or, preferably, via regeneration of the aggregate signal. Whilst a suitable technique has been proposed for a point to point link, relying on relative dispersion of the signals through an integral number of bit periods between control stations, deployment within a mesh network will encounter the same synchronisation issues as an OTDM network. Furthermore, in addition to stabilising the optical path lengths, it is necessary to equalise the relative dispersions throughout the network.

Alternatively, all of the advantages of OTDM systems are offered by packet switched OTDM systems³⁷⁴, but without the synchronisation constraints of OTDM. The successful development of full regeneration for a stream of asynchronous optical packets will thus allow infinitely scaleable optical networks, with complex interconnectivity and minimal management overhead within the core of the network. Furthermore, the packet switched nature of the transmission format implies that the SDH layer is also bypassed, providing a flat network architecture. In summary, this thesis has demonstrated that infinitely scaleable 40 Gbit/s OTDM networks may be readily constructed using a combination of

- electro-optic modulators for signal processing
- electronic phase locked loops for synchronisation
- fibre ring laser pulse sources.

Such networks offer an attractive alternative to both WDM and electrically multiplexed systems offering the same aggregate capacity. Networks of this type are most likely to

be deployed as national or global scale backbone networks. Studies of the transmission properties of 40 Gbit/s OTDM signals revealed that dispersion profiled fibre will be required for OTDM transmission at higher capacities due to the limitations imposed by the average soliton model, and the need to increase the signal to noise ratio for active soliton control.

Further work should focus on both the transmission and networking of ultra high speed OTDM signals (> 80 Gbit/s). In terms of transmission, the development of dispersion profiled fibres are likely to be required to allow soliton transmission with commercially acceptable repeater spacings, with active soliton control or all optical regeneration enabling transmission over global distances. In terms of networking, further developments of electro-absorption modulators, driven by simple base rate signals should allow the development of appropriate ADM's, with a maximum achievable line rate currently in the region of 8 times the modulator bandwidth (80 Gbit/s using latest devices). Similarly, Mach Zehnder modulators may be used for the deployment of OTDM systems at four times the maximum modulator drive frequency (160 Gbit/s using commercially available components). Beyond these line rates (≈ 200 Gbit/s) it may become necessary to investigate the potential of non-linear optical switches, although the development of high speed electro-optic modulators with a high frequency, narrow band response suitable for use in a high base rate OTDM system should not be ruled out.

8. Publications and Conference Presentations

July 1994 - June 1997.

Items shown in italics are not directly discussed in this thesis.

Books

D.M.Spirit, M.J.O'Mahony (eds), "High Capacity Optical Transmission, Explained", John Wiley and Sons, Chichester, 1995 : Main author, Chapters 4 and 6, Co-author Chapter 5.

D.W.Smith (ed), "Optical Networking Technology", Chapman and Hall, London, 1995, Co-author Chapter 4.

Journal Papers

A.D.Ellis, T.Widdowson, X.Shan, D.G.Moodie, "Three node, 40 Gbit/s OTDM network experiment using electro-optic switches", *Electronics Letters*, **30**, 16, pp1333, 1994.

D.G.Moodie, A.D.Ellis, C.W.Ford, "Generation of 6.3 ps optical pulses at a 10 GHz repetition rate using a packaged electroabsorption modulator", *Electronics Letters*, **30**, 20, pp1700, 1994.

T.Widdowson, A.D.Ellis, "20 Gbit/s soliton transmission over 125 Mm", *Electronics Letters*, **30**, 22, pp1866, 1994.

D.M.Spirit, A.D.Ellis, P.E.Barnsley, "Optical time division multiplexing: Systems and networks", *IEEE Communications Magazine*, December 1994, pp56, 1994.

*D.A.O.Davies, A.D.Ellis, T.Widdowson, G.Sherlock, "10 Gbit/s data switched semiconductor laser amplifier nonlinear loop mirror", *Electronics Letters*, **31**, 2, pp111, 1995.*

A.D.Ellis, M.C.Tatham, D.A.O.Davies, D.Nessett, D.G.Moodie, G.Sherlock, "40 Gbit/s transmission over 202 km of standard fibre using midspan spectral inversion", *Electronics Letters*, **31**, 4, pp299, 1995.

D.J.Richardson, R.P.Chamberlin, L.Dong, D.N.Payne, A.D.Ellis, T.Widdowson, D.M.Spirit, "Demonstration of 205 km transmission of 35 GHz, 5ps pulses generated from a diode driven, low jitter, beat signal to soliton train conversion source", *Electronics Letters*, **31**, 6, pp470, 1995.

*A.D.Ellis, D.M.Patrick, D.Flannery, R.J.Manning, D.A.O.Davies, D.M.Spirit, "Ultra high speed OTDM networks using semiconductor amplifier based processing nodes", *Journal of Lightwave Technology*, **13**, 5, pp761, 1995.*

*D.A.O.Davies, A.D.Ellis, G.Sherlock, "Regenerative 20 Gbit/s wavelength conversion and demultiplexing using a semiconductor laser amplifier nonlinear loop mirror", *Electronics Letters*, **31**, 12, pp1000, 1995.*

A.D.Ellis, T.Widdowson, "690 node global OTDM network demonstration", *Electronics Letters*, **31**, 14, pp1171, 1995.

*A.D.Ellis, D.A.O.Davies, A.Kelly, W.A.Pender, "Data driven operation of semiconductor amplifier loop mirror at 40 Gbit/s", *Electronics Letters*, **31**, 15, pp1245, 1995.*

A.D.Ellis, W.A.Pender, T.Widdowson, D.J.Richardson, R.P.Chamberlain, L.Dong, "All optical modulation of 40 GHz beat frequency conversion source", *Electronics Letters*, **31**, 16, pp1362, 1995.

D.G.Moodie, A.D.Ellis, A.R.Thurlow, M.J.Harlow, I.F.Lealman, S.D.Perrin, L.J.Rivers, M.J.Robertson, "Multi-quantum well electroabsorption modulators for 80 Gbit/s OTDM systems", *Electronics Letters*, **31**, 16, pp1370, 1995.

W.A.Pender, P.J.Watkinson, E.J.Greer, A.D.Ellis, "10 Gbit/s all optical regenerator", *Electronics Letters*, **31**, 18, pp1587, 1995.

A.Altuncu, L.Noel, W.A.Pender, A.S.Siddiqui, T.Widdowson, A.D.Ellis, M.A.Newhouse, A.J.Antos, G.Kar, P.W.Chu, "40 Gbit/s error free transmission over a 68 km distributed erbium doped fibre amplifier", *Electronics Letters*, **32**, 3, pp233, 1996.

D.J.Richardson, L.Dong, R.P.Chamberlain, A.D.Ellis, T.Widdowson, W.A.Pender, "Periodically amplified system based on loss compensating dispersion decreasing fibre", *Electronics Letters*, **32**, 4, pp373, 1996.

A.D.Ellis, T.Widdowson, X.Shan, "Wavelength dependence of 40 Gbit/s solitonic transmission over distances greater than 2000 km", *Electronics Letters*, **32**, 4, pp381, 1996.

W.A.Pender, T.Widdowson, A.D.Ellis, "Error free operation of a 40 Gbit/s all-optical regenerator", *Electronics Letters*, **32**, 6, pp567, 1996.

X.Shan, T.Widdowson, A.D.Ellis, A.S.Siddiqui, "Very simple method to stabilise mode-locked erbium fibre lasers", *Electronics Letters*, **32**, 11, pp1015, 1996.

A.Altuncu, A.S.Siddiqui, A.D.Ellis, M.A.Newhouse, A.J.Antos, "Gain and noise figure characterisation of a 68 km long distributed erbium doped fibre amplifier", *Electronics Letters*, **32**, 19, pp1800, 1996.

J.K.Lucek, P.Gunning, D.G.Moodie, K.Smith, A.D.Ellis, D.Pitcher, "Optical TDMA channel selection using electroabsorption modulator with dual frequency drive", *Electronics Letters*, **33**, 1, pp22, 1997.

D.D.Marcenac, D.Neset, A.E.Kelly, M.Brierley, A.D.Ellis, D.G.Moodie, C.W.Ford, "40 Gbit/s transmission over 400 km using mid-span spectral inversion by four-wave-mixing in a 2 mm long SOA", Submitted to *Electronics Letters*.

D.D.Marcenac, A.D.Ellis, D.G.Moodie, "80 Gbit/s OTDM using electro-absorption modulators", Submitted to *Electronics Letters*.

Conference Presentations

A.D.Ellis, D.M.Spirit, D.Flannery, D.A.O.Davies, G.Sherlock, R.J. Manning, "Ultra fast optical processing using semiconductor amplifiers", *Proc ECOC'94*, pp121, 1994.

A.D.Ellis, M.C.Tatham, D.M.Spirit, D.A.O.Davies, D.Neset, D.G.Moodie, G.Sherlock, "Ultra high speed OTDM over standard fibre", *IEE Colloquium Digest 1995/110*, Paper 9, 1995.

A.D.Ellis, "A comparison of WDM and OTDM systems for high capacity optical fibre transmission", *IEE Colloquium Digest 1996/091*, Paper 1, 1996.

A.D.Ellis, "Optical multiplexing for high capacity optical networks", Key Note Address, ACTS concertation meeting, 5th March, 1997.

A.D.Ellis, "OTDM and WDM, Technologies for Global Scale Networks ?", Invited Presentation, Rochester Theory Centre Workshop on Advanced Concepts in High Speed Optical Communications, Rochester, 23rd May 1997.

Other Conference Papers

D.G.Moodie, A.D.Ellis, A.R.Thurlow, I.F.Lealman, C.W.Ford, M.J.Robertson, "Electroabsorption modulators for ultra high speed OTDM systems", IEE Colloquium Digest 1995/110, Paper 3, 1995.

X.Shan, A.S.Siddiqui, A.D.Ellis, T.Widdowson, D.M.Spirit, M.A.Newhouse, A.J.Antos, "10 and 80 GHz soliton transmission over 60 km distributed erbium doped fibre", IEE Colloquium Digest 1995/110, Paper 15, 1995.

D.G.Moodie, A.D.Ellis, A.R.Thurlow, M.J.Harlow, I.F.Lealman, S.D.Perrin, L.J.Rivers, M.J.Robertson, "Electroabsorption modulators for 80 Gbit/s systems", Proc IOOC'95, paper FB3-3, 1995.

R.J.Manning, D.A.O.Davies, A.D.Ellis, D.M.Patrick, "Applications of high speed non-linearities of semiconductor amplifiers", Proc OAA'95, paper SaC1-1, pp226, 1995.

D.J.Richardson, R.P.Chamberlain, L.Dong, D.N.Payne, A.D.Ellis, T.Widdowson, W.A.Pender, D.M.Spirit, "High frequency bright and dark soliton sources based on dispersion profiled fibre circuitry and their applications", Proc UPS'95, 1995.

D.J.Richardson, L.Dong, R.P.Chamberlin, A.D.Ellis, T.Widdowson, W.A.Pender, "Periodically amplified transmission system based on loss compensating dispersion decreasing fibre", IEE Colloquium Digest 1996/090, Paper 4, 1996.

D.G.Moodie, M.J.Harlow, A.D.Ellis, C.W.Ford, S.D.Perrin, M.J.Guy, "High modulation depth electroabsorption modulator modules for OTDM systems", IEE Colloquium Digest 1996/091, Paper 5, 1996.

M.W.Street, D.Nesset, A.D.Ellis, J.H.Marsh, J.S.Aitchison, "Generation of high peak power (615 W) subpicosecond pulses using a gain switched distributed feedback laser diode and nonlinear fibre compression technique", Proc CLEO'96, Paper CMK5, 1996.

D.J.Richardson, L.Dong, A.D.Ellis, T.Widdowson, W.A.Pender, "Experimental demonstration of 10 Gbit/s, 4.7 ps pulse transmission over 4300 km in a low dispersion loss compensating dispersion decreasing fibre", Proc NGWA'96, Paper FA3-1, 1996.

J.K.Lucek, P.Gunning, D.G.Moodie, K.Smith, A.D.Ellis, "High granularity channel selection using an electroabsorption modulator for ultrafast TDMA LAN applications", Proc ECOC'96, paper ThD.1.8, 1996.

J.K.Lucek, P.Gunning, D.G.Moodie, K.Smith, A.D.Ellis, D.Pitcher, "40 Gbit/s Optical TDMA LAN", Proc ECOC'96, Paper ThC.3.4, 1996.

I.D.Phillips, P.N.Kean, N.J.Doran, I.Bennion, D.A.Pattison, A.D.Ellis, "Simultaneous clock recovery and data regeneration using a nonlinear optical loop mirror as an optical mixer", Proc OFC'97, Paper ThH5, 1997.

Papers in Related Fields

X.Gu, S.J.Pycock, D.M.Spirit, A.D.Ellis, C.J.Anderson, "10 Gbit/s, 138 km uncompensated duobinary transmission over installed standard fibre", Electronics Letters, 30, 23, pp1953, 1994.

T.Widdowson, J.P.Hueting, A.D.Ellis, D.J.Malyon, P.J.Watkinson, "Global fibre transmission using optically amplified regenerators for maximised repeater spacing", Electronics Letters, 30, 24, pp2056, 1994.

- E.M.Kimber, X.Gu, S.J.Pycock, E.Pittuck, B.L.Patel, D.M.Spirit, J.Wakefield, A.D.Ellis, C.J.Anderson, "Field technology demonstration of unrepeaters 2x10 Gbit/s narrow band WDM over 120 km of installed step index fibre", *Proc ECOC'94, Post-deadline papers*, pp31, 1994.
- L.Noel, X.Shan, A.D.Ellis, "Four WDM channel NRZ to RZ format conversion using a single semiconductor laser amplifier", *Electronics Letters*, 31, 4, pp277, 1995.
- E.M.Kimber, X.Gu, S.J.Pycock, E.Pittuck, B.L.Patel, D.M.Spirit, J.Wakefield, A.D.Ellis, C.J.Anderson, "Unrepeatered 2 x 10 Gbit/s narrow band WDM field technology demonstration over 120 km of installed step index fiber", *Proc OFC'95, Paper TuC4*, pp5, 1995.
- X.Gu, A.D.Ellis, D.M.Spirit, "Stimulated Brillouin scattering in installed standard fibre and its influence on a 10 Gbit/s system using binary and duobinary signalling", *Proc IOOC'95, paper WA3-3*, 1995.
- J.P.Huetting, T.Widdowson, A.D.Ellis, "10 Gbit/s NRZ global transmission using optically amplified electronic regeneration", *Electronics Letters*, 31, 13, pp1075, 1995.
- W.H.Loh, R.I.Laming, X.Gu, M.N.Zervas, M.J.Cole, T.Widdowson, A.D.Ellis, "10 cm chirped fibre Bragg grating for dispersion compensation at 10 Gbit/s over 400 km of non dispersion shifted fibre", *Electronics Letters*, 31, 25, pp2203, 1995.
- R.I.Laming, W.H.Loh, X.Gu, M.N.Zervas, M.J.Cole, A.D.Ellis, "Dispersion compensation with chirped fiber Bragg grating to 400 km at 10 Gbit/s in non-dispersion shifted fiber", *Proc OFC'96, Paper ThA5*, 1996.
- W.H.Loh, R.I.Laming, A.D.Ellis, D.Atkinson, "Dispersion compensated 10 Gbit/s transmission over 700 km of standard single mode fiber with 10 cm chirped fiber grating and duobinary transmitter", *Proc OFC'96, Paper PD30*, 1996.
- W.H.Loh, R.I.Laming, A.D.Ellis, D.Atkinson, "10 Gbit/s transmission over 700 km of standard single mode fibre with a 10 cm chirped fibre grating compensator and duobinary transmitter", *IEE Colloquium Digest 1996/091, Paper 10*, 1996.
- X.Gu, S.J.Dodds, L.C.Blank, D.M.Spirit, S.J.Pycock, A.D.Ellis, "Duobinary technique for dispersion reduction in high capacity optical systems - modelling experiment and field trial", *IEE Proceedings in Optoelectronics*, 143, 4, pp228, 1996.
- W.H.Loh, R.I.Laming, A.D.Ellis, D.Atkinson, "10 Gbit/s transmission over 700 km of standard single mode fibre with 10 cm chirped fiber grating compensator and duobinary transmitter", *IEEE Photonics Technology Letters*, 8, 9, pp1258, 1996.
- R.Kashyap, A.D.Ellis, D.J.Malyon, J.P.Huetting, H-G.Froelich, A.Swanton, D.J.Armes, "Four wavelength dispersion compensation over 125 km of single mode optical fibre at 10 Gbit/s using multiple in-line step chirped gratings", *Proc ECOC'96, Paper MoB.4.3*, 1996.
- R.Kashyap, A.D.Ellis, D.J.Malyon, H-G.Froelich, A.Swanton, D.J.Armes, "Eight wavelength x 10 Gbit/s simultaneous dispersion compensation over 100 km single mode fibre with a single 10 nm bandwidth 1.3 metre long super step chirped fibre Bragg grating with a continuous delay of 13.5 ns", *Proc ECOC'96, Paper ThB.3.2*, 1996.
- L.Dong, M.J.Cole, A.D.Ellis, M.Durkin, M.Ibsen, V.Gusmeroli, R.I.Laming, "40 Gbit/s, 1.55 μ m transmission over 100 km of non dispersion shifted fibre with long continuously chirped fibre gratings", *Proc OFC'97 Paper PD-6*, 1997.

9. References

- ¹ D.M.Spirit, M.J.O'Mahony, "High Capacity Optical Transmission Explained", John Wiley and Sons, Chichester, 1995.
- ² P.D.Chidgey, D.W.Smith, "Sampled optical time division multiplexing of asynchronous data", Electronics Letters, **23**, pp1228, 1987 .
- ³ E.D.Lowe, P.Botham, I.Hawker, "An upgrade route for core transport networks", Proc Globecom'96, 1996. and E.D.Lowe, "Europe's telcos gird for traffic onslaught", Photonics Spectra, 1997 .
- ⁴ A.S.Acampora, "A multichannel multihop local lightwave network", Proc Globecom'87, 1987
- ⁵ D.W.Smith, "Optical network technology", Chapman and Hall, London, 1995.
- ⁶ G.Prati, "Photonic networks", Springer Verlag, Berlin, 1997.
- ⁷ W.J.Tomlinson, "Wavelength multiplexing in multimode optical fibres", Applied Optics, **16**, 8, pp2180, 1977.
- ⁸ N.A.Olsson, "68.3 km transmission with 1.37 Tbit km/s capacity using wavelength division multiplexing of ten single frequency lasers at 1.5 μm ", Electronics Letters, **21**, 3, pp105, 1985 .
- ⁹ J.Hecht, "How persistence paid off for the pioneers of fibre optics", Physics World, pp 14, July 1996.
- ¹⁰ T.G.Lynch et al, "Experimental field trial demonstration of a managed multinode reconfigurable wavelength routed optical network", Proc ECOC'92, Paper ThA.12.4, 1992.
- ¹¹ T.Matsumoto, M.Jinno, K.Kimura, K.Noguchi, "Studies on optical digital cross-connect systems for very high speed optical communication networks", Proc ICC'94, pp1060, 1994.
- ¹² J.Zhou, M.J.O'Mahony, "Power management system design modelling of optical multi-wavelength transport networks", Proc Globecom'94, pp1, 1994 .
- ¹³ R.S.Vodhanel, J.-C.Chiao, G.-K.Chang, C.Gibbons, F.Sheladeh, T.Suzaki, "Performance of an 8 wavelength 8 node WDM ring network experiment with 80 Gbit/s capacity", Proc OFC'96, Paper PD28, 1996. .
- ¹⁴ M.Fukui, M.Fukutoku, T.Sakamoto, K.Shimano, K.Okamoto, M.Yamada, K.Oda, H.Toba, "Experimental verification of cascading of 12 channel x 2.5 Gbit/s WDM add drop multiplexer employing unequally spaced arrayed waveguide grating", Proc ECOC'96, Paper ThD.1.1, 1996.
- ¹⁵ M.Koga, A.Watanabe, S.Okamoto, K.Sato, H.Takahashi, M.Okuno, "Optical path cross connect demonstrator designed to achieve 320 Gbit/s", Proc ECOC'96, Paper ThC.3.1, 1996. .
- ¹⁶ L.Bertherton, C.Coeurjolly, P.A.Perrier, A.Noury, S.Ruggeri, P.Gavignet, V.Havard, S.Gauchard, H.Fevrier, "Over 40,000 km path across a layered network by recirculation through an experimental WDM network", Proc ECOC'96, Paper MoA.4.1, 1996.
- ¹⁷ R.Kashyap, "Photosensitive optical fibres: Devices and applications", Optical Fiber Technology, **1**, 1, pp17, 1994.
- ¹⁸ T.S.Kinsel, R.T.Denton, "Terminals for a high speed optical pulse code modulation communication system: II. Optical multiplexing and demultiplexing", Proceedings of the IEEE, **56**, 2, pp146, 1968.
- ¹⁹ S.Kawanishi, H.Takara, T.Morioka, O.Kamatani, K.Takiguchi, T.Kitoh, M.Saruwatari, "Single channel 400 Gbit/s time division multiplexed transmission of 0.98 ps pulses over 40 km employing dispersion slope compensation", Electronics Letters, **32**, 10, pp916, 1996.
- ²⁰ A.D.Ellis, T.Widdowson, "690 node global OTDM network demonstration", Electronics Letters, **31**, 4, pp1171, 1995.
- ²¹ C.Lin, "Optoelectronic technology and Lightwave Communications Systems", Van Nostrand Reinhold, New York, 1989.
- ²² C.K.Kao & G.Hockham "Dielectric fiber surface waveguides for optical frequencies", Proc IEE, **133**, pp1151, 1985.
- ²³ A.C.Newell, J.V.Moloney, "Nonlinear optics", Addison Wesley, Redwood City, 1992.
- ²⁴ G. P. Agrawal, "Nonlinear fibre optics", Academic Press, London, 1989.
- ²⁵ C.D.Poole & R.E.Wagner, "Phenomenological approach to polarisation dispersion in single mode fibres", Electronics Letters, **22**, pp1029-30.
- ²⁶ R.W.Eason, A.Miller, "Nonlinear optics in signal processing", Chapman and Hall, London, 1993.
- ²⁷ R.W.Boyd, "Nonlinear Optics", Academic Press, San Diego, 1992.
- ²⁸ E.Desurvire, "Erbium doped fiber amplifiers, principles and applications", John Wiley and Sons, New York, 1994.
- ²⁹ J.A.Arnaud, "Enhancement of optical receiver sensitivities by amplification of the carrier", IEEE Journal of Quantum Electronics, **4**, 11, pp893, 1968.

- ³⁰ A.Yariv, "Signal to noise ratio considerations in fibre links with periodic or distributed optical amplification", *Optics Letters*, **15**, 9, pp1064, 1990.
- ³¹ R.A.Fisher, W.K.Bischel, *Applied Physics Letters*, **23**, 661, 1973.
- ³² J.R.Taylor, "Optical solitons - theory and experiment", Cambridge University Press, Cambridge, 1992.
- ³³ A.Hasagawa, F.Tappert, "Transmission of stationary nonlinear pulses in dispersive dielectric fibres", *Applied Physics Letters*, **23**, pp142, 1973.
- ³⁴ L.F.Mollenauer, R.H.Stolen, J.P.Gordon, "Experimental observation of picosecond pulse narrowing and solitons in optical fibers", *Physics Review Letters*, **45**, pp1095, 1980.
- ³⁵ K.Iwatsuki, A.Takada, M.Saruwatari, "Optical soliton propagation using 3 GHz gain switched 1.3 μm laser diodes", *Electronics Letters*, **24**, pp1572, 1988.
- ³⁶ J.J.E.Reid, C.T.H.F.Liedenbaum, L.F.Tiemeijer, P.I.Kuindersma, "Realisation of 20 Gbit/s long haul soliton transmission at 1300 nm on standard single mode optical fibre", *Proc ECOC'94*, Paper PD-4, 1994.
- ³⁷ F.M.Knox, W.Forysiak, N.J.Doran, "10 Gbit/s soliton communications systems over standard fibre at 1.55 μm and the use of dispersion compensation", *Journal of Lightwave Technology*, **13**, 10, pp1955, 1995.
- ³⁸ A.Hasegawa, "Optical solitons in fibers", Springer Verlag, Berlin, 1990.
- ³⁹ J.P.Gordon, "Interaction forces among solitons in optical fibres", *Optics Letters*, **8**, 11, pp396, 1983.
- ⁴⁰ V.I.Karpman, V.V.Solov'ev, "A perturbational approach to the two soliton system", *Physica D3*, pp487, 1981.
- ⁴¹ K.J.Blow, N.J.Doran, "Bandwidth limits of nonlinear (soliton) optical communication systems", *Electronics Letters*, **19**, pp429, 1983.
- ⁴² B.Hermansson, D.Yeumerical investigation of soliton interaction", *Electronics Letters*, **19**, pp570, 1983.
- ⁴³ F.M.Mitschke, L.F.Mollenauer, "Experimental observation of interaction forces between solitons in optical fibers", *Optics Letters*, **12**, pp355, 1987.
- ⁴⁴ J.Satsuma, N.Yajima, "Initial value problems of one dimensional self modulation of nonlinear waves in dispersive media", *Progress Theoretical Physics, Supplement*, **55**, pp284, 1974.
- ⁴⁵ A.Hasegawa, Y.Kodama, "Signal transmission by optical solitons in monomode fibre", *Proceedings of the IEEE*, **69**, 9, pp1145, 1981
- ⁴⁶ H.Kubota, M.Nakazawa, "Long distance optical soliton transmission with lumped amplifiers", *IEEE Journal of Quantum Electronics*, **26**, 4, pp692, 1990.
- ⁴⁷ K.J.Blow, N.J.Doran, "Average soliton dynamics and the operation of soliton systems with lumped amplifiers", *IEEE Photonics Technology Letters*, **3**, 4, pp369, 1991.
- ⁴⁸ A.Hasegawa, Y.Kodama, "Guiding Centre Soliton", *Physical Review Letters*, **66**, 2, pp161, 1991.
- ⁴⁹ A.D.Ellis, J.D.Cox, D.Bird, J.Regault, J.V.Wright, W.A.Stallard, "5 Gbit/s soliton propagation over 350 km with large periodic dispersion coefficient perturbations using erbium doped fibre amplifier repeaters", *Electronics Letters*, **27**, 10, pp878, 1991.
- ⁵⁰ A.D.Ellis, D.A.Cleland, J.D.Cox, W.A.Stallard, "Two channel soliton transmission over 678 km", *Proc OFC'92*, paper WC3, 1992.
- ⁵¹ L.F.Mollenauer, E.Lichtman, G.T.Harvey, M.J.Neubelt, B.M.Nyman, "Demonstration of error free soliton transmission over more than 15000 km at 5 Gbit/s single channel and over more than 11000 km at 10 Gbit/s in a two channel WDM", *Electronics Letters*, **28**, pp792, 1992.
- ⁵² M.Nakazawa, H.Kubota, "Optical soliton communication in a positively and negatively dispersion allocated optical fibre transmission line", *Electronics Letters*, **31**, 3, pp216, 1995.
- ⁵³ J.M.Jacob, E.A.Golovchenko, A.N.Pilipetskii, G.M.Carter, C.R.Menyuk, "Experimental demonstration of soliton transmission over 28 Mn using mostly normal dispersion fibre", *IEEE Photonics Technology Letters*, **9**, 1, pp130, 1997.
- ⁵⁴ S.M.J.Kelly, "Characteristic sideband instability of periodically amplified average soliton", *Electronics Letters*, **28**, 8, pp806, 1992.
- ⁵⁵ N.J.Doran, "Nonlinear fibre devices and soliton communications", in : D.B.Ostrowsky, R.Reinsch (eds), "Guided Wave Nonlinear Optics", Kluwer Academic Publishers, 1992.
- ⁵⁶ J.V.Wright, S.F.Carter, "Constraints on the design of long haul soliton systems", *Proc NGWP'92*.

- ⁵⁷ J.P.Gordon, H.A.Haus, "Random walk of coherently amplified solitons in optical fiber transmission", *Optics Letters*, **11**, 10, pp665, 1986.
- ⁵⁸ L.F.Mollenauer, B.M.Nyman, M.J.Neubelt, G.Raybon, S.G.Evangelides, "Demonstration of soliton transmission at 2.4 Gbit/s over 12 000km", *Electronics Letters*, **27**, 2, pp178, 1991.
- ⁵⁹ M.Ding, K.Kikuchi, "Limits of long distance soliton transmission in optical fibers with laser diodes as pulse sources", *IEEE Photonics Technology Letters*, **4**, 6, pp667, 1992.
- ⁶⁰ K.Qiu, "Soliton position jitter caused by periodic amplification and self frequency shift", *Electronics Letters*, **30**, 5, pp439, 1994.
- ⁶¹ L.F.Mollenauer, J.P.Gordon, "Birefringence mediated timing jitter in soliton transmission", *Optics Letters*, **19**, 6, pp375, 1994.
- ⁶² E.M.Dianov, A.V.Luchnikov, A.N.Pilipetskii, A.M.Prokhorov, "Long range interaction of solitons in ultra long communication systems", *Soviet Journal of Lightwave Communication*, **1**, pp235, 1991.
- ⁶³ L.F.Mollenauer, K.Smith, J.P.Gordon, C.R.Menyuk, "Resistance of solitons to the effects of polarisation dispersion in optical fibres", *Optics Letters*, **14**, pp1219, 1989.
- ⁶⁴ D.Wood, "Constraints on the bit rates in direct detection optical communication systems using linear or soliton pulses", *Journal of Lightwave Technology*, **8**, 7, pp1097, 1990.
- ⁶⁵ A.B.Grudin, I.A.Goncharenko, "Increased amplifier spacing in soliton system with partial dispersion compensation", *Electronics Letters*, **32**, 17, pp1602, 1996.
- ⁶⁶ M.Suzuki, H.Tanaka, N.Edagawa, Y.Mitsushima, "New applications of a sinusoidally driven InGaAsP electroabsorption modulator to in line optical gates with ASE noise reduction effect", *Journal of Lightwave Technology*, **10**, pp1912, 1992.
- ⁶⁷ M.Jinno, "All optical signal regularising/regeneration using a nonlinear fiber Sagnac interferometer switch with signal clock walk off", *Journal of Lightwave Technology*, **12**, 9, pp1648, 1994.
- ⁶⁸ T.S.Kinsel, F.S.Chen, "Experimental evaluation of an optical time division demultiplexer for twenty four channels", *Applied Optics*, **11**, 6, pp1411, 1972.
- ⁶⁹ R.S.Tucker, G.Eisenstein, S.K.Korotky, "Optical time division multiplexing for very high bit rate transmission", *Journal of Lightwave Technology*, **6**, 11, pp1737, 1988.
- ⁷⁰ J.P.King, I.Hardcastle, H.J.Harvey, P.D.Greene, B.J.Shaw, M.G.Jones, D.J.Forbes, M.C.Wright, "Polarisation independent 20 Gbit/s soliton data transmission over 12,500 km using amplitude and phase modulation soliton transmission control", *Electronics Letters*, **31**, 13, pp1090, 1995.
- ⁷¹ J.M.Senior, "Optical Fiber Communications, Principles and Practice", Prentice Hall International (UK) Ltd, Hemel Hempstead, Second Edition, 1992.
- ⁷² D.M.Bird, R.M.Fatah, M.K.Cox, P.D.Constantine, J.C.Regault, K.H.Cameron, "Miniature packaged actively mode locked semiconductor laser with tuneable 20 ps transform limited pulses", *Electronics Letters*, **26**, 25, pp2086, 1990.
- ⁷³ A.D.Ellis, T.Widdowson, X.Shan, G.E.Wickens, D.M.Spirit, "Transmission of a true single polarisation 40 Gbit/s soliton data signal over 205 km using a stabilised erbium fibre ring laser and 40 GHz electronic timing recovery", *Electronics Letters*, **29**, 11, pp990, 1993.
- ⁷⁴ X.Shan, T.Widdowson, D.J.Malyon, A.D.Ellis, D.M.Spirit, "Comparison of soliton sources for communication applications", *IEE Colloquium Digest 1994/120*, paper 6, 1994.
- ⁷⁵ J.M.Wiesenfeld, J.Stone, "Chirp in picosecond film lasers and pulse compression by linear dispersion in optical fibers", *Optics Letters*, **8**, pp262, 1983.
- ⁷⁶ P-L.Liu, C.Lin, I.P.Kaminow, J.J.Hsieh, "Picosecond pulse generation from InGaAsP lasers at 1.25 and 1.3 μ m by electrical pulse pumping", *IEEE Journal of Quantum Electronics*, **17**, 5, pp671, 1981.
- ⁷⁷ S.Tarucha, K.Otsuka, "Response of semiconductor laser to deep sinusoidal injection current modulation", *IEEE Journal of Quantum Electronics*, **17**, 5, pp810, 1981.
- ⁷⁸ A.J.Taylor, J.M.Wiesenfeld, G.Eisenstein, R.S.Tucker, "Timing jitter in mode locked and gain switched InGaAsP injection lasers", *Applied Physics Letters*, **49**, 12, pp681, 1986.
- ⁷⁹ A.G.Weber, W.Rongham, E.Hoilger Böttcher, M.Schell, D.Binberg, "Measurement and simulation of the turn on delay and time jitter in gain switched semiconductor lasers", *IEEE Journal of Quantum Electronics*, **28**, 2, pp441, 1992.
- ⁸⁰ A.Takada, T.Sugie, M.Saruwatari, "Transform limited 5.6 ps optical pulse generation at 12 GHz repetition rate from gain-switched distributed feedback laser diode by employing pulse compression technique", *Electronics Letters*, **22**, 25, pp1347, 1986.
- ⁸¹ A.D.Ellis, D.A.O.Davies, A.Kelly, W.A.Pender, "Data driven operation of semiconductor amplifier loop mirror at 40 Gbit/s", *Electronics Letters*, **31**, 15, pp1245, 1995.

- ⁸² M.Schell, D.Huhse, D.Bimberg, "Generation of 2.5 ps light pulses with 15 nm wavelength tunability at 1.3 μm by self seeded gain switched semiconductor laser", *IEEE Photonics Technology Letters*, **5**, 11, pp1267, 1993.
- ⁸³ M.Vaa, B.Mikkelsen, K.S.Jepsen, K.E.Stubkjaer, M.Schilling, K.Daub, E.Lach, G.Laube, W.Idler, K.Wunstel, S.Bourhoule, C.Kazmierski, D.Mathoorasing, "A bit rate flexible and power efficient all optical demultiplexer realised by monolithically integrated Michelson interferometer", *Proc ECOC'96*, Paper ThB.3.3, 1996.
- ⁸⁴ F.Zamkotsian, K.Sato, H.Okamoto, K.Kishi, I.Kotaka, M.Yamamoto, Y.Kondo, H.Yasaka, Y.Yoshikuni, K.Oe, "An InP based optical multiplexer integrated with modulators for 100 Gbit/s transmission", *Proc ECOC'94*, PD Paper, pp 105, 1994, and "Generation and coding of a 100 Gbit/s signal by an InP-based optical multiplexer integrated with modulators", *Electronics Letters*, **31**, 7, pp578, 1995.
- ⁸⁵ M.Jinno, "Effect of timing jitter on an optically controlled picosecond optical switch", *Optics Letters*, **18**, 17, pp1409, 1993.
- ⁸⁶ K.Suzuki, K.Iwatsuki, S.Nishi, M.Saruwatari, "Error free demultiplexing of 160 Gbit/s pulse signal using optical loop mirror including semiconductor laser amplifier", *Electronics Letters*, **30**, 18, pp1501, 1994.
- ⁸⁷ K.J.Blow, D.Wood, "The evolution of solitons from non-transform limited pulses", *Optics Communications*, **58**, 5, pp349, 1986.
- ⁸⁸ D.S.Seo, K.Y.Kim, H.F.Liu, "Timing jitter reduction of gain switched DFB laser by external injection seeding", *Electronics Letters*, **30**, 20, pp1700, 1994.
- ⁸⁹ P.Gunning, J.K.Lucek, D.G.Moodie, K.Smith, R.P.Davey, S.V.Chernikov, M.J.Guy, J.R.Taylor, A.S.Siddiqui, "Gain switched DFB laser diode pulse source using continuous wave light injection for jitter suppression and an electroabsorption modulator for pedestal suppression", *Electronics Letters*, **32**, 11, pp1010, 1996.
- ⁹⁰ K.A.Ahmed, B.J.Eggleton, H.F.Liu, P.A.Krug, F.Ouellette, "Simultaneous mode selection and pulse compression of gain switched pulses from a Fabry-Perot laser using a 40 mm chirped optical fiber grating", *IEEE Photonics Technology Letters*, **7**, 158, 1995.
- ⁹¹ P.Gunning, R.Kashyap, A.S.Siddiqui, K.Smith, "Picosecond pulse generation of <5ps from gain switched DFB semiconductor laser diode using linearly step chirped fibre gratings", *Electronics Letters*, **31**, 13, pp1066, 1995.
- ⁹² M.Nakazawa, K.Suzuki, Y.Kimura, "Generation and transmission of optical solitons in the gigahertz region using a directly modulated distributed feedback laser diode", *Optics letters*, **15**, 10, pp588, 1990.
- ⁹³ J.M.Wiesenfeld, M.Kuznetsov, "Tunable picosecond pulse generation using a compressed modelocked laser diode source", *IEEE Photonics Technology Letters*, **2**, 5, pp319, 1990.
- ⁹⁴ A.S.Hou, R.S.Tucker, G.Eisenstein, "Pulse compression of an actively modelocked diode laser using linear dispersion in fiber", *IEEE Photonics Technology Letters*, **2**, 5, pp322, 1990.
- ⁹⁵ R.Ludwig, A.Erhrhardt, "Turnkey ready wavelength repetition rate and pulse width tunable femtosecond hybrid modelocked laser", *Electronics Letters*, **31**, 14, pp1165, 1995.
- ⁹⁶ A.Takada, K.Sato, M.Saruwatari, M.Yamamoto, "Pulse width tunable subpicosecond pulse generation from an actively modelocked monolithic MQW laser/MQW electroabsorption modulator", *Electronics Letters*, **30**, 11, pp898, 1994.
- ⁹⁷ R.P.Davey, K.Smith, A.McGuire, "High speed mode locked tunable integrated erbium fibre laser", *Electronics Letters*, **28**, 5, pp482, 1992.
- ⁹⁸ M.Nakazawa, E.Yoshida, "Direct generation of a 750 fs, 10GHz pulse train from a regeneratively mode locked fibre laser with multiple harmonic modulation", *Electronics Letters*, **32**, 14, pp1291, 1996.
- ⁹⁹ X.Shan, D.A.Cleland, A.D.Ellis, "Stabilising Er fibre soliton laser with pulse phase locking", *Electronics Letters*, **28**, 2, pp182, 1992.
- ¹⁰⁰ D.J.Kuizenga, A.E.Siegman, "FM and AM mode locking of the homogeneous laser - Part II: Experimental results in a Nd:YAG laser with internal FM modulation", *IEEE Journal of Quantum Electronics*, **6**, 11, pp700, 1970.
- ¹⁰¹ G.T.Harvey, L.F.Mollenauer, "Harmonically mode locked fiber ring laser with an internal Fabry Perot stabiliser for soliton transmission", *Optics Letters*, **18**, 2, pp107, 1993.

- ¹⁰² X.Shan, A.D.Ellis, T.Widdowson, G.E.Wickens, D.M.Spirit, "Stabilisation of a 10 GHz mode locked erbium fibre laser and its application in a 4x10Gbit/s soliton transmission", Proc NGWP'93, paper TuD4, 1993.
- ¹⁰³ T.Widdowson, D.J.Malyon, X.Shan, P.J.Watkinson, "Soliton propagation without transmission control using a phase locked erbium fibre ring laser", Electronics Letters, **30**, 8, pp661, 1994.
- ¹⁰⁴ H.Takara, S.Kawanishi, M.Saruwatari, "Stabilisation of a modelocked Er doped fibre laser by suppressing the relaxation oscillation frequency component", Electronics Letters, **31**, 4, pp292, 1995.
- ¹⁰⁵ M.Nakazawa, K.Tamura, E.Yoshida, "Supermode noise suppression in a harmonically mode locked fibre laser by selfphase modulation and spectral filtering", Electronics Letters, **32**, 5, pp1285, 1996.
- ¹⁰⁶ X.Shan, T.Widdowson, A.D.Ellis, A.S.Siddiqui, "Very simple method to stabilise mode locked erbium fibre lasers", Electronics Letters, **32**, 11, pp1015, 1996.
- ¹⁰⁷ D.J.Kuizenga, A.E.Siegman, "FM and AM mode locking of the homogeneous laser - Part I: Theory", IEEE Journal of Quantum Electronics, **6**, 11, pp695, 1970.
- ¹⁰⁸ M.DiDomenico, J.E.Geusic, H.M.Marcos, R.G.Smith, "Generation of ultrashort optical pulses by mode locking the YAIG:Nd laser", Applied Physics Letters, **8**, pp180, 1966.
- ¹⁰⁹ S.P.Dijaili, J.S.Smith, A.Dienes, "Timing synchronisation of a passively mode locked dye laser using a pulsed optical phase lock loop", Applied Physics Letters, **55**, 5, pp418, 1989.
- ¹¹⁰ B.P.Nelson, K.Smith, K.J.Blow, "Mode locked erbium fibre laser using an all optical nonlinear loop mirror", Electronics Letters, **28**, pp656, 1992.
- ¹¹¹ E.J.Greer, K.Smith, "All optical FM modelocking of fibre lasers", Electronics Letters, **28**, pp1741, 1992.
- ¹¹² A.D.Ellis, K.Smith, D.M.Patrick, "All optical clock recovery at bit rates up to 40 Gbit/s", Electronics Letters, **29**, 15, pp1323, 1993.
- ¹¹³ E.J.Greer, Y.Kimura, K.Suzuki, E.Yoshida, M.Nakazawa, "Generation of 1.2 ps 10 GHz pulse train from all optically modelocked erbium fibre ring laser with active nonlinear polarisation rotation", Electronics Letters, **30**, 21, pp1764, 1994.
- ¹¹⁴ K.Tamura, E.P.Ippen, H.A.Haus, L.E.Nelson, "77-fs pulse generation from a stretched pulse mode locked all fiber ring laser", Optics Letters, **18**, 13, pp1080, 1993.
- ¹¹⁵ H.A.Haus, S.T.Kirsch, K.Mathysek, F.J.Leonberger, "Picosecond Optical Sampling", IEEE Journal of Quantum Electronics, **16**, 8, pp870, 1980.
- ¹¹⁶ L.C.Blank, "High Capacity Optical Fibre Transmission Systems", PhD Thesis, School of Electronic Engineering Science, University of Wales, Bangor, Gwynedd, UK, 1992.
- ¹¹⁷ J.J.Veselka, S.K.Korotky, P.V.Mamyshev, A.H.Gnauck, G.Raybon, N.M.Froberg, "A soliton transmitter using a cw laser and an NRZ driven Mach-Zehnder modulator", IEEE Photonics Technology Letters, **8**, 7, pp950, 1996.
- ¹¹⁸ A.D.Ellis, T.Widdowson, X.Shan, D.G.Moodie, "Three node 40 Gbit/s OTDM network experiment using electro-optic switches", Electronics Letters, **30**, 16, pp1333, 1994.
- ¹¹⁹ P.A.Krug, D.M.Spirit, L.C.Blank, "Transmission study of optical pulses at 6.2 Gbit/s generated using LiNbO3 modulators to externally modulate cw lasers", Proc 17th ACOFT, 1992.
- ¹²⁰ M.Suzuki, H.Tanaka, K.Utaka, N.Edagawa, Y.Matsushima, "Transform limited 14 ps optical pulse generation with 15 GHz repetition rate by InGaAsP electroabsorption modulator", Electronics Letters, **28**, 11, pp1007, 1992.
- ¹²¹ D.G.Moodie, A.D.Ellis, A.R.Thurlow, M.J.Harlow, I.F.Lealman, S.D.Perrin, L.J.Rivers, M.J.Robertson, "Multi-quantum well electroabsorption modulators for 80 Gbit/s OTDM systems", Electronics Letters, **31**, 16, pp1370, 1995.
- ¹²² K.Wakita, K.Sato, I.Kotaka, M.Yamamoto, M.Asobe, "Transform limited 7 ps optical pulse generation using a sinusoidally driven InGaAsP / InGaAsP stained multiple quantum well DFB laser/modulator monolithically integrated", IEEE Photonics Technology Letters, **5**, 8, pp899, 1993.
- ¹²³ G.Raybon, M.G.Young, U.Koren, B.I.Miller, M.Chien, M.Zirngibl, C.Dragone, N.M.Froberg, C.A.Burrus, "Five channel WDM soliton pulse generation using sinusoidally driven electroabsorption modulators in 16 x 1 laser/modulator array", Electronics Letters, **31**, 14, pp1147, 1995.
- ¹²⁴ N.M.Froberg, G.Raybon, A.M.Johnson, Y.K.Chen, T.Tanbun-ek, R.A.Logan, A.Tate, A.M.Sargent, K.Weicht, P.F.Sciortino, "Pulse generation by harmonic modulation of an integrated DBR laser-modulator", Electronics Letters, **30**, 8, pp650, 1994.

- ¹²⁵ D.G.Moodie, A.D.Ellis, C.W.Ford, "Generation of 6.3 ps optical pulses at a 10 GHz repetition rate using a packaged electroabsorption modulator and dispersion decreasing fibre", *Electronics Letters*, **30**, 20, pp1700, 1994.
- ¹²⁶ D.G.Moodie, "Electroabsorption modulators and their impact on future telecommunication networks", MSc Thesis, Electronic and Electrical Engineering Department, University College London, London, UK, 1994.
- ¹²⁷ M.J.Guy, S.V.Chernikov, J.R.Taylor, D.G.Moodie, R.Kashyap, "Generation of transform limited optical pulses at 10 GHz using an electroabsorption modulator and a chirped fibre Bragg grating", *Electronics Letters*, **31**, 8, pp671, 1995.
- ¹²⁸ A.D.Ellis, M.C.Tatham, D.A.O.Davies, D.Nessett, D.G.Moodie, G.Sherlock, "40 Gbit/s transmission over 202 km of standard fibre using mid span spectral inversion", *Electronics Letters*, **31**, 4, pp299, 1995.
- ¹²⁹ D.D.Marcenac, A.D.Ellis, D.G.Moodie, "80 Gbit/s OTDM using electroabsorption modulators", Submitted to *Electronics Letters*.
- ¹³⁰ N.M.Froberg, G.Raybon, U.Koren, B.I.Miller, M.G.Young, M.Chien, G.T.Harvey, A.Gnauck, A.M.Johnson, "Generation of 2.5 Gbit/s soliton data stream with an integrated laser-modulator transmitter", *Electronics Letters*, **30**, 22, pp1880, 1994.
- ¹³¹ D.G.Moodie, P.J.Cannard, A.J.Dann, D.D.Marcenac, C.W.Ford, J.Reed, R.T.Moore, J.K.Lucek, A.D.Ellis, "Low polarisation sensitivity buried heterostructure electroabsorption modulators for ultra high speed networks", Submitted to ECOC'97.
- ¹³² J.K.Lucek, P.Gunning, D.G.Moodie, K.Smith, A.D.Ellis, "High granularity channel selection using an electroabsorption modulator for ultrafast LAN applications", *Proc ECOC'96*, paper ThD.1.8, 1996.
- ¹³³ J.K.Lucek, P.Gunning, D.G.Moodie, K.Smith, A.D.Ellis, D.Pitcher, "Optical TDMA channel selection using electroabsorption modulator with dual frequency drive", *Electronics Letters*, **33**, 1, pp22, 1997.
- ¹³⁴ J.T.Manassah, M.A.Mustafa, R.R.Alfano, P.P.Ho, "Spectral extent and pulse shape of the supercontinuum for ultrashort laser pulse", *IEEE Journal of Quantum Electronics*, **22**, 1, pp197, 1986.
- ¹³⁵ T.Morioka, S.Kawanishi, K.Mori, M.Saruwatari, "Nearly penalty free <4 ps supercontinuum Gbit/s pulse generation over 1535 - 1560 nm", *Electronics Letters*, **30**, 10, pp790, 1994.
- ¹³⁶ P.V.Mamyshev, "Dual wavelength source of high repetition rate transform limited optical pulses for soliton transmission", *Optics Letters*, **19**, pp2074, 1994.
- ¹³⁷ O.G.Okhotnikov, F.M.Araujo, "Pulse generation through optical switching in phase driven loop mirror", *Electronics Letters*, **31**, 25, pp2197, 1995.
- ¹³⁸ A.Boskovic, S.V.Chernikov, J.R.Taylor, "Femtosecond figure of eight Yb:Er fibre laser incorporating a dispersion decreasing fibre", *Electronics Letters*, **31**, 17, pp1446, 1995.
- ¹³⁹ S.Gray, A.B.Grudinn, "Passive harmonically modelocked fiber soliton laser with repetition rate above 2 GHz", *Optical Fiber Technology*, **2**, pp241, 1996.
- ¹⁴⁰ M.Nakazawa, K.Suzuki, "Generation of pseudorandom dark soliton data train and its coherent detection by one bit shifting with a Mach-Zehnder interferometer", *Electronics Letters*, **31**, 13, pp1084, 1995.
- ¹⁴¹ S.V.Chernikov, J.R.Taylor, "Multigigabit/s pulse source based on the switching of an optical beat signal in a nonlinear fibre loop mirror", *Electronics Letters*, **29**, 8, pp658, 1993.
- ¹⁴² P.A.Morton, V.Mizrahi, L.F.Mollenauer, T.Tanbun-Ek, R.A.Logan, H.M.Presby, T.Erdogan, A.M.Sergent, K.W.Weicht, "Packaged hybrid soliton pulse source results and 270 Terabit.km/sec soliton transmission", *IEEE Photonics Technology Letters*, **7**, 1, pp111, 1995.
- ¹⁴³ Z.Wang, J.M.Nielsen, S.D.Brorson, B.Christensen, T.Franck, N.G.Jensen, A.M.Larsen, J.Norregaard, E.Bodtker, "15.8 Gbit/s system transmission experiment using a 5.2 mm long monolithic colliding pulse modelocked quantum well laser diode", *Electronics Letters*, **31**, 4, pp272, 1995.
- ¹⁴⁴ D.M.Patrick, A.D.Ellis, "10GHz pulse train derived from a cw DFB laser using crossphase modulation in an optical fibre", *Electronics Letters*, **29**, 15, pp1391, 1993.
- ¹⁴⁵ R.A.Betts, J.W.Lears, S.J.Frisken, P.S.Atherton, "Generation of transform limited optical pulses using all-optical gate", *Electronics Letters*, **28**, 11, pp1035, 1992.
- ¹⁴⁶ A.D.Ellis, D.M.Spirit, "Compact 40 Gbit/s optical demultiplexer using a GaInAsP optical amplifier", *Electronics Letters*, **29**, 24, pp2115, 1993.

- ¹⁴⁷ L.Noel, X.Shan, A.D.Ellis, "Four WDM channel NRZ to RZ format conversion using a single semiconductor laser amplifier", *Electronics Letters*, **31**, 4, pp277, 1995.
- ¹⁴⁸ M.W.Street, D.Nesset, A.D.Ellis, J.H.Marsh, S.J.Aitchison, "Generation of high peak power (615 W) subpicosecond pulses using a gain switched distributed feedback laser diode and a nonlinear fiber compression technique", *Proc CLEO'96*, paper CMK5, 1996.
- ¹⁴⁹ W.J.Tomlinson, R.H.Stolen, C.V.Shank, "Compression of pulses chirped by self phase modulation in fibers", *Journal of the Optical Society of America*; B, **1**, 2, pp139, 1994.
- ¹⁵⁰ D.Grischowsky, A.C.Balant, "Optical pulse compression based on enhanced frequency chirping", *Applied Physics Letters*, **41**, 1, pp1, 1982.
- ¹⁵¹ A.D.Ellis, D.M.Patrick, D.Flannery, R.J.Manning, D.A.O.Davies, D.M.Spirit, "Ultra high speed OTDM networks using semiconductor amplifier based processing nodes", *Journal of Lightwave Technology*, **13**, 5, pp761, 1995.
- ¹⁵² H.H.Kuehl, "Solitons on an axially nonuniform optical fiber", *Journal of the Optical Society of America* B, **5**, 3, pp709, 1988.
- ¹⁵³ V.A.Bogatryrev, M.M.Bubnov, E.M.Dianov, A.S.Kurkov, P.V.Mamyshev, A.M.Prokhorov, S.D.Rumyantsev, V.A.Semenov, S.L.Semenov, A.J.Sysoliatin, S.V.Chernikov, A.N.Gur'yanov, G.G.Devyatykh, S.I.Miroshnichenko, "A single mode fiber with chromatic dispersion varying along the length", *Journal of Lightwave Technology*, **9**, 5, pp561, 1991.
- ¹⁵⁴ S.V.Chernikov, D.J.Richardson, E.M.Dianov, D.N.Payne, "Picosecond soliton pulse compressor based on dispersion decreasing fibre", *Electronics Letters*, **28**, 19, pp1842, 1992.
- ¹⁵⁵ K.Suzuki, K.Iwatsuki, S.Nishi, M.Saruwatari, K.Sato, K.Wakita, "2.5 ps soliton pulse generation at 15 GHz with monolithically integrated MQW-DFB-LD/MQW-EA modulator and dispersion decreasing fibre", *Electronics Letters*, **29**, 19, pp1713, 1993.
- ¹⁵⁶ N.J.Doran, K.J.Blow, "Solitons in optical communications", *IEEE Journal of Quantum Electronics*, **19**, 12, pp1883, 1983.
- ¹⁵⁷ K.Tajima, "Compensation of soliton broadening in nonlinear optical fibres with loss", *Optics Letters*, **12**, pp54, 1987.
- ¹⁵⁸ K.J.Blow, N.J.Doran, D.Wood, "Generation and stabilization of short soliton pulses in the amplified nonlinear Schrodinger equation", *Journal of the Optical Society of America* B, **5**, 2, pp381, 1988.
- ¹⁵⁹ D.J.Richardson, Private communication, 1996.
- ¹⁶⁰ M.Nakazawa, K.Kurokawa, H.Kubota, K.Suzuki, Y.Kimura, "Femtosecond erbium doped fibre amplifier", *Applied Physics Letters*, **57**, pp653, 1990.
- ¹⁶¹ M.Nakazawa, K.Kurokawa, H.Kubota, E.Yamada, "Observation of the trapping of an optical soliton by adiabatic gain narrowing and its escape", *Physical Review Letters*, **65**, 15, pp1881, 1990.
- ¹⁶² M.Nakazawa, E.Yoshida, H.Kubota, Y.Kimura, "Generation of a 170 fs, 10 GHz transform limited pulse train at 1.55 μ m using a dispersion decreasing, erbium doped active soliton compressor", *Electronics Letters*, **30**, 24, pp2038, 1994.
- ¹⁶³ M.J.Guy, S.V.Chernikov, J.R.Taylor, D.G.Moodie, R.Kasyap, "200 fs soliton pulse generation at 10 GHz through nonlinear compression of transform limited pulses from an electroabsorption modulator", *Electronics Letters*, **31**, 9, pp740, 1995.
- ¹⁶⁴ F.Koyama, K.Iga, "Frequency Chirping in external modulators", *Journal of Lightwave Technology*, **6**, 1, pp87, 1988.
- ¹⁶⁵ E.M.Dianov, P.V.Mamyshev, A.M.Prokhorov, S.V.Chernikov, "Generation of a train of fundamental solitons at a high repetition rate in optical fibers", *Optics Letters*, **14**, 18, pp1008, 1989.
- ¹⁶⁶ P.V.Mamyshev, S.V.Chernikov, E.M.Dianov, "Generation of fundamental soliton trains for high bit rate optical fiber communication lines", *IEEE Journal of Quantum Electronics*, **27**, 10, pp2347, 1991.
- ¹⁶⁷ A.V.Shipulin, E.M.Dianov, D.J.Richardson, D.N.Payne, "40 GHz soliton train generation through multisoliton pulse propagation in a dispersion varying optical fiber circuit", *IEEE Photonics Technology Letters*, **6**, 11, pp1380, 1994.
- ¹⁶⁸ E.A.Swanson, S.R.Chin, K.Hall, K.A.Rauschenbach, R.S.Bondurant, J.W.Miller, "A near transform limited 100 GHz soliton pulse train using soliton compression of two phase sidebands from a single laser", *Proc OFC'94*, Paper PD15-1, 1994.
- ¹⁶⁹ S.V.Chernikov, J.R.Taylor, R.Kashyap, "Integrated all optical fibre source of multigigahertz soliton pulse train", *Electronics Letters*, **29**, 20, pp1788, 1993.

- ¹⁷⁰ D.Wake, C.R.Lima, P.A.Davies, "Optical generation of millimetre wave signals for fibre-radio systems using a dual mode DFB semiconductor laser", *IEEE Transactions on Microwave Theory and Technology*, **43**, pp2270, 1995.
- ¹⁷¹ U.Gliese, T.N.Nielsen, M.Bruun, E.L.Christensen, K.E.Stubkjaer, S.Lindergren, B.Broberg, "Wideband heterodyne optical phase locked loop for generation of 3-18 GHz microwave carriers", *IEEE Photonics Technology Letters*, **4**, 936, 1992.
- ¹⁷² D.Cotter, "Stimulated Brillouin scattering in monomode optical fibre", *Journal of Optical Communications*, **4**, pp10, 1983.
- ¹⁷³ S.V.Chernikov, J.R.Taylor, P.V.Mamyshev, E.M.Dianov, "Generation of soliton pulse train in optical fibre using two cw singlemode diode lasers", *Electronics Letters*, **28**, 10, pp931, 1992.
- ¹⁷⁴ E.A.Swanson, S.R.Chin, "40-GHz pulse train generation using soliton compression of Mach-Zehnder modulator output", *IEEE Photonics Technology Letters*, **7**, 1, pp114, 1995.
- ¹⁷⁵ S.V.Chernikov, D.J.Richardson, R.I.Laming, E.M.Dianov, D.N.Payne, "70 Gbit/s fibre based source of fundamental solitons at 1550 nm", *Electronics Letters*, **28**, 13, pp1210, 1992.
- ¹⁷⁶ D.J.Richardson, R.P.Chamberlin, L.Dong, D.N.Payne, A.D.Ellis, T.Widdowson, D.M.Spirit, "Demonstration of 205km transmission of 35 GHz, 5 ps pulses generated from a diode driven low jitter beat signal to soliton train conversion source", *Electronics Letters*, **31**, 6, pp470, 1995.
- ¹⁷⁷ G.E.Wickens, D.M.Spirit, L.C.Blank, "Nonlinear transmission of 20 Gbit/s optical time division multiplexed data over 205 km of dispersion shifted fibre", *Electronics Letters*, **28**, pp117, 1992.
- ¹⁷⁸ M.Eiselt, "Optical loop mirror with semiconductor amplifier", *Electronics Letters*, **28**, 16, pp1505, 1992.
- ¹⁷⁹ T.Morioka, S.Kawanishi, H.Takara, M.Saruwatari, "Multiple output 100 Gbit/s all optical demultiplexer based on multichannel four wave mixing pumped by a linearly chirped square pulse", *Electronics Letters*, **30**, 23, pp1959, 1994.
- ¹⁸⁰ K.J.Blow, N.J.Doran, B.K.Nayar, B.P.Nelson, "Two-wavelength operation of the nonlinear fiber loop mirror", *Optics Letters*, **15**, 4, pp248, 1990.
- ¹⁸¹ D.M.Patrick, A.D.Ellis, D.M.Spirit, "Bit rate flexible all-optical demultiplexing using a nonlinear optical loop mirror", *Electronics Letters*, **29**, 8, pp702, 1993.
- ¹⁸² D.M.Patrick, A.D.Ellis, "Demultiplexing using crossphase modulation-induced spectral shifts and Kerr polarisation rotation in optical fibre", *Electronics Letters*, **29**, 2, pp227, 1993.
- ¹⁸³ ARTEMIS, "RACE project R2015 Final Report", Document R2015/FCL/COE/FR/P/01/b1.
- ¹⁸⁴ S.Bigo, O.Audouin, E.Desurvire, "Analysis of soliton inline regeneration through two wavelength nonlinear loop mirror as synchronous amplitude/phase modulator", *Electronics Letters*, **31**, 25, pp2191, 1995.
- ¹⁸⁵ M.Jinno, T.Matsumoto, "Ultrafast, low power and highly stable all optical switching in an all polarisation maintaining fiber Sagnac interferometer", *IEEE Photonics Technology Letters*, **2**, 5, pp349, 1990.
- ¹⁸⁶ W.S.Lee, A.Hadjifotiou, "Optical transmission over 140 km at 40 Gbit/s by optical time division multiplexing/demultiplexing", *Electronics Letters*, **31**, 12, pp997, 1995.
- ¹⁸⁷ M.Nakazawa, K.Suzuki, E.Yamada, T.Kitoh, M.Kawachi, "160 Gbit/s soliton data transmission over 200 km", *Electronics Letters*, **31**, 7, pp565, 1995.
- ¹⁸⁸ L.F.Mollenauer, P.V.Mamyshev, M.J.Neubelt, "Measurement of timing jitter in filter guided soliton transmission at 10 Gbit/s and achievement of 375 Gbit/s-Mm error free at 12.5 Gbit/s and 15 Gbit/s", *Optics Letters*, **19**, 10, pp704, 1994.
- ¹⁸⁹ J.K.Lucek, K.Smith, "Remotely programmable all optical routing device with optical clock division", *Proc OFC'95*, paper TuD5, 1995.
- ¹⁹⁰ P.E.Barnsley, G.E.Wickens, H.J.Wickes, D.M.Spirit, "A 4x5 Gbit/s transmission system with all optical clock recovery", *IEEE Photonics Technology Letters*, **4**, 1, pp83, 1992.
- ¹⁹¹ M.Nakazawa, K.Suzuki, E.Yamada, "NOLM oscillator and its injection locking technique for timing clock extraction and demultiplexing", *Electronics Letters*, **32**, 12, pp1122, 1996.
- ¹⁹² S.Kawanishi, M.Saruwatari, "Ultra high speed PLL type clock recovery circuit based on all optical gain modulation in travelling wave laser diode amplifier", *Journal of Lightwave Technology*, **11**, 12, pp2123, 1993.
- ¹⁹³ O.Kamatani, S.Kawanishi, "Ultrahigh speed clock recovery with phase lock loop based on four wave mixing in a travelling wave laser diode amplifier", *Journal of Lightwave Technology*, **14**, 8, pp1757, 1996.

- ¹⁹⁴ Y.G.Wey, K.S.Giboney, J.E.Bowers, M.J.W.Rodwell, P.Silvestre, P.Thigarajan, G.Y.Robinson, "108 GHz GaInAs/InP p-i-n photodiodes with integrated bias tees and matched resistors", IEEE Photonics Technology Letters, **5**, 11, pp1310, 1993.
- ¹⁹⁵ K.Smith, J.K.Lucek, "All optical clock recovery using a mode locked laser", Electronics Letters, **28**, pp1814, 1992.
- ¹⁹⁶ S.Bigo, E.Desurvire, "20 GHz all-optical clock recovery based on fibre laser mode locking with fibre nonlinear loop mirror as variable intensity/phase modulator", Electronics Letters, **31**, 21, pp1855, 1995.
- ¹⁹⁷ N.J.Smith, K.J.Blow, W.J.Firth, K.Smith, "Suppression of soliton interactions by periodic phase modulation", Optics Letters, **19**, pp16, 1994.
- ¹⁹⁸ M.Obro, P.Thorsen, S.B.Andreasen, "All optical frame synchronisation recovery", Electronics Letters, **30**, 15, pp1243, 1994.
- ¹⁹⁹ U.Feiste, D.J.As, A.Ehrhardt, "18 GHz all optical frequency locking and clock recovery using a self pulsating two section DFB laser", IEEE Photonics Technology Letters, **6**, 1, pp106, 1994.
- ²⁰⁰ P.Monteiro, J.N.Matos, J.R.F.daRocha, "20 Gbit/s DR based timing recovery circuit", Electronics Letters, **30**, 10, pp799, 1994.
- ²⁰¹ O.Kamatani, S.Kawanishi, "Prescaled timing extraction from 400 Gb/s optical signal using a phase lock loop based on four wave mixing in a laser diode amplifier", IEEE Photonics Technology Letters, **8**, 8, pp1094, 1996.
- ²⁰² D.M.Patrick, R.J.Manning, "20 Gbit/s all optical clock recovery using semiconductor nonlinearities", Electronics Letters, **31**, 20, pp1760, 1995.
- ²⁰³ L.E.Adams, E.S.Kintzer, J.G.Fujimoto, "All optical timing extraction at 40 GHz using a modelocked figure eight laser with an SLA", Electronics Letters, **31**, 20, pp1759, 1995.
- ²⁰⁴ T.Ono, T.Shimizu, Y.Yano, H.Yokayama, "Optical clock extraction from 10 Gbit/s data pulses by using monolithic mode locked laser diodes", Proc OFC'95, paper ThL4, 1995.
- ²⁰⁵ R.Ludwig, W.Pieper, E.Jahn, N.Agrawal, A.Ehrhardt, L.Kuller, H.G.Weber, "10 GHz all optical clock recovery using a mode locked semiconductor laser in a 40 Gbit/s 100 km transmission experiment", Proc OFC'96, paper WH2, 1996.
- ²⁰⁶ M.Jinno, T.Matsumoto, "Optical tank circuits used for all optical timing recovery", IEEE Journal of Quantum Electronics, **28**, 4, pp895, 1992.
- ²⁰⁷ S.Kawanishi, M.Saruwatari, "New type phase locked loop using travelling wave laser diode optical amplifier for very high speed optical transmission", Electronics Letters, **24**, 23, pp1452, 1988.
- ²⁰⁸ K.L.Hall, K.A.Rauschenbach, E.A.Swanson, S.R.Chinn, G.Raybon, "Picosecond accuracy all optical bit phase sensing using a nonlinear optical loop mirror", IEEE Photonics Technology Letters, **7**, 8, pp935, 1995.
- ²⁰⁹ Y.Miyamoto, T.Kataoka, K.Hagimoto, K.Kato, "Data and clock WDM transmission using 20 Gbit/s electrical demultiplexer with waveguide pin photodiode interface", Proc ECOC'94, 1994.
- ²¹⁰ W.A.Pender, T.Widdowson, A.D.Ellis, "Error free operation of a 40 Gbit/s all optical regenerator", Electronics Letters, **32**, 6, pp567, 1996.
- ²¹¹ E.A.Marcatili, "Optical subpicosecond gate", Applied Optics, **19**, 9, pp1468, 1980.
- ²¹² H.Haga, M.Izutsu, T.Sueta, "An integrated 1x4 high speed optical switch and its applications to a time demultiplexer", Journal of Lightwave Technology, **3**, 1, pp116, 1985.
- ²¹³ G.Ishikawa, H.Ooi, Y.Akiyama, S.Taniguchi, H.Nishimoto, "80 Gbit/s (2x40 Gbit/s) transmission experiments over 667 km dispersion shifted fibre using Ti:LiNbO₃ OTDM modulator and demultiplexer", Proc ECOC'96, Paper ThC.3.3, 1996.
- ²¹⁴ D.M.Patrick, A.D.Ellis, D.A.O.Davies, M.C.Tatham, G.Sherlock, "Demultiplexing using polarisation rotation in a semiconductor laser amplifier", Electronics Letters, **30**, 4, pp341, 1994.
- ²¹⁵ T.Morioka, S.Kawanishi, K.Uchiyama, H.Takara, M.Saruwatari, "Polarisation-independent 100 Gbit/s all optical demultiplexer utilising four wave mixing in a polarisation maintaining fibre loop", Electronics Letters, **30**, 7, pp591, 1994.
- ²¹⁶ T.Morioka, H.Takara, S.Kawanishi, T.Kitoh, M.Saruwatari, "Error free 500 Gbit/s all-optical demultiplexing using low noise, low jitter supercontinuum short pulses", Electronics Letters, **32**, 9, pp833, 1996.
- ²¹⁷ T.Morioka, H.Takara, S.Kawanishi, K.Uchiyama, M.Saruwatari, "Polarisation independent all optical demultiplexing up to 200 Gbit/s using four wave mixing in a semiconductor laser amplifier", Electronics Letters, **32**, 9, pp840, 1996.

- ²¹⁸ K.Mori, K.Uchiyama, T.Morioka, M.Saruwatari, "Wavelength conversion with an optical parametric loop mirror", *Electronics Letters*, **32**, 23, pp2171, 1996.
- ²¹⁹ K.Uchiyama, H.Takara, S.Kawanishi, T.Morioka, M.Saruwatari, "100 Gbit/s all optical demultiplexing using nonlinear optical loop mirror with gating width control", *Electronics Letters*, **29**, 21, pp1870, 1993.
- ²²⁰ K.Uchiyama, S.Kawanishi, H.Takara, T.Morioka, M.Saruwatari, "100 Gbit/s to 6.3 Gbit/s demultiplexing experiment using polarisation independent nonlinear optical loop mirror", *Electronics Letters*, **30**, 11, pp873, 1994.
- ²²¹ E.Jahn, N.Agrawal, W.Pieper, H.-J.Ehrke, D.Franke, W.Furst, C.M.Weinert, "Monolithically integrated nonlinear Sagnac interferometer and its application as a 20 Gbit/s all optical demultiplexer", *Electronics Letters*, **32**, 9, pp782, 1996.
- ²²² E.Jahn, N.Agrawal, M.Arbert, H.-J.Ehrke, D.Franke, R.Ludwig, W.Pieper, H.G.Weber, C.M.Weinert, "40 Gbit/s demultiplexing using a monolithically integrated Mach Zehnder interferometer with semiconductor laser amplifiers", *Electronics Letters*, **31**, 21, pp1857, 1995.
- ²²³ B.Mikkelsen, M.Vaa, N.Storkfelt, T.Durhuus, C.Jorgensen, R.J.S.Pedersen, S.L.Danielsen, K.E.Stubkjaer, M.Gustavsson, W.van Berlo, M.Janson, "Monolithic integrated Michelson interferometer with SOAs for high speed all optical signal processing", *Proc OFC'95*, paper TuD4, 1995.
- ²²⁴ C.Jorgensen, S.L.Danielsen, B.Mikkelsen, M.Vaa, K.E.Stubkjaer, P.Doussiere, F.Pommerau, L.Goldstein, R.Ngo, M.Goix, "All optical 40 Gbit/s OTDM to 2 x 20 Gbit/s WDM signal format conversion", *Electronics Letters*, **32**, 15, pp1384, 1996.
- ²²⁵ L.D.Westbrook, D.G.Moodie, "Simultaneous bi-directional analogue fibre optic transmission using an electroabsorption modulator", *Electronics Letters*, **32**, 19, pp1806, 1996.
- ²²⁶ L.D.Westbrook, D.G.Moodie, "Telecommunications Network", European Patent Number EP96305315.2, 1995.
- ²²⁷ D.J.Malyon, A.D.Ellis, W.A.Stallard, "Laser amplifier control in a 280 Mbit/s optical transmission system", *Electronics Letters*, **25**, 3, pp235, 1989.
- ²²⁸ D.G.Moodie, Private Communication (Project IA073815, 1996 Milestone Report, Development and Application of *Electroabsorption Modulators*), 1996.
- ²²⁹ M.Nakazawa, Y.Kimura, K.Suzuki, H.Kubota, T.Komukai, E.Yamada, T.Sugawa, E.Yoshida, T.Yamamoto, T.Imai, A.Sahara, H.Nakazawa, O.Yamauchi, M.Umezawa, "Field demonstration of soliton transmission at 10 Gbit/s over 2000 km in Tokyo metropolitan optical loop network", *Electronics Letters*, **31**, 12, pp992, 1995.
- ²³⁰ X.Gu, S.J.Dodds, L.C.Blank, D.M.Spirit, S.J.Pycock, A.D.Ellis, "Duobinary technique for dispersion reduction in high capacity optical systems - modelling, experiment and field trial", *IEE Proceedings on Optoelectronics*, **143**, 4, pp228, 1996.
- ²³¹ B.Wedding, "New method for optical transmission beyond dispersion limit", *Electronics Letters*, **28**, pp1298, 1992.
- ²³² A.D.Ellis, D.M.Spirit, "Unrepeated transmission over 80 km standard fibre at 40 Gbit/s", *Electronics Letters*, **30**, 1, pp72, 1994.
- ²³³ K.Iwashita, N.Takachino, "Compensation of 202 km single mode fibre chromatic dispersion in a 4 Gbit/s optical CPFSK transmission experiment", *Electronics Letters*, **24**, 12, pp759, 1988.
- ²³⁴ A.Yariv, D.Fekete, D.M.Pepper, "Compensation for channel dispersion by nonlinear optical phase conjugation", *Optics Letters*, **4**, 2, pp52, 1979.
- ²³⁵ W.Pieper, C.Kurtzke, R.Schnabel, D.Bruer, R.Ludwig, K.Petermann, "Nonlinearity insensitive standard fibre transmission based on optical phase conjugation in a semiconductor amplifier", *Electronics Letters*, **30**, 9, pp724, 1992.
- ²³⁶ R.Ludwig, W.Pieper, H.G.Weber, D.Bruer, K.Petermann, F.Kuppers, A.Mattheus, "Unrepeated 40 Gbit/s RZ single channel transmission over 150 km of standard single mode fibre at 1.55 μm ", *Electronics Letters*, **33**, 1, 1997.
- ²³⁷ A.Sano, T.Kataoka, Y.Miyamoto, K.Hagimoto, K.Takiguchi, K.Sato, "Unrepeated transmission of an OTDM 40 Gbit/s signal over 110 km using a dispersion adjustable PLC delay equaliser", *Electronics Letters*, **31**, 12, pp1003, 1995.
- ²³⁸ M.J.Cole, H.Geiger, R.I.Laming, S.Y.Set, M.N.Zervas, W.H.Loh, V.Gusmeroli, "Broadband dispersion compensating chirped fibre gratings in a 10 Gbit/s NRZ standard fibre link", *Proc ECOC'96*, Paper ThB.3.5, 1996.

- ²³⁹ L.Dong, M.J.Cole, A.D.Ellis, M.Durkin, M.Ibsen, V.Gusmeroli, R.I.Laming, "40 Gbit/s, 1.55 μm transmission over 100 km of non dispersion shifted fibre with long continuously chirped fibre gratings", Proc OFC'97, Paper PD-6, 1007.
- ²⁴⁰ M.C.Tatham, X.Gu, L.D.Westbrook, G.Sherlock, D.M.Spirit, "Transmission of 10 Gbit/s directly modulated DFB signals over 200 km standard fibre using mid-span spectral inversion", Electronics Letters, **30**, 16, pp1335, 1994.
- ²⁴¹ D.J.Richardson, R.I.Laming, D.Traverner, D.N.Payne, "Simulation of 50 GHz transmission over 50 km of standard fibre using midpoint spectral inversion for dispersion compensation", NGWP'93, Paper TuD2, 1993.
- ²⁴² A.H.Gnuack, R.M.Jopson, P.P.Iannone, R.M.Derosier, "Transmission of two wavelength multiplexed 10 Gbit/s channels over 560 km of dispersive fibre", Electronics Letters, **30**, 9, pp727, 1994.
- ²⁴³ A.D'Ottavi, E.Iannone, A.Mecozzi, S.Scotti, P.Spano, R.Dall'Ara, G.Guekos, J.Eckner, "4.3 terahertz four wave mixing spectroscopy of InGaAsP semiconductor amplifiers", Applied Physics Letters, **65**, 21, pp2633, 1994.
- ²⁴⁴ A.D'Ottavi, F.Martelli, P.Spano, A.Mecozzi, S.Scotti, R.Dall'Ara, J.Eckner, G.Guekos, "Very high efficiency four wave mixing in a single semiconductor travelling wave amplifier", Applied Physics Letters, **68**, 16, pp2186, 1996.
- ²⁴⁵ K.J.Valhala, J.Zhou, D.Geraghty, R.Lee, M.Newkirk, B.I.Miller, "Four wave mixing in semiconductor travelling wave amplifiers for wavelength conversion in all optical networks", International Journal of High Speed Electronics, **7**, 1, pp153, 1996.
- ²⁴⁶ J.Zhou, N.Park, J.W.Park, K.J.Vahala, M.A.Newkirk, B.I.Miller, "Efficiency of broadband four wave mixing wavelength conversion using semiconductor travelling wave amplifiers", IEEE Photonics Technology Letters, **6**, 1, pp50, 1994.
- ²⁴⁷ J.Zhou, N.Park, K.J.Vahala, M.A.Newkirk, B.I.Miller, "Broadband wavelength conversion with amplification by four wave mixing in semiconductor travelling wave amplifiers", Electronics Letters, **30**, 11, pp859, 1994.
- ²⁴⁸ A.D.Ellis, T.Widdowson, X.Shan, G.E.Wickens, D.M.Spirit, "Transmission of a true single polarisation 40 Gbit/s soliton data signal over 205 km using a stabilised erbium fibre ring laser and 40 GHz electronic timing recovery", Electronics Letters, **29**, 11, pp990, 1993.
- ²⁴⁹ X.Xhang, B.F.Jorgensen, "Extending transmission distance limitation for a 40 Gbit/s signal over standard fibre using optical phase conjugation", Optical Fibre Technology, **2**, pp188, 1996
- ²⁵⁰ D.D.Marcenac, D.Nesset, A.E.Kelly, M.Brierley, A.D.Ellis, D.G.Moodie, C.W.Ford, "40 Gbit/s transmission over 400 km using midspan spectral inversion by four wave mixing in a 2 mm long SOA", Submitted to Electronics Letters.
- ²⁵¹ K.Takiguchi, S.Kawanishi, H.Takara, O.Kamatani, K.Uchiyama, A.Himeno, K.Jinguji, "Dispersion slope equalising experiment using planar lightwave circuit for 200 Gbit/s time division multiplexed transmission", Electronics Letters, **32**, 22, pp2083, 1996.
- ²⁵² M.Suzuki, N.Edagawa, H.Tagawa, H.Tanaka, S.Yamamoto, S.Akiba, "Feasibility demonstration of 20 Gbit/s single channel soliton transmission over 11500 km using alternating amplitude solitons", Electronics Letters, **30**, 13, pp1083, 1994.
- ²⁵³ K.Iwatsuki, K.Suzuki, S.Nishi, M.Saruwatari, "40 Gbit/s optical soliton transmission over 65km", Electronics Letters, **28** pp1821, 1992.
- ²⁵⁴ M.Nakazawa, K.Suzuki, E.Yamada, H.Kubota, Y.Kimura, "Straight line soliton data transmission over 2000 km at 20 Gbit/s and 1000 km at 40 Gbit/s using erbium doped fibre amplifiers", Electronics Letters, **29**, 16, pp1474, 1993.
- ²⁵⁵ S.Kawanishi, H.Takara, O.Kamatani, T.Morioka, "100 Gbit/s, 500 km optical transmission experiment", Electronics Letters, **31**, 9, pp737, 1995 and S.Kawanishi, H.Takara, O.Kamatani, T.Morioka, M.Saruwatari, "100 Gbit/s, 560 km optical transmission experiment with 80 km amplifier spacing employing dispersion management", Electronics Letters, **32**, 5, pp470, 1996.
- ²⁵⁶ S.Kawanishi, H.Takara, T.Morioka, O.Kamatani, M.Saruwatari, "200 Gbit/s 100 km TDM transmission using supercontinuum pulses with prescaled PLL timing extraction and all optical demultiplexing", Proc OFC'95, paper PD28, 1995.
- ²⁵⁷ D.Leguen, F.Favre, R.Boittin, J.Debeau, F.Devaux, M.Henry, C.Thebault, T.Georges, "Demonstration of sliding filter controlled soliton transmission at 20 Gbit/s over 14 Mm", Electronics Letters, **31**, 4, pp301, 1995.

- ¹⁵⁸ T.Widdowson, A.D.Ellis, "20 Gbit/s soliton transmission over 125 Mm", *Electronics Letters*, **30**, 22, pp1866, 1994.
- ¹⁵⁹ Y.Kodama, S.Wabnitz, "Reduction of soliton interaction forces by bandwidth limited amplification", *Electronics Letters*, **27**, 21, pp1931, 1991.
- ¹⁶⁰ T.Georges, F.Favre, "Influence of soliton interaction on amplifier noise induced jitter: a first order analytical solution", *Optics Letters*, **16**, 21, pp1656, 1991.
- ¹⁶¹ A.Mecozzi, J.D.Moores, H.A.Haus, Y.Lai, "Soliton transmission control", *Optics Letters*, **16**, 23, pp1841, 1991.
- ¹⁶² D.Marcuse, "Simulations to demonstrate reduction of the Gordon Haus effect", *Optics letters*, **17**, 1, pp34, 1992.
- ¹⁶³ Y.Kodama, A.Hasegawa, "Generation of asymptotically stable optical solitons and suppression of the Gordon Haus effect", *Optics Letters*, **17**, 1, pp31, 1992.
- ¹⁶⁴ M.Nakazawa, H.Kubota, "Physical interpretation of reduction of soliton interaction by bandwidth limited amplification", *Electronics Letters*, **28**, 10, pp958, 1992.
- ¹⁶⁵ A.N.Pilipetskii, C.R.Menyuk, "Acoustic effect and correlated errors in soliton information transmission", *Optics Letters*, **21**, 2, pp119, 1996.
- ¹⁶⁶ A.Mecozzi, H.A.Haus, "Effect of filters on soliton interactions in wavelength division multiplexing systems", *Optics Letters*, **17**, 14, pp987, 1992.
- ¹⁶⁷ J.P.Gordon, "Interaction forces among solitons in optical fibres", *Optics Letters*, **8**, 11, pp396, 1983.
- ¹⁶⁸ P.L.Chu, C.Desem, "Mutual interaction between solitons of unequal amplitudes in optical fibre", *Electronics Letters*, **21**, 24, pp1133, 1985.
- ¹⁶⁹ L.F.Mollenauer, J.P.Gordon, S.G.Evangelides, "The sliding frequency guiding filter: an improved form of soliton jitter control", *Optics Letters*, **17**, 22, pp1575, 1992.
- ¹⁷⁰ P.V.Mamyshev, L.F.Mollenauer, "Stability of soliton propagation with sliding frequency guiding filters", *Optics Letters*, **19**, 24, pp2083, 1994.
- ¹⁷¹ M.Romagnoli, S.Wabnitz, Y.Kodama, F.Fontana, L.Bossalini, P.Franco, M.Midrio, "Stabilisation of optical solitons by acousto-optic modulators, theory and experiments", *Proc COST Workshop on Optical Telecommunications, Nice, France*, pp25, 1994.
- ¹⁷² E.Kolltveit, B.Biotteau, F.Pitel, I.Riant, O.Audouin, P.Brindel, E.Brun, P.Sansonetti and J-P.Hamaide, "Soliton frequency guiding in a 2x5 Gbit/s WDM system using a UV-written fibre Fabry-Perot filter", *ECOC'95*, paper Mo.A.3.6
- ¹⁷³ E.Kolltveit, B.Biotteau, I.Riant, F.Pitel, O.Audouin, P.Brindel, E.Brun, P.Sansonetti and J-P.Hamaide, "Soliton frequency guiding by UV-written fibre Fabry-Perot filter in a 2x5 Gbit/s wavelength division multiplexing transmission over transoceanic distances", *IEEE Photonics Technology Letters*, **7**, 12, pp1498, 1995.
- ¹⁷⁴ E.Yamada, K.Suzuki, M.Nakazawa, "10 Gbit/s single pass soliton transmission over 1000 km", *Electronics Letters*, **27**, 14, pp1289, 1991
- ¹⁷⁵ L.F.Mollenauer, E.Lichtman, M.J.Nuebelt, G.T.Harvey, "Demonstration, using sliding frequency guiding filters, of error free soliton transmission over more than 20 Mm at 10 Gbit/s single channel and over more than 13 Mm at 20 Gbit/s in a two channel WDM", *Electronics Letters*, **29**, 10, pp910, 1993.
- ¹⁷⁶ G.Aubin, T.Montalant, J.Moulu, B.Nortier, F.Pirio, J.-B.Thomine, "Demonstration of soliton transmission at 10 Gbit/s up to 27 Mm using signal frequency sliding technique", *Electronics Letters*, **31**, 1, pp52, 1995.
- ¹⁷⁷ L.F.Mollenauer, P.V.Mamyshev, M.J.Nuebelt, "Demonstration of soliton WDM transmission at 6 and 7 x 10 Gbit/s, error free over transoceanic distances", *Electronics Letters*, **32**, 5, pp471, 1996.
- ¹⁷⁸ P.V.Mamyshev, L.F.Mollenauer, "NRZ to soliton data conversion by a filtered transmission line" *Proc OFC'95*, paper FB2, 1995.
- ¹⁷⁹ F.Favre, D.LeGuen, "20 Gbit/s soliton transmission over 19 Mm using sliding frequency guiding filters", *Electronics Letters*, **31**, 12, pp991, 1995
- ¹⁸⁰ K-I.Suzuki, S.Kawai, K.Iwatsuki, "40 Gbit/s adiabatic and phase stationary soliton transmission with sliding frequency filter over 4000 km reciprocating dispersion managed fibre", *Electronics Letters*, **32**, 23, 1996.
- ¹⁸¹ M.Nakazawa, E.Yamada, H.Kubota, K.Suzuki, "10 Gbit/s soliton data transmission over one million kilometers", *Electronics Letters*, **27**, 14, pp1270, 1991.

- ²⁸² M.Nakazawa, H.Kubota, E.Yamada, K.Suzuki, "Infinite distance soliton transmission with soliton controls in time and frequency.", *Electronics Letters*, **28**, 12, pp1099, 1992.
- ²⁸³ N.J.Smith, K.J.Blow, W.J.Firth, K.Smith, "Soliton dynamics in the presence of phase modulators.", *Optics Communication*, **103**, pp324, 1993.
- ²⁸⁴ H.Kubota, M.Nakazawa, "Soliton transmission control for ultra high speed system", *IEICE Transactions on Electronics*, **E78-C**, 1, pp5, 1995.
- ²⁸⁵ H.Kubota, M.Nakazawa, "Soliton transmission with long amplifier spacing under soliton control", *Electronics Letters*, **29**, 20, pp1780, 1993
- ²⁸⁶ "The Guinness Book of Records 1997", Guinness Publishing, 1996, United Kingdom, pp114.
- ²⁸⁷ S.Wabnitz, "Suppression of soliton interactions by phase modulation", *Electronics Letters*, **29**, 19, pp1711, 1993.
- ²⁸⁸ T.Widdowson, D.J.Malyon, A.D.Ellis, K.Smith, K.J.Blow, "Soliton Shepherding: All optical transmission control over global distances", *Electronics Letters*, **30**, 12, pp990, 1994.
- ²⁸⁹ H.J.Harvey, "An alternative derivation of soliton transmission control", *Proc OAA'94*, 1994.
- ²⁹⁰ O.Leclerc, E.Desurvire, O.Audouin, "Assessment of 80 Gbit/s (4x20Gbit/s) regenerated WDM soliton transoceanic transmission", *Electronics Letters*, **32**, 12, pp1118, 1996.
- ²⁹¹ M.Nakazawa, K.Suzuki, H.Kubota, Y.Kimura, Y.Yamada, K.Tamura, T.Komukai, T.Imai, "40 Gbit/s WDM (10 Gbit/s x 4 unequally spaced channels) soliton transmission over 10000km using synchronous modulation and narrowband optical filtering", *Electronics Letters*, **32**, 9, pp828, 1996.
- ²⁹² M.Nakazawa, K.Suzuki, H.Kubota, E.Yamada, "60 Gbit/s WDM (20 Gbit/s x 3 unequally spaced channels) soliton transmission over 10,000km using in-line synchronous modulation and optical filtering", *Electronics Letters*, **32**, 18, pp1686, 1996.
- ²⁹³ M.Nakazawa, K.Suzuki, E.Yamada, "20 Gbit/s, 1020 km penalty free soliton transmission using erbium doped fibre amplifiers", *Electronics Letters*, **28**, 11, pp1046, 1992.
- ²⁹⁴ M.Nakazawa, Y.Kimura, K.Suzuki, H.Kubota, T.Komukai, E.Yamada, T.Sugawa, E.Yoshida, T.Yamamoto, T.Imai, A.Sahara, O.Yamauchi, M.Umezawa, "Soliton transmission at 20 Gbit/s over 2000 km in Tokyo metropolitan optical network", *Electronics Letters*, **31**, 17, pp1478, 1995.
- ²⁹⁵ M.Nakazawa, K.Suzuki, H.Kubota, E.Yamada, Y.Kimura, "Straight line soliton data transmission at 20 Gbit/s beyond Gordon Haus limit", *Electronics Letters*, **30**, 16, pp1331, 1994.
- ²⁹⁶ N.J.Smith, K.J.Blow, I.Andonovic, "Sideband generation through perturbations to the average soliton model", *Electronics Letters*, **10**, pp1329, 1992.
- ²⁹⁷ F.Matera, A.Mecozzi, M.Romagnoli, M.Settembre, "Sideband instability induced by periodic power variation in long distance fiber links", *Optics Letters*, **18**, 18, pp1499, 1993.
- ²⁹⁸ F.Devaux, Y.Sorel, J.F.Kerdiles, "Simple measurement of fiber dispersion and of chirp parameter of intensity modulated light emitter", *Journal of Lightwave Technology*, **11**, 12, pp1937, 1993.
- ²⁹⁹ A.Takada, H.Miyazawa, "30 GHz picosecond pulse generation from actively mode locked erbium doped fibre laser", *Electronics Letters*, **26**, 3, pp216, 1990.
- ³⁰⁰ Th.Pfeiffer, G.Veith, "40 GHz pulse generation using a widely tunable all-polarisation preserving erbium fibre ring laser", *Electronics Letters*, **29**, 21, pp1849, 1993.
- ³⁰¹ Th.Pfeiffer, Private communication, September 1995.
- ³⁰² K.Iwatsuki, S.Kawai, S.Nishi, M.Saruwatari, "Timing jitter due to carrier linewidth of laser diode pulse sources in ultra high speed soliton transmission", *Journal of Lightwave Technology*, **13**, 4, pp639, 1995.
- ³⁰³ A.Naka, T.Matsuda, S.Saito, K.Sato, "5200 km straight line soliton transmission experiment at 10 Gbit/s", *Electronics Letters*, **31**, 19, pp1679, 1995.
- ³⁰⁴ W.Forysaik, F.M.Knox, N.J.Doran, "Average soliton propagation in periodically amplified systems with stepwise dispersion profiled fibre", *Optics Letters*, **19**, 3, pp174, 1994.
- ³⁰⁵ M.Suzuki, I.Morita, N.Edagawa, S.Yamamoto, H.Tagawa, S.Akiba, "Reduction of Gordon-Haus timing jitter by periodic dispersion compensation", *Electronics Letters*, **31**, 23, pp2027, 1995.
- ³⁰⁶ M.Nakazawa, A.Sahara, K.Tamura, "Marked increase in the power margin through the use of a dispersion allocation technique", *IEEE Photonics Technology Letters*, **8**, 8, pp1088, 1996.
- ³⁰⁷ Y.Kodama, H.Ramagnoli, S.Wabnitz, "Soliton stability and interactions in fibre lasers", *Electronics Letters*, **28**, 21, pp1981, 1992.
- ³⁰⁸ F.M.Knox, P.Harper, P.N.Kean, N.J.Doran, I.Bennion, "Low jitter long distance pulse transmission of near net fibre dispersion zero wavelength", *Electronics Letters*, **31**, 17, pp1467, 1995.

- ³⁰⁹ V.V.Afanasjev, W.H.Loh, A.B.Grudinin, D.Atkinson, D.N.Payne, "Unlimited soliton propagation and noise suppression in a system with spectral filtering and saturable absorption.", CLFO'94, paper CThN1, 1994.
- ³¹⁰ K.Smith, N.J.Doran, P.G.J.Wigley, "Pulse shaping, compression and pedestal suppression employing a nonlinear-optical loop mirror", *Optics Letters*, **15**, 22, pp1294, 1990.
- ³¹¹ M.Matsumoto, H.Ikeda, A.Hasegawa, "Suppression of noise accumulation in bandwidth limited soliton transmission by means of nonlinear loop mirrors", *Optics Letters*, **19**, 3, pp183, 1994.
- ³¹² N. J. Smith, N. J. Doran, "Picosecond soliton propagation using nonlinear optical loop mirrors as intensity filters", *Electronics Letters*, **30**, 13, pp1084, 1994.
- ³¹³ S.Bigo, E.Desurvire, O.Audouin, "Dual control nonlinear optical loop mirrors for all optical soliton synchronous modulation", *Optics Letters*, **21**, 18, pp1463, 1996.
- ³¹⁴ K.J.Blow, N.J.Doran, "Average soliton dynamics and the operation of soliton systems with lumped amplifiers", *IEEE Photonics Technology Letters*, **3**, 4, pp369, 1991.
- ³¹⁵ A.D.Ellis, T.Widdowson, X.Shan, "Wavelength dependence of 40 Gbit/s solitonic transmission over distances greater than 2000 km", *Electronics Letters*, **32**, 4, pp381, 1996.
- ³¹⁶ M.Nakazawa, K.Kurokawa, "Femtosecond soliton transmission in 18 km long dispersion shifted distributed erbium doped fibre amplifier", *Electronics Letters*, **27**, 15, pp1369, 1991.
- ³¹⁷ M.Nakazawa, "Ultralong dispersion shifted EDFA and its application to soliton transmission", *IEEE Journal of Quantum Electronics*, **26**, 12, pp2103, 1990.
- ³¹⁸ D.M.Spirit, I.W.Marshall, P.D.Constantine, D.L.Williams, S.T.Davey, B.J.Ainslie, "Nonlinear dispersion free 10 GHz optical pulse train transmission in distributed erbium doped fibre", *Electronics Letters*, **27**, 3, pp222, 1991.
- ³¹⁹ K.Kurokawa, M.Nakazawa, "Femtosecond soliton transmission characteristics in ultralong distributed EDFA with different pumping configurations", *IEEE Journal of Quantum Electronics*, **28**, 9, pp1922, 1992.
- ³²⁰ C.Lester, K.Bertilsson, K.Rottwitt, P.A.Andrekson, M.A.Newhouse, A.J.Antos, "Soliton transmission over more than 90 km using distributed erbium doped fibres", *Electronics Letters*, **31**, 3, pp219, 1995.
- ³²¹ A.J.Stentz, R.W.Boyd, A.F.Evans, "Dramatically improved transmission of ultrashort solitons through 40 km of dispersion decreasing fibre", *Optics Letters*, **20**, pp1770, 1995.
- ³²² A.Altuncu, L.Noel, W.A.Pender, A.S.Siddiqui, T.Widdowson, A.D.Ellis, M.A.Newhouse, A.J.Antos, G.Kar, P.W.Chu, "40 Gbit/s error free transmission over a 68 km distributed erbium doped fibre amplifier", *Electronics Letters*, **32**, 3, pp233, 1996.
- ³²³ D.M.Spirit, G.E.Wickens, T.Widdowson, G.R.Walker, D.L.Williams, L.C.Blank, "137 km, 4x5 Gbit/s optical time division multiplexed unrepeated system with distributed erbium amplifier", *Electronics Letters*, **28**, 13, pp1362, 1992.
- ³²⁴ G.Aubin, E.Jeanney, T.Montalant, J.Moulu, F.Pirio, J-B.Thomine, F.Devaux, N.Souli, "Record 20 Gigabit-per-second 200-km repeater span transoceanic soliton transmission using in line remote pumping", *IEEE Photonics Technology Letters*, **8**, 9, pp1267, 1996.
- ³²⁵ E.Desurvire, "Analysis of distributed erbium doped fiber amplifiers with fibre background loss", *IEEE Photonics Technology Letters*, **3**, 7, pp625, 1991.
- ³²⁶ C.J.Anderson, A.D.Ellis, Working records, 1994.
- ³²⁷ X.Shan, A.D.Ellis, T.Widdowson, D.M.Spirit, "10 and 80 GHz soliton transmission over 60 km distributed erbium fibre amplifier", *IEE Colloquium Digest 1995/110*, paper 15, 1995.
- ³²⁸ A.Altuncu, A.S.Siddiqui, A.D.Ellis, M.A.Newhouse, A.J.Antos, "Gain and noise figure characterisation of a 68 km long distributed erbium doped fibre amplifier", *Electronics Letters*, **32**, 19, pp1800, 1996.
- ³²⁹ R.Ohira, A.Hasegawa, Y.Kodama, "Methods of constructing a long haul soliton transmission system with fibres having a distribution in dispersion", *Optics Letters*, **20**, 7, pp702, 1995.
- ³³⁰ D.J.Richardson, L.Dong, R.P.Chamberlin, A.D.Ellis, T.Widdowson, W.A.Pender, "Periodically amplified system based on loss compensating dispersion decreasing fibre", *Electronics Letters*, **32**, 4, pp373, 1996.
- ³³¹ D.J.Richardson, L.Dong, A.D.Ellis, T.Widdowson, W.A.Pender, "Experimental demonstration of 10 Gbit/s 4.7 ps pulse transmission over 4,300 km in a low dispersion, loss compensating dispersion decreasing fibre", *NGWA'96*, Paper FA3-1, pp8, 1996.

- ³³² S.V.Chernikov, P.V.Mamyshev, "Femtosecond soliton propagation in fibers with slowly decreasing dispersion", *Journal of the Optical Society of America B*, **8**, 8, pp1633, 1991.
- ³³³ D.J.Richardson, R.P.Chamberlin, L.Dong, D.N.Payne, "High quality soliton loss compensation in a 38 km dispersion decreasing fibre", *Electronics Letters*, **31**, pp1681, 1995.
- ³³⁴ D.J.Richardson, L.Dong, R.P.Chamberlin, W.A.Pender, A.D.Ellis, T.Widdowson, "Periodically amplified system based on loss compensating dispersion decreasing fibre", *IEE Colloquium Digest 1996/090*, Paper 4, 1996
- ³³⁵ J.P.Gordon, "Theory of the soliton self frequency shift", *Optics Letters*, **11**, pp662, 1996.
- ³³⁶ G.P.Agrawal, M.J.Potasek, "Nonlinear pulse distortion in single mode optical fibers at the zero dispersion wavelength", *Physical Review A*, **33**, 3, pp1765, 1986.
- ³³⁷ M.Desaix, D.Anderson, M.Lisak, "Solitons emerging from pulses launched in the vicinity of the zero dispersion point in a single mode optical fibre", *Optics Letters*, **15**, 1, pp18, 1990.
- ³³⁸ S.Kawai, K.Iwatsuki, S.Nishi, "Demonstration of error free optical soliton transmission over 30,000 km at 10 Gbit/s with signal frequency sliding technique", *Electronics Letters*, **31**, 17, pp1463, 1995.
- ³³⁹ W.Forysiak, N.J.Doran, "Reduction of Gordon-Haus jitter in soliton transmission systems by optical phase conjugation", *Journal of Lightwave Technology*, **13**, 5, pp850, 1995.
- ³⁴⁰ R-J.Essiambre, G.P.Agrawal, "Ultrahigh bit rate soliton communication systems using dispersion decreasing fibers and parametric amplifiers", *Optics Letters*, **21**, 2, pp116, 1996.
- ³⁴¹ C.R.Giles, T.Li, T.H.Wood, C.A.Burrus, D.A.B.Miller, "All Optical Regenerator", *Electronics Letters*, **24**, 14, pp848, 1988.
- ³⁴² A.D.Ellis, D.A.Cleland, "Ultrafast all optical switching in two wavelength amplifying nonlinear optical loop mirror", *Electronics Letters*, **28**, 4, pp405, 1992.
- ³⁴³ M.Jinno, M.Abe, "All optical regenerator based on nonlinear fibre Sagnac interferometer", *Electronics Letters*, **28**, 14, pp1350, 1992.
- ³⁴⁴ M.Eiselt, W.Pieper, H.G.Weber, "Decision gate for all optical data retiming using a semiconductor laser amplifier in a loop mirror configuration", *Electronics Letters*, **29**, 1, pp107, 1993.
- ³⁴⁵ J.K.Lucek, K.Smith, "All optical signal regenerator", *Optics Letters*, **18**, 15, pp1226, 1993.
- ³⁴⁶ K.Weich, R.Eggmann, J.Hörler, D.J.As, M.Möhrle, E.Patzak, "10 Gbit/s all-optical clocked decision circuit using two section semiconductor lasers", *Electronics Letters*, **30**, 10, pp784, 1994.
- ³⁴⁷ D.A.O.Davies, A.D.Ellis, G.Sherlock, "Regenerative 20 Gbit/s wavelength conversion and demultiplexing using a semiconductor laser amplifier nonlinear loop mirror", *Electronics Letters*, **31**, 12, pp1000, 1995.
- ³⁴⁸ Y.Yano, T.Ono, N.Henmi, "Noise compression and waveform restoration by an optical signal regenerator", *Proc OFC'95*, paper WH4, 1995.
- ³⁴⁹ A.D.Ellis, W.A.Pender, T.Widdowson, D.J.Richardson, R.P.Chamberlain, L.Dong, "All optical modulation of 40 GHz beat frequency conversion source", *Electronics Letters*, **31**, 16, pp1362, 1995.
- ³⁵⁰ W.A.Pender, P.J.Watkinson, E.J.Greer, A.D.Ellis, "10 Gbit/s all optical regenerator", *Electronics Letters*, **31**, 18, pp 1587, 1995.
- ³⁵¹ W.Pieper, K.Weich, R.Ludwig, E.Patzak, H.G.Weber, "All optical polarisation and wavelength independent 3R signal regenerator", *Electronics Letters*, **32**, 14, pp1316, 1996.
- ³⁵² I.D.Phillips, P.N.Kean, N.J.Doran, I.Bennion, D.A.Pattison, A.D.Ellis, "Simultaneous clock recovery and data regeneration using a nonlinear optical loop mirror as an all optical mixer", *Proc OFC'97*.
- ³⁵³ X.Shan, "Mode-locked erbium fibre lasers and their applications in high capacity optical communications", PhD Thesis, University of Essex, Department of Electronic Systems Engineering, Colchester, UK, 1994.
- ³⁵⁴ A.Felder, M.Möller, J.Popp, J.Böck, H-M Rein, "46 Gb/s DEMUX, 50 Gb/s MUX and 30 GHz static frequency divider in silicon bipolar technology", *IEICE Transactions on Electronics*, **E79-C**, 7, pp892, 1996 and *IEEE Journal of Solid State Circuits*, **31**, 4, 1996.
- ³⁵⁵ K.Satzke, D.Baums, U.Cebulla, H.Haisch, D.Kaiser, E.Lach, E.Kühn, J.Weber, R.Weinmann, P.Wiedemann, E.Zielinski, "Ultrahigh bandwidth (42GHz) polarisation independent ridge waveguide electroabsorption modulator based on tensile strained InGaAsP MQW", *Electronics Letters*, **31**, 23, pp2030, 1995.

- ³⁵⁶ S.Kuwano, N.Takachio, K.Iwashita, T.Otsuji, T.Enoki, K.Wakita, "160 Gbit/s (4 ch x 40 Gbit/s electronically multiplexed data) WDM transmission over 320 km dispersion shifted fibre", Proc OFC'96, Paper PD25, 1996.
- ³⁵⁷ P.B.Hansen, L.Eskilden, S.G.Grubb, A.M.Vengsarkar, S.K.Korotky, T.A.Stasser, J.E.J.Alphonsus, J.J.Veselka, D.J.DiGiovanni, D.W.Peckham, E.C.Beck, D.Truxal, W.Y.Cheung, S.G.Kosiniski, D.Gasper, P.F.Wysocki, V.L.DaSilva, J.R.Simpson, "529 km unrepeated transmission at 2.488 Gbit/s using dispersion compensation, forward error correction, and remote post and preamplifiers pumped by diode pumped Raman lasers", Electronics Letters, **31**, 17, pp1460, 1995.
- ³⁵⁸ G.Aubin, T.Montalant, J.Moulu, F.Pirio, J.-B.Thomine, F.Devaux, "40 Gbit/s OTDM soliton transmission over transoceanic distances", Electronics Letters, **32**, 24, pp2188, 1996.
- ³⁵⁹ E.Brun-Maunand, P.Brindel, O.Leclerc, F.Pitel, E.Desurvire, "Parametric study of chromatic dispersion influence in 20 Gbit/s, 20Mm regenerated soliton systems with up to 140 km amplifier spacing", Electronics Letters, **32**, 11, pp1022, 1996.
- ³⁶⁰ I.Morita, M.Suzuki, N.Edagawa, S.Yamamoto, S.Akiba, "Single channel 40 Gbit/s, 5000 km straight line soliton data transmission experiment using periodic dispersion compensation", Proc ECOC'96, Paper TuD.3.1, 1996.
- ³⁶¹ D.M.Spirit, L.C.Blank, "Optical time division multiplexing for high capacity network applications", BT Technology Journal, **11**, 2, pp34, 1993.
- ³⁶² T.Morioka, M.Saruwatari, "Ultrafast all-optical switching utilising the optical Kerr effect in polarisation maintaining single mode fibres", IEEE Journal on Selected Areas in Communications, **6**, 7, pp1186, 1988.
- ³⁶³ T.Morioka, H.Takara, K.Mori, M.Saruwatari, "Ultrafast reflective optical Kerr demultiplexer using polarisation rotation mirror", Electronics Letters, **28**, 6, pp521, 1992.
- ³⁶⁴ D.M.Patrick, A.D.Ellis, D.M.Spirit, "Bit rate flexible all optical demultiplexing using a nonlinear optical loop mirror", Electronics Letters, **29** 8, pp702, 1993.
- ³⁶⁵ A.D.Ellis, D.M.Spirit, "The use of GaInAsP amplifiers for 40 Gbit/s signal processing", Proc NGWP'93, Paper PD2, 1993.
- ³⁶⁶ K.Suzuki, K.Iwatsuki, S.Nishi, M.Saruwatari, "160 Gbit/s single polarisation subpicosecond transform limited pulse signal demultiplexing using ultrafast optical loop mirror including MQW travelling wave semiconductor laser amplifier", Electronics Letters, **30**, 8, pp660, 1994.
- ³⁶⁷ E.Jahn, N.Agrawal, H-J, Ehrke, R.Ludwig, W.Pieper, H.G.Weber, "Monolithically integrated asymmetric Mach Zehnder interferometer as a 20 Gbit/s all-optical add/drop multiplexer for OTDM systems", Electronics Letters, **32**, 3, pp216, 1996.
- ³⁶⁸ D.M.Patrick, A.D.Ellis, D.M.Spirit, "Bit rate flexible all optical demultiplexing using nonlinear optical loop mirror", Proc ECOC'93, pp281, 1993.
- ³⁶⁹ O.Kamatani, S.Kawanishi, "Add/drop operation for 100 Gbit/s optical signal based on optical wavelength conversion by four wave mixing", Electronics Letters, **32**, 10, pp911, 1996.
- ³⁷⁰ J.K.Lucek, P.Gunning, D.G.Moodie, K.Smith, A.D.Ellis, D.Pitcher, "40 Gbit/s optical TDMA LAN", Proc ECOC'96, Paper ThC.3.4, 1996.
- ³⁷¹ A.Lord, L.C.Blank, J.M.Boggis, E.Bryant, W.A.Stallard, "Theory of control mechanism for an optically time division multiplexed system", Electronics Letters, **24**, 1, pp29, 1988.
- ³⁷² F.M.Knox, W.Forysiak, N.J.Doran, "10 Gbit/s soliton communication systems over standard fibre at 1.55 μ m and the use of dispersion compensation", Journal of Lightwave Technology, **13**, 10, pp1955, 1995
- ³⁷³ F.M.Knox, P.Harper, P.N.Kean, I.Bennion, N.J.Doran, "10 Gbit/s soliton transmission over standard fibre", IEE Colloquium Digest 1996/090, paper 13, 1996.
- ³⁷⁴ D.Cotter, J.K.Lucek, D.D.Marcenac, "Ultra high bit rate networking: from the transcontinental backbone to the desktop", IEEE Communications Magazine, pp2, April 1997.